SECTION A

JOURNAL OF RESEARCH

of the NATIONAL BUREAU OF STANDARDS

JNBAAS 81A(2 & 3) 243-344 (March - June 1977)

U.S. DEPARTMENT OF COMMERCE / National Bureau of Standards

Physics and Chemistry

Journal of Research

of the

National Bureau of Standards

A. Physics and Chemistry

Mar.–June • 1977

VOLUME • 81A

NUMBERS • 2&3

Associate Editor: D. D. Wagman

Publication dates:
Feb. 1, Apr. 1, June 1, Aug. 1, Oct. 1, Dec. 1, 1977

J. Res. Nat. Bur. Stand. (U.S.), A

JOURNAL OF RESEARCH

The National Bureau of Standards Journal of Research reports research and development in the fields of activities shown at right. Also included from time to time are survey articles on topics closely related to the Bureau's scientific and technical program.

The Journal is published in two separate sections as follows:

A. Physics and Chemistry

Contains papers of interest primarily to scientists working in these fields. Issued six times a year. Annual subscription: domestic, $17.00; foreign, $21.25. Single copy, varies.

B. Mathematical Sciences

Presents studies and compilations designed mainly for the mathematician and the theoretical physicist. Issued quarterly. Annual subscription: domestic, $9.00; foreign, $11.25. Single copy, $2.25.

To begin publication as a single journal, July–August, 1977

IMPORTANT NOTICE TO OUR READERS

Effective with the next issue, Section A "Physics and Chemistry" and Section B "Mathematical Sciences" will be combined into one publication entitled "Journal of Research of the National Bureau of Standards." The consolidated Journal will extend its coverage to include the results of research and development in all technical areas in which the Bureau is active. These include physics, chemistry, engineering, mathematics and computer science. The Journal will thus provide better overall coverage of NBS work, with major emphasis on measurement methodology, the basic technology underlying standardization, and survey articles on topics closely related to the Bureau's scientific and technical programs. It will also continue to bring to our readers abstracts with complete citations for all other papers published by Bureau staff, whether in government publications or in non-NBS media.

Long-time followers of NBS will recognize the full circle for the Journal. In 1959, the Journal of Research—published since 1928—began publication as four separate sections. During the intervening years, program spin-offs and changes in program emphasis led to a reduction of the Journal of Research to the current two sections. The Bureau now feels that a return to the single combined Journal is in the best interest of our readers.

The "new" Journal will continue the same six-times-a-year schedule as for the present Section A. Subscribers to Section A and Section B will automatically continue to receive the combined Journal for their present subscription, unless they indicate that they wish otherwise. They will recieve a notice of adjustment or expiration from the Journal's subscription management, the Superintendent of Documents, U.S. Government Printing Office.

On matters other than subscriptions, please feel free to contact the undersigned or correspond directly with the Journal subject-matter editors named below. Your patience and understanding during this transition period will be very much appreciated.

W.R.Tilley
Chief, Office of Technical Publications

Board of Editors

Churchill Eisenhart, Executive Editor (Mathematics)
John W. Cooper (Physics)
Donald D. Wagman (Chemistry)
Andrew J. Fowell (Engineering)
Joseph O. Harrison (Computer Science)
Stephen J. Smith (Boulder Labs.)

U.S. DEPARTMENT OF COMMERCE
Juanita M. Kreps, Secretary

NATIONAL BUREAU OF STANDARDS
Ernest Ambler, Acting Director

Order all publications from the Superintendent of Documents
U.S. Government Printing Office, Washington, D.C. 20402

The Secretary of Commerce has determined that the publication of this periodical is necessary in the transaction of the public business required by law of this Department. Use of funds for printing this periodical has been approved by the Director of the Office of Management and Budget through June 30, 1981.

JOURNAL OF RESEARCH of the National Bureau of Standards—A. Physics and Chemistry
Vol. 81A, Nos. 2 and 3, March–June 1977

Diffusion with Discontinuous Swelling

III. Type II Diffusion as a Particular Solution of the Conventional Diffusion Equation

Anton Peterlin

Institute for Materials Research, National Bureau of Standards, Washington, D.C. 20234

(May 3, 1977)

Very often a non-solvent diffuses into a glassy polymer with a steep concentration profile proceeding at an almost constant rate v yielding a weight gain proportional to time. Such a diffusion is called type II diffusion in order to distinguish it from the more usual "Fickian" diffusion proceeding without such a constant concentration front and yielding, at least in the beginning, a weight gain proportional to the square root of time. It turns out that the conventional diffusion equation without any special new term but with a diffusion coefficient rapidly increasing with concentration has a series of solutions representing exactly such type II diffusion with v as a completely free parameter which determines the steepness of concentration front. With the usual boundary conditions and infinite medium the diffusion coefficient has to become infinite at the highest penetrant concentration. This case can be considered as an extreme limit which is approached to a high degree in an actual experiment. The finite sample thickness, however, requires only a very large but not an infinite diffusion coefficient. Hence type II diffusion is only a special case of possible diffusion processes compatible with the conventional diffusion equation without any need for new terms if only the diffusion coefficient increases sufficiently fast with penetrant concentration.

Key words: Concentration dependent diffusion coefficient; concentration front; discontinuous swelling; unconventional diffusion; velocity of concentration front propagation.

1. Introduction

In recent years a large amount of experimental [1–12] and theoretical [13–21] work was done on diffusion of liquids in polymer glasses with almost discontinuous swelling which is now generally referred to as type II diffusion [2]. It is characterized by three basic conditions: (1) As solvent penetrates the polymer, a sharp advancing boundary separates the inner glassy core from the outer swollen and rubbery shell, (2) Behind the solvent's advancing front, the swollen gel is in an almost equilibrium swelling state, (3) the boundary between swollen gel and glassy core advances at almost constant rate varying in polystyrene, depending on temperature, penetrant and its activity, between 0.2 and 10×10^{-6} cm/s. As a consequence the specific weight gain per unit cross section of the diffusing front, W increases almost linearly with time as expected from the almost constant velocity, v, of progress of the swelling boundary between the low and high concentration of the penetrant. An effect of minor importance for the diffusion process itself is the partial destruction of polymer with craze and crack formation in the swollen region of the polymer.

As a glassy polymer is cooled the speed of advancing front falls off and a critical point is reached with zero velocity v. Type II diffusion is replaced by a more or less conventional Fickian diffusion. In this case the polymer has both a glassy shell and glassy core. The swelling by the penetrant is not sufficient for the reduction of the glass transition point of the swollen material below or to the temperature of the experiment. According to some analyses of the low molecular weight paraffin diffusion into polystyrene, the effect occurs at relatively high penetrant activity [17], between 0.5 and 1, while older data on methyl acetate diffusion into poly(methyl methacrylate) and on acetone diffusion in cellulose nitrate show the linear increase of W with time most clearly at very low activity [1a].

Since the advancing of a sharp boundary between low and high solvent concentration at an almost constant velocity is a most unexpected feature of a diffusion process, a new name, type II diffusion was created [2] and the phenomenon tried to be explained by a new term in the diffusion equation depending on the divergence of the stress field originating at the boundary between the conspicuously swollen and the almost nonswollen material [15, 16]. An analysis of the diffusion process in a nonlinear sorption and diffusion range, however, shows that the effect is neither so strange nor so unexpected to need a new name and a new term in the diffusion equation. It follows automatically from the classical formulation of diffusion if the sorption (S) and diffusion (D) coefficient are strongly dependent on concentration c of diffusant or its chemical potential μ.

In this paper it will be demonstrated that the general diffusion equation in an infinite medium can have a steady state solution with a time independent concentration profile progressing uniformly through the polymer at a constant velocity. The sole condition for such a solution is that the mobility becomes infinite at the maximum concentration c_0 or maximum chemical potential of the diffusant. This condition is a natural consequence of the geometrical boundaries of the

[1] Figures in brackets indicate the literature references at the end of this paper.

sample extending from $-\infty$ to $+\infty$. A constant current j from the boundary at $-\infty$ can be only sustained if D increases to infinity while $(dc/\partial x)_{-\infty}$ goes to zero. The more realistic consideration of the finite dimensions of the sample removes the need for an infinitely large diffusion coefficient but also makes the mathematics a little more complicated than attempted in this paper.

For the sake of simplicity only the linear case will be treated. The swelling boundary has a constant cross-section and proceeds with constant velocity in the x-axis direction. The specific weight gain of the sample per unit time, dW/dt, is constant as in the case of type II diffusion if one neglects the transients at the beginning and the end of the experiment. The transients are of course completely neglected in the consideration of the steady state boundary propagation through an infinitely thick sample extending from $-\infty$ to $+\infty$.

In the actual membrane the diffusant mobility may increase quite drastically with glass to rubber transformation but still remains finite. Yet the changes are quite substantial, from $D = 10^{-12}$ cm^2/s in a glass to 10^{-6} cm^2/s in a gel. The above mentioned steady state solution in the infinite medium is therefore the asymptotic approximation to the actual diffusion process if the mobility increases by a few orders of magnitude while the sorbent concentration increases from $c = 0$ to c_0. This is indeed the case with a diffusant which transforms the glassy polymer into a rubbery gel. The gel must be so much lower in polymer content that the sorbate flows through it almost freely and thus easily supplies the amount of liquid requested for the swelling at the propagating concentration front.

Transient from the start at $t = 0$ with $c = 0$ throughout the sample to the steady state solution is a combination with the usual type I diffusion with the initial weight gain proportional to the square root of time. During this transition time the steady state of the concentration tail gets established in front of the almost constant concentration profile. The shape of the profile depends on the propagation velocity [14]. The total weight gain is a sum of two terms, one proportional to $t^{1/2}$ and one proportional to t [13]. The former soon tapers off while the latter remains practically unchanged. Another transient effect occurs at the end of the experiment when the steadily progressing concentration fronts nearly meet each other in the center of the film if the liquid enters the film from both surfaces. According to Hopfenberg et al. [8, 9], the specific weight gain slightly increases in the case of propagation of *n*-pentane into glassy polystyrene just before the diffusion process is completed. Such an effect finds a simple explanation in the superposition of the concentration tails in front of the concentration discontinuities as they approach the center plane of the film. Hence the concentration at each point between the advancing fronts increases faster than formerly when the fronts were farther apart. As a consequence the critical concentration for the transformation from glass to gel is reached earlier. This shows up in an acceleration of specific weight gain at the end of type II diffusion.

The diffusion equation and the boundary conditions do not impose any limitation on v and hence do not determine the velocity of profile propagation. The velocity must be connected with some independent material property. It seems to be a good suggestion that the increase of concentration of the penetrant produces by the ensuing membrane swelling a sufficiently high stress on the polymer network for the rupture or partial disentanglement of most strained chains. But since the chain rupture or the pulling out of chains is not an instantaneous process an effect of this type sufficiently large to permit a substantial swelling is only achieved if the stress persists for a sufficiently long time. This condition determines the propagation velocity of the concentration profile. If the condition cannot be met the transport of permeant proceeds in the usual way as type I diffusion, i.e., without a discontinuous concentration front and with a weight increase which is for a long while proportional to the square root of time.

2. Mathematical Description of Type II Diffusion

All the theoretical work up till now is purely descriptive without any serious attempt of explanation. Peterlin [13, 14] based his description on the diffusion and sorbate concentration dependence on time in front of a sorption discontinuity, i.e., a jump from c^* to c_0, moving through the sample at constant velocity v. In this area the Fickian diffusion equation reads [13]

$$\frac{\partial}{\partial x'}\left(D\frac{\partial c}{\partial x'} + vc\right) = \frac{\partial c}{\partial t} \tag{1}$$

with the diffusion current

$$j' = -D\frac{\partial c}{\partial x'} - vc. \tag{2}$$

Here $x' = x - vt$, D is the constant diffusion coefficient, and c^* the maximum concentration of liquid in the glass beyond which a discontinuous transformation to a gel with concentration c_0 and so high diffusivity takes place that practically no driving gradient is needed for the supply of liquid to the proceeding discontinuity front. The point x corresponding to a constant x' moves with the constant velocity v to larger x as does the concentration discontinuity. The Fickian formulation with the current proportional to the negative gradient of concentration instead of that of chemical potential is fully legitimate because the sorption coefficient is assumed constant although much smaller in front than behind the concentration discontinuity.

Behind the discontinuity the sorbate concentration is practically constant (c_0) and hence the current j' in the x',t frame equal to zero. In the laboratory system x,t the diffusion current j is by vc larger than j'. Hence it turns out to be $-D\,\partial c/\partial x$ in front of discontinuity and vc_0 behind it. Exactly speaking the very large value of D in the swollen region permits even a higher value of current than vc_0 in order to supply the liquid needed for the gradual establishment of the steady state concentration tail in front of discontinuity.

From these equations one obtains the weight gain per unit cross section of the film as function of time

$$W = c^*(2D/\pi)^{1/2}t^{1/2} + c_0vt \qquad v^2t/4D \to 0 \tag{3}$$

for small t and

$$W = c^*D/v + c_0vt \qquad v^2t/4D \to \infty \tag{4}$$

for large t after the concentration profile in front of the discontinuity has reached its stationary value. The concentration is measured in g of sorbate per cm^3 of sorbent.

The first term describes the effect of Fickian diffusion with constant diffusion coefficient D in front of the discontinuity which after the initial proportionality to $t^{1/2}$ *reaches the constant value* c^*D/v. The second term describes the weight gain in the highly swollen region behind the discontinuity proportional to the uniform increase of the volume of the swollen region as a consequence of constant velocity v of the profile propagation. In these expressions one assumed that the diffusivity in the gel is so much higher than in the glass that there practically no measurable gradient is needed for the transport of the liquid. A rather similar approach was used by Crank [22] in his description of different cases of diffusion in solids.

In the initial state the coexistence of the square root and linear term in time according to eq (3) yields over appreciable time intervals a constant power m relationship between weight gain and time, $W = Bt^m$, as can be seen from figure 1. where log W is plotted versus log t. At small t one has the square root, $m = 0.5$, and at high t the linear, $m = 1$, dependence. A rather constant m, i.e., a rather constant slope, applies to intervals extending over almost two decades of time. One can guess that within experimental errors such a theoretical prediction may sufficiently well fit the power law of weight gain observed in some cases of unconventional sorption [7].

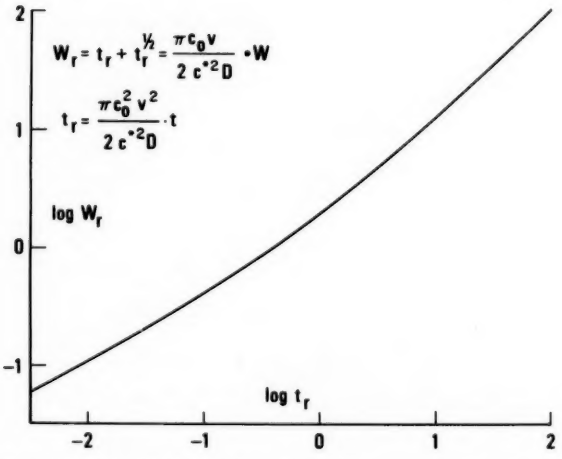

FIGURE 1. *Bilogarithmic plot of weight gain* W *over time* t *according to* eq (3).

There is no limitation about v in eqs 1 to 4 although the time dependence of the concentrations profile in front of the concentration discontinuity [14] and the asymptotic steady state value c^*D/v depend on v. The dimensionless time parameter $a = (v^2t/4D)^{1/2}$ increases and the total equilibrium sorption c^*D/v in that region decreases with increasing v. The constant rate progression of the concentration discontinuity yielding the linear weight gain according to eqs (3) and (4) characteristic for type II diffusion hence is a distinct possibility compatible with the classical diffusion equation as long as the supply of the sorbate through the highly swollen section of the film is sufficiently high. This flux has to fill continuously with the solvent a volume increasing in depth by v per second in spite of the steadily increasing length of the supply route from the outer surface of the film to the steadily progressing discontinuity. In all practical cases that requires that the diffusion coefficient of the gel (D_2) is some orders of magnitude higher than in the not swollen glass (D_1). In the ideal case of an infinite extension of the film in the direction perpendicular to the front this condition amounts to an infinite value of D_2.

One concludes that the type II diffusion can be sufficiently well approximated on the basis of the classical diffusion equation by the limiting case of constant rate propagation of a concentration discontinuity. The very beginning ($t = 4Da^2/v^2$ with $a \to 0$) with the weight gain proportional to $t^{1/2}$ may be over in such a short time that it is practically unobservable. After that a linear increase of weight gain with time is established. In a sample with a very large distance between the border where the liquid enters and the concentration discontinuity the weight gain must show some incipient drop as soon as the influence of diffusion time through the swollen region becomes preceptible on the solvent supply at the concentration discontinuity. This does not occur in the above-quoted experiments by Hopfenberg et al. [7–9], where for a polystyrene (PS) film of 38μm thickness the diffusion from both surfaces of the film was completed between 12 min and 400 hours, dependent on temperature, activity of n-pentane vapor, and on polymer orientation. The velocity of concentration front propagation in the same cases varied between 1.3×10^{-9} (cast annealed PS, 25 °C, n-pentane gas activity 0.63) and 2.65×10^{-6} cm.s^{-1} (biaxially oriented PS, 35 °C, activity 1). Since the maximum liquid concentration was about 13 g per 100 g of polymer one needs indeed such an extremely small gradient for steady supply of so small an amount of liquid increase per unit time that its decrease would be hard to detect.

Hence the contrast between types I and II diffusion is one of the consequences of the extreme nonideality of transport properties in the latter case. A discontinuous substantial increase of sorption and diffusion takes place after a limiting concentration c^* of sorbent is attained in the film by more or less conventional type I diffusion. The constant rate propagation of the concentration discontinuity represents a pseudostationary state of diffusion in such a nonideal medium. The velocity v, however, is not derivable from the diffusion equation and boundary conditions and must be determined by some other mechanism of solvent-polymer interaction.

The non-ideality of the medium, i.e., an almost discontinuous increase of diffusion coefficient as soon as the penetrant concentration reaches a critical value c^* was already suggested by King [1] for explanation of the unconventional diffusion of alcohol vapor into wool and keratine. His results cannot be directly compared with eqs (1 to 4) because he uses an expansion of D in powers of c which makes the results more complicated, dependent on the coefficients of the power expansion. But he actually estimates the effect of rapidly increasing D with concentration yielding a steep concentration front propagating with almost constant velocity into the medium.

Frisch et al. [15, 16] assume that the diffusion current density is caused by the gradient of chemical potential and the divergence of the partial stress tensor of the penetrant

$$j = -Bc[\partial\mu/\partial x - (1/c)\partial S_{xx}/\partial x] \qquad (5)$$

if one puts

$$S_{xx} = s\int_0^x c(x',t)dx' \tag{6}$$

i.e., if one makes the assumption that the partial stress tensor S of the penetrant at any location and time is proportional to the total uptake of the penetrant up to that location and time. With a constant proportionality factor s one obtains from

$$\partial S_{xx}/\partial x = sc(x,t) \tag{7}$$

a current

$$\begin{aligned} j &= -Bc\partial\mu/\partial x + Bsc = -Bc(x,t)(\partial\mu/\partial x - s) \\ &= -Bc\partial\mu/\partial x + vc. \end{aligned} \tag{8}$$

With constant D and $\mu = RT\ \ell n\ c$ one obtains

$$\begin{aligned} c(x,t) = (c_0/2)\{&\exp(xv/D)\mathrm{erfc}[(x + vt)/2(Dt)^{1/2}] \\ &+ \mathrm{erfc}[(x - vt)/2(Dt)^{1/2}]\} \end{aligned} \tag{8a}$$

for diffusion into the half space with $x \geq 0$. According to this solution the steepness of concentration "discontinuity" at $c_0/2$ soon tapers off in exactly the same manner as in conventional diffusion. The point with $c = c_0/2$ proceeds into the medium at almost constant velocity v. Points with smaller c move faster and those with higher c move more slowly so that the maximum slope, located at $c = c_0/2$, gradually diminishes and finally becomes zero. The weight gain W/c_0 is initially proportional to $t^{1/2}$. With increasing time it approaches strict proportionality to t. The assymptote goes exactly through the origin of W,t coordinate system.

The "theory" depends on the "natural" assumption formulated in eq (6) that the partial stress tensor of the liquid S_{xx} in the highly swollen section of the sample linearly increases with x and hence goes to infinity in an infinite medium. Since to our knowledge no such stress exists one gets the impression that all the naturalness of the above assumption is rather pragmatic based on the success, i.e., on the yielding of a constant term in eq (5) one wants to have in order to fit the experimental data. There is no correlation between any property of the polymer or penetrant and the coefficient s which together with B determines the velocity of propagation $v = Bs$ of the concentration front. Hence the derivation of the authors, the introduction of the new term depending on the stress gradient, and the choice of stress which yields the constant component Bsc of the current can be labelled mathematical description but not explanation of the type II diffusion.

The difference between the solution of Frisch et al. and that of Peterlin is in the shape of concentration profile and in limiting weight gain. According to the former concept the shape of concentration front gets gradually less steep and finally becomes perfectly flat as at the end of conventional diffusion. In the latter formulation it rather soon reaches a finite shape which after that does not change any more. The asymptotic weight gain is strictly proportional to time in the former case and still contains a square root term in time in the latter case.

None of the two concepts yields a front propagation containing linear and square root terms in time. Both yield a constant or almost constant velocity of propagation of concentration front if this is taken as the point of fastest concentration increase, i.e., at $c = c_0/2$ (model of Frisch), or at the point where the concentration jumps from c^* to c_0 (model of Peterlin). Hence the experimental data of Kwei and Zupko [6] yielding such a combination of linear and square root of time terms cannot be described by any of the two concepts.

A further difficulty for the model of Frisch et al. shows up in desorption experiments [4, 8] which correspond to purely Fickian diffusion. Peterlin's formulation is not affected because it only describes the diffusion process if a concentration front moves with a constant velocity through the medium. If there is none the diffusion is conventional. Frisch's formulation, however, starts with a large S_{xx} which at completed sorption increases linearly from 0 at the first boundary, $x = 0$, to sc_0d at the other boundary, $x = d$. The gradient $\partial S_{xx}/\partial x$ would simply continue to pump the liquid through the film at the same rate v and in the same direction as during the preceding type II diffusion. There is no end to the process. The way out of this impass is the simultaneous consideration of the identical type II diffusion pumping the liquid at the same rate v and in opposite direction from the other boundary as a consequence of $S_{xx}(d)$ starting with value 0 at $x = d$ and increasing to sc_0d at $x = 0$. At the end of sorption the sum of $S_{xx}(0)$and $S_{xx}(d)$ is constant, sc_0d, throughout the sample. Its gradient disappears and so does the current corresponding to type II diffusion. This happy end effect has however the disadvantage that it yields the same negative result for all previous and later times. The sum of both S_{xx} is a constant as far as x is concerned although it increases with time during sorption and decreases during desorption as does the total uptake of penetrant. Hence it cannot generate any steady flow as observed in type II diffusion. The modification of S_{xx} in eqs (5) and (6) which explains the end of sorption and the Fickian type of desorption process excludes the explanation of the unconventional sorption the equations were formulated for.

The formulation according to eq (5) leads to another quite unexpected consequence. The coefficient s in the stress tensor, eq (6), which multiplied by B yields the velocity of concentration front propagation seems to be a constant of the penetrant-polymer system and hence independent of c. All the concentration dependence is in the factor B which affects equally the type I (the first term) and type II (the second term) diffusion. Hence v is proportional to the conventional diffusion coefficient. The proportionality factor s depends on the penetrant-polymer combination but not on concentration. That leads to the peculiar consequence that the normal type of diffusion is not the classical "Fickian" diffusion but the type II diffusion.

In contrast to that the experiments by Hopfenberg et al. [7, 8] on the dependence of type II diffusion on vapor activity convincingly show a rapid decrease of v with decreasing activity a and the complete cessation of such diffusion below a limiting activity $a^* \sim 0.3$. Hence s cannot be a constant but must be a function of a-a^* vanishing at a^* and for any a below a^*. Although this dependence is the crucial point of explanation of type II diffusion it was never attempted to be derived from material properties.

Moreover the presence of the term B_s in diffusion equation completely changes the concentration increase in time ahead of the concentration front as soon as the local concentration c surpasses the value c^* corresponding to the limiting activity a^*. This consequence may be less disturbing if one assumes that ahead of concentration front c is always smaller than c^* and behind it larger than or equal to c^*. But it still may cause

some problems in the front itself if the concentration does not jump discontinuously from $c_1 = c^*$ ahead of the front to c_2 behind the front. The variation of propagation velocity with c must create a special type of front profile which was never yet analyzed from this point of view. Without any more detailed analysis one can only guess that any concentration increase in the front will become steeper until it will be almost discontinuous.

3. Constant Rate Propagation of Concentration Profile

On the basis of the general diffusion equation with S and D dependent on chemical potential one can easily formulate the conditions for a constant rate propagation of a concentration profile

$$c(x,t) = C(x - vt) = C(x'). \tag{9}$$

The coordinate system x' moves to the right with the same velocity v as the concentration profile. Hence in this system the concentration C is constant at each x' and the current density $j' = 0$. With these assumptions the solution of the diffusion problem is truly conventional without a need for any additional more or less arbitrary term in the diffusion equation.

According to the thermodynamics of irreversible processes the diffusion current density in the laboratory fixed system x is proportional to the chemical potential gradient of the diffusant

$$j = -(c/f)\,\partial\mu/\partial x = -DS\,\partial p/\partial x = -P\,\partial p/\partial x \tag{10}$$

where f is the frictional resistance yielding the diffusion coefficient $D = RT/f$. The chemical potential μ can be expressed as function of vapor pressure $p(x,t)$ in equilibrium with the sorbate at position x at time t

$$\mu = RT\,\ell\mathrm{n}\,p(x,t) + \mu^0 \tag{11}$$

The constant μ^0 is still a function of T and of any other parameter independent of p and x. The concentration c is a product of sorption $S(p)$ and pressure. The conservation of mass yields the concentration variation with time

$$\partial c/\partial t = \partial(Sp)/\partial t = -\partial j/\partial x = \partial(P\partial p/\partial x)/\partial x. \tag{12}$$

In this well-known classical one dimensional diffusion equation the sorption S, the diffusion coefficient D and permeability P are functions of p or concentration c and not constants as assumed in the ideal Fickian case. But they are independent of time and location. The membrane is homogenous and does not change although at each point x its swelling and diffusivity vary drastically with time. There is also no temperature effect considered.

The drastic change of sorption in the transition from glass to gel implies quite a substantial swelling of the polymer causing eventually the formation of macroscopic cracks as observed in the earlier experiments [2, 3]. For simplicity sake, these dimensional changes are not at all considered in the above formulation of the diffusion equation. Such an omission affects the numerical results but not the functional properties of the solutions as for instance the existence of the steady state solution and the conditions for a constant velocity of profile propagation.

The thermodynamic equilibrium correlation between concentration and vapor pressure permits to express the concentration profile according to eq (9) as a profile of vapor pressure proceeding with a constant velocity v

$$p(x,t) = q(x - vt) \tag{13}$$

because the material property $S(p)$ is independent of x and t. Hence the values $p(x,t)$ can be expressed as functions of a single variable $x' = x - vt$. That means that the partial derivatives in eq (10) can be expressed as total derivatives by x'. In such a case the differentiation on time is equivalent to differentiation on location

$$\partial q/\partial t = -v\,dq/dx' \tag{14}$$

which with constant v transforms eq (10) into the straightforwardly integrable total differential equation

$$\frac{d}{dx'}\left(-P\frac{dq}{dx'} - vSq\right) = \frac{dj'}{dx'} = 0. \tag{15}$$

This formulation actually means that there is neither a current nor a change of concentration since the coordinate system x' travels with the same velocity v as the concentration or vapor pressure profile. This yields

$$v dx' = -D(q)\,dq/q \tag{16}$$

with the solution

$$-vx' = \int_{q(0)}^{q(x')} D(q)d\ln q. \tag{17}$$

The boundary condition $q = p(+\infty) = 0$ at $x' = +\infty$ is met automatically with a finite, not vanishing D at $q = 0$. The finite $q = p_0$ at $x' = -\infty$ demands an infinite value of $D(p_0)$. Equation (17) is completely general not imposing any condition on the choice and continuity of D beyond those mentioned in connection with the boundary condition, i.e., at $x' = -\infty$. Note that the value of S and its dependence on p or c do not enter eqs (16) and (17) explicitely.

One sees that in an infinite medium the diffusion eq (10) permits solutions with a constant concentration or thermodynamically equivalent pressure profile moving with a constant velocity v if only the diffusion coefficient goes to infinity at the maximum pressure p_0 applied at the infinitely distant negative boundary $x' = -\infty$ of the medium. The profile $q(x')$ depends on $D(p)$ and v as shown in eq (17). For a very simple dependence of D on p

$$D = A + Bp_0/(p_0 - p) \tag{18}$$

yielding $D_0 = A + B$ at $p = 0$ and $D = \infty$ at $p = p_0$, i.e., at the maximum pressure of the sorbate at the infinitely distant film boundary, $x' = -\infty$, one obtains the profile

$$\ell\mathrm{n}\,(q(x')/p_0) - (B/D_0)\,\ell\mathrm{n}\,(1 - q(x')/p_0) = -vx'/D_0 + \text{const.} \tag{19}$$

shown in figure 2 as function of $vx'/D_0 = y$ for different values of B/D_0. If the constant is equaled to zero one only displaces the $q(x')/p_0$ curves horizontally. This does not affect their shape which is our primary interest. The larger v and the smaller D_0 the steeper the true profile if plotted against x' (figure 3). The constant pressure profile q starts at high positive y with a long tail which only slightly differs from that calculated formerly [14] for a constant D_1, continues with a sharp rise of pressure and asymptotically approaches the limiting pressure p_0 at $y = -\infty$. The time independent concentration profile is obtained by multiplication of q by $S(p)$ which exhibits a large increase with p approaching p_0 if one wishes to describe the transition from a glass at $p = 0$ (S small) to a highly swollen gel with $c = c_0$ at $p = p_0$ (S large). Hence the concentration profile is expected to vary substantially faster than the pressure profile.

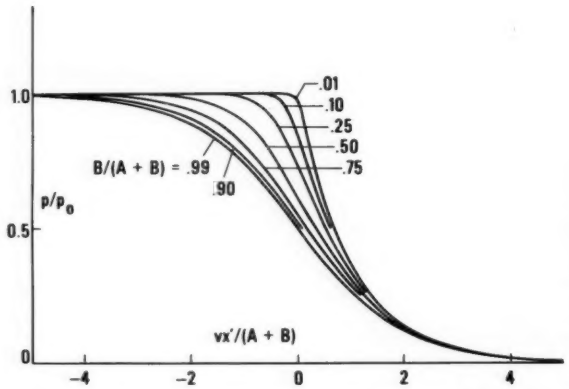

FIGURE 2. *Pressure profiles according to eq (19) moving to the right with constant velocity* v *for different values of* B/(A + B) *as functions of* vx'/(A + B).
The smaller the increase of diffusivity with p as measured by $B/(A + B)$ the steeper is the profile in this representation.

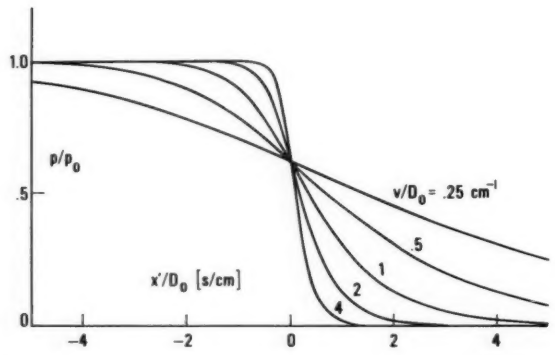

FIGURE 3. *Pressure profiles according to eq (19) moving to the right with constant velocity* v (*parameter of the curves*) *for* B/(A + B) = 0.5 *as functions of* $x'/(A + B)\ 1 = x'/D_0$.

The shape of the profile can be varied as freely as the dependence of D and S on p. In particular, one can choose constant D and S in the glass and rubber with a discontinuity at p^* thus producing a change of slope of P and a step-like concentration profile at p^* (figure 4) as already partially treated by Crank [22]. Hence the case treated formerly [13, 14] with two concentration independent diffusion constants, $D_1 \ll D_2$, is contained in the present more general treatment.

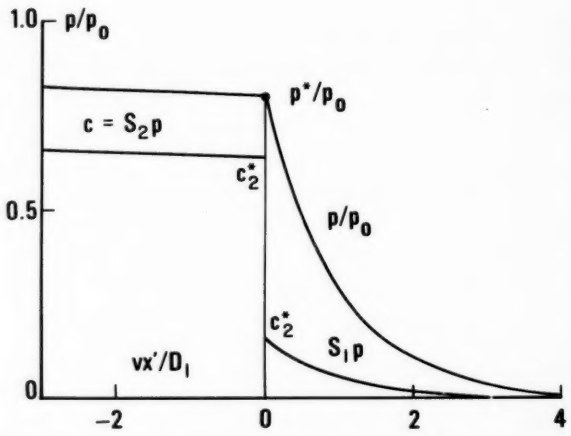

FIGURE 4. *Pressure and concentration profile moving to the right with constant velocity* v *as functions of* vx'/D *for a discontinuous change of diffusion constant from* D_1 *to* $D_2 = 100\ D_1$ *and of sorption from* S_1 *to* $S_2 = 4S_1$ *at* $p = p^* = 0.8\ p_0$.
Note the continuity of p and the discontinuity of c at the boundary between glass and gel. The constancy of D and S in the glass (to the right) and in the gel (to the left) yields $p = p_0$ at a finite value $x'_0 = D/v$ instead of at $x'_0 = -\infty$ as postulated by the steady state solution (eqs (9) and (13)). As a consequence the propagation velocity v has to slow down as soon as $x'_0 - vt$ approaches and reaches the outer boundary of the medium by which the penetrant enters because from that moment on the diffusion through the gel is unable to supply the necessary amount of diffusant. Note that one has assumed that up to this time the equilibrium pressure at the entrance to the medium rises continuously and at a constant rate from p^* to p_0.

The boundary between unswollen and swollen region moves with the constant velocity v. The value of v is still completely free and is not at all determined by the diffusion equation or the boundary conditions. From the uniform translation of the concentration profile one derives the weight gain

$$w = j(-\infty) \cdot t = vSp_0t = vc_0t \qquad (20)$$

proportional to time in perfect agreement with the observations of the steady state of type II diffusion.

One hence has the rather unexpected result that the same mathematical formalism (eq (12)) yields both types of diffusion: Type I for constant or approximately constant and Type II for extremely pressure or concentration dependent D, S, and P. Actually the diffusion constant must be infinite for $p = p_0$ in order to satisfy the boundary condition at $x' = -\infty$. From a pure mathematical point of view the values of S are irrelevant and can be chosen at will. Type I diffusion is a very special case confined to ideally linear systems with constant D and S. Type II diffusion is more or less close to the diffusion in actual polymer-sorbent systems with D and S rapidly increasing with p, after the initial transient has abated and before the great transport length from the boundary to the moving front starts to reduce perceptibly the velocity of front propagation.

The diffusion coefficient D of the penetrant or permeability P of an actual medium certainly may become very large but can never assume infinite values. In going from a glass to a swollen rubber or gel the increase in D may be many orders of magnitude, from 10^{-12} to 10^{-6} cm^2/s, so that the steady state

solution with $D(p_0)/D(o) \sim \infty$ is a very good asymptotic approximation of the actual material transport. But the finite maximum value of D imposes a reduction of the permeant supply with increasing transport length l_{tr} because the pressure gradient at the outer boundary of the sample, $(dp/dx)_{x=0} \sim (p_0 - p(\ell_{tr}))/\ell_t$, decreases with this length. That means a slow but steady decrease of propagation velocity of the concentration profile with increasing distance of the profile from the outer boundary of the sample. In a very thick sample the initially constant velocity propagation of the profile and hence the linear increase of weight gain with time are expected to show an observable decrease. But since the most precise measurements were made on extremely thin films with total liquid path less than 0.1 mm one was never faced with this limitation.

A very instructive general picture of the effects caused by the finite although very large diffusion coefficient D_2 in the highly swollen material can be derived from the very schematic figure 4. It is based on a constant D_2, independent of concentration which varies from c^*_2 at the concentration front to the maximum c_0 in thermodynamic equilibrium with the penetrant pressure p_0 at the outer boundary of the sample. In order to simplify the matter one assumes in that which follows that the profile shown in figure 4 is established immediately, at time $t = 0$, at the outer boundary, $x = 0$, so that the initial transient effects can be completely neglected. At $t = 0$ one hence has $x' = x - vt = 0$.

One first notices that the concentration $c(0)$ at the outer boundary has the initial value c^*_2 which steadily increases with time up to the maximum value c_0. If one assumes that during this time the concentration front moves with a constant velocity v one deduces a slight increase of current density and a more than linear increase of weight gain with time

$$\begin{aligned} j &= vc^*_2/(1 - v^2t/D_2) \\ W &= -(c^*_2\, D_2/v)\, \ell\mathrm{n}\, (1 - v^2t/D_2) \qquad (21) \\ &= c^*_2\, vt\, (1 + v^2t/2D_2 + \cdots) \\ c(0) &= c^*_2/(1 - v^2t/D_2). \end{aligned}$$

The parameter v^2t/D_2 remains small during the whole experiment. Its maximum value is reached at the moment when the front hits the opposite boundary of the sample or meets the front proceeding from this boundary. In the latter case one derives from film thickness d and $t_{max} = d/2v$ the maximum value of this parameter

$$(v^2t/D_2)_{max} = d^2/4D_2t_{max}. \qquad (22)$$

In the diffusion of n-pentane into cast annealed PS film [8] the film thickness was 38 μm = 3.8×10^{-3} cm, $t_{max} = 60$ hours = 2.16×10^5s for $p_0 = 550$ mmHg at 30 °C. From these data one obtains maximum values for the parameter between 1.7×10^{-4} and 1.7×10^{-2} if D_2 varies between 10^{-7} and 10^{-9} cm^{2}s^{-1}. In biaxially oriented film at penetrant activity 1 and $T = 35$ °C the values are up to 300 times higher so that a sufficiently small value of the parameter is only obtainable with the higher diffusion coefficient which is indeed more probable than the lower limit. One can be rather certain that in most cases the parameter is so small that the current j is practically constant, the weight increase W almost linear with time, and a very small difference $c(0) - c^*_2$ required for a constant supply of liquid to the progressing concentration front. The small value of the parameter also tells that the ideal case, eqs (9) through (20), is a good approximation of the actual polymer-penetrant systems displaying type II diffusion.

But the finite increase in time of penetrant concentration at the sample boundary in contact with the liquid or gas seems to be an important feature of type II diffusion. It is a consequence of the fact that the polymer glass simply cannot expand instantaneously to such an extent that the equilibrium concentration of penetrant could be accommodated. Since the polymer is quite inhomogeneous on molecular scale it exhibits a wide variation of penetrability in very small regions. The more penetrable areas expand substantially more and faster than the less penetrable sections. The forces exerted by the penetrant on taut molecules connecting the latter sections across the former regions will either rupture these chains or pull them out slowly. Both effects require a finite time. As a consequence of such enforced polymer expansion the sample crazes and even cracks. One gets convinced that just this relaxation of the specimen under the osmotic pressure of the penetrant determines the velocity of propagation of the concentration front which is independent of D and of any other parameter of the diffusion equation.

In a more realistic approach the inability of the polymer to expand sufficiently for the accommodation of the equilibrium amount of penetrant most likely starts at a substantially smaller concentration than c^*_2, let us say c^*_1. This means that at low activity with $c(0) < c^*_1$ the sorption and diffusion are conventional without any concentration front propagating at constant velocity through the glass. If, however, the activity is so high that $c(0) > c^*_1$ a finite time is needed for proper polymer expansion thus creating the circumstances observed with type II diffusion. The higher the driving force $c(0) - c^*_1$ as compared with c^*_1 and the higher the volume change with the linear expansion of the polymer the more rapidly the glass adjusts to the space requirements of the penetrant, i.e., the higher the velocity of concentration front propagation in perfect agreement with observations.

On the other hand, the steady state profile cannot be established instantaneously. Even if a constant propagation rate is imposed it takes a certain time before the pressure or concentration distribution in the frontal tail assumes time independent values. This was explicitly demonstrated for a concentration discontinuity moving with a constant velocity [14]. The result can be generalized for any profile. In first approximation the weight gain in this transient is proportional to the square root of time. The duration of a substantial contribution of the transient can be unobservably short so that the weight gain does not exhibit a significant initial component proportional to the square root of time but instead is directly proportional to time.

4. Conclusions

The steady state solution of the simple diffusion equation with the constant rate of propagation of the fixed concentration profile according to eq (9) is a good approximation of the pseudo-stationary situation of Type II diffusion. Its range is between the usual initial transient with concentration and weight gain dependence on $t^{1/2}$ and the final stage with the weight gain less than proportional to t because at fixed maximum values of D and P the sorbate has to be transported

to the concentration front through a steadily increasing depth of the fully swollen film. The large ratio between D_{max} and D_{min} and the small maximum linear extension $\ell_{tr,\,max}$ of films through which the material transport takes place may make very short the duration and rather difficult the observation of the initial and final stages. Therefore, as a rule, the scene is dominated by the pseudo-stationary type II diffusion as formulated in eqs (9) and (19). In the case of thin film with the liquid entering from both plane surfaces the superposition of concentration tails in front of the propagating concentration discontinuity may overcompensate the latter effect and yield a final increase of weight gain rate.

But one also sees that type II diffusion is nothing exceptional requesting any change or modification of diffusion equation. It is a simple consequence of a very rapid change of P, i.e., of S and D with sorbate activity. The increase in S is only needed for a rapid increase of penetrant mobility. There is no need for introduction of a new mechanism although a new name may have some practical use. The old Fickian formulation in concentration terms is of course rather inadequate for the description of such less conventional effects because it is applicable only to perfectly ideal material with activity independent sorption. But this limitation was already so thoroughly demonstrated [23] that it has no sense to reopen the subject again.

An important result of this investigation is also the confirmation of the very early finding [13] that the velocity v of propagation of concentration discontinuity is not in the slightest manner determined or limited by the diffusion equation and the dependence of D on concentration. Experiments, however, very clearly show a drastic increase of v with activity of the permeant and temperature of experiment. There is also a substantial dependence of v on thermodynamic properties of penetrant and polymer and on mechanical and thermal history of the polymer. Hence one will have to consider the molecular effects connected with swelling much more thoroughly than it was done up till now in order to be able to find the connection between the velocity and the mechanical and thermodynamic properties of the penetrant-polymer system. A next paper will try to discuss some possible approaches to such a molecular theory of unconventional diffusion.

References

[1] King, G., Trans. Farad. Soc. **41,** 325 (1945).
[1a] Kishimoto, A., Fujita, H., Odani, H., Kurata, M., and Tamura, M., J. Phys. Chem. **64,** 594 (1960).
[2] Alfrey, T., Jr., Chem. Eng. News **43,** 64 (Oct. 11, 1965).
[3] Alfrey, T., Jr., Gurnee, E. F., and Lloyd, W. G. J., Polymer Sci. C. **12,** 249 (1966).
[4] Michaels, A. S., Bixler, H. J., and Hopfenberg, H. B., J. Appl. Polymer Sci. **12,** 991 (1968).
[5] Bray, J. C., and Hopfenberg, H. B., J. Polymer Sci. B, **7,** 679 (1969).
[6] Kwei, T. K., and Zupko, H. M., J. Polymer Sci. A-2, **7,** 867 (1969).
[7] Hopfenberg, H. B., Holley, R. H., and Stannett, V., Polymer Eng. & Sci. **9,** 242 (1969).
[8] Holley, R. H., Hopfenberg, H. B., and Stannett, V., Polymer Eng. Sci. **10,** 376 (1970).
[9] Baird, B. R., Hopfenberg, H. B., and Stannett, V., Polymer Eng. Sci. **11,** 274 (1971).
[10] Kwei, T. K., Wang, T. T., and Zupko, H. M., Macromol. **5,** 645 (1972).
[11] Jaques, C. H. M., Hopfenberg, H. B., and Stannett, V., Polymer Eng. Sci. **13,**81 (1973).
[12] Jaques, C. H. M., Hopfenberg, H. B., and Stannett, V., J. Appl. Polymer Sci. **18,** 223 (1974).
[13] Peterlin, A., J. Polymer Sci. **B3,** 1083 (1965).
[14] Peterlin, A., Makromol. Chem. 124, 136 (1969).
[15] Frisch, H. L., Wang, T. T., and Kwei, T. K., J. Polymer Sci. A-2, **7,** 879 (1969).
[16] Wang, T. T., Kwei, T. K., and Frisch, H. L., J. Polymer Sci. A-2, **7,** 2019 (1969).
[17] Hopfenberg, H. B., and Frisch, H. L., J. Polymer Sci. **B7,** 405 (1969).
[18] Hopfenberg, H. B. "Membrane Science and Technology", Ed. by J. E. Flinn (Plenum Press 1970), p. 16.
[19] Park, G. S., Diffusion in Polymers, Ed. by J. Crank and G. S. Park (Academic Press, New York 1968), Chapter 5.
[20] Wang, T. T., and Kwei, T. K., Macromol. **6,** 919 (1973).
[21] Kwei, T. K., and Wang, T. T., "Permeability of Plastic Films and Coatings", Ed. by H. B. Hopfenberg (Plenum Publ. Co., New York 1975), p. 63.
[22] Crank, J., Mathematics of Diffusion (Oxford Univ. Press, 1956), Chapter 7.
[23] Peterlin, A., Permeability of Plastic Films and Coatings, Ed. by H. B. Hopfenberg, (Plenum Publ. Co., New York 1974), p. 9.

(Paper 81A2&3-926)

JOURNAL OF RESEARCH of the National Bureau of Standards—A. Physics and Chemistry
Vol. 81A, Nos. 2 and 3, April–June 1977

Thermophysical Measurements on 90Ti-6Al-4V Alloy Above 1450 K Using a Transient (Subsecond) Technique*

A. Cezairliyan, J. L. McClure, and R. Taylor**

Institute for Materials Research, National Bureau of Standards, Washington, D.C. 20234

(March 5, 1977)

Simultaneous measurements are described of specific heat capacity, electrical resistivity and hemispherical total emittance of the ternary alloy 90Ti-Al-4V in the temperature range 1450 to 1900 K, and the melting point and and the radiance temperature at the melting point of the alloy by a subsecond duration transient technique. The results are expressed by the relations:

$$c_p = 1.3833 - 9.943 \times 10^{-4}T + 3.745 \times 10^{-7}T^2$$

$$\rho = 152.65 + 1.9304 \times 10^{-2}T - 3.9548 \times 10^{-6}T^2$$

where c_p is in $J \cdot g^{-1} \cdot K^{-1}$, ρ is in $\mu\Omega \cdot cm$, and T is in K. The value of the hemispherical total emittance is 0.39 in the range 1700 to 1900 K. The melting point and the radiance temperature at the melting point are 1943 and 1796 total emittance of the ternary alloy 90Ti-6A1-4V in the temperature range 1450 to 1900 K, and the melting point 0.395. Estimated inaccuracies of measured properties are: 3 percent for specific heat capacity, 1 percent for electrical resistivity, 5 percent for hemispherical total emittance and 8 K for melting point and radiance temperature at the melting point.

Key words: Electrical resistivity; heat capacity; high-speed measurements; high temperatures; melting; normal spectral emittance; radiance temperature; specific heat capacity; thermal radiation properties; thermodynamics; titanium alloy.

1. Introduction

In this paper, application of a transient technique to the measurement of selected thermophysical properties (specific heat capacity, electrical resistivity, hemispherical total emittance, melting point,[1] radiance temperature[2] at the melting point) of the alloy 90Ti-6Al-4V above 1450 K is described.

The method is based on rapid resistive self-heating of the specimen from room temperature to its melting point in less than one second by the passage of an electrical current pulse through it; and on measuring, with millisecond resolution, such experimental quantities as current through the specimen, potential drop across the specimen, and specimen temperature. Detailes regarding the construction and operation of the measurement system, the formulation of relations for properties, the methods of measuring experimental quantities, and other pertinent information are given in earlier publications [1, 2][3].

2. Measurements

2.1. Specimens

The measurements of specific heat capacity, electrical resistivity, hemispherical total emittance, and melting point were performed on four specimens in the form of tubes. The tubes were fabricated from rods by removing the center portion using an electro-erosion technique. The nominal dimensions of the specimens were: length: 76.2 mm; outside diameter, 6.3 mm; and wall thickness, 0.5 mm. A small rectangular hole (0.5 × 1 mm) fabricated in the wall at the middle of the specimen approximated blackbody conditions for optical temperature measurements. The outer surfaces of the specimens were polished to reduce heat loss due to thermal radiation.

The radiance temperature measurements at the melting point were performed on specimens in the form of strips fabricated from a plate. The nominal dimensions of the strips were: length, 51 mm; width, 4.7 mm, and thickness, 0.25 mm. Before the experiments, the surface of the specimens was treated using abrasive; three different grades of abrasive were used yielding three different surface roughnesses (ranging from approximately 0.4 to 0.9 μm RMS) for different specimens.

The specimen material in rod and plate form was furnished by the U. S. Air Force Materials Laboratory, Wright Patterson Air Force Base, Ohio, and comprised two different lots of material. Chemical analyses of the material which are listed in table 1, show slight differences in composition. The rod material, from which the tube-shape specimens were fabricated, was hot swaged and the structure was composed of primary alpha titanium together with some acicular alpha + retained beta. The plate material, from which strip-shape specimens were fabricated, showed evidence of an elongated grain structure comprising primary alpha and beta. Photomicrographs of the two structures are shown in figure 1.

* This work was supported in part by the U. S. Air Force Office of Scientific Research.
** Guest scientist from the University of Manchester Institute of Science and Technology, Manchester, United Kingdom.
[1] Alloys have a melting range instead of a melting point, however for convenience, in the present work the solidus point of the alloy is referred to as the melting point.
[2] Radiance temperature (sometimes referred to as brightness temperature) is the apparent temperature of the specimen surface as measured by the pyrometer.
[3] Figures in brackets indicate the literature references at the end of this paper.

TABLE 1. *Composition of the titanium alloy*[a]

Material Form	in wt. %			in ppm																			
	Ti	Al	V	B	Ca	Cr	Cu	Fe	Mg	Mn	Mo	Ni	Nb	Pb	Si	Sn	Ta	W	Zr	C	H	N	O
Rod	89.2	6.1	4.2	10	50	15	30	1500	50	30	150	15	—	50	300	300	100	50	30	220	80	120	1700
Plate	89.2	6.1	4.2	30	150	30	80	1500	30	60	80	30	100	15	80	80	100	15	30	390	30	90	1500

[a] Information was furnished by Dr. S. R. Lyon of the U. S. Air Force Materials Laboratory.

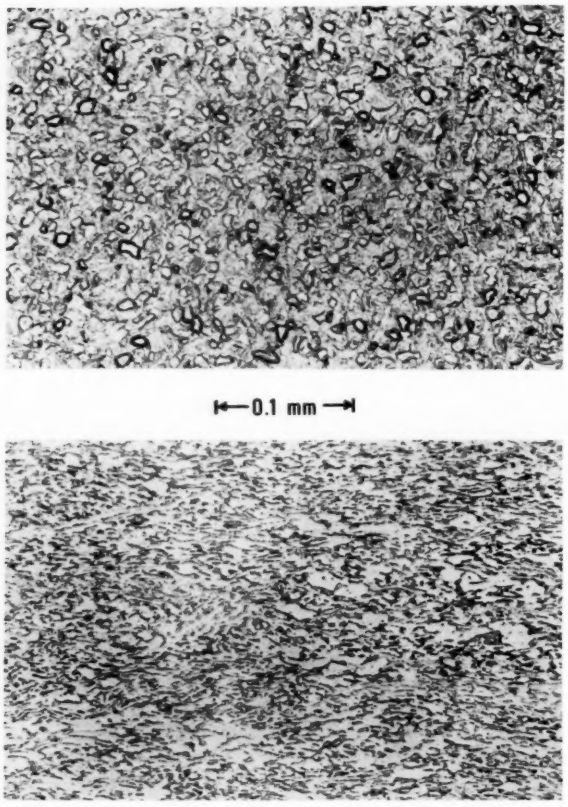

FIGURE 1. *Photomicrographs of titanium alloy specimens: tube-shape (upper photograph), and strip-shape (lower photograph), obtained before the experiments.*

At low temperatures and at vanadium contents greater than 3 percent, the equilibrium structure of this alloy comprises a mixture of the alpha and beta phases, although the actual structure will depend upon the heat treatment conditions. Above about 1300 K, the exact temperature depending upon composition, the alloy transforms to wholly beta. To ensure that the transformation was completed below 1450 K an additional experiment was performed in which the electrical resistance of a tube-shape specimen was measured during its heating from room temperature to the melting point (in 480 ms). The results, as shown in figure 2 indicate that the transformation occurred over a wide temperature range and that it was completed at about 1400 K, which is below the range of the results on thermophysical properties obtained in the present investigation.

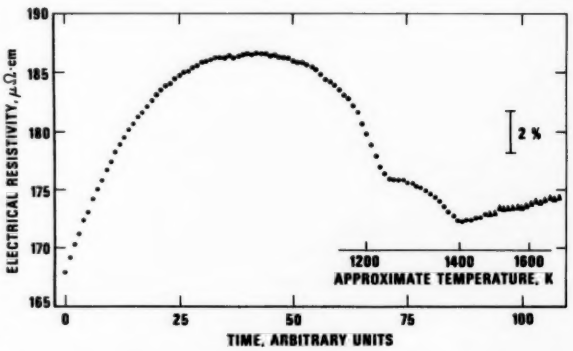

FIGURE 2. *Variation of the electrical resistivity of the titanium alloy (specimen-2) as a function of time during its heating from near room temperature to 1700 K (1 time unit = 5 ms).*

The plotted points are the results of two consecutive experiments (dots: near room temperature to 1450 K, and triangles: 1450 to 1700 K). An approximate temperature scale (non-linear) is shown for the latter part of the heating.

2.2. Procedure

All the experiments were performed with the specimen in an argon environment at atmospheric pressure. To optimize the operation of the high-speed pyrometer, the temperature interval (1450 to 1943 K) was divided into three ranges. This yielded a total of twelve experiments on four tube-shape specimens. Duration of the current pulses in experiments on tube-shape specimens ranged from 400 to 500 ms, with heating rates ranging from 2600 to 3800 $K \cdot s^{-1}$. Duration of the current pulses in experiments on strip-shape specimens ranged from 400 to 800 ms, with heating rates ranging from 1300 to 2200 $K \cdot s^{-1}$. Radiative heat loss from the tube-shape specimens was, in all cases, less than 2 percent at 1500 K and less than 5 percent at 1900 K of the input power.

3. Results

The thermophysical properties reported in this paper are based on the International Practical Temperature Scale of 1968 [3]. In all computations, the geometrical quantities are based on their room temperature (298 K) dimensions. The experimental results on specific heat capacity and electrical resistivity are represented by polynomial functions in temperature obtained by least squares approximation of the individual points. The final values on these properties, at 50 degree temperature intervals, computed using the functions are presented in table 2. The results obtained from individual experiments are given in the Appendix.

Specific Heat Capacity: Specific heat capacity was computed from data taken during the heating period. A correction

TABLE 2. *Specific heat capacity and electrical resistivity of the titanium alloy*

T (K)	c_p ($J \cdot g^{-1} \cdot K^{-1}$)	ρ ($\mu\Omega \cdot cm$)
1450	0.729	172.3
1500	.734	172.7
1550	.742	173.1
1600	.751	173.4
1650	.762	173.7
1700	.775	174.0
1750	.790	174.3
1800	.807	174.6
1850	.826	174.8
1900	.846	175.1

for power loss due to thermal radiation was made using the results on hemispherical total emittance. The function for specific heat capacity (standard deviation = 0.7%) that represents the results in the temperature range 1450 to 1900 K is:

$$c_p = 1.3833 - 9.943 \times 10^{-4}T + 3.745 \times 10^{-7}T^2 \quad (1)$$

where T is in K, and c_p is in $J \cdot g^{-1} \cdot K^{-1}$.

Electrical Resistivity: The electrical resistivity was determined from the same experiments that were used to calculate specific heat capacity. The function for electrical resistivity (standard deviation = 0.2%) that represents the results in the temperature range 1450 to 1900 K is:

$$\rho = 152.65 + 1.9304 \times 10^{-2}T - 3.9548 \times 10^{-6}T^2 \quad (2)$$

where T is in K and ρ is in $\mu\Omega \cdot cm$. In the computations of the specimen's cross-sectional area, which is needed for the computations of electrical resistivity, the density of the specimen was taken as $4.422\ g \cdot cm^{-3}$. The measurement, before the pulse experiments, of the electrical resistivity of the four tube-shape specimens at 293 K with a Kelvin bridge yielded an average value of 166.2 $\mu\Omega \cdot cm$ with an average absolute deviation of 0.1 percent and a maximum absolute deviation of 0.2 percent.

Hemispherical Total Emittance: Hemispherical total emittance was computed using data taken during both heating and initial free radiative cooling periods. The results of measurements in the temperature range 1700 to 1900 K did not show any significant variation in emittance. A value of 0.39 was obtained by averaging all the results (standard deviation = 2%).

Melting Point: Temperature of the tube-shape specimens was measured near and during the initial melting period until the specimen collapsed. A plateau in temperature indicated the transition from solid to liquid phase. Typical results for the variation of the specimen temperature during melting are shown in figure 3. The melting point for each specimen was obtained by averaging the temperature points on the plateau.

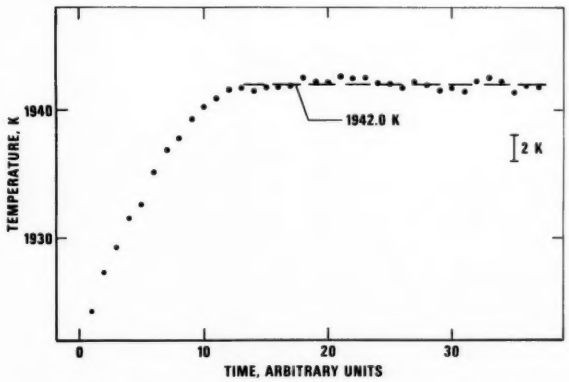

FIGURE 3. *Variation of the temperature of the titanium alloy (specimen-3) as a function of time near and at its melting point (1 time unit = 0.833 ms).*

The results are presented in table 3. The average melting point of the four specimens is 1942.6 K with an average absolute deviation from the mean of 0.4 K and a maximum absolute deviation of 0.8 K. It may be concluded that the melting point of the titanium alloy measured in this work is 1943 K.

TABLE 3. *Summary of measurements of the melting point of the titanium alloy*

Specimen number	Number of temperatures at plateau	Melting point (K)	Standard deviation (K)
1	10	1942.7	0.4
2	23	1943.5	.6
3	25	1942.0	.3
4	15	1942.4	.2

Radiance Temperature at the Melting Point: Radiance temperature measurements were performed on the strip-shape specimens at 653 nm which corresponds to the effective wavelength of the pyrometer's interference filter. The bandwidth of the filter was 10 nm. The circular area viewed by the pyrometer was 0.2 mm in diameter. Typical results for the variation of the specimen radiance temperature during melting are shown in figure 4. A single value for the radiance temperature at the plateau was obtained by averaging the temperatures at the plateau. The results are presented in table 4. The average radiance temperature at the melting point for the specimens is 1795.6 K with an average absolute deviation of 0.2 K and a maximum absolute deviation of 0.4 K. It may be concluded that the radiance temperature of the titanium alloy measured in this work is 1796 K.

Normal Spectral Emittance: The normal spectral emittance at the melting point was determined using the results of the radiance temperature (obtained from the measurements on strip-shape specimens) and the melting point (obtained from the measurements on tube-shape specimens). The results yield a value of 0.395 for the normal spectral emittance (at 653 nm) at the melting point of the alloy.

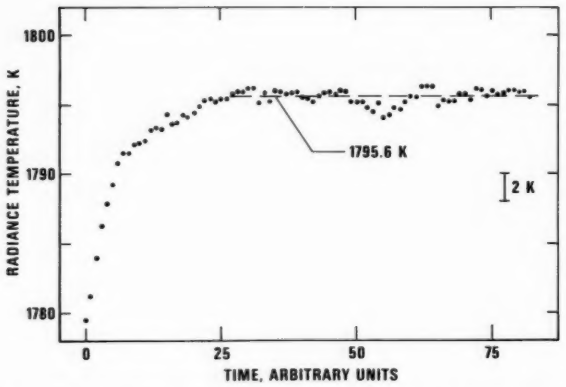

FIGURE 4. *Variation of the radiance temperature (at 653 nm) of the titanium alloy (specimen-2) as a function of time near and at its melting point (1 time unit = 0.833 ms).*

TABLE 4. *Summary of measurements of the radiance temperature (at 653 nm) of the titanium alloy during melting*

Specimen number	Typical surface Roughness (μm)	Number of temperatures at plateau	Radiance temperature (K)	Standard deviation (K)
1	0.4	27	1795.4	0.2
2	.5	56	1795.6	.5
3	.5	64	1795.2	.3
4	.4	36	1795.8	.4
5	.9	43	1795.9	.3

Estimate of Errors: The details of estimating errors in measured and computed quantities using the present measurement system are given in an earlier publication [2]. In this paper, the specific items were recomputed whenever the present conditions differed from those in the earlier publication. The results are summarized in table 5.

TABLE 5. *Estimate of errors*

Quantity	Imprecision[a]	Inaccuracy[b]
Specific heat capacity	0.7%	3%
Electrical resistivity	0.2%	1%
Hemispherical total emittance	2%	5%
Melting point	0.6 K	8 K
Radiance temperature (at melting point)	0.5 K	8 K
Normal spectral emittance (at melting point)	—	3%

[a] Imprecision refers to the standard deviation of a quantity as computed from the difference between measured value and that from the smooth function obtained by the least squares method.

[b] Inaccuracy refers to the estimated total error (random and systematic).

4. Discussion

Considering the wealth of literature data on 90Ti-6Al-4V there is remarkably little information on the physical properties of this alloy and data at temperatures above 1000 K does not appear to have been obtained. In figures 5 and 6 the smoothed values for specific heat capacity and electrical resistivity listed in table 2 are plotted together with the limited amount of low temperature data available in the literature. From figure 5, it can be seen that the specific heat capacity data of Ziegler and Mullins [4] may be reasonably extrapolated to join up with the present data.

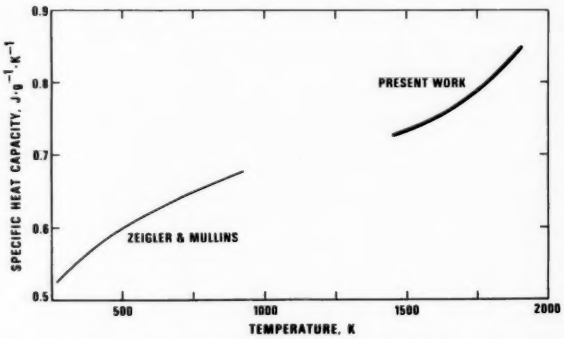

FIGURE 5. *Specific heat capacity of titanium alloy reported in the literature. The alloy used by Zeigler and Mullins [4] contained 5.9 percent Al and 3.9 percent V.*

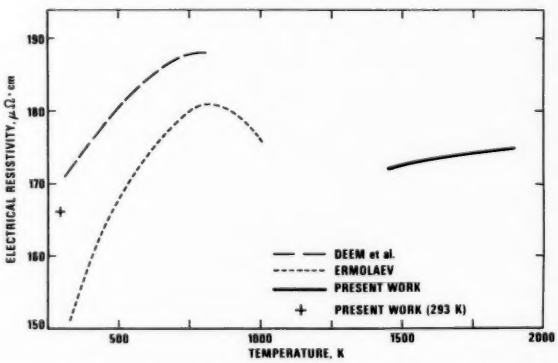

FIGURE 6. *Electrical resistivity of titanium alloy reported in the literature. The alloy used by Deem et al. [5] contained 6 percent Al and 4 percent V, while that used by Ermolaev [6] contained 5 percent Al and 4 percent V.*

The electrical resistivity data on 90Ti-6Al-4V reported by Deem et al. [5] covers the temperature range 310 to 810 K and shows evidence of a maximum around 800 K. Ermolaev [6] has measured the electrical resistivity of a titanium alloy containing 5 percent Al and 4 percent V up to 1000 K and his results are some 4 to 12 percent lower than the data of Deem et al. However, a definite maximum is observed around 800

K. These results, together with those of the present work, are presented in figure 6. The room temperature value obtained in the present work is about 2.5 percent below the value of Deem et al., but such a difference can be accounted for by variations in specimen structure. If figure 6 is inspected together with figure 2 then it is apparent that low temperature resistivity values follow the trend indicated by Deem et al. and Ermolaev, namely that resistivity increases to a maximum and then decreases. The data of the present work indicate that electrical resistivity decreases until 1250 K where the curve shows a kink but still decreases until 1400 K above which resistivity begins to increase steadily up to 1900 K. Above 1400 K, the resistivity results pertain to the beta phase. Below 1400 K however, a number of solid state reactions may be occurring, chief of which are the reactions whereby alpha prime decomposes to alpha + beta and, at high temperatures, alpha will decompose to beta. Additionally, beta is metastable at low temperatures and will itself decompose to alpha. Since these are kinetic processes affected by the heating rate, it is difficult to predict the behavior of this alloy unless further work is done involving the heating of alloys carefully heat treated to produce different structures.

No data have been found in the literature on the hemispherical total emittance of the alloy 90Ti-6Al-4V that correspond to the specimen conditions and the temperature range of the measurements of the present work. The value of the hemispherical total emittance for a similar alloy at the highest reported temperature (about 1200 K) in the literature [7] is 0.47 which corresponds to a specimen with a rough surface. This high value compared to 0.39 (the value of the present work) may be attributed primarily to the differences in the specimen surface conditions.

Measurements of the normal spectral emittance at 665 nm on several titanium alloy specimens under different conditions were reported in the literature [8] for temperatures up to about 1700 K. The reported results for the specimen and conditions that closely match those of the present work indicate a nearly linear variation of emittance with temperature in the range 1200 to 1700 K. Extrapolation of these results to the melting point of the alloy (1943 K) yields a value of 0.369 for the normal spectral emittance, which is about 7 percent lower than the value of 0.395 obtained in the present work. This difference may not be very significant due to the fact that specimens were different and the literature results were extrapolated to the melting point.

According to a compilation on melting points [9], the results, reported by different investigators, of the melting point of pure titanium are in the range 1933 to 1953 K. The value 1943 K obtained in the present work for the alloy is compatible with the above.

In the present experiments related to melting (true temperature obtained using tube-shape specimens and radiance temperature obtained using strip-shape specimens), it was not possible to follow the entire melting process because the specimen collapsed and opened the main electrical circuit prior to the completion of melting. However, good quality horizontal plateaus were obtained during the initial melting period which are more of a characteristic of pure metals.

The authors express their gratitude to M. S. Morse for his help with the electronic instrumentation.

5. Appendix

TABLE A-1. *Experimental results on specific heat capacity of the titanium alloy*

Range	Temperature (K)	Specimen-1		Specimen-2		Specimen-3		Specimen-4	
		c_p ($J \cdot g^{-1} \cdot K^{-1}$)	Δc_p[a] (%)	c_p ($J \cdot g^{-1} \cdot K^{-1}$)	Δc_p[a] (%)	c_p ($J \cdot g^{-1} \cdot K^{-1}$)	Δc_p[a] (%)	c_p ($J \cdot g^{-1} \cdot K^{-1}$)	Δc_p[a] (%)
I	1450	0.7247	−0.58	0.7230	−0.81	0.7213	−1.05	0.7345	+0.76
	1500	.7332	−0.16	.7327	−0.23	.7305	−0.53	.7380	+0.49
	1550	.7431	+0.18	.7437	+0.26	.7414	−0.05	.7441	+0.31
	1600	.7550	+0.52	.7556	+0.60	.7544	+0.44	.7540	+0.39
	1650	.7693	+0.92	.7679	+0.74	.7700	+1.01	.7691	+0.90
II	1650	0.7595	−0.36	.7620	−0.03	.7619	−0.04	.7615	−0.09
	1700	.7710	−0.55	.7733	−0.25	.7747	−0.07	.7767	+0.19
	1750	.7862	−0.50	.7880	−0.27	.7902	+0.01	.7928	+0.34
	1800	.8059	−0.12	.8064	−0.06	.8091	+0.28	.8100	+0.39
	1850	.8311	+0.68	.8295	+0.48	.8320	+0.78	.8286	+0.38
III	1700	0.7775	+0.29	.7771	+0.24	.7820	+0.87	.7812	+0.77
	1750	.7820	−1.04	.7858	−0.55	.7836	−0.83	.7860	−0.52
	1800	.7952	−1.47	.7999	−0.87	.7948	−1.52	.7983	−1.07
	1850	.8182	−0.89	.8206	−0.60	.8175	−0.98	.8197	−0.71
	1900	.8538	+0.92	.8492	+0.44	.8557	+1.13	.8529	+0.81

[a] The quantity Δc_p is percentage deviation of the individual results from the smooth function represented by equation (1).

TABLE A-2. *Experimental results on electrical resistivity of the titanium alloy*

Range	Temperature (K)	Specimen-1		Specimen-2		Specimen-3		Specimen-4	
		ρ ($\mu\Omega$·cm)	$\Delta\rho$[a] (%)	ρ ($\mu\Omega$·cm)	$\Delta\rho$[a] (%)	ρ ($\mu\Omega$·cm)	$\Delta\rho$[a] (%)	ρ ($\mu\Omega$·cm)	$\Delta\rho$[a] (%)
I	1450	172.19	−0.08	172.80	+0.27	172.04	−0.17	172.31	−0.01
	1500	172.56	−0.09	173.21	+0.29	172.37	−0.20	172.59	−0.07
	1550	172.94	−0.08	173.57	+0.29	172.74	−0.19	173.02	−0.03
	1600	173.32	−0.05	173.90	+0.28	173.13	−0.16	173.47	+0.03
	1650	173.66	−0.04	174.22	+0.28	173.50	−0.14	173.77	+0.02
II	1650	173.75	+0.01	174.22	+0.28	173.41	−0.19	173.68	−0.03
	1700	174.09	+0.03	174.54	+0.29	173.72	−0.18	174.00	−0.02
	1750	174.41	+0.05	174.83	+0.30	174.03	−0.17	174.28	−0.02
	1800	174.70	+0.06	175.12	+0.30	174.32	−0.15	174.56	−0.02
	1850	175.00	+0.10	175.45	+0.35	174.56	−0.15	174.85	+0.01
III	1700	174.18	+0.08	174.18	+0.08	173.51	−0.30	173.72	−0.18
	1750	174.52	+0.11	174.51	+0.11	173.79	−0.31	174.02	−0.17
	1800	174.80	+0.12	174.81	+0.13	174.13	−0.26	174.29	−0.17
	1850	175.06	+0.13	175.07	+0.14	174.45	−0.22	174.54	−0.17
	1900	175.36	+0.17	175.30	+0.14	174.62	−0.25	174.77	−0.16

[a] The quantity $\Delta\rho$ is percentage deviation of the individual results from the smooth function represented by equation (2).

TABLE A-3. *Experimental results on hemispherical total emittance of the titanium alloy*

Specimen	T (K)	ϵ
1	1714	0.394
	1896	.388
2	1705	0.380
	1885	.376
3	1706	0.392
	1879	.392
4	1710	0.386
	1879	.380

6. References

[1] Cezairliyan, A., Design and Operational Characteristics of a High-Speed (Millisecond) System for the Measurement of Thermophysical Properties at High Temperatures, J. Res. Nat. Bur. Stand. (U.S.), **75C** (Eng. and Instr.), No. 1, 7–18 (Jan.–Mar. 1971).

[2] Cezairliyan, A., Morse, M. S., Berman, H. A., and Beckett, C. W., High-Speed (Subsecond) Measurement of Heat Capacity, Electrical Resistivity, and Thermal Radiation Properties of Molybdenum in the Range 1900 to 2800 K, J. Res., Nat. Bur. Stand. (U.S.), **74A,** (Phys. and Chem.), No. 1, 65–92 (Jan.–Feb.1970).

[3] International Practical Temperature Scale of 1968, Metrologia **5,** 35 (1969).

[4] Ziegler, W. T., and Mullins, J. C., Specific Heat of Titanium Alloys, Georgia Inst. Tech., Final Report, Project No. A504 (1961).

[5] Deem, H. W., Wood, W. D., and Lucks, C. F., The Relationship Between Electrical and Thermal Conductivities of Titanium Alloys, Trans. Met. Soc. AIME, **212,** 520 (1958).

[6] Ermolaev, B. I., Thermal Conductivity and Electrical Conductivity of Materials Based on Titanium and Its Alloys from 20–80 to 1000 K, Metal Science and Heat Treatment, **16,** 1049 (1974).

[7] de L'Estoile, H., and Rosenthal, L., Advisory Group for Aeronautical Research and Development, Paris, France, AGARD-211 N63-21549, (1958).

[8] Betz, H. T., Olson, O. H., Schurin, B. D., and Morris, J. C., WADC-TR-56-222 (Part 2), (1957) (AD202493).

[9] Charlesworth, J. H., Melting Points of Metallic Elements and Selected Compounds, Air Force Materials Laboratory Report, TR-70-137 (1970).

(Paper 81A2&3-927)

JOURNAL OF RESEARCH of the National Bureau of Standards—A. Physics and Chemistry
Vol. 81A, Nos. 2 and 3, March–June 1977

Evaporation of a Liquid Droplet

Richard Kayser, Jr., and Herbert S. Bennett

Institute for Materials Research, National Bureau of Standards, Washington, D.C. 20234

(March 22, 1977)

Two idealized models for the preheat stage of liquid droplets are analyzed theoretically. These models contain the effects of transient heat conduction and evaporation. It is assumed that the droplet surface area decreases linearly with time. This assumption necessitates the solution of moving boundary problems. These models, however, do not consider gas-phase mass transport. In the finite-gradient model, the temperatures of both the droplet and surrounding hot gases vary spatially and temporally. In the zero-gradient model the gas temperature varies spatially and temporally but the droplet temperature varies only temporally, i.e., the droplet temperature is spatially uniform. Numerical examples, which require extensive calculations of confluent hypergeometric functions, are presented for typical values of the droplet latent heat and evaporation rate constant. The temperature profiles given by the finite-gradient and zero-gradient models agree to within 20 percent of each other for all cases examined.

Key words: Confluent hypergeometric functions; droplet; moving boundary problem; preheat; transient heat conduction.

1. Introduction

The ignition of a droplet of conventional fuel consists essentially of two stages [1][1]. During the first or preheat stage heat flows from the hot surrounding gas to the droplet, causing the droplet temperature to rise and liquid fuel to evaporate from the droplet surface. In the second stage, ignition occurs in the gaseous mixture of fuel and oxidizer surrounding the droplet. The preheat stage is dominated by transient processes and provides the motivation for the subject of this paper.

Wise and Ablow [2], Parks, et al. [3], and Waldman [4] have previously analyzed the effects of transient droplet heating by neglecting the existence of internal circulation and by neglecting selected terms in the heat conduction equations. In addition they assume that the droplet surface regresses linearly with time. In a previous publication, Bennett and Kayser [5] included the effects of internal circulation but also neglected evaporation and regression of the droplet surface. We now include these effects in the present paper.

The neglect of internal circulation can in many instances lead to gross underestimates of the heat transfer rates within the droplet. Available experimental evidence indicates that in most cases the heat transfer rate inside the droplet is much faster than is possible with heat conduction alone. El Wakil, et al. [6] observed vigorous circulation within the droplet and showed that the droplet temperature is uniform even during the initial transient period. This indicates that the rate at which heat is transferred to the droplet is much slower than the rate of internal mixing. As pointed out by Law [7], assuming the droplet temperature to be uniform in a sense circumvents the difficult task of describing internal circulation but still includes the effects due to its presence; that is, uniform droplet temperature represents the limit of rapid internal circulation.

Two models for the transient preheat stage are presented. In the first model, called the finite-gradient model, the effects of transient heat conduction and evaporation with linear surface regression rate are analyzed. The droplet and gas temperatures vary spatially and temporally and the effects of internal circulation are neglected. In the second model, called the zero-gradient model, we include the effects of transient heat flow, evaporation, and internal circulation. The latter is included by assuming the droplet temperature to be temporally varying but spatially uniform as discussed above. The gas temperature is again both time and space dependent.

The results of the finite-gradient and zero-gradient models are applied to the preheat stage of droplets in hot gases. The temperature profiles are used to predict the time duration between introduction of the droplet into a hot atmosphere and its reaching a given temperature. In addition we compare the analogous times predicted by a particularly simple and accurate approximation to the exact expression derived for the zero-gradient model.

In the next section we describe the physical assumptions for the preheat stage common to both models. Section 3 contains the mathematical description of these assumptions. We derive in section 4 the temperature profiles of the droplet and gas predicted by the finite-gradient model while in section 5 we give the corresponding expressions for the zero-gradient model. We present in the last section numerical examples for both models. The temperature profiles obtained are very similar for both models and are within 20 percent of each other in all cases examined.

2. Preheat Stage

Williams has examined the problem of the assumptions underlying droplet vaporization and combustion theories in some detail [8]. In models for preheating, many researchers consider the droplet to be a sphere with temperature independent thermal properties and neglect diffusion effects [1]. Others include thermal diffusion effects but later in their theoretical analyses neglect some terms in the diffusion equa-

[1] Figures in brackets indicate the literature references at the end of this paper.

tions [3]. In addition, most theoretical investigators neglect the influence of gravity, forced convection, and radiant heat transfer. Combustion chambers and experimental techniques such as freely falling droplets exist to eliminate gravitational effects. Proper selection of some experimental parameters such as ambient pressure and initial droplet size may minimize the other effects not included in the model for preheating. Several researchers have shown that except for the very heavy fuel oils, radiant heat transfer from the hot gas or from adjacent droplets is negligible [7, 9].

The models examined in this paper contain only thermal diffusion effects. We assume that a spherical liquid droplet of initial radius $r = r_{d0}$ is inserted at time $t = 0$ into a hot atmosphere (e.g., air). The initial temperature of the droplet at time $t = 0$ is T_{d0}. The hot gas is unbounded and initially at a constant temperature T_{g0}. For $t > 0$ the temperature at infinity is kept at T_{g0}.

The inclusion of evaporation demands that the droplet radius change with time. In the present work a linear surface regression rate is assumed:

$$R^2(t) = r_{d0}^2 = k_e t \tag{1}$$

$R(t)$ is a direct specification of the motion of the interface $r = R(t)$ with time and k_e denotes the evaporation rate constant. A self-contained theory would obtain $R(t)$ indirectly by adding to the boundary conditions at the interface the requirement that the local vapor pressure be determined in the solution process. A moving boundary problem in which $R(t)$ is directly specified falls into the general class of problems called inverse-Stefan problems while those in which it is determined in the solution process are called Stefan problems [10]. It must be stressed at this point that the solutions which we will obtain will be applicable only in those time regimes for which eq (1) is an accurate representation of the actual surface regression rate.

We denote the density, specific heat, and the thermal conductivity of the droplet respectively by d_d, C_d, and K_d and of the gas respectively by d_g, C_g and K_g. We assume that these thermal properties remain spatially and temporally constant during preheat. In addition, the ambient pressure of the host gas does not change. Using these and the above assumptions we seek to compute the dependence of the temperature $T(r, t)$ upon the radial distance r and time t. In particular, we shall compute the time required for a droplet to reach a given temperature.

3. Theoretical Analysis

We first consider the finite-gradient model. The distribution of temperature within the system is governed by the Fourier heat conduction equation for the case in which the isothermal surfaces are concentric spheres. Let $T_d(r, t)$, $T_g(r, t)$, $a_d^2 = (K_d/d_d C_d)$, and $a_g^2 = (K_g/d_g C_g)$ denote the temperatures and thermal diffusivities of the droplet and surrounding gas respectively. The governing equation for $t \geq 0$ and $0 \leq r < R$ (inside the droplet) reads

$$\frac{\partial T_d(r, t)}{\partial t} = a_d^2\left(\frac{\partial^2 T_d(r, t)}{\partial r^2} + \frac{2}{r}\frac{\partial T_d(r, t)}{\partial r}\right) \tag{2}$$

and for $t \geq 0$ and $r > R$ (outside the droplet)

$$\frac{\partial T_g(r, t)}{\partial t} = a_g^2\left(\frac{\partial^2 T_g(r, t)}{\partial r^2} + \frac{2}{r}\frac{\partial T_g(r, t)}{\partial r}\right) \tag{3}$$

The quantity $R(t)$ specifies the motion of the interface with time and is given in eq. (1).

The specification of the boundary conditions completes the statement of the problem. The temperature $T(r, t)$ has the form

$$T_d(r, t) = T_{d0} \text{ for } 0 \leq r < R \text{ and } t \leq 0 \tag{4}$$

and

$$T_g(r, t) = T_{g0} \text{ for } r > R \text{ and } t \leq 0 \tag{5}$$

and it becomes for $t > 0$

$$T(r, t) = \begin{cases} T_d(r, t) \text{ for } 0 \leq r < R \\ T_g(r, t) \text{ for } r > R. \end{cases}$$

The temperature is finite everywhere, namely $T_d(0, t)$ is finite and

$$\lim_{r \to \infty} T_g(r, t) = T_{g0} \tag{6}$$

The symmetry condition that no heat flux exists at the center of the droplet is

$$\frac{\partial T_d(0, t)}{\partial r} = 0 \tag{7}$$

$\partial T_d(0, t)/\partial r$ is of course taken to mean the partial derivative of $T_d(r, t)$ which respect to r evaluated at $r = 0$. The problem statement for the finite-gradient model is completed by two conditions at the interface $r = R$ which match the temperature and heat flux

$$T_d(R^-, t) = T_g(R^+, t) \tag{8}$$

$$K_d \frac{\partial T_d(R^-, t)}{\partial r} = K_g \frac{\partial T_g(R^+, t)}{\partial r} + L_d d_d \frac{dR(t)}{dt} \tag{9}$$

where $R^{\pm} = \lim_{\zeta \to 0} (R \pm \zeta)$ and L_d is the latent heat of vaporization per unit mass of the condensed material. From eq (1) we note that dR/dt goes off to infinity near the end of the droplet lifetime so that the difference between the thermal conductivities times the temperature gradients must become unbounded. More will be said about this point in subsequent sections.

We find it convenient at this point to introduce dimensionless quantities which in this paper will be denoted by Greek letters. They are defined as follows:

(1) The time τ is chosen to move the singular point of complete droplet evaporation to infinity, $\tau = 2(a_d^2/k_e) \ln (r_{d0}/R(t))$. As the evaporation rate constant k_e goes to zero τ reduces to $\tau_0 = a_d^2 t/r_{d0}^2$.

(2) The distance coordinate η is chosen to remove the time dependence of the position of the boundary, $\eta = r/R(t)$. Distance is thus measured in instantaneous droplet radii.

When $k_e = 0$, $\eta = \eta_0 = r/r_{d0}$.

(3). The dimensionsless temperature ratios are defined by

$$\Theta_j(\eta, \tau) = (T_j(r, t) - T_{d0})/(T_{g0} - T_{d0}), \qquad j = d \text{ or } g.$$

$\Theta_d(\eta, \tau)$ is the fraction of the maximum possible temperature rise. In addition, we define $\alpha = a_d/a_g$, $\beta = K_g/K_d$, $\epsilon = k_e/a_d^2$, and $\lambda = L_d/[C_d(T_{g0} - T_{d0})]$.

With the above definitions, eqs (2)–(9) become

$$\frac{\partial\Theta_d(\eta, \tau)}{\partial\tau} = \frac{\partial^2\Theta_d(\eta, \tau)}{\partial\eta^2} + \left(\frac{2}{\eta} - \frac{\epsilon\eta}{2}\right)\frac{\partial\Theta_d(\eta, \tau)}{\partial\eta} \qquad (0 \le \eta < 1) \quad (10)$$

$$\alpha^2\frac{\partial\Theta_g(\eta, \tau)}{\partial\tau} = \frac{\partial^2\Theta_g(\eta, \tau)}{\partial\eta^2} + \left(\frac{2}{\eta} - \frac{\alpha^2\epsilon\eta}{2}\right)\frac{\partial\Theta_g(\eta, \tau)}{\partial\eta} \qquad (\eta > 1) \quad (11)$$

$$\Theta_d(\eta, 0) = 0 \quad (12)$$

$$\Theta_g(\eta, 0) = 1 \quad (13)$$

$$\lim_{\eta\to\infty} \Theta_g(\eta, \tau) = 1 \quad (14)$$

$$\frac{\partial\Theta_d(0, \tau)}{\partial\eta} = 0 \quad (15)$$

$$\Theta_d(1^-, \tau) = \Theta_g(1^+, \tau) \quad (16)$$

$$\frac{\partial\Theta_d(1^-, \tau)}{\partial\eta} = \beta\frac{\partial\Theta_g(1^+, \tau)}{\partial\eta} - \lambda\epsilon/2 \quad (17)$$

Equations (10)–(17) are the complete statement in dimensionless form for the finite-gradient model.

We now consider the zero-gradient model. As was mentioned in section 1, the internal circulation inside the droplet may be sufficient in many cases to maintain a spatially uniform temperature within the droplet. When such conditions prevail, the Fourier heat conduction equation for the droplet, eq (2), and the boundary condition (9) are replaced by a single heat transfer equation. The temperatures in the zero-gradient model are denoted by $T_{dz}(t)$ and $T_{gz}(r, t)$ for the droplet and gas respectively. For the case in which the droplet temperature is spatially uniform, $T_d(r, t) = T_{dz}(t) = T_g(R^+, t) = T_{gz}(R^+, t)$ and the heat flux into the droplet,

$$(4\pi R^3/3)d_dC_d\frac{dT_{dz}(t)}{dt}/(4\pi R^2) \quad (18)$$

must equal the heat flux from the gas. Equations (2) and (9) are thus replaced by the following equality

$$\frac{d_dC_dR}{3}\frac{dT_{dz}(t)}{dt} = K_g\frac{\partial T_{gz}(R^+, t)}{\partial r} + L_dd_d\frac{dR(t)}{dt}. \quad (19)$$

Equations (3)–(8) with $T_d(r, t)$ and $T_g(r, t)$ replaced respectively by $T_{dz}(t)$ and $T_{gz}(r, t)$ and eq (19) are the mathematical statement of the zero-gradient model.

In terms of the dimensionless quantities introduced earlier, the working equations in the zero-gradient model are

$$\alpha^2\frac{\partial\Theta_{gz}(\eta, \tau)}{\partial\tau} = \frac{\partial^2\Theta_{gz}(\eta, \tau)}{\partial\eta^2} + \left(\frac{2}{\eta} - \frac{\alpha^2\epsilon\eta}{2}\right)\frac{\partial\Theta_{gz}(\eta, \tau)}{\partial\eta} \qquad (\eta > 1) \quad (20)$$

$$\Theta_{dz}(0) = 0 \quad (21)$$

$$\Theta_{gz}(\eta, 0) = 1 \quad (22)$$

$$\lim_{\eta\to\infty} \Theta_{gz}(\eta, \tau) = 1 \quad (23)$$

$$\Theta_{dz}(\tau) = \Theta_{gz}(1^+, \tau) \quad (24)$$

$$\frac{1}{3}\frac{d\Theta_{dz}(\tau)}{d\tau} = \beta\frac{\partial\Theta_{gz}(1^+, \tau)}{\partial\eta} - \frac{\lambda\epsilon}{2} \quad (25)$$

In the next two sections we solve the equations for the finite-gradient and zero-gradient models by taking their Laplace transforms. The Laplace transform of the reduced temperature $\Theta(\eta, \tau)$ is denoted by

$$\Phi(\eta, \sigma) = \int_0^\infty \exp(-\sigma\tau)\Theta(\eta, \tau)d\tau \quad (26)$$

where σ is the dimensionless Laplace transform variable. The Bromwich integral

$$\Theta(\eta, \tau) = \lim_{\delta\to\infty}\frac{1}{2\pi i}\int_{\gamma-i\delta}^{\gamma+i\delta} \exp(\sigma\tau)\Phi(\eta, \sigma)d\sigma \quad (27)$$

expresses the temperature in terms of the Laplace transform. The quantity γ is chosen sufficiently large so that the integral

$$\int_0^\infty \exp(-\sigma\tau)|\Theta(\eta, \tau)|d\tau$$

exists.

4. Finite-Gradient Model

From eqs (2)–(9), the Laplace transform of the reduced temperature $\Theta(\eta, \tau)$ satisfies the following equations and conditions:

$$\left[\frac{\partial^2}{\partial\eta^2} + \left(\frac{2}{\eta} - \frac{\epsilon\eta}{2}\right)\frac{\partial}{\partial\eta} - \sigma\right]\Phi_d(\eta, \sigma) = 0 \qquad (0 \le \eta < 1) \tag{28}$$

$$\left[\frac{\partial^2}{\partial\eta^2} + \left(\frac{2}{\eta} - \frac{\alpha^2\epsilon\eta}{2}\right)\frac{\partial}{\partial\eta} - \alpha^2\sigma\right]\Phi_g(\eta, \sigma) + \alpha^2 = 0 \qquad (\eta > 1) \tag{29}$$

$$\frac{\partial\Phi_d(0, \sigma)}{\partial\eta} = 0 \tag{30}$$

$$\lim_{\eta\to\infty} \Phi_g(\eta, \sigma) = 1 \tag{31}$$

$$\Phi_d(1^-, \sigma) = \Phi_g(1^+, \sigma) \tag{32}$$

$$\frac{\partial\Phi_d(1^-, \sigma)}{\partial\eta} = \beta\frac{\partial\Phi_g(1^+, \sigma)}{\partial\eta} - \frac{\lambda\epsilon}{2\sigma}. \tag{33}$$

To solve the subsidiary differential eqs (28) and (29), we make a change of variable. Letting $\zeta = \epsilon\eta^2/4$ gives

$$\left[\zeta\frac{\partial}{\partial\zeta} + \left(\frac{3}{2} - \zeta\right)\frac{\partial}{\partial\zeta} - \frac{\sigma}{\epsilon}\right]\Psi_d(\zeta, \sigma) = 0 \tag{34}$$

$$\left[\alpha^2\zeta\frac{\partial^2}{\partial(\alpha^2\zeta)^2} + \left(\frac{3}{2} - \alpha^2\zeta\right)\frac{\partial}{\partial(\alpha^2\zeta)} - \frac{\sigma}{\epsilon}\right]\Psi_g(\alpha^2\zeta, \sigma) + \sigma^{-1} = 0 \tag{35}$$

where $\Phi_d(\eta, \sigma) = \Psi_d(\zeta, \sigma)$ and $\Phi_g(\eta, \sigma) = \Psi_g(\alpha^2\zeta, \sigma)$.

The operator in square brackets is the confluent hypergeometric differential operator and eqs (34) and (35) are confluent hypergeometric differential equations. We obtain the general solutions to eqs (28) and (29) as

$$\Phi_d(\eta, \sigma) = AM(\sigma/\epsilon, 3/2, \epsilon\eta^2/4) + BU(\sigma/\epsilon, 3/2, \epsilon\eta^2/4) \tag{36}$$

for the droplet and

$$\Phi_g(\eta, \sigma) = \sigma^{-1} + CM(\sigma/\epsilon, 3/2, \alpha^2\epsilon\eta^2/4) + DU(\sigma/\epsilon, 3/2, \alpha^2\epsilon\eta^2/4) \tag{37}$$

for the hot surrounding gas. The quantities $M(a, b, z)$ and $U(a, b, z)$ are two independent solutions to the confluent hypergeometric differential equation and are called confluent hypergeometric functions. Their most useful general properties may be found in Chapter 13 of Ref. [11].

The constants A, B, C, and D must be determined from the conditions (30)–(33). The condition that no heat flux exists at the center of the droplet requires that $B = 0$ since $U(\sigma/\epsilon, 3/2, \epsilon\eta^2/4)$ is not well-behaved at $\eta = 0$. Similarly, the condition that the reduced gas temperature goes to unity at large distances requires $C = 0$ since $M(\sigma/\epsilon, 3/2, \alpha^2\epsilon\eta^2/4)$ is not well-behaved at infinity. The two remaining conditions at the interfacial boundary $\eta = 1$ constitute two inhomogeneous simultaneous equations for the remaining constants A and D. Solving these, we obtain the Laplace transformed solutions for the reduced temperatures:

$$\Phi_d(\eta, \sigma) = \frac{3\left[\alpha^2\beta\sigma U\left(\frac{\sigma}{\epsilon} + 1, \frac{5}{2}, \frac{\alpha^2\epsilon}{4}\right) - \lambda\epsilon U\left(\frac{\sigma}{\epsilon}, \frac{3}{2}, \frac{\alpha^2\epsilon}{4}\right)\right]M\left(\frac{\sigma}{\epsilon}, \frac{3}{2}, \frac{\epsilon\eta^2}{4}\right)}{\sigma^2 H(\sigma/\epsilon)} \tag{38}$$

for the droplet, and

$$\Phi_g(\eta, \sigma) = \sigma^{-1} - \frac{\left[2\sigma M\left(\frac{\sigma}{\epsilon} + 1, \frac{5}{2}, \frac{\epsilon}{4}\right) + 3\lambda\epsilon M\left(\frac{\sigma}{\epsilon}, \frac{3}{2}, \frac{\epsilon}{4}\right)\right]U\left(\frac{\sigma}{\epsilon}, \frac{3}{2}, \frac{\alpha^2\epsilon\eta^2}{4}\right)}{\sigma^2 H(\sigma/\epsilon)} \tag{39}$$

for the gas where

$$H(\sigma/\epsilon) = 2M\left(\frac{\sigma}{\epsilon} + 1, \frac{5}{2}, \frac{\epsilon}{4}\right)U\left(\frac{\sigma}{\epsilon}, \frac{3}{2}, \frac{\alpha^2\epsilon}{4}\right) + 3\alpha^2\beta M\left(\frac{\sigma}{\epsilon}, \frac{3}{2}, \frac{\epsilon}{4}\right)U\left(\frac{\sigma}{\epsilon} + 1, \frac{5}{2}, \frac{\alpha^2\epsilon}{4}\right). \tag{40}$$

The differential relations of M and U have been used in deriving these equations. These expressions have been derived in a form suitable for going to the limit of zero evaporation rate constant, $\epsilon = 0$. The correct limiting cases may be found in Ref. [6] and the details of the limiting process in appendix A.

The reduced temperature distributions of the droplet and surrounding gas are obtained by evaluating the Bromwich integrals of eq (8):

$$\Theta(\eta, \tau) = \lim_{\delta\to\infty} \frac{1}{2\pi i} \int_{\gamma-i\delta}^{\gamma+i\delta} \exp(\sigma\tau)\Phi(\eta, \sigma)d\sigma. \tag{41}$$

To evaluate the Bromwich integrals it is first necessary to investigate the nature of the integrand $\exp(\sigma\tau)\Phi(\eta, \sigma)$. No distinction will be made in this discussion between the droplet and the gas as the integrands in both cases exhibit the same general properties. First of all, $\exp(\sigma\tau)\Phi(\eta, \sigma)$ is a single-valued, analytic function of σ except at its singularities. It has a simple second order pole at $\sigma = 0$ and an infinity of real, negative simple first order poles at the zeroes of $H(\sigma/\epsilon)$ given in eq (40). To show that $H(\sigma/\epsilon)$ possesses no complex, imaginary or positive zeros is straight-foreward. General methods for locating such zeros may be found, for example, in Carslaw and Jaeger [12] and Ince [13].

We now evaluate the Bromwich integral. We complete the contour of eq (41) by a large semicircular arc in the left-hand complex plane and take γ to be an arbitrarily small positive number. The final reduced temperature distributions are then obtained by applying the Cauchy Residue Theorem and letting δ and the radius of the large semicircular arc tend to infinity. The integral along the large semicircular arc vanishes and we find

$$\Theta_d(\eta, \tau) = \frac{3}{H(0)}\left[\frac{\lambda}{H(0)}\frac{\partial H(\rho)}{\partial\rho}\bigg|_{\rho=0} - \lambda\frac{\partial U\left(\rho, \frac{3}{2}, \frac{\alpha^2\epsilon}{4}\right)}{\partial\rho}\bigg|_{\rho=0}\right.$$
$$\left. - \lambda\frac{\partial M\left(\rho, \frac{3}{2}, \frac{\epsilon\eta^2}{4}\right)}{\partial\rho}\bigg|_{\rho=0} + \alpha^2\beta U\left(1, \frac{5}{2}, \frac{\alpha^2\epsilon}{4}\right) - \epsilon\lambda\tau\right] \tag{42}$$
$$+ 3\sum_{n=1}^{\infty} \frac{\exp(\epsilon\rho_n\tau)\left[\rho_n\alpha^2\beta U\left(\rho_n + 1, \frac{5}{2}, \frac{\alpha^2\epsilon}{4}\right) - \lambda U\left(\rho_n, \frac{3}{2}, \frac{\alpha^2\epsilon}{4}\right)\right] M\left(\rho_n, \frac{3}{2}, \epsilon\eta^2/4\right)}{\rho^2{}_n\partial H(\rho)/\partial\rho|_{\rho=\rho_n}}$$

and

$$\Theta_g(\eta, \tau) = 1 + \frac{1}{H(0)}\left[\frac{3\lambda}{H(0)}\frac{\partial H(\rho)}{\partial\rho}\bigg|_{\rho=0} - 3\lambda\frac{\partial M\left(\rho, \frac{3}{2}, \frac{\epsilon}{4}\right)}{\partial\rho}\bigg|_{\rho=0}\right.$$
$$\left. - 3\lambda\frac{\partial U\left(\rho, \frac{3}{2}, \frac{\alpha^2\epsilon\eta^2}{4}\right)}{\partial\rho}\bigg|_{\rho=0} - 2M\left(1, \frac{5}{2}, \frac{\epsilon}{4}\right) - 3\epsilon\lambda\tau\right] \tag{43}$$
$$- \sum_{n=1}^{\infty} \frac{\exp(\epsilon\rho_n\tau)[2\rho_n M\left(\rho_n + 1, \frac{5}{2}, \frac{\epsilon}{4}\right) + 3\lambda M\left(\rho_n, \frac{3}{2}, \frac{\epsilon}{4}\right)]U\left(\rho_n, \frac{3}{2}, \alpha^2\epsilon\eta^2/4\right)}{\rho^2{}_n\partial H(\rho)/\partial\rho|_{\rho=\rho_n}}.$$

where $H(\rho_n) = 0$, $n = 1, 2, 3 \cdots$; i.e., the ρ_n are the zeros of $H(\rho)$.

We pause to make several comments about the expressions obtained for $\Theta_d(\eta, \tau)$ and $\Theta_g(\eta, \tau)$. Both contain a term proportional to the reduced time τ which is a consequence of the second order pole at $\sigma = 0$. As mentioned after eq (9), the choice of linear surface regression rate implies that the difference between the thermal conductivities times the temperature gradients evaluated at the interface goes to infinity at large times. By large times of course, we mean times close to the end of the droplet's lifetime. These are times for which the linear surface regression rate of eq (1) is no longer an accurate representation of the true physical situation. For λ, ϵ, and τ of the orders of magnitude of interest here, the linear term in τ may be considered an artifact of the model and makes only a very small contribution to the reduced temperatures. We remark also that eqs (42) and (43) are not suitable for going directly to the limit $\epsilon = 0$. Further discussion of this point may be found in appendix A.

In section 6 are presented plots of $\Theta_d(1, \tau)$ versus τ for typical values of the dimensionless quantities λ and ϵ. In the next section we derive expressions for the reduced temperatures for the zero-gradient model.

5. Zero-Gradient Model

The analysis for the zero-gradient model is mathematically very similar to that for the finite-gradient model and will not be quite as detailed. Equations (20)–(25) are the working equations for the zero-gradient model. The Laplace transformed system of equations is

$$\left[\frac{\partial^2}{\partial\eta^2} + \left(\frac{2}{\eta} - \frac{\alpha^2\epsilon\eta}{2}\right)\frac{\partial}{\partial\eta} - \alpha^2\sigma\right]\Phi_{gz}(\eta, \sigma) + \alpha^2 = 0 \quad (44)$$

$$\lim_{\eta\to\infty} \Phi_{gz}(\eta, \sigma) = 1 \quad (45)$$

$$\Phi_{dz}(\sigma) = \Phi_{gz}(1^+, \sigma) \quad (46)$$

$$\frac{\sigma}{3}\Phi_{dz}(\sigma) = \beta\frac{\partial\Phi_{gz}(1^+, \sigma)}{\partial\eta} - \frac{\lambda\epsilon}{2\sigma} \quad (47)$$

The general solution to the differential eq (44) which satisfies the condition (45) is

$$\Phi_{gz}(\eta, \sigma) = \sigma^{-1} + AU(\sigma/\epsilon, 3/2, \alpha^2\epsilon\eta^2/4) \quad (48)$$

Combining eqs (46) and (47) to eliminate $\Phi_{dz}(\sigma)$ yields the relation

$$\frac{\sigma}{3}\Phi_{gz}(1^+, \sigma) = \beta\frac{\partial\Phi_{gz}(1^+, \sigma)}{\partial\eta} - \frac{\lambda\epsilon}{2\sigma} \quad (49)$$

which is then used to determine the single unknown constant A of eq (48). Doing this yields the Laplace transformed reduced temperature distributions

$$\Phi_{dz}(\sigma) = \Phi_{gz}(1^+, \sigma) \quad (50)$$

for the droplet, and

$$\Phi_{gz}(\eta, \sigma) = \sigma^{-1} - \frac{(2\sigma + 3\lambda\epsilon)U(\sigma/\epsilon, 3/2, \alpha^2\epsilon\eta^2/4)}{\sigma^2 I(\sigma/\epsilon)} \quad (51)$$

for the gas where

$$I(\sigma/\epsilon) = 2U(\sigma/\epsilon, 3/2, \alpha^2\epsilon/4) + 3\beta\alpha^2 U(1 + \sigma/\epsilon, 5/2, \alpha^2\epsilon/4) \quad (52)$$

These expressions have been derived in a form suitable for going to the limit $\epsilon = 0$, which represents the nonevaporative problem solved in Ref. [6]. That they in fact reduce to the correct limit is shown in appendix A.

All that remains to be done is to evaluate the Bromwich integral of eq (8) with $\Phi(\eta, \sigma) = \Phi_{gz}(\eta, \sigma)$

$$\Theta_{gz}(\eta, \tau) = \lim_{\delta\to\infty}\frac{1}{2\pi i}\int_{\gamma-i\delta}^{\gamma+i\delta} \exp(\sigma\tau)\Phi_{gz}(\eta, \sigma)d\sigma. \quad (53)$$

The same general comments made about the corresponding integrands in the finite-gradient model are applicable here also. We complete the contour by a large semicircular arc in the left-hand complex plane, apply the Cauchy Residue Theorem and let δ and the radius of the semicircular arc tend to infinity. Following this sequence of steps were find

$$\Theta_{dz}(\tau) = \Theta_{gz}(1^+, \tau) \quad (54)$$

and

$$\Theta_{gz}(\eta, \tau) = 1 + \frac{1}{I(0)}\left[\frac{3\lambda}{I(0)}\frac{\partial I(\rho)}{\partial\rho}\bigg|_{\rho=0} - 2 - 3\lambda\frac{\partial U(\rho, 3/2, \alpha^2\epsilon\eta^2/4)}{\partial\rho}\bigg|_{\rho=0} - 3\epsilon\lambda\tau\right] - \sum_{n=1}^{\infty}\frac{\exp(\epsilon\rho_n\tau)(2\rho_n + 3\lambda)U(\rho_n, 3/2, \alpha^2\epsilon\eta^2/4)}{\rho^2{}_n\partial I(\rho)/\partial\rho|_{\rho=\rho_n}} \quad (55)$$

where $I(\rho_n) = 0$, $n = 1, 2, 3, \cdots$; i.e., the ρ_n are the negative real zeros of $I(\rho)$. Note that the linear term in τ also appears in the zero-gradient model solutions.

It is possible to obtain some very simple and accurate approximations to eqs (54) and (55). The thermal diffusivity of the droplet is several orders of magnitude smaller than that of the surrounding gas. This suggests that before applying the Laplace inversion formula we expand the subsidiary solution $\Phi_{gz}(\eta, \sigma)$ into a power series in $\alpha = a_d/a_g$. We obtain only the simplest approximation by letting α go to zero in eq (51):

$$\lim_{\alpha \to 0} \Phi_{gz}(\eta, \sigma) \equiv \Phi_{g0}(\eta, \sigma) \tag{56}$$

$$= \sigma^{-1} - \frac{2\sigma + 3\epsilon\lambda}{2\eta\sigma(\sigma + 3\beta)}$$

The inverse Laplace transform of this remarkably simple expression yields the following approximations for the reduced temperatures in the zero-gradient model.

$$\Theta_{d0}(\tau) = \left(1 - \frac{\lambda\epsilon}{2\beta}\right)\left(1 - \exp(-3\beta\tau)\right) \tag{57}$$

for the droplet, and

$$\Theta_{g0}(\eta, \tau) = 1 - \eta^{-1}\exp(-3\beta\tau) - (\lambda\epsilon/2\beta\eta)(1 - \exp(-3\beta\tau)) \tag{58}$$

for the surrounding gas. Note that the term linear in τ has disappeared to the order of approximation used. However, if $\Phi_{gz}(\eta, \sigma)$ is expanded out to first order in α, then a relatively simple infinite series and the linear term in τ show up in the approximation of $\Theta_{gz}(\eta, \tau)$. Unfortunately, the expressions obtained by letting α go to zero in the finite-gradient model are much the same as the exact solutions.

In the next section, we present plots of $\Theta_{dz}(\tau)$ versus τ for typical values of λ and ϵ. In addition, the times predicted by $\Theta_d(\eta, \tau)$, $\Theta_{dz}(\eta, \tau)$ and $\Theta_{d0}(\tau)$ for the droplet to reach a given temperature are compared and discussed.

6. Numerical Examples and Conclusions

In this section, we give some illustrative numerical examples for the predictions made by finite-gradient and zero-gradient models. The input data for the calculations are the four dimensionless quantities α, β, λ and ϵ. We take $\alpha = 0.057$, $\beta = 0.186$ and $\lambda = 0.01, 0.055, 0.10$ and $\epsilon = 0.10, 0.55, 1.0$, independently, so that there are nine cases. These values correspond roughly to those of medium weight fuel oil in hot air at atmospheric pressure. Typical values of the physical parameters K, d, and C which yield the chosen values of α and β are given in table 1. In table 2, we give the values of L_d corresponding to $\lambda = 0.01, 0.055$, and 0.10 and k_e corresponding to $\epsilon = 0.10, 0.55$, and 1.0. The temperature difference $T_{g0} - T_{d0}$ is taken to be 1666.67 K (corresponding to $T_{d0} = 300$ K and $T_{g0} = 1966.67$ K) and a_d^2 and C_d are assigned the values given them in table 1.

Figures 1a, 1b, and 1c compare the numerical predictions

TABLE 1. *Typical values of the thermal conductivity* K, *density* d, *specific heat* C *at constant volume, and thermal diffusivity* a^2 *which yield* $\alpha = a_d/a_g = 0.057$ *and* $\beta = K_g/K_d = 0.186$

Property	Droplet	Gas
K(J/cm s °C)	1.45×10^{-3}	2.69×10^{-4}
d(g/cm^3)	0.90	1.3×10^{-3}
C(J/g °C)	2.39	1.0
a^2(cm^2/s)	6.5×10^{-4}	0.20

TABLE 2. *The values of the droplet latent heat of vaporization per gram,* L_d, *and the evaporation rate constant,* k_e, *corresponding to the values of the dimensionless parameters* $\lambda = L_d/\{C_d(T_{go} - T_{do})\}$ *and* $\epsilon = k_e/a_d^2$ *used.* The temperature difference $T_{go} - T_{do}$ is taken to be 1666.67 K and a_d^2 and C_d are assigned the values given in table 1.

λ	L_d(J/g)	ϵ	k_e(cm^2/s)
0.01	39.83	0.1	6.5×10^{-5}
0.055	219.08	0.55	3.575×10^{-4}
0.10	398.33	1.0	6.5×10^{-4}

of the finite-gradient and zero-gradient models for oil droplets in air for λ equal to 0.01, 0.055, and 0.10, respectively. $\Theta_d(1^-, \tau)$ and $\Theta_{dz}(\tau)$, the reduced surface temperatures, are computed from eqs (42) and (54). It should be noted that due to the presence of the linear term in τ, neither $\Theta_d(1^-, \tau)$ nor $\Theta_{dz}(\tau)$ reach steady state during the droplet lifetime. Even if that term were absent, $\Theta_d(\eta, \tau)$ would never become uniform throughout the droplet. We must stress at this point that the apparent large difference between the temperature profiles for fixed λ but different ϵ is deceiving. Although shown on the same graph, the curves are plotted versus $\epsilon\tau/2$ which is a function of ϵ, i.e., each curve has its own distinct time scale. The results have been shown in this fashion for clarity only. If they were all plotted on the same scale, real time t for example, the entire group of curves would lie very close to one another. As can be seen from the figures, $\Theta_d(1^-, \tau)$ and $\Theta_{dz}(\tau)$ are quite similar. Their difference is greatest when $\epsilon\tau/2$ is small. This is to be expected. The thermal gradients inside the droplet are largest near the beginning of its lifetime and for such times the approximations of the zero-gradient model are more suspect. Although not plotted, the simple approximation $\Theta_{d0}(\tau)$ to $\Theta_{dz}(\tau)$, obtained in the last section, is an extremely good one as long as $\epsilon\tau/2$ is neither too large nor too small. The difference between $\Theta_{dz}(\tau)$ and $\Theta_{d0}(\tau)$ is less than about 15 percent in the worst case ($\lambda = 0.1$ and $\epsilon = 1.0$) and much smaller in the other cases for the τ's we have considered. Due to its simple analytic form, accuracy, and ease of mathematical computation, we suspect that $\Theta_{d0}(\tau)$ is potentially a very useful expression for analyses of the initial preheat period of droplets in hot atmospheres.

A quantity of interest in the design of combustion chambers is the time required for fuel droplet to reach a given temperature T_s. Let us denote this time by t_e and consider a fuel droplet with the same physical parameters given in table 1 and an initial radius $r_{d0} = 50$ μm. For illustrative purposes, let us assume that $T_{SL} = 550$ K, the initial droplet temperature $T_{d0} = 300$ K, and the initial gas temperature $T_{g0} = 1966.67$ K. The droplet reading T_s corresponds to $\Theta_s = 0.15$. Using the data displayed graphically as figs. 1a, 1b, and 1c, we compute the times required for Θ to increase from zero to 0.15. The results are shown in figure 2 as a plot of t_e versus ϵ. It can be seen that the times, t_e, predicted by the finite-gradient and zero-gradient models are within about 20 percent of each other. For comparison, the t_e's predicted by $\Theta_{d0}(\tau)$ are also presented and are seen to be within 10–20 percent of those predicted by $\Theta_{dz}(\tau)$ as long as $\epsilon \lesssim 0.55$. Figure 2 also provides an extremely powerful cross check on the analytic and numerical results of this paper and those of Ref. [9]. By solving a totally different problem, Bennett and Kayser [9] obtained the times t_e for the case of $\epsilon = 0$. These are the points on the t-axis of figure 2. By extrapolating the

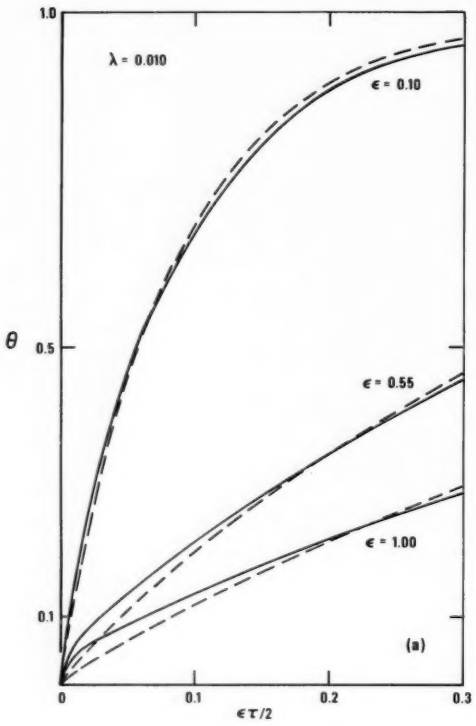

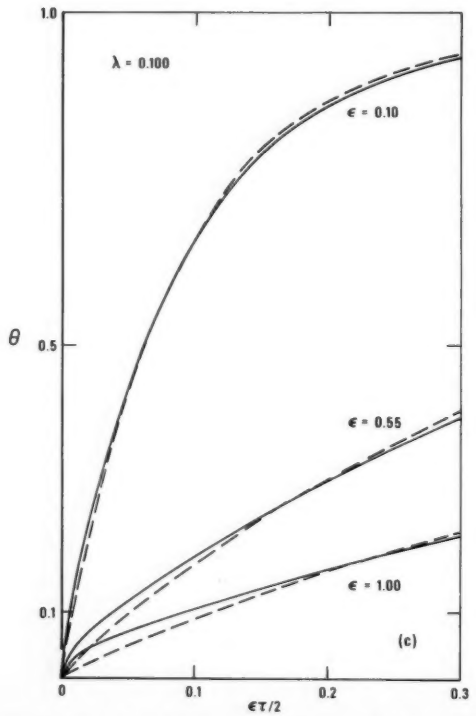

FIGURE 1. *The reduced temperature $\Theta_d(1^-, \tau)$ (solid lines) and $\Theta_{dz}(\tau)$ (dashed lines) plotted as a function of $\epsilon\tau/2$ with $\alpha = 0.057$, $\beta = 0.186$ and $\epsilon = 0.10, 0.55$, and 1.0 for λ equal to (a) 0.01, (b) 0.055, and (c) 0.10.*
The initial droplet radius, r_{do}, is 50 μm.

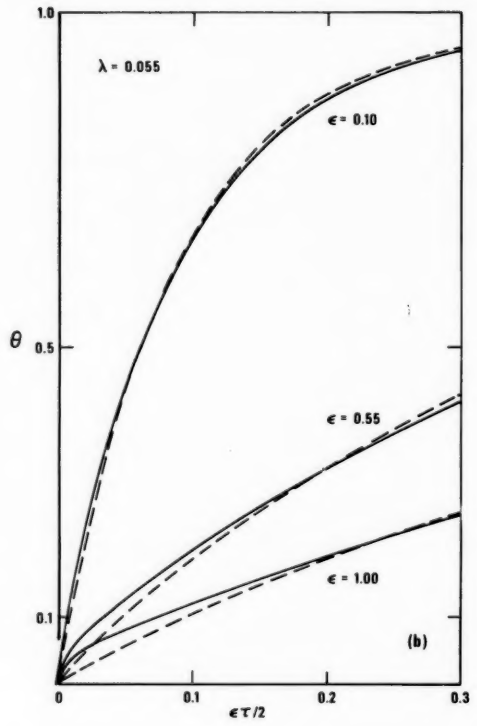

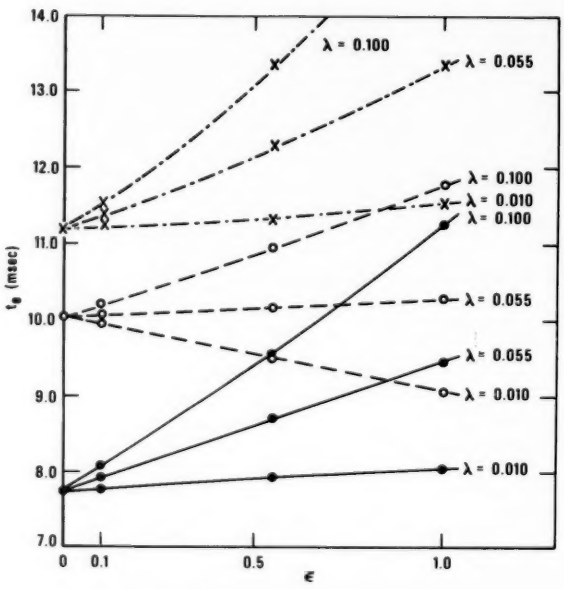

FIGURE 2. *The times t_e required for a droplet to reach obtained from $\Theta_d(1^-, \tau)$ (solid lines and closed circles), $\Theta_{dz}(\tau)$ (dashed lines and crosses) plotted as a function of ϵ for various values of λ.*
The physical properties used are those of table 1 and the initial droplet radius, r_{do}, is 50 μm.
The temperature T_S corresponds to $\Theta(t_e) = 0.15$.

results obtained here for nonzero ϵ to ϵ equal to zero, it can be seen that the results are in agreement and this indicates that this work and that of Ref. [9] are internally consistent.

Figure 3 contains a plot of the volume fraction of the droplet that has evaporated away by the time $t = t_e$ versus ϵ. For $\epsilon = 0.1$, an evaporation rate constant fairly characteristic of the initial preheat stage, the volume fraction evaporated is less than 5 percent. If ϵ is fairly small, this perhaps justifies neglecting evaporation and surface regression rate in analyzing the initial droplet preheat stage. A fairly decent approximate procedure for predicting the times t_e and the droplet size at $t = t_e$ is to neglect evaporation, compute the time required for the droplet to reach a given temperature, and then to use that time and a relation like eq (1) to calculate the volume fraction evaporated.

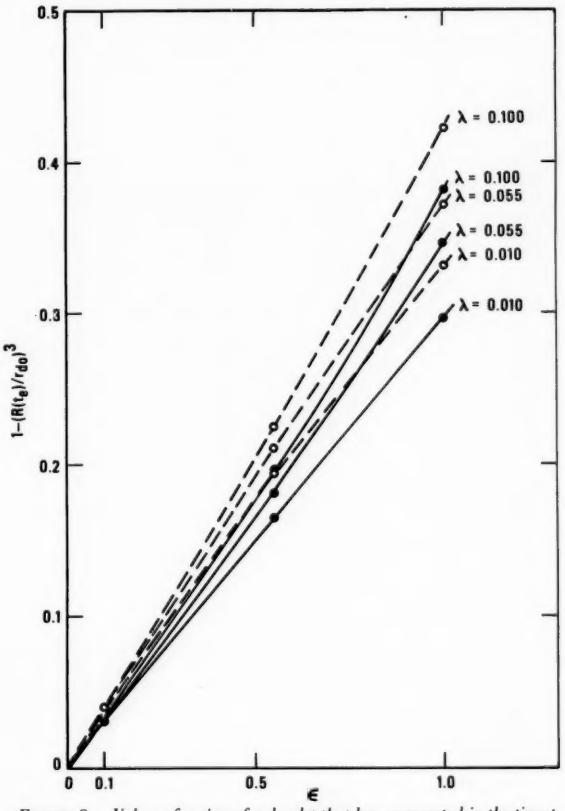

FIGURE 3. *Volume fraction of a droplet that has evaporated in the time t_e plotted as a function of ϵ for various values of λ.*
The closed circles and solid lines are for the finite-gradient model ($\Theta_d(1^-, \tau)$) and the open circles and dashed lines are for the zero-gradient model ($\Theta_{dz}(\tau)$). The physical properties used are those in table 1 and the initial droplet radius, r_{d0}, is 50 μm. The times t_e are those of figure 2.

The authors thank members of the Applied Mathematics Division and the Computer Sciences Division at the National Bureau of Standards for their assistance in preparing and using computer programs. They have benefited from helpful discussions with T. D. Coyle, K. G. Krieder, and M. B. McNeil. One of us, Richard Kayser, Jr., gratefully acknowledges support from the National Science Foundation.

7. Appendix A

In this appendix, we show that intermediate results such as those of eqs (38) and (51) reduce to the correct limits as ϵ, the reduced evaporation rate constant, goes to zero. We also make some general remarks concerning this limiting process.

The results of the $\epsilon = 0$ problem corresponding to eqs (38) and (51) will be denoted by a superscript '0' and are [6]:

$$\Phi_d^0(\eta_0, \sigma) = \frac{\beta(1 + \alpha\sigma^{1/2}) \sinh(\sigma^{1/2}\eta_0)}{\sigma\eta_0[\{\beta(1 + \alpha\sigma^{1/2}) - 1\} \sinh \sigma^{1/2} + \sigma^{1/2} \cosh \sigma^{1/2}]} \tag{A1}$$

for the droplet in the finite-gradient model and

$$\Phi_{gz}^0(\eta_0, \sigma) = \sigma^{-1} - \exp[-\alpha\sigma^{1/2}(\eta_0 - 1)]/[\eta_0(\sigma + 3\beta\alpha\sigma^{1/2} + 3\beta)] \tag{A2}$$

for the gas in the zero-gradient model. The quantities η_0 and τ_0 are defined in section 3. We use the relations [11]

$$dM(a, b, z)/dz = aM(a + 1, b + 1, z)/b \tag{A3}$$

$$dU(a, b, z)/dz - aU(a + 1, b + 1, z) \tag{A4}$$

to rewrite eqs (38) and (51) as

$$\Phi_d(\eta, \sigma) = \frac{-\left[\beta \frac{d}{d\eta} U\left(\frac{\sigma}{\epsilon}, \frac{3}{2}, \frac{\alpha^2\epsilon\eta^2}{4}\right)\Big|_{\eta=1} - \frac{1}{4}\epsilon\lambda U\left(\frac{\sigma}{\epsilon}, \frac{3}{2}, \frac{\alpha^2\epsilon}{4}\right)\right] M\left(\frac{\sigma}{\epsilon}, \frac{3}{2}, \frac{\epsilon\eta^2}{4}\right)}{\sigma\left[\frac{d}{d\eta} M\left(\frac{\sigma}{\epsilon}, \frac{3}{2}, \frac{\epsilon\eta^2}{4}\right)\Big|_{\eta=1} U\left(\frac{\sigma}{\epsilon}, \frac{3}{2}, \frac{\alpha^2\epsilon}{4}\right) - \beta M\left(\frac{\sigma}{\epsilon}, \frac{3}{2}, \frac{\epsilon}{4}\right) \frac{d}{d\eta} U\left(\frac{\sigma}{\epsilon}, \frac{3}{2}, \frac{\alpha^2\epsilon\eta^2}{4}\right)\Big|_{\eta=1}\right]} \tag{A5}$$

$$\Phi_{gz}(\eta, \sigma) = \sigma^{-1} + \frac{(2\sigma + 3\epsilon\lambda) U(\sigma/\epsilon, 3/2, \alpha^2\epsilon\eta^2/4)}{2\sigma[3\beta(d/d\eta) U(\sigma/\epsilon, 3/2, \alpha^2\epsilon\eta^2/4)|_{\eta=1} - \sigma U(\sigma/\epsilon, 3/2, \alpha^2\epsilon/4)]} \tag{A6}$$

Again from Ref. [11] we obtain

$$\lim_{a\to\infty} [M(a, b, z/a)/\Gamma(b)] = z^{1/2-1/2b} I_{b-1}(2z^{1/2}) \tag{A7}$$

$$\lim_{a\to\infty} [\Gamma(1 + a - b) U(a, b, z/a)] = 2z^{1/2-1/2} K_{b-1}(2z^{1/2}) \tag{A8}$$

where I and K are modified Bessel functions. Using these two limiting expressions, we find

$$\lim_{\epsilon\to 0} M(\sigma/\epsilon, 3/2, \epsilon\eta^2/4)/\Gamma(3/2)] = \frac{2 \sinh(\sigma^{1/2}\eta_0)}{\sqrt{\pi}\eta_0\sigma^{1/2}} \tag{A9}$$

$$\lim_{\epsilon\to 0} \left[\Gamma\left(\frac{\sigma}{\epsilon} - \frac{1}{2}\right) U(\sigma/\epsilon, 3/2, \alpha^2\epsilon\eta^2/4)\right] = \frac{2\sqrt{\pi} \exp(-\alpha\eta_0\sigma^{1/2})}{\alpha\eta_0\sigma^{1/2}}. \tag{A10}$$

Multiplying the numerator and denominator of eq (A5) by $\Gamma\left(\frac{\sigma}{\epsilon} - \frac{1}{2}\right) \Big/ \Gamma\left(\frac{3}{2}\right)$, substituting the results of eqs. (A9) and (A10), replacing $d/d\eta$ by $d/d\eta_0$, and rearranging the resulting expression yields eq (A1); that is

$$\lim_{\epsilon\to 0} \Phi_d(\eta, \sigma) = \Phi_d^0(\eta_0, \sigma). \tag{A11}$$

Multiplying numerator and denominator of eq (A6) by $\Gamma\left(\frac{\sigma}{\epsilon} - \frac{1}{2}\right)$ and then performing the same sequence of operations as for the finite-gradient model leads to eq (A2):

$$\lim_{\epsilon\to 0} \Phi_{gz}(\eta, \sigma) = \Phi_{gz}^0(\eta_0, \sigma). \tag{A12}$$

The same general procedure may easily be used to show that other intermediate results also tend to the correct limit as ϵ goes to zero.

It is the intermediate results which may be checked and not the final results obtained by evaluating the Bromwich integrals. It is not permissible, as may be verified by trying it, to take the expressions $\Theta_d(\eta, \tau)$ and $\Theta_{gz}(\eta, \tau)$ of eqs (42) and (55) to the limit of ϵ being zero to obtain $\Theta_d^0(\eta_0, \tau_0)$ and $\Theta_{gz}^0(\eta_0, \tau_0)$. This limiting process is improper for the following reason. Inspection of eqs (A1), (A2), (A5) and (A6) shows the first two to be double-valued functions of σ with a branch points at $\sigma = 0$ and the last two to be single-valued analytic functions of σ. As one proceeds to the limit of zero ϵ, an infinity of simple first order poles coalesces into a branch point at the origin, $\sigma = 0$. The evaluation of the Bromwich integrals leading to $\Theta_d(\eta, \tau)$ and $\Theta_{gz}(\eta, \tau)$ is thus only valid for nonzero ϵ. The expressions representing $\Theta_d(\eta, \tau)$ and $\Theta_{gz}(\eta, \tau)$ only do so for nonzero ϵ and this explains why it is impermissible, in fact impossible, to obtain $\Theta_{d0}^0(\eta_0, \tau_0)$ and $\Theta_{gz}^0(\eta_0, \tau_0)$ from them by any limiting process.

8. References

[1] Williams, A., Combustion and Flame, **21,** 1 (1973).
[2] Wise, H. and Ablow, C. M., J. Chem. Phys. **27,** 389 (1957).
[3] Parks, J. M., et al., AIAA Journal, **4,** 1632 (1966).
[4] Waldman, C. H., The Fifteenth (International) Symposium on Combustion. (The Combustion Institute, Pittsburgh, 1976) p. 429.
[5] Bennett, H. S. and Kayser, R., Jr., to be published.
[6] El Wakil, M. M., et al., NACA TN 3490 (1956).
[7] Law, C. K., Combustion and Flame, **26,** 17 (1976).
[8] Williams, F. A., J Chem. Phys. **33,** 133 (1960).
[9] Friedman, M. H. and Churchill, S. W., Chemical Engineering Progress Symposium Series, Heat Transfer-Boston, American Institute of Chemical Engineering, **61,** 1 (1965).
[10] Ockendon, J. R. and Hodgekins, W. R., editors, Moving Boundry Problems in Heat Flow and Diffusion (Oxford Univ. Press, London, 1975).
[11] Abramowitz, M. and Stegun, I., editors, Handbook of Mathematical Functions, Natl. Bur. Stds. (U.S.) Applied Math. Series No. 55 (U.S. GPO, Washington, D. C., 1964), Chap. 13.
[12] Carslaw, H. S. and Jaeger, J. C., Conduction of Heat in Solids (Oxford Univ. Press, London, 1947), p. 266.
[13] Ince, E. L., Ordinary Differential Equations (Dover Publications, New York, 1926), Chap. 10.

(Paper 81A2&3-928)

JOURNAL OF RESEARCH of the National Bureau of Standards—A. Physics and Chemistry
Vol. 81A, Nos. 2 and 3, March–June 1977

Isotope Effects in the Association Reactions of Methyl and Ethyl Iodide Cations*

L. Wayne Sieck

Institute for Materials Research, National Bureau of Standards, Washington, D. C. 20234

(March 10, 1977)

Rate coefficients for production of stabilized dimeric parent cations at 295 K have been determined in CH_3I, CD_3I, CH_3I-CD_3I mixtures, C_2H_5I, CH_3CD_2I, CD_3CH_2I, and C_2D_5I. These processes are the most rapid reported for association reactions, the various individual values falling within the limits 0.33×10^{-24} (CH_3I) and 10.1×10^{-24} cm^6 molecule^{-2} sec^{-1} (C_2H_5I). The temperature dependence of the stabilization coefficients in CH_3I and CD_3I was also measured over the range 220 ± 3 to 320 ± 1 K, as well as the efficiencies of other third bodies in the stabilization process. The differences observed for the variously labelled analogues are interpreted in terms of vibrational level (energy) depression upon deuteration, which affects the intrinsic lifetime of the collision complex.

Key words: Alkyl iodides; ion-molecule reactions; isotope effects; mass spectrometry; photo-ionization; rate constants.

1. Introduction

Several years ago [1][1] we reported a study of parent dimer cation formation in the methyl halides using high pressure photoionization mass spectrometry, which extended earlier work by Hamill and co-workers [2–4] concerned with association ion production in the ethyl and propyl bromides and iodides. The common characteristic of these systems is the high overall efficiency for the third order process

$$A^+ + 2A \rightarrow (A)_2^+ + A \qquad (1)$$

where A^+ denotes the parent molecular ion. More recently [5] we completed an investigation of dimer formation in low molecular weight aromatic hydrocarbons in which we found that production of $(C_6D_6)_2^+$ in C_6D_6 was a factor of 2.7 times faster than $(C_6H_6)_2^+$ formation in C_6H_6 at 295 K. In view of this pronounced isotope effect, we initiated a new photoionization study involving the methyl and ethyl iodides emphasizing the effect of isotopic substitution on the rate coefficient for process 1. These molecules were considered to be ideal systems for detailing some of the general factors influencing stabilization of ion-molecule complexes since >90 percent of the parent ions produced initially via photoionization are in $v = 0$ of the ground electronic state [6] (internal energy effects are minimal), the variously labelled deuterium analogues are readily available, and the room temperature stabilization coefficients are sufficiently high to permit experiments at reduced collision frequencies under controlled conditions.

2. Experimental Procedure

The NBS high pressure photoionization mass spectrometer equipped with a field-free reaction chamber was used for all experiments. Ionization of methyl iodide (I.P. $^2E_{1/2} = 9.54$ eV) and ethyl iodide (I.P. $^2E_{1/2} = 9.34$ eV, I.P. $^2E_{3/2} = 9.93$ eV) [7] was induced via photoabsorption at 123.6 nm (10.0 eV) using a Kr resonance lamp equipped with MgF_2 optics. Measurements other than those at 295 K were taken with a variable temperature modification described elsewhere [8].

3. Results

3.1. General Behavior

Typical composite spectra found for methyl and ethyl iodides as a function of pressure are given in figure 1 for CD_3I

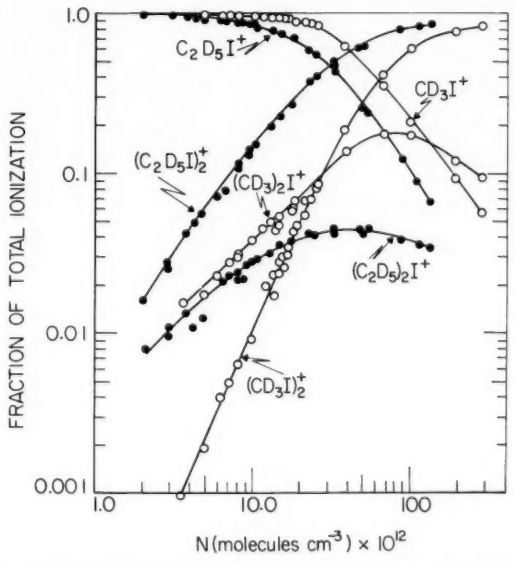

FIGURE 1. *Composite spectra obtained in photoionized* CD_3I *and* C_2D_5I *as a function of concentration.*

* This work was partially supported by ERDA.

[1] Figures in brackets indicate the literature references at the end of this paper.

and C_2D_5I. In every system the competing reactions

$$RI^+ + RI \underset{k_{-2}}{\overset{k_2}{\rightleftarrows}} (RI)_2^{+*} \quad (2)$$

followed by

$$(RI)_2^{+} \rightarrow R_2I^+ + I \quad (3)$$

or

$$(RI)_2^{+*} + RI \rightarrow (RI)_2^{+} + RI \quad (4)$$

where RI = methyl or ethyl iodide, were observed. Process 2 involves bimolecular formation of a transient collision complex $(RI)_2^{+*}$, which either dissociates to reform reactants or eliminates an iodine atom (process 3) at lower densities. At higher densities collisional stabilization (process 4) is facilitated, as indicated in figure 1 by the rapid formation of $(CD_3I)_2^+$ and $(C_2D_5I)_2^+$ and the concurrent decrease in the relative fractional yields of the respective dialkyliodium ions.

3.2. Reaction Rates

Rate coefficients for process 3 at 295 K were derived from the initial slopes of the growth curves found for R_2I^+ when the respective fractional yields were plotted in semilogarithmic form versus RI concentration. Residence times (τ's) for various RI^+ ions at the zero pressure limit were approximated by first evaluating average τ's for several ions of differing *m/e* ratios at 295 K under molecular flow conditions (<1–2 millitorr)[2] using calibration reactions [9] and assuming the usual (mass)$^{1/2}$ dependence for relative τ's. Calibration reactions included $t-C_4H_9^+ + CH_3NH_2 \rightarrow CH_3NH_3^+$ ($k = 1.30 \pm 0.15 \times 10^{-9}$),[3] $C_3H_7^+ + i-C_4H_{10} \rightarrow C_4H_9^+$ ($k = 4.2 + 0.2 \times 10^{-10}$), $C_3H_6^+ + C_3H_6 \rightarrow$ products ($k = 8.0 \pm 0.5 \times 10^{-10}$), and $NH_3^+ + NH_3 \rightarrow NH_4^+$ ($k = 1.9 \pm 0.2 \times 10^{-9}$). Third order stabilization coefficients (process 4) were calculated from the initial slopes of the logarithm[2] of the fractional intensities of $(RI)_2^+$ versus (concentrations) using the same respective τ's for the various RI^+ ions. Residence times at other temperatures were calculated by applying the appropriate velocity corrections.

3.3. Methyl Iodides

Rate coefficients for production of dialkyliodium ions in CH_3I, CD_3I, and CH_3-CD_3I (1:1) mixtures at 295 K are given in table 1, along with values for CH_3I and CD_3I at 220 ± 3 and 320 ± 1 K. Within the indicated reproducibility limits, the coefficients for $(CH_3)_2I^+$ formation in CH_3I and $(CD_3)_2I^+$ in CD_3I were invariant at 2.4 ± 0.1 and 2.25 ± 0.1 × 10^{-11}, respectively, over this temperature range. The overall 295 K coefficient for production of $(CX_3)_2I^+$ in CH_3I-CD_3I (1:1) mixtures was found to be 2.3 ± 0.2 × 10^{-11}. Products indicating isotopic scrambling such as $(CH_2D)(CH_3)I^+$, $(CD_2H)(CH_3)I^+$, etc., were not observed; the only second order products detected were $(CH_3)_2I^+$, $(CH_3)(CD_3)I^+$, and $(CD_3)_2I^+$, with an essentially statistical distribution (0.26:0.50:0.24).

In contrast to the near equivalency of the halogen elimination rates, substantial isotope effects were found in the third order coefficients for collisional stabilization of $(CX_3I)_2^{+*}$ (X = H or D). Data for CH_3I, CD_3I, and CH_3I-CD_3I (1:1) mixtures are shown in figure 2, which gives the appropriate $(CX_3I)_2^+/(CX_3)_2I^+$ ratios versus CX_3I concentration. Relative stabilization efficiencies are given by the slope ratios after correction for the slight differences found in the production rates for $(CX_3)_2I^+$, and were determined to be 1.0, 1.8(3), and 2.8(0) in CH_3I-CD_3I (1:1), and CD_3I respectively. Absolute values, as well as those determined at 220 ± 3 and 320 ± 1 K in CH_3I and CD_3I, are listed in table 1. The isotopic compositions of the $(CX_3I)_2^+$ dimer ions formed in a (1:1) CH_3I-CD_3I mixture as a function of concentration and percent reaction of CX_3I^+ are given in figure 3. Again no evidence was found for hydrogen-scrambled species such as $(CH_2D)(CD_3)_2^+$, etc.; i.e., the methyl groups retain their isotopic integrity during stabilization.

A number of measurements were also taken to estimate the stabilization efficiencies for other third bodies relative to methyl iodide itself. These results, which were obtained in mixtures containing ~5 percent CH_3I or CH_3I in the bulk additive, are shown in figure 4. Approximate relative values in CH_3I were derived from the additive concentration at which the intensity of $(CH_3I)_2^+$ was equal to that for $(CH_3)_2I^+$.

[2] 1 torr = 133.32 Nm^{-2}.
[3] Bimolecular units are cm^3 $molecule^{-1}$ s^{-1}.

TABLE 1. *Rate coefficients for second and third order reactions in methyl and ethyl iodide*

System	Temp. (K)	$k(R)_2I^{+a}$	$k(RI)_2{}^{+b}$	Relative $k(RI)_2{}^{+c}$
CH_3I	295 ± 1	2.37 ± 0.12 × 10^{-11}	0.33 × 10^{-24}	1.0
CH_3I	220 ± 3	2.46 ± 0.25 × 10^{-11}	0.45 × 10^{-24}	1.0
CH_3I	320 ± 1	2.37 ± 0.05 × 10^{-11}	0.24 × 10^{-24}	1.0
CD_3I	295 ± 1	2.23 ± 0.05 × 10^{-11}	0.94 × 10^{-24}	2.8
CD_3I	220 ± 3	2.04 ± 0.12 × 10^{-11}	1.26 × 10^{-24}	2.8
CD_3I	320 ± 1	2.16 ± 0.12 × 10^{-11}	0.67 × 10^{-24}	2.8
CH_3I-CD_3I (1:1)	295 ± 1	2.3 ± 0.1 × 10^{-11}	0.61 × 10^{-24}	1.8
C_2H_5I	295 ± 1	2.0 ± 0.1 × 10^{-11}	4.1 × 10^{-24}	1.0
CH_3CD_2I	295 ± 1	2.0 ± 0.1 × 10^{-11}	5.3 × 10^{-24}	1.28
CD_3CH_2I	295 ± 1	2.0 ± 0.1 × 10^{-11}	7.4 × 10^{-24}	1.79
C_2D_5I	295 ± 1	2.0 ± 0.1 × 10^{-11}	10.1 × 10^{-24}	2.44
C_6H_6	295 ± 1		0.194 × 10^{-24}[d]	1.0
C_6D_6	295 ± 1		0.526 × 10^{-24}[d]	2.71

[a] Units are cm^3 $molecule^{-1}$ s^{-1}.
[b] Units are cm^6 $molecule^{-2}$ s^{-1}.
[c] Relative value taking $k = 1.0$ for unlabeled analogue at that temperature.
[d] Values taken from Reference 5.

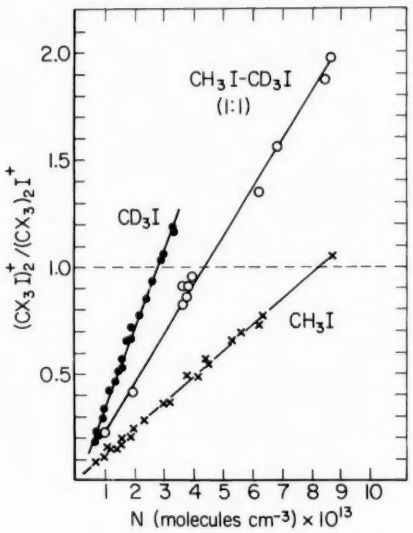

FIGURE 2. $(CX_3I)_2^+/(CX_3)_2I^+$ *ratio* (X = H or D) *versus concentration in* CH_3I, CH_3I-CD_3I *mixtures* (1:1), *and* CD_3I.

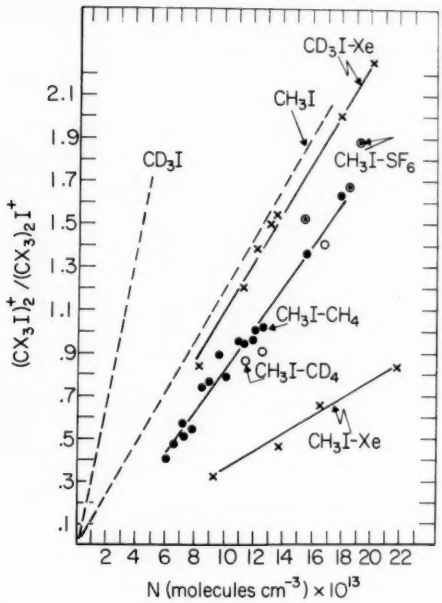

FIGURE 4. $(CX_3I)_2^+/(CX_3)_2I^+$ *ratio* (X = H or D) *versus concentration of added* CH_4, CD_4, Xe, *and* SF_6.

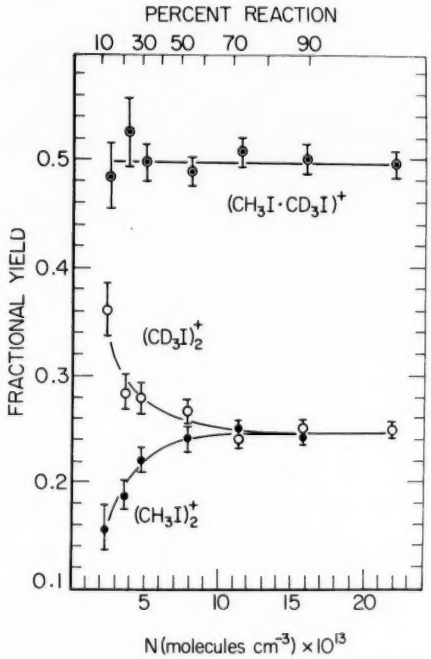

FIGURE 3. *Fractional yields of* $(CH_3I)_2^+$, $(CH_3I-CD_3I)^+$, *and* $(CD_3I)_2^+$ *versus concentration in* CH_3I-CD_3I *mixtures* (1:1).

Taking 1.0 as the efficiency for CH_3I as M in the overall reaction

$$CX_3I^+ + CX_3I \rightarrow (CX_3I)_2^{+*} \xrightarrow{M} (CH_3I)_2^+ + M \qquad (5)$$

(X = H or D) relative experimental values of 0.68 ± 0.1, 0.65 ± 0.1, 0.31 ± 0.03, 0.87 ± 0.13 were obtained for CH_4, CD_4, Xe, and SF_6 respectively. Mixtures of Xe with CD_3I gave an efficiency for Xe of 0.30 ± 0.03 relative to CD_3I = 1.0 in pure CD_3I. The experimentally determined efficiencies were then modified to take into account the differences in collision frequencies between $(CX_3I)_2^{+*}$ and CX_3I, CH_4, etc., which can be calculated directly from Langevin [10] or ADO theory [11]. After applying the appropriate corrections, the relative third-body efficiencies were found to be CH_3 = 1.0, CH_4 = 0.57 ± 0.1, CD_4 = 0.55 ± 0.1, Xe = 0.52 ± 0.05, and SF_6 = 1.45 ± 0.22 in CH_3I. Again, taking CD_3I = 1.0, the relative value for Xe in CD_3I was determined to be 0.51 ± 0.05, which is equivalent to that derived for Xe in CH_3I.

3.4. Ethyl Iodides

Measurements in C_2H_5I, CH_3CD_2I, CD_3CH_2I, and C_2D_5I were taken at 295 K only. The rate coefficients for production of diethyliodium ions, $(C_2X_5)_2I^+$, were determined to be 2.0 ± 0.15 × 10^{-11} for all analogues. Stabilization rates (process 4) were again found to increase with increasing deuteration in the order C_2H_5I = 1.0, CH_3CD_2I = 1.28, CD_3CH_2I = 1.79, and C_2D_5I = 2.44. On an absolute scale, the third order coefficient for stabilization of $(C_2H_5I)_2^{+*}$ was deter-

mined to be 4.1×10^{-24}, or a factor of 12 higher than that observed in CH_3I (see table 1).

Biomolecular formation of long-lived dimeric ions was also directly detected in the ethyl iodides. Figure 5, which gives plots of $(C_2X_5I)_2^+/(C_2X_5)_2I^+$ versus concentration, indicates non-zero intercepts for all of the analogues, including C_2H_5I. Observation of these entities corresponds to lifetimes for detected $(C_2X_5I)_2^{+*}$ on the order of several milliseconds, which is the total transit time in our apparatus for ions of these approximate masses. The plots also exhibit downward curvature at higher conversions (higher densities), which is ascribed to formation of undetected trimeric ions having masses beyond the operational range of the quadrupole mass filter used in these experiments ($\sim m/e$ 400). Association ions such as $[(C_2H_5)_2I \cdot C_2H_5I]^+$, etc., which correspond to solvation of dialkyliodium ions, were not detected in either the ethyl or methyl iodides at pressures up to 0.1 torr, which was the maximum in the present study.

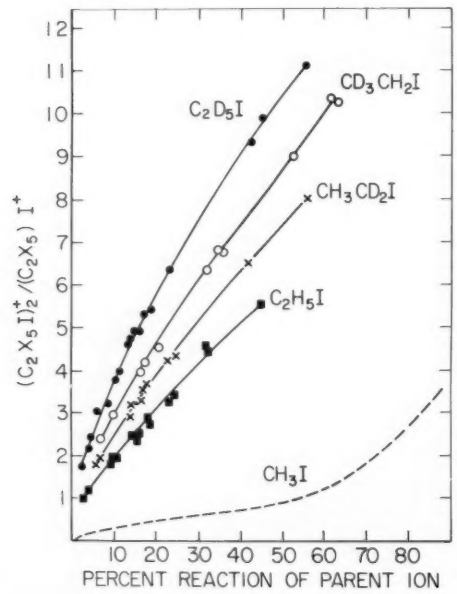

FIGURE 5. *$(C_2X_5I)_2^+/(C_2X_5)_2I^+$ ratio (X = H or D) as a function of the extent reaction of C_2H_5I, CH_3CD_2I, CD_3CH_2I, and C_2D_5I.*

4. Discussion

As expected [12] for association reactions, a negative temperature coefficient was observed for the third order stabilization of $(CX_3I)_2^+$ in CH_3I and CD_3I (see table 1). However, the variation with temperature does not yield a straight line when k(stab.) is plotted versus T^{-n} for any values of n from 0.1 to 5, although unique fits of this form have been obtained for other systems. The lack of a unique functional form or profound temperature effect in methyl iodide is ascribed to the fact that the stabilization coefficients are extremely high over the range studied, so that no substantial dependence would be anticipated except at much higher temperatures (other studies [12] have been restricted to association reactions having 300 K stabilization coefficients 2–5 orders of magnitude slower than those characteristic of the alkyl iodides). In addition, the ratios of the third order coefficients in CD_3I and CH_3I at any temperature are constant at 2.8, which would be expected since the physical factors involved in the stabilization mechanism are presumably the same for both analogues.

Consideration of the relative stabilization efficiencies for the labelled ethyl iodides (table 1) indicates that deuteration on either the methyl or methylene carbon facilitates stabilization (comparison of CH_3CD_2I and CD_3CH_2I with C_2H_5I or C_2D_5I). Based on the relative values, attempts were made to calculate the effect of D substitution on both carbons choosing various trial isotope effects at each site. However, no unique self-consistent set of relative or individual contributions compatible with the experimental ratios could be computer-generated due to the fact that all models predicted a substantially higher relative value for CH_3CD_2I ($\geq$15 percent higher, which was considered outside the possible error in measurement). The only common result of all calculations was that substitution of D for H on the methylene carbon has a slightly lower effect ($\sim$10 percent) than exchanging a D for an H on the methyl group.

Among all of the active vibrational fundamentals in the alkyl halides, the methyl deformation and the methylene rocking modes (ethyl iodide), which lie substantially lower in energy than the C—H stretch, are the most easily excited. The effect of deuteration is to reduce the C—H stretching, CH_3 deformation, and CH_2 rocking frequencies by a factor of $\sim$0.3, while the C—I stretching frequency remains essentially unaffected [13]. The large differences observed in the third order stabilization coefficients for the variously labeled iodides are therefore ascribed to a depression of the deformation and rocking frequencies (shift to lower energies and higher state densities) upon deuterium substitution. This depression is manifested by an increased dissociative lifetime for the unstable initial ion-molecule collision complex, as evidenced by the fact that the relative yields of the bimolecularly produced ethyl iodide dimer ions which survived ion transit (extrapolated zero conversion intercepts in figure 4) also appear to increase with increasing deuteration. The lack of isotopic scrambling also indicates that both reacting partners retain their structural integrity within the excited collision complex, facilitating a favorable energy level match between the third body and the excited dimeric ion in the pure halide systems. This favorable condition would account for the magnitude of the stabilization coefficients, which are the highest recorded for third order association reactions at 295 K.

With respect to the measured stabilization efficiencies of other third bodies relative to methyl iodide itself, it is somewhat surprising that methane and Xe exhibit the same relative value ($\sim$0.5) since Xe can only deactivate via vibrational to translational energy conversion. Also, CH_4 and CD_4 are found to be equally effective even though there is a 30 percent decrease in the vibrational frequencies for CD_4 relative to CH_4, which should increase the probability for energy transfer. The low overall efficiency found for methane may be due either to the fact that the duration of the collision between excited dimeric ions and methane is less than the duration with Xe, SF_6, or CH_3I (based on relative velocity considerations), or that the active vibrational frequencies in

the excited dimers are substantially lower than those associated with the methane fundamentals ($\geq \sim 1000\ cm^{-1}$). Sulfur hexafluoride has both a high mass (146 a.m.u.) and several very low-lying vibrational modes ($<800\ cm^{-1}$) which accounts for the observation that it is slightly more effective than CH_3I itself as a deactivator for $(CH_3I)_2^+$.

In conclusion we would like to emphasize the intriguing fact that the stabilization efficiencies for CD_3I, C_2D_5I, and C_6D_6 (see table 1) are all 2.6 ± 0.2 times higher than those for the perprotonated analogues. Whether this equivalence is fortuitous, is due to common physical property of the excited dimer cation in these particular systems, or is generally characteristic of polyatomic organic ion-molecule collision complexes which have no highly exothermic or favorable fragmentation channels, deserves further study.

5. References

[1] Sieck, L. W., and Gorden, R., Jr., Int. J. Chem. Kinet. **5,** 445 (1973).
[2] Pottie, R. F., and Hamill, W. H., J. Phys. Chem. **63,** 877 (1959).
[3] Pottie, R. F., Barker, R., and Hamill, W. H., Radiat. Res. **10,** 664 (1959).
[4] Theard,L. P., and Hamill, W. H., J. Am. Chem. Soc. **84,** 1134 (1962).
[5] Sieck, L. W., and, Gordon, R., Jr., Int. J. Mass Spectrom. Ion Phys. **19,** 269 (1976).
[6] Turner, D. W., Baker, C., Baker, A. D., and Brundle, C. R., Molecular Photoelectron Spectroscopy, (Wiley-Interscience, London, 1970.)
[7] Where ionization potentials (I.P.'s) are given, the values are taken from Rosenstock, H. M., Draxl, K., Steiner, B. W., and Herron, J. T., Energetics of Gaseous Ions, J. Phys. Chem. Ref. Data **6,** Suppl. 1 (1977).
[8] Sieck, L. W., to be published.
[9] Sieck, L. W., and Lias, S. G., J. Phys. Chem. Ref. Data **5**(4), (1976).
[10] Gioumousis, G., and Stevenson, D. P., J. Chem. Phys. **29,** 294 (1958).
[11] Su, T., and Bowers, M. T., J. Chem. Phys. **58,** 3027 (1973); Su, T., and Bowers, M. T., Int. J. Mass Spectrom. Ion Phys. **12,** 347 (1973).
[12] See, for example, Porter, R. F., in, Interactions Between Ions and Molecules, Ausloos, P., Ed., NATO Advanced Study Institutes, Series B Physics **6,** 231 (1975).
[13] See, for example, Pinchas, S., and Laulicht, I., Infrared Spectra of Labelled Compounds, (Academic Press, N.Y., 1971.)

(Paper 81A2&3-929)

JOURNAL OF RESEARCH of the National Bureau of Standards—A. Physics and Chemistry
Vol. 81A, Nos. 2 and 3, March–June 1977

Solubility of $Ca_5(PO_4)_3OH$ in the System $Ca(OH)_2$-H_3PO_4-H_2O at 5, 15, 25, and 37 °C*

H. McDowell, T. M. Gregory,*** and W. E. Brown******

Institute for Materials Research, National Bureau of Standards, Washington, D.C. 20234

(January 19, 1977)

Solubility isotherms of hydroxyapatite, $Ca_5(PO_4)_3OH$ (OHAp), prepared by titrating a boiling aqueous suspension of $Ca(OH)_2$ with 0.5 *M* H_3PO_4, were determined in the ternary system $Ca(OH)_2$-H_3PO_4-H_2O at 5, 15, 25, and 37 °C in the pH range 3.7–6.7 by equilibration with dilute H_3PO_4 solutions. The solubility product K_s, determined as a function of temperature by a generalized least-squares procedure from 41 experimental points, is given by the equation

$$\log K_s = -8219.41/T - 1.6657 - 0.098215T.$$

The values of K_s and its dispersion at 25 and 37 °C are 3.04 (0.25) and 2.35 (0.27) $\times 10^{-59}$. There is a maximum in K_s near 16 °C, which may be due to the form of temperature dependence found earlier for the stability constants of the ion pairs $CaH_2PO_4^+$ and $CaHPO_4^0$.

The relative positions of the isotherms show that OHAp has a negative thermal coefficient of solubility. Thermodynamic functions for the dissolution of the salt are reported.

The solubility data previously reported by others for OHAp at 25 °C were reviewed. The solubility products obtained by three of these investigators were comparable with our value of 3.0×10^{-59}; their data were re-evaluated by the method described here. We conclude that the best value for the solubility product at 25 °C is 4.7 (2.0) $\times 10^{-59}$.

Key words: Dissolution; hydroxyapatite; ion pairs; solubility; solubility isotherms; solubility product; thermal coefficient of solubility; thermodynamics; tooth mineral.

1. Introduction

Hydroxyapatite, $Ca_5(PO_4)_3OH$, is an important component of bones and teeth and of many industrial products. Despite the profusion of papers on the chemistry of hydroxyapatite [1–5][1] the exact solubility of this salt is still questioned. Its existence as a compound with a fixed crystalline form having a well-defined solubility product has been disputed [2, 4]. This is due, in part, to the fact that its preparations vary in composition. Recently it has been found that this salt exists in two modifications, one monoclinic, the other (statistically) hexagonal [6]. Some of the difficulties encountered in solubility measurements on hydroxyapatite and the experimental principles that can be used to overcome them are described in greater detail elsewhere [7]. Much of the uncertainty regarding the solubility of the salt also stems from a combination of factors related to the difficulty of preparing pure samples and to the fact that it usually precipitates in a very finely divided state so that contamination by adsorption and occlusion of impurities readily occurs. Solubility measurements on this salt are difficult because its relatively low solubility and its slow rate of equilibration from supersaturation make the establishment of equilibrium uncertain. The solubility data previously reported on this salt have all been for 25 °C.

In making solubility measurements on hydroxyapatite workers have used two approaches. On the one hand, precipitates formed from aqueous solutions at low temperatures have been separated and redispersed directly in an equilibrating medium [1]. On the other, the solubility measurements have been made following treatment of the precipitate by exposure to elevated temperatures [5]. Both procedures have yielded apatites with a constant solubility product over a wide range of aqueous compositions, although the two types of treatments give materials with somewhat different values for the solubility product. Here we report the results of solubility measurements at 5, 15, 25, 37 °C on a precipitate that was not heat treated (except for drying at 110 °C). A precipitated product was used because it should be more representative of the apatites found in biological and other natural systems. The data were used to calculate solubility products and thermodynamic functions for this salt taking into account ion pair formation. In addition to the work reported here, we have re-examined solubility data obtained at 25 °C in other studies [8–10] of hydroxyapatites prepared in a manner similar to the one used here. The adjustment procedure [5, 11–15] used in treating the data is unusually rigorous and provides a superior assessment of the reliability of the derived constants.

2. Experimental Methods and Materials

2.1 Preparation of Materials

Hydroxyapatite was prepared by titrating a boiling aqueous suspension of $Ca(OH)_2$ with 0.5 *M* H_3PO_4. The $Ca(OH)_2$ suspension was prepared by adding 194 g of CaO, made by calcination of $CaCO_3$ for 24 hours at 1000 °C, to seven liters of freshly boiled distilled water. The titration was carried out

* This investigation was supported in part by Research Grant DE00572 to the American Dental Association Health Foundation from the National Institute of Dental Research, and is part of the dental research program conducted by the National Bureau of Standards in cooperation with the American Dental Association.

** Department of Chemistry, Federal City College, Washington, D. C.
*** Research Associate, American Dental Association Health Foundation Research Unit, National Bureau of Standards, Washington, D. C. 20234
**** Director, American Dental Association Health Foundation Research Unit, National Bureau of Standards, Washington, D. C. 20234

[1] Figures in brackets indicate the literature references at the end of this paper.

in a 15 liter, Teflon-coated,[2] stainless steel pot equipped with a gold plated stirrer, a reflux condenser protected from the atmosphere by a CO_2-absorbing trap, and ports for introducing N_2 and the titrant. The H_3PO_4 solution was added to the stirred suspension at a rate of 1 mL/min until a Ca/P ratio of 1.70 was reached. After the titration was complete, boiling and stirring were continued for two days. The solid was then allowed to settle and the supernatant liquid was removed by siphoning. Five liters of freshly boiled distilled water were then added to the reaction vessel and the resulting suspension was boiled and stirred for two days to remove the $Ca(OH)_2$. The supernatant was then siphoned off and the washing process was repeated three times with distilled water and finally with 0.001 *M* H_3PO_4. The slurry was then transferred to a three liter Erlenmeyer flask and dried in an oven at 110 °C under a stream of dry N_2.

Doubly crystallized phosphoric acid hemihydrate, $2H_3PO_4 \cdot H_2O$, and freshly boiled distilled water were used to prepare a 1 *M* stock solution. The H_3PO_4 solutions used for the titration and equilibrations were prepared by diluting the stock solution with freshly boiled distilled water.

Examination of the solid with a petrographic microscope gave a mean refractive index of 1.636; this agrees with the values usually found for precipitated $Ca_5(PO_4)_3OH$ [5]. The material was free of extraneous phases but the crystallites were too small to be resolved. The infrared spectrum of the material indicated that it was crystalline and essentially free of carbonate. The BET surface area[3] of the solid was 16.7 m^2/g. Chemical analysis yielded: Ca, 39.25 percent and P, 18.13 percent. (Theoretical: Ca, 39.89 percent and P, 18.50 percent.) From the analytical results the molar Ca/P ratio of the solid was 1.67_3 with a standard error of 0.042.

2.2. Equilibration Experiments

To each of a series of glass-stoppered bottles, 4 g of hydroxyapatite were added and washed several times with small volumes of the H_3PO_4 solution with which the salt was to be equilibrated. About 125 mL of this acid were then added and the bottle was sealed with paraffin wax and rotated end-over-end at 7 rpm in a thermostatted water bath held to within 0.1 °C of the selected temperature. In preliminary experiments lasting up to 21 days, it was shown that equilibrium was attained within 7 days. Thereafter, solutions equilibrated for at least 7 days were filtered, using a syringe equipped with a millipore filter, and the pH values and calcium and phosphorus concentrations of the filtrates were determined.

2.3. Analyses

Calcium, phosphorus, and pH were determined using the methods and instruments described in earlier publications [11, 15]. The estimated errors for Ca (1.5%), P (1.0%), and pH (0.015) guided the assignment of weights (sec. 5).

[2] In order to adequately describe materials and experimental procedures, it was occasionally necessary to identify commercial products by manufacturer's name or label. In no instances does such identification imply endorsement by the National Bureau of Standards, nor does it imply that the particular product or equipment is necessarily the best available for the purpose.

[3] The surface area measurement was made by Dr. W. V. Loebenstein, Dental & Medical Materials Section, NBS.

3. Calculations

Details of the method used for the calculation of solubility products and ion pair association constants by generalized least squares have been reported previously [11]. The specific equations and conditions needed to describe equilibrium systems containing solid $Ca_5(PO_4)_3OH$ are given here. Curly brackets will be used to denote equation, section and table numbers used in Reference [11]. The purpose of these calculations was to obtain the solubility product, K_s, of $Ca_5(PO_4)_3OH$ as a function of temperature, allowing for the presence of ion pairs, and to compute the adjusted values of the observations. The values used for the association constants of the ion pairs $CaHPO_4^0$ and $CaH_2PO_4^+$ are those given in table {12}[4]. In 30 systems (out of 41 reported here) the weighted sum of squares of residuals of four observations per system (concentration of total calcium, Ca; and total phosphorus, P; initial phosphoric acid concentration, P_0; and pH) was minimized subject to three condition functions: saturation with respect to $Ca_5(PO_4)_3OH$, electroneutrality, and congruent dissolution (sec. 5.2) of the salt. In the remaining 11 systems (3 at 5 °C, 5 at 15 °C, and 3 at 37 °C) the condition of congruent dissolution was omitted and the variable P_0 was accordingly not adjusted for these systems (see discussion). The solubility product K_s was computed by the least squares estimation of the coefficients A_j in the expression $\ln K_s = A_1/T + A_2 + A_3T$, where T is the temperature in Kelvins (eq {16}).

3.1. Balance Equations, Solubility Product, and Activity Coefficients

The equations of mass balance are given by eqs {1} to {4}. Activity coefficients (Debye-Hückel) and ionic strength are defined in eqs {10} and {11a}. (All quantities were calculated on the molar basis.) The ionic activity product is defined for all $Ca_5(PO_4)_3OH$ as

$$K_{HA} = (Ca^{2+})^5(PO_4^{3-})^3(OH^-) \quad (1)$$

where the first factor (activity of ionic calcium) and the second (activity of orthophosphate ion) are defined as follows:

$$(Ca^{2+}) = (Ca - \tau)/g_{Ca} \quad (2a)$$

$$(PO_4^{3-}) = (P - \tau)k_3/(H^+)N. \quad (2b)$$

The quantities g_{Ca}, k_3, and N are defined in the equations of [11] already referred to; $(H^+) = 10^{-pH}$, and τ is the sum of ion pair concentrations, eq {8}. The apparent solubility product K'_{HA} was calculated taking τ to be zero.

3.2. Condition Functions, Parameters, and Standard Deviation

The condition functions imposed on the systems reported here have been enumerated above. The electroneutrality condition is given by eq {14}. The other two conditions are defined here as:

(1) Saturation with respect to $Ca_5(PO_4)_3OH$

[4] The ion pair $CaPO_4^-$ need not be considered for pH < 8.

$$(Ca^{2+})^5(PO_4^{3-})^3(OH^-) - K_s = 0, \quad (3)$$

where the activities are given by eqs (2a) and (2b), and by $(OH^-) = k_w/(H^+)$, where k_w is the dissociation constant of water;

(2) Congruent dissolution of $Ca_5(PO_4)_3OH$

$$Ca/(P - P_0) - R = 0, \quad (4)$$

where R is the expected value of the ratio, 5/3.

Since the ion pair association constants were not subject to adjustment in these calculations, the number of constants is just one (K_s); the number of adjustable parameters (p) is one or three corresponding to separate ($ln\ K_s = A_2$) or combined ($ln\ K_s = A_1/T + A_2 + A_3T$) data adjustments, respectively (see sec. {3.5b}). The standard deviation is given by eq {22} with the denominator (degrees of freedom) in that equation replaced by $\Sigma_t(2N_t + 3M_t) - p$. Here N_t and M_t denote the number of systems at temperature t constrained by 2 and 3 conditions, respectively.

4. Results

4.1. Solubility and Solubility Product

The compositions of saturated $Ca_5(PO_4)_3OH$ solutions at 5, 15, 25, and 37 °C are presented in tables 1 through 4. At all temperatures except 25 °C there were one or more systems whose dissolution ratios (col. 5) were inconsistent with congruent dissolution (expected value = 5/3). These data, however, yielded values (eq (1)) of the apparent solubility product, K'_{HA} (col. 6) which clearly belonged to the population being sampled. These points were therefore included in the analysis (see sec. 5.4). The values of K_{HA} computed with the data shown in these tables and with the assumption of ion pairs are shown in the last column of the tables as K^0_{HA}. It is noteworthy that in the more acid solutions, values of K'_{HA} that might be suspected to represent outliers on the high side are better behaved when ion pairs are taken into account.

The data adjustments as found for the combined data are summarized in tables 5 through 8. Values of the ionic strength, μ, shown in column 5, indicate the broad range of solution compositions included in the investigation. The data segregated in the lower portion of the tables were adjusted without the congruent dissolution condition (eq (4)) and hence the initial acid concentration, P_0, of these systems was ignored in the adjustment. The ratios $Ca/(P - P_0)$ for the other systems computed with the untruncated adjusted data and subsequently rounded to 6 digits are uniformly equal to 1.66667. Similarly, the adjusted values of K_{HA} at temperature T in the last columns are identical (to five digits or better) to the value of the least-squares constant K_s, which is given to sufficient accuracy by eq (5):

$$\log K_s = -8219.41/T - 1.6657 - 0.098215\,T. \quad (5)$$

Values of the solubility product, its logarithm, and the associated standard errors (eq {25}) at the four temperatures are listed in table 9. (The standard error of the adjustment, s, is discussed in sec. 5.1.)

TABLE 1. *Solubility of hydroxyapatite at 5 °C Unadjusted quantities*

Initial Acid P_0 $M \times 10^3$	Composition of equil. solns pH	Ca $M \times 10^3$	P $M \times 10^3$	$\frac{Ca}{P-P_0}$	$K'_{HA} \times 10^{59}$	$K°_{HA} \times 10^{59}$
0.846	5.91_2	0.630	1.19_5	1.81	3.73	3.17
1.04_4	5.81_3	.748	1.45_5	1.82	3.03	2.56
3.22	5.26_9	2.40	4.75	1.57	2.80	2.14
6.22	5.02_2	4.46	8.88	1.68	4.28	2.92
10.2_4	4.79_8	7.45	14.6_6	1.69	3.87	2.32
26.0	4.45_9	18.6	37.3	1.65	7.64	3.10
26.0	4.45_6	18.7	36.7	1.75	7.11	2.92
26.0	4.44_0	18.7	36.9	1.72	5.58	2.29
0.410	6.29_5	0.307	0.544	[a](2.29)	5.18	4.48
.410	6.29_4	.302	.540	(2.32)	4.66	4.04
.410	6.29_0	.297	.532	(2.44)	3.88	3.37

[a] Value inconsistent with congruent dissolution.

TABLE 2. *Solubility of hydroxyapatite at 15 °C Unadjusted quantities*

Initial Acid P_0 $M \times 10^3$	Composition of equil.solns. pH	Ca $M \times 10^3$	P $M \times 10^3$	$\frac{Ca}{P-P_0}$	$K'_{HA} \times 10^{59}$	$K°HA$ 10^{59}
1.04_4	5.70_2	0.751	1.47_7	1.73	5.25	4.75
1.89	5.44_2	1.31	2.59	1.87	5.22	4.61
6.25	4.90_0	4.36	8.62	1.84	4.78	3.76
10.4_0	4.67_1	7.32	14.6_1	1.74	4.33	3.10
25.9	4.31_4	18.0	36.1	1.76	5.53	3.07
25.9	4.31_4	18.3	36.3	1.76	5.94	3.29
25.9	4.30_7	18.6	36.7	1.72	5.84	3.22
0.132	6.66_3	0.111	0.177	(2.47)	3.47	3.25
.433	6.20_3	.259	.460	(9.59)	3.27	3.04
.433	6.19_1	.262	.472	(6.72)	3.04	2.83
.433	6.16_1	.281	.521	(3.19)	3.57	3.31
.857	5.80_2	.583	1.10_4	(2.36)	3.45	3.16

TABLE 3. *Solubility of hydroxyapatite at 25 °C Unadjusted quantities*

Initial Acid P_0 $M \times 10^3$	Composition of equil.solns. pH	Ca $M \times 10^3$	P $M \times 10^3$	$\frac{Ca}{P-P_0}$	$K'_{HA} \times 10^{59}$	$K°_{HA} \times 10^{59}$
0.130	6.46_6	0.117	0.203	1.60	2.77	2.63
.414	5.96_2	.306	.599	1.65	2.81	2.65
.994	5.53_6	.695	1.39_1	1.75	1.72	1.61
5.11	4.84_2	3.52	7.30	1.61	3.68	3.11
10.8_9	4.52_3	7.53	15.5_2	1.63	4.01	3.07
20.9	4.27_1	14.5	29.3	1.73	5.15	3.45
20.9	4.26_3	14.5	29.5	1.69	4.61	3.08
53.0	3.92_2	36.0	73.6	1.75	6.35	3.14
53.0	3.92_1	35.5	72.4	1.83	5.70	2.84

TABLE 4. *Solubility of hydroxyapatite at 37 °C Unadjusted quantities*

Initial Acid P_0 $M \times 10^3$	Composition of equil.solns. pH	Ca $M \times 10^3$	P $M \times 10^3$	$\frac{Ca}{P-P_0}$	$K'_{HA} \times 10^{59}$	$K°_{HA} \times 10^{59}$
0.994	5.43_6	0.686	1.40_3	1.68	3.02	2.81
1.92	5.12_9	1.35	2.69	1.75	3.07	2.80
1.92	5.10_7	1.34	2.75	1.61	2.21	2.02
10.8_9	4.35_7	7.56	15.6_3	1.59	2.44	1.92
20.9	4.10_1	14.7	29.8	1.65	3.01	2.11
52.9	3.75_4	35.6	73.9	1.70	3.30	1.78
0.140	6.40_4	0.0980	0.178	(1.32)	2.86	2.69
.433	5.94_0	.245	.471	(6.45)	3.13	2.94
4.21	4.79_4	2.83	5.66	(1.95)	2.92	2.56

TABLE 5. *Solubility of hydroxyapatite at 5 °C Adjusted quantities*

Initial Acid P_0 $M \times 10^3$	Composition of equil.solns.			$\mu \times 10^3$	$\frac{Ca}{P-P_0}$	$K_{HA} \times 10^{59}$
	pH	Ca $M \times 10^3$	P $M \times 10^3$			
0.834 (7)[b]	5.898 (7)	0.641(5)	1.219(10)	1.94	[a]1.67	2.92
1.023 (8)	5.806 (7)	.777(6)	1.489(12)	2.33	1.67	2.92
3.255 (26)	5.293 (7)	2.385(19)	4.686(38)	6.98	1.67	2.92
6.201 (50)	5.019 (7)	4.499(36)	8.900(72)	12.94	1.67	2.92
10.26 (8)	4.814 (7)	7.404(59)	14.70(12)	20.94	1.67	2.92
26.02 (21)	4.455 (7)	18.64(15)	37.20(30)	50.26	1.67	2.92
25.93 (21)	4.457 (7)	18.58(15)	37.07(30)	50.10	1.67	2.92
25.99 (21)	4.456 (7)	18.62(15)	37.16(30)	50.21	1.67	2.92
[c]*	6.272 (8)	0.301(4)	0.546(7)	0.939	*	2.92
*	6.276 (8)	.299(4)	0.541(7)	.932	*	2.92
*	6.283 (8)	.295(3)	0.533(7)	.920	*	2.92

[a] Machine value = 5/3 to seven significant figures.
[b] Standard error in the last digit(s) calculated by eq {26}.
[c] P_0 not adjusted.

TABLE 6. *Solubility of hydroxyapatite at 15 °C Adjusted quantities*

Initial Acid P_0 $M \times 10^3$	Composition of equil.solns.			$\mu \times 10^3$	$\frac{Ca}{P-P_0}$	$K_{HA} \times 10^{59}$
	pH	Ca $M \times 10^3$	P $M \times 10^3$			
1.029 (8)	5.668 (6)	0.770(6)	1.491(12)	2.33	1.67	3.23
1.843 (15)	5.406 (6)	1.354(11)	2.656(21)	4.05	1.67	3.23
6.141 (50)	4.883 (6)	4.431(35)	8.810(71)	12.97	1.67	3.23
10.32 (8)	4.669 (6)	7.400(59)	14.76(12)	21.39	1.67	3.23
25.68 (21)	4.312 (6)	18.28(15)	36.64(30)	51.13	1.67	3.23
25.77 (21)	4.311 (6)	18.35(15)	36.78(30)	51.30	1.67	3.23
25.91 (21)	4.309 (6)	18.44(15)	36.97(30)	51.56	1.67	3.23
*	6.665 (8)	0.110(1)	0.178(2)	0.366	*	3.23
*	6.210 (7)	.255(3)	.465(6)	.802	*	3.23
*	6.201 (7)	.260(3)	.475(6)	.816	*	3.23
*	6.158 (7)	.283(3)	.519(7)	.883	*	3.23
*	5.805 (7)	.579(7)	1.109(14)	1.76	*	3.23

TABLE 7. *Solubility of hydroxyapatite at 25 °C Adjusted quantities*

Initial Acid P_0 $M \times 10^3$	Composition of equil. solns.			$\mu \times 10^3$	$\frac{Ca}{P-P_0}$	$K_{HA} \times 10^{59}$
	pH	Ca $M \times 10^3$	P $M \times 10^3$			
0.1307(11)	6.475(6)	0.1179(8)	0.2014(16)	0.385	1.67	3.04
.4094(34)	5.958(6)	.3189(24)	0.6007(48)	.986	1.67	3.04
.978(8)	5.561(6)	.726(6)	1.414(11)	2.20	1.67	3.04
5.074(41)	4.832(6)	3.645(29)	7.261(58)	10.77	1.67	3.04
10.83(9)	4.516(6)	7.726(6)	15.46(12)	22.52	1.67	3.04
20.75(17)	4.259(6)	14.72(12)	29.58(24)	42.16	1.67	3.04
20.79(17)	4.258(6)	14.75(12)	29.65(24)	42.25	1.67	3.04
52.40(42)	3.913(6)	36.80(29)	74.48(60)	101.3	1.67	3.04
52.07(42)	3.916(6)	36.57(29)	74.02(60)	100.7	1.67	3.04

TABLE 8. *Solubility of hydroxyapatite at 37 °C Adjusted quantities*

Initial Acid P_0 $M \times 10^3$	Composition of equil. solns.			$\mu \times 10^3$	$\frac{Ca}{P-P_0}$	$K_{HA} \times 10^{59}$
	pH	Ca $M \times 10^3$	P $M \times 10^3$			
0.977(8)	5.411(8)	0.718(6)	1.408(11)	2.16	1.67	2.35
1.900(15)	5.111(8)	1.375(11)	2.725(22)	4.11	1.67	2.35
1.911(15)	5.109(8)	1.383(11)	2.741(22)	4.13	1.67	2.35
10.88(9)	4.365(8)	7.719(62)	15.51(13)	22.57	1.67	2.35
20.91(17)	4.107(7)	14.73(12)	29.75(24)	42.41	1.67	2.35
52.49(43)	3.765(7)	36.42(29)	74.34(60)	101.4	1.67	2.35
*	6.390(9)	0.101(1)	0.175(2)	0.325	*	2.35
*	5.925(9)	.247(3)	.468(6)	0.764	*	2.35
*	4.789(8)	2.835(35)	5.655(70)	8.41	*	2.35

TABLE 9. *Temperature dependence of the solubility product*

$\log K_s = -8219.41/T - 1.6657 - 0.098215\,T$ [eq (5)]		
°C	$\log K_s + 59$	$K_s \times 10^{59}$
5	0.4656	2.92
	(0.044)[a]	(0.30)
15	0.5090	3.23
	(0.033)	(0.25)
25	0.4835	3.04
	(0.036)	(0.25)
37	0.3716	2.35
	(0.049)	(0.27)

[a] Standard error.

Figure 1 illustrates the temperature dependence of the solubility product. The smooth curve represents eq (5) (95% confidence intervals come from table 9). The preliminary values of K_s from separate adjustments at the four temperatures (table 12) are shown for comparison. The values plotted in the figure as experimental points are those listed in column 7 of tables 1 through 4.

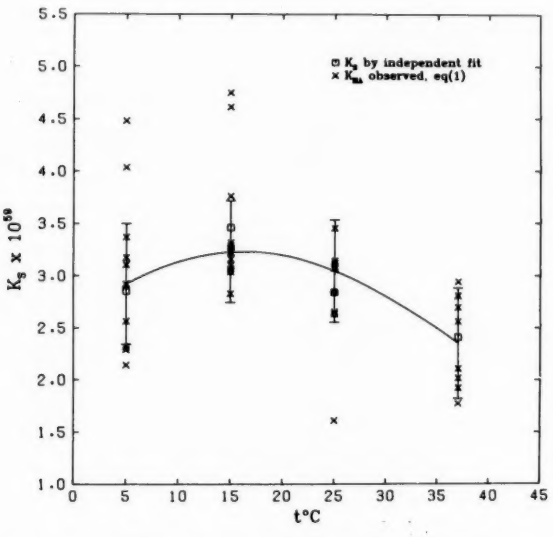

FIGURE 1. *Variation in the solubility product of hydroxyapatite as a function of temperature.*
The curve represents eq (5); the 95 percent confidence intervals come from table 9.

The solubility isotherms for $Ca_5(PO_4)_3OH$ are plotted in figure 2 in terms of log (total Ca concentration) against pH. The smooth curves were generated as described in reference [21]. The experimental points are from tables 1 through 4. The adjusted values of the observations (not indicated in the figure) lie on the curves. The relative positions of the curves and corresponding data sets indicate that the solubility of hydroxyapatite decreases with increasing temperature even though it can be seen from figure 1 that the solubility product does not decrease monotonically with temperature. This type of behavior has been previously established for $CaHPO_4 \cdot 2H_2O$ [11], $CaHPO_4$ [15], and β-$Ca_3(PO_4)_2$ [13].

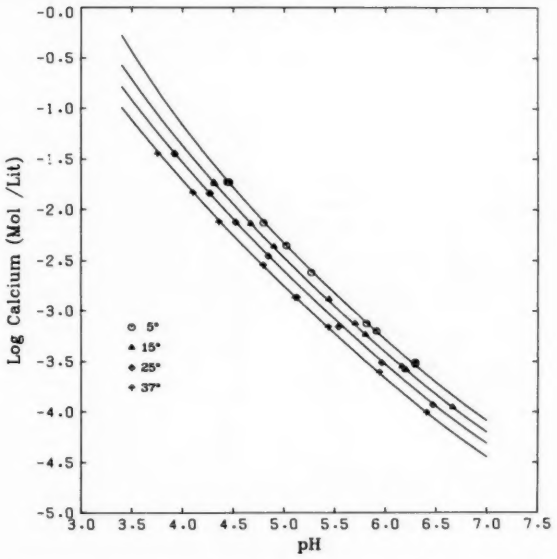

FIGURE 2. *Solubility isotherms (log calcium concentration versus pH) for hydroxyapatite in the system* $Ca(OH)_2$-H_3PO_4-H_2O *at 5, 15, 25, and 37 °C.*

4.2. Ion Pairs

The concentrations of the ion pairs $CaHPO_4^0$ and $CaH_2PO_4^+$ in saturated solutions of $Ca_5(PO_4)_3OH$ at 25 °C are given in table 10. These values[5] were computed in the adjustment procedure, making use of the known values [11] of the corresponding stability constants. The percentage of bound calcium (sum of ion pair conc. × 100/total Ca conc.) shown in column 4 is seen to increase markedly in the more acid solutions due to the rapid increase in the concentration of the ion $CaH_2PO_4^+$ (col. 3) with decreasing pH. The corresponding effect on the values of the "observed" solubility product, columns 6 and 7 of tables 1 through 4, is quite evident. (Values of the ion pair concentrations at the other temperatures are similar to those shown in table 10.)

TABLE 10. *Concentration of ion pairs and bound calcium at 25 °C*

pH	$[CaHPO_4^0]$ $M \times 10^3$	$[CaH_2PO_4^+]$ $M \times 10^3$	100 τ^a/Ca
6.475	0.0008(<1)[b]	0.0001(<1)	0.79(1)
5.958	.0022(<1)	.0008(<1)	.93(1)
5.561	.0045(1)	.0039(1)	1.18(1)
4.832	.0166(2)	.077(1)	2.80(2)
4.516	.0294(4)	.282(5)	4.61(3)
4.259	.0473(6)	.820(13)	7.06(4)
4.258	.0473(6)	.823(14)	7.07(4)
3.913	.0900(12)	3.46(6)	12.5(1)
3.916	.0896(12)	3.43(6)	12.4(1)

[a] τ is sum of ion pair concentrations.
[b] Standard error in the last digit(s). See sec. 4.2.

[5] The standard errors listed in the table were computed for each system with the aid of the covariance matrix (eq {A-10}) of the adjusted observations and the appropriate derivatives of equations {8-9} which define τ and the ion pair concentrations.

4.3. Thermodynamic Quantities

The dissolution of $Ca_5(PO_4)_3OH$ may be described by the reaction

$$Ca_5(PO_4)_3OH = 5Ca^{2+} + 3PO_4^{3-} + OH^-. \quad (6)$$

The quantities $\Delta G°$, $\Delta H°$, and $\Delta S°$ associated with the dissolution reaction were calculated from eq (5) for log K_s following the procedure of eqs {27–29}. The results, along with their standard errors, are set out in table 11.

TABLE 11. *Thermodynamic quantities*

°C	$\Delta G°$ kcal/mol	$\Delta H°$ kcal/mol	$\Delta S°$ cal[a]/mol·K
5	74.5	2.8	−258
	[b] (0.06)	(2.5)	(10)
15	77.1	0.3	−267
	(0.04)	(1.2)	(4)
25	79.8	−2.3	−276
	(0.05)	(1.1)	(4)
37	83.2	−5.6	−286
	(0.07)	(2.9)	(9)

[a] 1 cal = 4.1840 J.
[b] Standard error.

5. Discussion

5.1. Standard Deviation, Weights and Goodness of Fit

Table 12 summarizes the results of preliminary adjustments that were carried out to examine the temperature dependence of K_{HA} and to test for uniformity of variance (s^2, eq {22}) among the four temperature sets. The variances listed there were homogeneous by Bartlett's test [16]. These results in table 12 were obtained with the following assignment of errors: Ca, 2.0 percent; P, 1.5 percent; P_0, 1.0 percent; pH, 0.020 (absolute). The corresponding weights (eq {12}, with $s_0 = 1 \times 10^{-4}$) were then utilized in the final adjustment of the combined data. The overall variance was found to be $s^2 = 1.13 \times 10^{-8}$, based on 109 degrees of freedom, f (sec. 3.2). The critical values of χ^2_{109} (95%), 82.0 and 139.8, nicely bracket the value of f, thus confirming the adequacy of the weights used and establishing the goodness of fit of the adjustment. The standard deviation is then 1.06×10^{-4}, and the 95 percent confidence interval for s is $(0.94 < s < 1.22 \times 10^{-4})$.

TABLE 12. *Results of preliminary calculations*

°C	Number of functions (r)	Number of points (N)	f[c]	Variance $s^2 \times 10^8$	$K_s \times 10^{59}$
5	3[a]	8	29	0.89	2.85
	2[b]	3			
15	3	7	30	1.13	3.46
	2	5			
25	3	9	26	1.43	2.84
37	3	6	23	1.10	2.41
	2	3			

[a] Saturation, electroneutrality, and congruent dissolution.
[b] Saturation and electroneutrality.
[c] Degrees of freedom = $\Sigma Nr - 1$.

5.2. Solubility Isotherms

The data reported in tables 1 through 4 were obtained from phosphoric acid solutions of widely varying initial concentration (less than 1 to over 50 mM) equilibrated with pure solid $Ca_5(PO_4)_3OH$. It is evident from the plots in figure 2 that the experimental points at each temperature are well represented by the corresponding calculated curves. The latter resulted from the adjustment procedure which for all points assumes (i) equilibrium (saturation) and (ii) electroneutrality (i.e., all species known and accounted for, including ion pairs). In addition a third requirement, that of congruent dissolution (no extraneous solid phases are formed), was imposed on 30 out of the total of 41 systems. Since the remaining 11 systems, adjusted with only conditions (i) and (ii), are not distinguishable in figure 2 from those subjected to all three conditions, it appears that the smaller set of systems was indeed saturated with respect to $Ca_5(PO_4)_3OH$. The question of stoichiometry will be dealt with in more detail below (sec. 5.4). It suffices to emphasize here that failure to exhibit congruent dissolution is not in itself a sufficient reason to doubt the attainment of the equilibrium state.

The success of the adjustment procedure applied to these data is further illustrated by reference to tables 5 through 8. The standard errors (in parentheses) are generally within 1 percent of the adjusted observations. The individually computed solubility products, K_{HA} (eq (1)), shown in column 7, using the adjusted observations, are identical to the corresponding least-squares value of K_s (eq (5); table 9). Both the dissolution ratio, column 6 (where applicable) and the electroneutrality condition (not shown) were satisfied to better than 1 ppm. Additional insight as to the validity of the adjustment under the given conditions may be gained from the following results (not reported). The magnitudes of the largest relative adjustments (residual/observed) were: Ca, 0.046 at 37 °C; P, 0.025, and P_0, 0.023 at 15 °C. The size of the maximum residual in pH was 0.036 at 15 °C. The sizes of the corresponding standardized residuals (residual/S.E. of residual) were 2.4, 1.8, 3.3, and 1.8.

Effect of Temperature on the Solubility of $Ca_5(PO_4)_3OH$

The relative positions of the solubility isotherms depicted in figure 2 indicate, as mentioned in section 4, that the solubility of this preparation of hydroxyapatite has a negative temperature coefficient. It is of interest to examine this behavior under the condition of uniform initial acid concentration. Since at each of the four temperatures there were values of the adjusted initial acid (P_0, tables 5 through 8) near 1 mM and 10 mM, it was feasible to compute the conditional values [17] of Ca, P, and pH, and the corresponding concentrations of the ion pairs, at these two rounded values of P_0. The results are given in the following table:

°C	P_0 = 1 mM			P_0 = 10 mM		
	Ca	P	pH	Ca	P	pH
5	0.761	1.457	5.82	7.22	14.33	4.82
15	.750	1.450	5.68	7.17	14.30	4.68
25	.742	1.445	5.55	7.14	14.28	4.55
37	.734	1.440	5.40	7.10	14.26	4.40

Although the concentration differences between temperatures are small, on the order of the standard errors, the trend is consistently toward lower concentration with increasing temperature. The percentage of bound calcium, $100\tau/Ca$ (not listed), shows a marked reduction of over 50 percent between 5 and 37 °C; fom 2.7 to 1.2 (P_0 = 1 mM), and from 8.6 to 3.9 (P_0 = 10 mM).

5.3. Solubility Product Temperature Dependence and Models

Equation (5) for $\log K_s$ derived by the least squares adjustment possesses a maximum near 16 °C, as seen in figure 1. Maxima have also been shown to occur in the vicinity of 20 °C for the solubility products of $CaHPO_4 \cdot 2H_2O$ [11] and $Ca_3(PO_4)_2$ [13]. In the case of $CaHPO_4 \cdot 2H_2O$ it was argued that the maximum is a possible consequence of the thermodynamic properties of the solid. In the present work the influence of the ion pair assumption on the nature of the temperature dependence of the solubility product of $Ca_5(PO_4)_3OH$ was investigated. A least squares adjustment was accordingly carried out without the assumption of the presence of ion pairs. The equation corresponding to eq (5) gave the following values of K_s at the four experimental temperatures: 4.2, 4.0, 3.6, and 2.9×10^{-59}. The standard deviation of the adjustment was 1.08×10^{-4}, with a slightly wider confidence interval than was reported in section 5.1 for the model with ion pairs included. It is evident that the maximum in K_s for $Ca_5(PO_4)_3OH$ can be ascribed, at least in part, to the nature of the temperature dependence of the ion pair stability constants as reported in [11].

5.4. Stoichiometry. Potential Diagrams

Equilibrium between a solid calcium phosphate and an aqueous solution, and the stoichiometry of the saturating solid, may be demonstrated by a "potential diagram" [18], in which the coordinates are defined as $-\log[(Ca^{2+})(OH^-)^2]$ and $-\log[(H^+)^3(PO_4^{3-})]$. These are linearly related to the chemical potentials of the solution components $Ca(OH)_2$ and H_3PO_4. The saturation condition in such a diagram is defined by a straight line, whose slope is the negative of the Ca/P ratio in the solid. Figures 3 and 4 show the data of tables 1 through 4, as well as results at 25 °C reported by some other workers, plotted in this manner. The lines in figure 3 were fitted by least squares to the data of tables 1 through 4 only. The slopes at 5, 15, 25, and 37 °C are −1.643, −1.666, −1.682, and −1.645, respectively. When the fitting was done with a forced common slope, the value obtained was −1.660. (The standard error of the slope in all cases is less than 0.01). These values compare favorably with the values for the Ca/P ratio, 1.67_3, found by analysis of the solid (sec. 2.1) and the theoretical value for $Ca_5(PO_4)_3OH$, 1.667 (5/3). It is evident that the subset of 11 systems that failed to show congruent dissolution (sec. 5.2) cannot be distinguished in these plots from those that did satisfy that condition; thus all of the data represent solutions saturated with respect to a solid of very nearly the theoretical stoichiometry of 5/3. The results of the other workers shown in the figures are discussed in the following section.

5.5. Comparison With Reported Data

Avnimelech, Moreno, and Brown [9] reported solubility measurements at 25 °C on a sample of hydroxyapatite prepared by a method very similar to the one described in this paper. Their data (20 points), included in figure 3, very closely parallel our results at this temperature except that stoichiometric dissolution (i.e., a Ca/P ratio of 5/3) was the exception. This is not surprising because the objective of their research was to show that the surface Ca and P contribute significantly to the apparent stoichiometry of the overall dissolution reaction even though the stoichiometry of the final equilibrium reaction was shown to have the stoichiometry 5/3 (see their fig. 3). They reported a K_{HA} of 6.32 (2.1) $\times 10^{-59}$ (arithmetic mean) and a value of −1.66 (.02) for the slope of the line (not shown in our fig. 3); the Ca/P ratio of their solid was 1.69. We have recalculated the solubility product using the adjustment procedure described in this report; the resulting value of K_s is 5.23 (0.41) $\times 10^{-59}$.

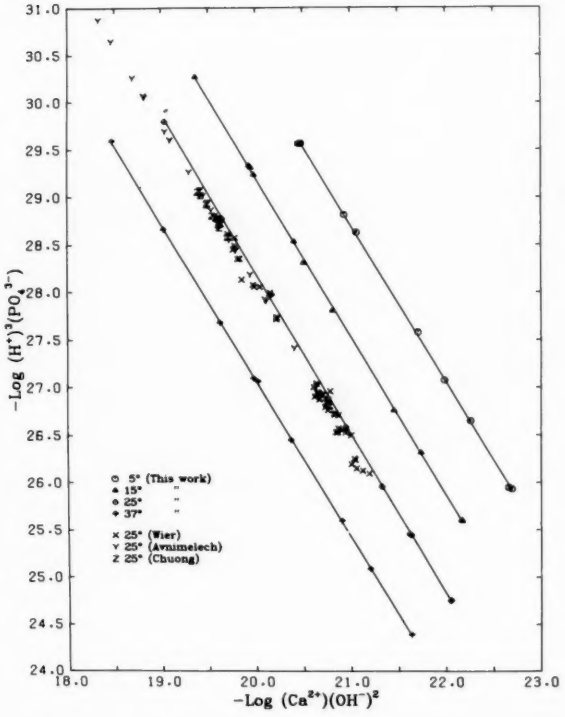

FIGURE 3. *"Potential plot"* (-log H_3PO_4 *activity versus -log* $Ca(OH)_2$ *activity) for hydroxyapatite at 5, 15, 25, and 37 °C. Solid lines are least-square fits of data in tables 1–4.*

Chuong [10] reported a series of 18 measurements on the four component system $Ca(OH)_2-H_3PO_4-H_2O-HCl$ at 25 °C to ascertain the effect of varying the solid-to-solution ratio; his solid was a portion of the same preparation that was used in the present study. His results, shown in figure 3, cover only a narrow range of the potential diagram, but are seen to be consistent with the data of Avnimelech et al. There was a slight trend in K_{HA} with increasing HCl concentration (mean values were 6.2, 5.4 and 5.0×10^{-59} at HCl concentrations of 0.70, 1.0 and 10.0 mmol/L, respectively), but no trend was observed at fixed acid concentration with solid-to-solution ratios varying from 0.2 to 2.0 g/100 mL. An overall estimate of the solubility product was not reported; we have

computed a least-squares value of 5.36 (0.19) × 10^{-59} from his data.

Wier, Chien, and Black [8] have reported an extensive series of hydroxyapatite solubility measurements (112 equilibrations at 25 °C) in which the ratio of solid-to-solution varied from 0.1 to 10.0 g/100 mL. They reported their solubility constants as pK_{HA} based on the formula $Ca_{10}(PO_4)_6(OH)_2$ which we have converted into K_{HA} values based on the formula $Ca_5(PO_4)_3OH$. The hydroxyapatite used in their equilibrations was a commercial product. In five of their six series of equilibrations, this hydroxyapatite had been boiled in water for 24 hours; in the sixth series, the hydroxyapatite had been treated with 1 *N* NH_4Cl solution at 120 °C in an autoclave for 50 days, replacing the NH_4Cl solution every 4 to 6 days. The purpose of the latter treatment was to further stabilize the hydroxyapatite and thereby to demonstrate the existence of a form of hydroxyapatite that is less soluble than the material used in their first five series of experiments. The first five series included 44 equilibrations with solid-to-solution ratios between 0.5 and 10.0. This set of points is included in figure 3 (Wier). Although there is considerable scatter, these points are comparable with the others at 25 °C in the figure. Wier et al. reported a solubility product equal to 5.0 × 10^{-59} for 32 systems of this set (solid-to-solution ratio of 1.0 g/100 mL). Making use of their measurements on all 44 systems, we derive a value of K_s equal to 6.18 (0.70) × 10^{-59}.

In addition to the above values, Moreno et al. [5] reported two values for K_s at 25 °C, one for a preparation heated in steam at 1000 °C, 3.7 (0.5) × 10^{-58}, and one heated in air at the same temperature, 2.5 (0.4) × 10^{-55}. The latter is four orders of magnitude larger than the value reported here and reflects changes in the structure induced by heating in air at 1000 °C. Hydroxyapatite is unstable when heated in air at 1000 °C and tends to disproportionate into $Ca_3(PO_4)_2$ and $Ca_4(PO_4)_2O$. Moreno et al. reported evidence for the presence of β-$Ca_3(PO_4)_2$ in the air-heated sample. For this reason, very little weight should be given to the K_s of the air-heated sample.

Hydroxyapatite is believed to be the stable phase when heated at 1000 °C in a steam atmosphere. As noted below, the K_s for the steam-heated sample is significantly higher than the value reported here; thus, the steam-heat treatment may have altered the structure of the hydroxyapatite in some way.

Clark [1] has reported a value of similar magnitude, 20 × 10^{-59}, for a sample of hydroxyapatite prepared by precipitation at 90 °C.

The values of K_s that we derived from the data of the above mentioned investigators are summarized in table 13 along with the value obtained from our data. Clearly the values of Clark and of Moreno et al. are substantially different from the other four values. When the average of the latter four values is taken with weights inversely proportional to the squares of the given standard errors, we derive a value of 4.7 (0.1) × 10^{-59} as the most probable value for the solubility product constant at 25 °C of hydroxyapatite that has not received thermal treatment. In view of the spread of these four values, an estimate of 2.0 × 10^{-59} is a reasonable value of the uncertainty to be assigned to the derived K_s.

Wier et al. gave two values for the K_{HA} of the autoclaved hydroxyapatite, one obtained with 0.1 g of solid per 100 mL of solution, 5.6 × 10^{-61} (15 points) and the other with 1.0 g of solid per 100 mL, 2.2 × 10^{-60} (22 points). These data are displayed in the potential plot of figure 4; our results at 25 °C are again shown for comparison. Because there appear to be substantial differences among the three sets, we have re-evaluated the data of Wier et al. for the sixth series with the procedures and constants used by us so as to put all the data in figure 4 on a comparable basis. (Some uncertainty was encountered in estimating the ionic strength; unspecified amounts of HCl had been added to the equilibrating solu-

TABLE 13. *Summary of adjusted values of the solubility product of* $Ca_5(PO_4)_3OH$ *at 25 °C.*

Investigator	Ref.	$K_s \times 10^{59}$	Comments
Moreno et al.	[5]	37.(5.)[a]	Heated in steam at 1000 °C.
Clark	[1]	20.[b](3.)	Precipitated at 90 °C.
Wier et al.	[8]	6.18(0.70)	0.5 to 10.0 gm/100 mL.
Chuong	[10]	5.36(0.19)	0.2 to 2.0 gm/100 mL.
Avnimelech et al.	[9]	5.23(0.41)	
This work	—	3.04(0.25)	

[a] Estimated standard error of K_s.
[b] Antilog of 1/2 times the mean of 27 values in table 1 of ref. [1]. (No allowance made for ion pairs).

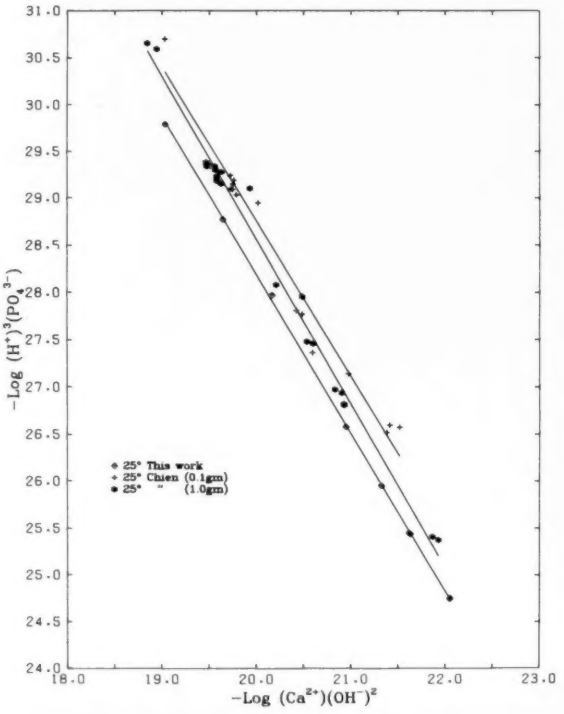

FIGURE 4. *"Potential plot" for hydroxyapatite at 25 °C comparing our data with those of Chien et al. [8] for the "autoclaved" sample.*

tions. We used the apparent electroneutrality imbalance, always positive in these solutions, as a measure of chloride concentration.) We obtained K_s values of 0.46 (0.14) and 1.95 (0.48) $\times 10^{-60}$, respectively, for the autoclaved samples. Ninety-five percent confidence intervals for the solubility products of the 0.1 and 1.0 gm/100 mL sets are, respectively, $0.17 < K_s < 0.75 \times 10^{-60}$, and $0.97 < K_s < 2.93 \times 10^{-60}$. It may be remarked that a value of 1×10^{-60} corresponds to a substantially lower Gibbs energy, about 2 kcal per mol, in the autoclaved sample as compared to the sample used by us and the one used by them in their first five series of equilibrations.

We concur with the principal conclusion of Wier et al., that hydroxyapatite may have a variable solubility product. Variability in the solubility of hydroxyapatite is indicated by the study of Moreno et al. [5], on synthetic hydroxyapatite, the studies of Patel et al. [19], on enamel, and that of Mattamal and Brown [20], on bone. Furthermore, it is known that hydroxyapatites have variable indices of refraction, unit-cell dimensions, impurity contents, degrees of disorder in the OH positions, and may possibly vary in their Ca and OH contents. Thus, there is ample basis for ascribing variable solubility to hydroxyapatites. The question then arises as to whether the low values reported by Wier et al. for the autoclaved sample represent solubility products for more completely annealed and stabilized hydroxyapatite or are a consequence of experimental errors. This warrants examination of the experimental technique which produced these results.

Wier et al. [8] used an equilibration apparatus consisting of two chambers separated by a cellulose acetate dialysis membrane. The same initial equilibration solution was present in both chambers, but the solid was present in only one and the solution for analysis was taken from the other. Thus, for the solution in the sample chamber to be in equilibrium with the solid, it is necessary for the solution in the first chamber to be saturated with respect to the solid, and for the two solutions to be in equilibrium across the membrane. Equilibrium across the membrane requires that the chemical potentials (or activities) of both $Ca(OH)_2$ and H_3PO_4 must be the same in the two solutions. The use of a membrane undoubtedly slows the approach to equilibrium, particularly if the membrane possesses some permselectivity. In the present case one might anticipate that the membrane would be somewhat permselective to cations in accord with the usual character of cellulose acetate membranes; the data for the autoclaved sample do provide an indication of this. The $\Delta Ca/\Delta P$ ratios in many of the equilibrations fall in a range much higher than the theoretical value, 1.67, thus indicating that the phosphate ions passed through the membrane less readily than the calcium ions and that trans-membrane equilibrium with respect to the component H_3PO_4 may not have been attained. If so, this may account for the relatively large variation in their solubility products. We believe this is the main reason for the difference in the values 0.046 (0.014) and 0.195 (0.048) $\times 10^{-59}$ for K_s obtained with the two solid-to-solution ratios, 0.1 and 1.0, respectively. No such variation with solid-to-solution ratio was observed by Chuong. Furthermore, the lower value for K_{HA} obtained by them with the smaller solid-to-solution ratio would be in accord with the view that these equilibrations had not reached saturation.

The true minimum value for the solubility product of hydroxyapatite continues to be of considerable interest because it would represent the most appropriate standard state for this solid, and it would be the structural condition toward which biological and other hydroxyapatites would tend to convert. It remains to be seen if a hydroxyapatite with K_{HA} significantly lower than the mean value reported here, 4.7×10^{-59}, can exist.

6. References

[1] Clark, J. S., Can. J. Chem. **33,** 1696 (1955).
[2] Neuman, W. F., and Neuman, M. W., The Chemical Dynamics of Bone Mineral. p. 30 (University of Chicago Press, Chicago, Ill., 1958).
[3] Rootare, H. M., Deitz, V. R., and Carpenter, F. G., J. Colloid Sci. **17,** 179 (1962).
[4] LaMer, V. K., J. Phys. Chem. **66,** 973 (1962).
[5] Moreno, E. C., Gregory, T. M., and Brown, W. E., J. Res. Nat. Bur. Stand. (U.S.), **72A** (Phys. and Chem.), No. 6, 773–782 (Nov.–Dec. 1968).
[6] Elliott, J. C., Mackie, P. E., and Young, R. A., Science **180,** 1055 (1973).
[7] Brown, W. E., p. 203 in Environmental Phosphorus Handbook (John Wiley and Sons, New York, N. Y., 1973).
[8] Wier, D. R., Chien, S. H., and Black, C. A., Soil Sci. **111,** 107 (1971).
[9] Avnimelech, Y., Moreno, E. C., and Brown, W. E., J. Res. Nat. Bur. Stand. (U.S.), **77A** (Phys. and Chem.), No. 1, 149–155 (Jan.–Feb. 1973).
[10] Chuong, R., J. Dent. Res. Supplement to No. 5, **52,** 911 (1973).
[11] Gregory, T. M., Moreno, E. C., and Brown, W. E., J. Res. Nat. Bur. Stand. (U.S.), **74A** (Phys. and Chem.), No. 4, 461–475 (July–Aug. 1970).
[12] Patel, P. R., Moreno, E. C., and Gregory, T. M., J. Res. Nat. Bur. Stand. (U.S.), **73A** (Phys. and Chem.), No. 1, 43–49 (Jan.–Feb. 1969).
[13] Gregory, T. M., Moreno, E. C., Patel, J. M., and Brown, W. E., J. Res. Nat. Bur. Stand. (U.S.), **78A** (Phys. and Chem.), No. 6, 667–674 (Nov.–Dec. 1974).
[14] Patel, P. R., Gregory, T. M., and Brown, W. E., J. Res. Nat. Bur. Stand. (U.S.), **78A,** (Phys. and Chem.), No. 6, 675–681 (Nov.–Dec. 1974).
[15] McDowell, H., Brown, W. E., and Sutter, J. R., Inorg. Chem. **10,** 1638 (1971).
[16] Dixon, W. J., and Massey, F. J., Jr., Introduction to Statistical Analysis, 2nd Ed., p. 179 (McGraw-Hill Book Company, New York, N. Y., 1957).
[17] Anderson, T. W., Introduction to Multivariate Statistical Analysis, p. 27 (John Wiley and Sons, New York, N. Y., 1958).
[18] Moreno, E. C., Lindsay, W. L., and Osborn, G., Soil Sci. **90,** 59 (1960).
[19] Patel, P. R., and Brown, W. E., J. Dent. Res. **54,** 728 (1975).
[20] Mattamal, G. J., and Brown, W. E. (Abstract), Internat. Assoc. Dent. Res., 53rd General Meeting, London, England (1975).
[21] Manuscript in preparation.

(Paper 81A2&3-930)

JOURNAL OF RESEARCH of the National Bureau of Standards—A. Physics and Chemistry
Vol. 81A, Nos. 2 and 3, March–June 1977

Thermodynamics of the Densification Process for Polymer Glasses

John E. McKinney

Institute for Materials Research, National Bureau of Standards, Washington, D. C. 20234

and

Robert Simha

Department of Macromolecular Science, Case Western Reserve University, Cleveland, Ohio 44106

(May 3, 1977)

A quantitative description is given for the densification process of glasses resulting from glass formation at elevated pressures. Phenomenological relations are derived, or justified, which allow estimation of the densification rate κ' (with respect to formation pressure) from various thermodynamic quantities and glass transition behavior. In addition, the estimation of κ' may be facilitated by the application of the hole theory of Simha and Somcynsky. Using these relations κ' is estimated, and the results from the different methods are compared for data from 23 different organic polymers with glass transition temperatures ranging from 150 to 455 K. The amount of densification appears to be limited by the apparent convergence of the glass temperature and effective decomposition temperature with increasing pressure. Some estimates of limiting values are presented. Finally, changes of refractive index resulting from densification are estimated from the observed, or predicted, densification rates.

Key words: Compressibility; densification; glass; glass transition; liquid; polymer; pressure; *PVT*; pyrolysis; refractive index; thermal expansion; thermodynamic.

1. Introduction

The density of a glass, as well as certain other properties, depend upon the thermodynamic history by which the glass is formed. For example, as shown schematically in figure 1a, an amorphous polymer subjected to an elevated pressure in the melt, followed by isobaric cooling at constant rate to a temperature well below the glass temperature, T_g, and then depressurized, will have a larger density than that obtained by isobaric cooling at the same rate at atmospheric pressure to the same temperature in the glass. From the former procedure the pressure induced densification rate is defined as

$$\kappa' = -(1/V)(\partial V/\partial P')_{T,P,k} \tag{1}$$

where V is the volume at temperature T and pressure P, and P' is the formation pressure maintained during constant rate of cooling k. Note that this definition parallels the usual one for the isothermal compressibility,

$$\kappa = -(1/V)(\partial V/\partial P)_{T,P',k}, \tag{2}$$

the difference being that P and P' are interchanged.

It is expected that the final depressurized volume in the glass will lie between the atmospheric and the pressurized value, as shown in figure 1a. It is then clear that the inequality,

$$\kappa_g > \kappa' > 0$$

where κ_g is the compressibility of the glass, is obeyed.

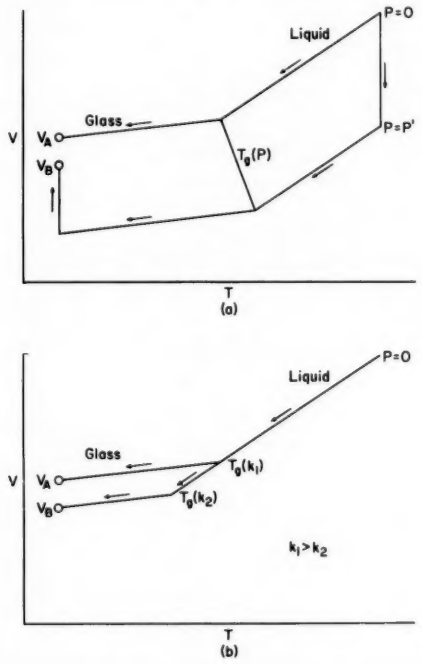

FIGURE 1. *Schematic illustration of two methods used to obtain densified glasses.*
(a) Densification by elevating the formation pressure at the same cooling rate k_1. (b) The same densification is obtained by commensurately decreasing the cooling rate at atmospheric pressure.

Although we may intuitively expect this relation to hold, as apparent from experiment, we do not know of any proof.

A well known alternative method of densifying glasses is simply to decrease the cooling rate as illustrated in figure 1b. In principle one can obtain the same volume in the glass by this procedure as by elevating the pressure, except that the times required for the former are much longer. For example, it is estimated [1][1] that a poly (vinyl acetate) glass obtained by isobaric cooling at 800 bar[2] in 8 hours would require 500 years to reach the same volume at the same terminal temperature by cooling slowly at atmospheric pressure. It should be recognized, however, that the states of glasses at the same volume, temperature, and pressure, but obtained through different histories, are not necessarily the same. As pointed out by Bree and coworkers [2], volume changes during isobaric-isothermal volume relaxation [3] have a large effect on relaxation times for creep compliance, whereas almost no effect is observed from volume changes obtained by isobaric cooling at elevated pressures. Accordingly, it appears that the state of a glass is not determined by its volume, temperature, and pressure alone. Moreover, pressure induced densification does have an influence on physical properties. According to the data of Dale and Rogers [4] over a 5 kbar range, the compressive modulus of polystyrene appears to increase slightly with formation (or molding) pressure, leveling off at higher pressures, with the yield stress going through a maximum between 1 and 1.5 kbar. Wetton and Moneypenny [5] have studied the dynamic mechanical and dielectric properties of several polymeric glasses formed at pressures up to slightly beyond 5 kbar. Both the real part of Young's modulus and its loss tangent, as well as the real part of the dielectric constant, increase with formation pressure. For poly(vinyl acetate) McKinney and Goldstein [1] have observed a 3 percent increase in the bulk modulus at 0 ° C, corresponding to a formation pressure of 800 bar. This difference increases with decreasing temperature.

Thermal properties also seem to depend on the amount of pressure induced densification. Although the heat capacity C_p is found to be independent [6] of formation pressure, the enthalpy H seems to vary significantly at formation pressures above a certain value. According to Price [7], very little change in the enthalpy of poly(methyl methacrylate) is observed up to about 800 bar, followed by a nearly constant rate of increase of about 0.015 cm^3/g up to 3 kbar, their maximum value. For polystyrene [8], the data have been evaluated as $\Delta H = H(\text{densified}) - H(\text{normal})$ first decreasing slightly and then going back to zero at about 800 bar, followed by an increase with nearly constant slope up to the maximum pressure. Weitz and Wunderlich [9] have also observed this behavior and interpreted it in terms of two opposing mechanisms arising from holes and rotational isomers. It is not clear, however, that the apparent negative values of ΔH obtained by experiment are significant.

The purpose of this paper is to describe the thermodynamics of the pressure induced densification process by applying both phenomenological and molecular theory. Simple phenomenological relationships are derived between the densification rate κ' and other thermodynamic properties for which values are more readily available in the literature. Moreover, it is shown how the hole theory of Simha and Somcynsky [10] may be used to facilitate the estimation of the densification rates for polymers using a minimum amount of experimental information. In both cases the derived relationships are tested using appropriate experimental data. An example of the utility of these results is demonstrated by estimating the change in the index of refraction corresponding to changes in molding pressure, assuming that the index of refraction is related to the volume by the Lorentz-Lorenz equation. The results have potential application to the adjustment of the refractive indices of lenses by varying the molding pressure.

2. Phenomenological Relationships

Two types of thermodynamic histories, shown schematically in figure 2, are pertinent to the development of the phenomenological relationships for pressure induced densification. In the first (Fig. 2a) the *PVT* surface of the glass is obtained from repeated isobaric cooling runs at the same constant rate, but at difference pressures, with all pressure changes occurring in the melt prior to each run. This procedure is called the variable formation history because the structure of the glass is different for each experimental pressure (which is the formation pressure, since $P = P'$). The glass transition at each pressure is assumed to occur at a constant mean relaxation time. Hence, the intersection of the liquid and glass *PVT* surfaces gives the proper $T_g(P)$, from which dT_g/dP is expected to approximate that obtained from the dynamic mechanical and dielectric frequency-temperature-pressure superposition. On the other hand, as a consequence of the varied structure, the glass *PVT* surface is not proper in the thermodynamic sense.

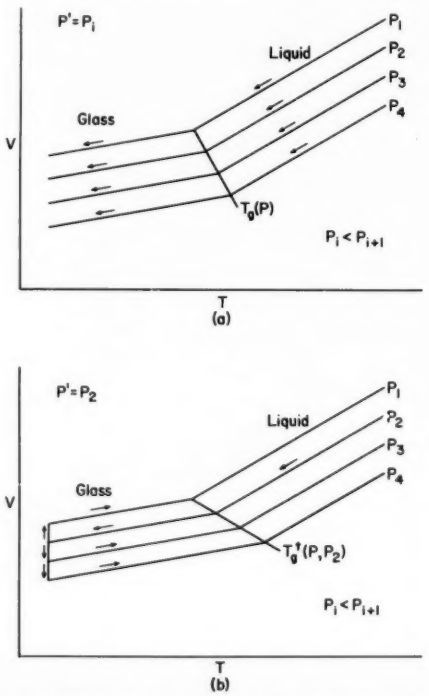

FIGURE 2. *Schematic illustration of two thermodynamic histories used to form glasses.*
(a) Variable formation. (b) Constant formation.

[1] Figures in brackets indicate literature references at the end of this paper.
[2] For conversion to SI units, 1 MPa = 10 bar.

With the other history (fig. 2b) the glass is formed also by isobaric cooling at constant rate at an arbitrary pressure, P' (which is usually atmospheric, but elevated in figure 2b to illustrate the more general case). At temperatures well below T_g, where viscoelastic relaxation times are large in comparison to effective experimental times, a thermodynamically reversible PVT surface for the glass is obtained by observing the volumetric response to "fast" changes in temperature and pressure. Since all of the data in the glass pertain to the same P', the PVT surface gives the proper values of the derivable thermodynamic quantities (for example, thermal expansion, isothermal compressibility, and internal pressure). The intersection of the liquid and glass surfaces defines the fictive temperature $T_g^\dagger(P, P')$.

The principal distinction in procedure between the two histories is that with variable formation all pressure changes are made in the melt, whereas with constant formation they are made in the glass. Note that the number of independent variables is different for $T_g(P)$ and $T_g^\dagger(P, P')$. The redundancy of using two arguments in the former arises from the fact that the formation and experimental pressure are always identical. Accordingly, T_g may be regarded as a special case of $T_g^\dagger$ when $P = P'$. The implicit argument k is deleted here because only one value appplies to these discussions for each case. For further details and interpretations of these histories, see Ref. [1].

In all of the schematic diagrams in this paper the glass transition is shown as a discrete intersection. With isobaric cooling at constant rate through T_g a gradual transition process is observed. The discrete intersections shown correspond to those obtained by extrapolation of the equilibrium isobars and the isochronal (nonrelaxing) ones for the glass.

We now proceed to evaluate the thermodynamic diagram in figure 3, in order to determine relationships for κ' in terms of other measured quantities. Volume A is obtained by isobaric cooling at constant rate and atmospheric pressure ($P = P' = 0$). Volume B is reached by pressurizing to $P = P' = \Delta P$ in the melt, followed by isobaric cooling at the same constant rate as for A, with subsequent depressurizing in the glass at the same terminal temperature as for A. Note that T_g (in lieu of $T_g^\dagger$) applies here, since the transition is observed at the formation pressure ($P = P'$) in both cases. The isobaric extension of V_B with increasing T (see dashed line) to its intersection with the liquid line yields the fictive temperature $T_g^\dagger(P, P') = T_g^\dagger(O, \Delta P)$.

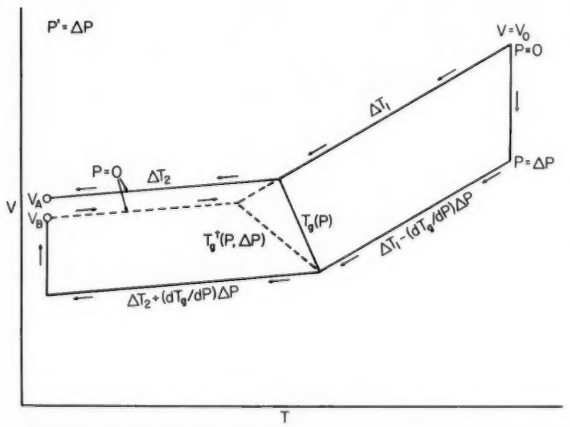

FIGURE 3. *Schematic illustration of the procedure used to derive the densification equation [See eqs (3) and (4)], and the distinction between $T_g(P)$ and $T_g^\dagger(P, P')$.*

In summing the thermodynamic contributions for small changes in T and P near $T_g(P)$ in the range where linear approximations are valid, we find

$$V_A = V_0(1 - \alpha_l \Delta T_1 - \alpha_g \Delta T_2)$$
$$V_B = V_0\{1 - \kappa_l \Delta P - \alpha_l[\Delta T_1 - (dT_g/dP)\Delta P] - \alpha_g[\Delta T_2 + (dT_g/dP)\Delta P] + \kappa_g \Delta P\} \quad (3)$$

where α is the usual isobaric thermal expansivity, the Δ's indicate differences as shown on figure 3, and the subscripts l and g pertain to liquid and glass. For small changes eq (1) may be written in the form

$$\kappa' = (V_A - V_B)/(V_0 \Delta P) \quad (4)$$

Substitution of eqs (3) for V_A and V_B yields

$$\kappa' = \Delta\kappa - \Delta\alpha \, dT_g/dP \quad (5a)$$

where the Δ's here indicate the usual differences in the respective quantities between liquid and glass. Since

$$dT_g^\dagger/dP = \Delta\kappa/\Delta\alpha \quad (6a)$$

along $T_g^\dagger$, [11], κ' may be expressed in terms of the difference between the two transition rates, i.e.,

$$\kappa' = \Delta\alpha(dT_g^\dagger/dP - dT_g/dP) \quad (5b)$$

Equation (5a) may also be written as an Ehrenfest-type relation, viz.,

$$dT_g/dP = \Delta\kappa/\Delta\alpha - \kappa'/\Delta\alpha \quad (5c)$$

which is consistent with the experimentally observed inequality

$$dT_g/dP \leq \Delta\kappa/\Delta\alpha$$

provided the densification rate is non-negative. Expressions fully equivalent to eqs (5) have been derived by Goldstein [11] and given previously in Ref. [12]. From eqs (5) it is evident (as also pointed out by Goldstein [11]) that the necessary and sufficient condition (assuming $\Delta\alpha \neq 0$) for the PVT surface to be independent of formation pressure is the validity of the first Ehrenfest equation

$$dT_g/dP = \Delta\kappa/\Delta\alpha. \quad (6b)$$

The analogous argument applies to the entropy surfaces. Since the second Ehrenfest equation,

$$dT_g/dP = T_g V \Delta\alpha/\Delta C_P \quad (7)$$

where C_P is the usual heat capacity at constant pressure, appears to be a good approximation [11, 13], there should be

a single entropy surface with respect to formation pressure in contrast to the manifold/surface observed for volume. This view is confirmed by the DSC[3] measurements of Yourtee and Cooper [6] on normal and densified polystyrene, which reveal no significant effect on the thermal properties of glasses by vitrification at elevated pressures. The authors did find some differences in the thermal behavior between these properties and those from vitrification by isothermal compression; however, these were attributed to inhomogeneous freezing processes during compression. Accordingly, if eq (7) is a good approximation, it leads to a convenient experimental determination of the initial ($P = 0$) value of dT_g/dP through volume-temperature and heat capacity measurements required at atmospheric pressure only. Equation (7) will be tested by means of experimental data later in this paper.

As stated above κ' may be determined (near T_g) from the values of $\Delta\alpha$, dT_g/dP, and $\Delta\kappa$ using eq (5a). The relative difficulty in obtaining these quantities experimentally increases in the order given above, as does the difficulty of obtaining their values from the literature. For these reasons it is desirable to be able to estimate $\Delta\kappa$ (or $\Delta\kappa/\Delta\alpha$) independently of existing PVT data. It will be shown how the hole theory of Simha-Somcynsky [10] may be used to arrive at values of $dT_g^\dagger/dP = \Delta\kappa/\Delta\alpha$.

As indicated previously, eqs (5) are based on several linearizations. It is assumed that the coefficients α_l, α_g, κ_l and κ_g are independent of pressure and temperature and that T_g is a linear function of pressure. Thus strictly, the reference temperature in the glass as well as the initial temperature in the melt should be appropriately close to T_g. Moreover, the pressure P' should be appropriately small. In the Appendix the general relationships are developed, based on the equations of state of the liquid and both glasses.

As an example, integral relations are evaluated over the two paths shown on figure 1a for PVAc, for which extensive data are available [1], and the Tait parameters are known [14] for the liquid and both glasses. The results are tabulated and compared with the corresponding linear approximations.

3. Application of Molecular Theory

The hole theory, which is used here to estimate the values of $dT_g^\dagger/dP$, is a corresponding states theory based on a lattice model. The partition function is defined in terms of a single ordering parameter, the hole fraction h, which gives the ratio of the number of vacant to total sites, each of which may be occupied by a polymer segment. The corresponding states are given in terms of the reduced (universal) variables

$$\tilde{T} = T/T^*,\ \tilde{P} = P/P^*,\ \tilde{V} = V/V^* \tag{8}$$

where T^*, P^*, and V^* are the scaling factors applicable to each polymer. Although these are defined explicitly by the theory, they are usually derived from a superposition of equilibrium PVT data along the master curves evaluated from the theory. For an illustration of this procedure, see Ref. [14].

The partition function Z is expressed uniquely in terms of the three independent variables $\tilde{T}$, $\tilde{V}$, and h. From the thermodynamic definition

$$P = -kT[\partial \ell nZ(T, V, h)/\partial V]_T$$

and the equilibrium constraint $(\partial Z/\partial h)_{T,V} = 0$, the following equilibrium equations [10] are obtained, respectively:

$$\tilde{P}\tilde{V}/\tilde{T} = [1 - 2^{-1/6}y(y\tilde{V})^{-1/3}]^{-1} + (2y/\tilde{T})(y\tilde{V})^{-2}[1.011(y\tilde{V})^{-2} - 1.2045] \tag{9}$$

$$(s/3c)[(s-1)/s + y^{-1}\ell n(1-y)] = [2^{-1/6}y(y\tilde{V})^{-1/3} - 1/3][1 - 2^{-1/6}y(y\tilde{V})^{-1/3}]^{-1} + [y/(6\tilde{T})](y\tilde{V})^{-2}[2.409 - 3.003(y\tilde{V})^{-2}] \tag{10}$$

where $y = 1 - h$ is the fraction of occupied sites, and s and $3c$ are the number of segments per molecule and the external degrees of freedom per molecule, respectively. As in previous work, we take $s/3c = 1$. Note that the term $(s-1)/s$ in eq (10) approaches unity for large molecules.

A basic assumption sufficient for the application of the hole theory to our densification model is

$$dT_g^\dagger/dP = (\partial T/\partial P)_h. \tag{11}$$

Gee [15] has shown that such an equation is valid for a single ordering parameter which is frozen in the glass. However, since h has been found to vary slightly with temperature and pressure in the glass [16, 17, 18], eq (11) must be revaluated to assess its validity for the more general case.

Consider the single-valued function $V = V(T, P, h)$ for which, by the usual definitions,

$$-\kappa = (\partial \ell nV/\partial P)_T = (\partial \ell nV/\partial P)_{T,h} + (\partial \ell nV/\partial h)_{T,P}(\partial h/\partial P)_T$$

$$\alpha = (\partial \ell nV/\partial T)_P = (\partial \ell nV/\partial T)_{P,h} + (\partial \ell nV/\partial h)_{T,P}(\partial h/\partial T)_P.$$

Since there are three independent variables (in the general case, the derivatives with two fixed arguments (suscripts) are the same for liquid and glass. (For the glass it is understood that these derivatives pertain to constant P' and k.) The differences become

$$-\Delta\kappa = (\partial \ell nV/\partial h)_{T,P}[(\partial h/\partial P)_{T,\ell} - (\partial h/\partial P)_{T,g}]$$

$$\Delta\alpha = (\partial \ell nV/\partial h)_{T,P}[(\partial h/\partial T)_{P,\ell} - (\partial h/\partial T)_{P,g}],$$

where the subscripts ℓ and g again pertain to liquid and glass. Recalling that $dT_g^\dagger/dP = \Delta\kappa/\Delta\alpha$, the ratio of the above equations is

$$dT_g^\dagger/dP = (\partial T/\partial P)_{h,\ell}F_P/F_T \tag{12}$$

where the "freezing fractions" F_P and F_T are

$$F_P = 1 - (\partial h/\partial P)_{T,g}/(\partial h/\partial P)_{T,\ell}$$

$$F_T = 1 - (\partial h/\partial \mathrm{T})_{P,g}/(\partial h/\partial T)_{P,\ell} \tag{13}$$

as defined in ref. [14]. Note that when $F_T = F_P$, eqs (11) and (12) coincide.

[3] Differential scanning calorimetry

Since the variables T, P, and h are continuous at $T_g^\dagger$, it follows that

$$(\partial T/\partial P)_{h,\ell} = (\partial T/\partial P)_{h,g} = (\partial T/\partial P)_h$$

along this transition line. From partial differential equations, i.e.

$$(\partial T/\partial P)_h = -(\partial h/\partial P)_{T,\ell}/(\partial h/\partial T)_{P,\ell}$$
$$= -(\partial h/\partial P)_{T,g}/(\partial /h/\partial T)_{T,g},$$

it follows that

$$(\partial h/\partial P)_{T,g}/(\partial h/\partial P)_{T,\ell} = (\partial h/\partial T)_{P,g}/(\partial h/\partial T)_{P,\ell},$$

which, as seen from eq (13), is tantamount to $F_T = F_P$. Accordingly, since eqs (12) and (13) coincide, the validity of eq (12) is extended to a single ordering parameter which need not be "frozen" in the glass.

To our knowledge both of the above freezing fractions have been evaluated for only two systems, namely poly(vinyl acetate) [16] and selenium [19]. According to the best analysis given in ref. [16], $F_P = 0.88$ and $F_T = 0.82$ for which the ratio $F_P/F_T = 1.07$, which corresponds to a 7 percent discrepancy in eq (11) for poly(vinyl acetate). A similar conclusion follows for Se. Since the above analysis shows that $F_T = F_P$, these differences are taken to be artifacts resulting from numerical inaccuracies.

The next step is the evaluation of $(\partial\tilde{T}/\partial\tilde{P})_h$ at equilibrium. From simultaneous numerical solutions of eqs (9) and (10), values of $h = 1 - y$ are obtained at a given set of reduced temperatures and pressures. For computational purposes it is convenient to replace $(\partial\tilde{T}/\partial\tilde{P})_h$ by the ratio $-(\partial h/\partial\tilde{P})_{\tilde{T}}/(\partial h/\partial\tilde{T})_{\tilde{P}}$. With constant increments $\Delta x (x = T \text{ or } P)$, it is easily shown for a quadratic dependence of y on x that

$$(dy/dx)_i = (y_{i+1} - y_{i-1})/(2\Delta x).$$

This procedure is used to generate a set of $(\partial h/\partial\tilde{P})_{\tilde{T}}$ and $(\partial h/\partial\tilde{T})_{\tilde{P}}$ values over the desired range from the sets of quadratic arcs defined by three adjacent points. Using a least squares fit, the approximation

$$(\partial\tilde{T}/\partial\tilde{P})_h = 0.00502 + 0.198\,\tilde{T} + 31.476\tilde{T}^2 \qquad (14)$$

is found to be accurate within a residual standard deviation of 0.2 percent at atmospheric pressure over the range $0.01 \leq \tilde{T} \leq 0.04$. From eqs (8) and (11)

$$dT_g^\dagger/dP = T^*(\partial\tilde{T}/\partial\tilde{P})_h/P^*. \qquad (15)$$

Substitution of eq (15) into eq (5b) gives the desired relation for the densification rate,

$$\kappa' = \Delta\alpha[T^*(\partial\tilde{T}/\partial\tilde{P})_h/P^* - dT_g/dP], \qquad (16)$$

where all quantities are evaluated at $T = T_g$.

Equation (16) may be rewritten (see for example eq (14) in Ref. [14]) as

$$\kappa' = -\Delta\alpha[(\partial T/\partial h)_P \times dh/dP] \qquad (16')$$

where the total derivative on the right hand side is to be taken along the $T_g(P)$ line. Provided the pressure coefficient of T_g has been determined with sufficient accuracy, there apparently is no numerical advantage in using eq (16').

It is mentioned in the last section that eq (7) appears to be a good approximation for most polymers. Assuming this relation, we may estimate κ' from volume-temperature and heat capacity data using the relation

$$\kappa' = \Delta\alpha[T^*(\partial\tilde{T}/\partial\tilde{P})_h/P^* - T_gV\ \Delta\alpha/\Delta C_P]. \qquad (17)$$

Olabisi and Simha [17] have shown for most polymers studied by them that the scaling factor P^* may be determined from the other two by means of the empirical relation

$$P^* = (T^*/V^*)\exp(1.319 - 1.493 \times 10^{-4}T^*) \qquad (18)$$

where the dimensions are K, bar, and cm^3/g. Thus it appears feasible to estimate κ' from appropriate data at atmospheric pressure only. This possibility is tested later in this paper.

According to Wunderlich [20] it is possible to estimate ΔC_P at T_g to within about ± 2 J/(mol−K) by applying the "rule of constant ΔC_P". The molecular repeat units are broken up into fundamental units or "beads" which loosen up in the T_g process. Each bead is assigned the value 11.3 J/(mol−K). The contributions of the beads to ΔC_P are assumed to be additive. Accepting the validity of this rule, it appears possible to obtain a crude estimate of κ' from hole theory applied to volume-temperature measurements alone.

4. Results

4.1. Data Sources

Although we refer usually to the original sources, there are collections of data on the pertinent quantities in the literature, which are sometimes cited here. Extensive lists of polymers and their values of T_g appear in refs. [21–23], where the last is restricted to fluorine-containing systems. Tables of T_g and $\Delta\alpha$ are included in Refs. [24–26], and T_g and ΔC_p in Refs. [27] and [28]. Reference [29], which is occasionally cited here, contains a more critical evaluation of C_p data on polymers for which the values on the same substance are often based on averages from different sources over wide ranges of temperature. Lists of polymers and their scaling factors based on the hole theory appear in Refs. [17] and [30]; however, P^* is not available in the latter. Pyrolysis data on polymers are contained in refs. [31–34]. These are useful to prevent degradation during the densification process and to optimize the amount of densification. Finally, ref. [35] gives an extensive list of refractive indices for polymers.

The number of digits for the values given in the subsequent tables is not intended to be an indication of precision or accuracy. Usually these numbers correspond to those given by the data sources. It is our opinion that most of the entries in these tables have more digits than can be justified as significant.

Table 1 gives the lists of polymers studied, abbreviations used here, and their values of T_g. In all tables the sequence is in order of increasing T_g.

TABLE 1. *List of polymers studied, abbreviations, and glass temperatures*

Abbreviations	Polymer of	T_g(K)
PDMSi	Dimethyl siloxane	150
PIB	Isobutylene	202
NR	Natural Rubber	204
PP	Propylene	244
SBR[a]	Styrene-butadiene	257
PMA	Methyl acrylate	282
PnBMA	*n*-butyl methacrylate	293
PVAc	Vinyl acetate	304
i-PMMA	Isotatic methyl methacrylate	320
PEMA	Ethyl metacrylate	337
PET	Ethylene terephthalate	340
PVC	Vinyl chloride	349
P4POS	4-phenoxystyrene	352
P3CS	3-chlorostyrene	363
PS	Styrene	363
a-PMMA	Atatic methyl methacrylate	378
PCHMA	Cyclohexyl methacrylate	380
P4MOS	4-methoxy styrene	381
P4CS	4-chlorostyrene	400
PoMS	*o*-methyl styrene	404
Pcarb	Carbonate of bis(phenol A)	416
PαMS (1)	α-methyl styrene (67% syndiotatic)	448
PαMS (2)	α-methyl styrene (95% syndiotatic)	455

[a] 55 percent Styrene.

4.2. Scaling Factors

Table 2 gives the scaling factors based on the hole theory of Simha and Somcynsky [10]. These are determined through superposition of experimental equilibrium data on each polymer with respect to the theoretical equation of state. In this work the scaling factors are used solely to estimate $dT_g^\dagger/dP = \Delta\kappa/\Delta\alpha$ for each polymer using eq (15). When two numbers appear in the reference column (in table 2 only), the first applies to the data source, and the second to the work by which the scaling factors are evaluated. When only one number appears, the scaling factors are either evaluated in the reference given, or by us.

TABLE 2. *Polymer scaling factors*

Polymer	Ref.	T* K	V* cm³/g	P* bar	P*calc bar	Δ P*/P %
PDMSi	36, 30[a]	7893	0.9602	5061	9461	87
PDMSi	37	7893[b]	.9602[b]	5061	9461	87
PIB	38, 30[a]	11220	1.0902	—	7208	—
PIB	37	11220[b]	1.0902[b]	7316	7208	−1.4
NR	39	8344	1.0353	—	8672	—
PP	40	8966	1.1230	8437	7829	−7.2
SBR[c]	41	9800	0.9892	—	8577	—
PMA	42, 17	9200	.7925	—	10990	—
PnBMA	43, 17	9988	.9299	8456	9402	11
PVAc	1, 14	9419	.8141	9380	10600	13
PVAc	37	9419[b]	.8141[b]	9158	10600	16
i-PMMA	44	11170	.8160	10090	9659	−4.3
PEMA	45, 30[a]	11540	.8862	—	8694	—
PET	46	10870	.7406	—	10830	—
PVC	47[d], 17	11320	.7105	10350	10990	6.2
PVC	48	11363	.7083	9783	11000	12
PS	15	12880	.9601	6628	7333	11
PS	47[d], 17	12700	.9625	7638	7409	−2.9
PS	49	11630	.9480	7881	8082	2.6
PS	50	12680	.9598	7453	7440	−0.2
a-PMMA	48	11490	.8220	8987	9403	4.6
a-PMMA	43, 17	11920	.8370	9147	8984	−1.8
a-PMMA	47[d], 17	11890	.8350	9303	9024	−3.0
PCHMA	43, 17	11290	0.8906	8382	8786	4.8
PoMS	50	12740	.9762	7458	7285	−2.3
Pcarb	51, 30[a]	12130	.8100	—	9156	—
PαMS (1)	52, 30[a]	12700	.9152	—	7792	—
PαMS (2)	52, 30[a]	12790	.8433	—	8403	—

[a] T* and V* only are determined in this reference.
[b] Volume-temperature data at atmospheric pressure taken from previous listing.
[c] 55 per cent Styrene.
[d] For additional comments of interpretation on these experimental data and evaluation of Tait parameters, see Ref. [53].

Two values of P^* for each polymer (or row) usually appear. The first of these (P^*) is determined in the usual way through superposition as mentioned above. The second (P^*_{calc}) is obtained from eq (18). When volume-temperature data are available at atmospheric pressure only, it is necessary to use eq (18) to estimate P^*. With the exception of PDMSi, P^* and P^*_{calc} agree to within 17 percent with an 8 percent relative standard deviation of differences over 17 pairs. With PDMSi the disparity of 87 percent is outstanding, and it is to be noted that the reduced glass temperature lies significantly outside the range for which eq (18) was deduced. Similarly, V^* and T^* are obtained at considerably higher temperatures than those employed here. A decrease of T^* by 7.2 percent and a concomitant decrease of V^* by 2.4 percent over 100 K has been estimated [30] for this polymer. Accordingly, the scaling factors cannot be assigned significant constant values over the experimental range.

In order to obtain some measure of the uncertainty in the scaling factors, several data sources on each polymer are sometimes included.

4.3. Densification Rates from *PVT* Data

Table 3 gives the results of calculations of the densification rates from *PVT* data without recourse to molecular theory. κ_1' is determined from the definition:

$$\kappa_1' = (V_A - V_B)/V_A P' \qquad (4')$$

which is identical to eq (4) setting $\Delta P = P'$, except that V_A replaced V_0. The difference between the values of κ_1' determined from eqs (4) and (4′) are insignificant in comparison with experimental uncertainty. κ_2' is determined from eq (5b). Note that there are only two polymers, PVAc and PαMS for which we found sufficient information to determine both κ_1' and κ_2'. Although the two methods are not necessarily fully equivalent because of the assumptions used to derive eqs (5), the agreement in both cases is good. In instances of more than one set of values per polymer, it is clear that the deviations in $dT_g^\dagger/dP$ have the largest effect on the uncertainty of κ_2'. These apparent discrepancies are usually consistent with the differences in $\Delta\kappa$. With polystyrene the maximum deviation in $dT_g^\dagger/dP$ is 38 percent compared with those for dT_g/dP, 23 percent and $\Delta\alpha$, 10 percent. Since κ_2' involves the difference between the two transition rates, its maximum deviation is magnified to 56 percent with its relative standard deviation over the five values being 26 percent. It is interesting to note that the direct method giving κ_1' which one might expect to be more reliable, yields values for which the maximum deviation (for polystyrene) is 86 percent with relative standard deviation over seven values being 35 percent. The ratio of average values, $\bar{\kappa}_2'/\bar{\kappa}_1'$, is 1.6. These discrepancies are a measure of the difficulties in obtaining reliable *PVT* data on glassy polymers.

In many instances the values of $\Delta\alpha$ at T_g and the required transition rates are not tabulated in the data sources and, therefore, had to be evaluated. The accuracy of these evalua-

tions may be considerably limited when the data are presented in graphical form only. In ref. [47] the values of $\Delta\kappa$ are determined by a different definition from the one used by us. In our definition κ_g is taken to be an isochronal (nonrelaxing) function of temperature and pressure and therefore must be derived from data at temperatures below (or pressures above) the glass transition region. $\Delta\kappa$ at T_g is then obtained by extrapolation. This, apparently, was not done by Hellwege et al. [47], at least over the appropriate temperature range for the data to be effectively isochronal. The distinction between the two definitions is clearly illustrated by Boyer [57]. Our larger values of $\Delta\kappa$ are determined from the Tait parameters given in ref. [53], which apply to the data of Hellwege et al. [47]. Note that the values of $dT_g^\dagger/dP$ from reevaluating [53] their data are in good agreement with most of the others on the same polymers except for PMMA. This discrepancy would be increased by using their value of $\Delta\kappa$ given in ref. [47], along with poorer overall agreement with the other two polymers.

In ref. [1] the transition rates are given as tangent values along the transition lines at each experimental pressure. Here, we use the secant values dT_g/dP and $dT_g^\dagger/dP$ between 0 and 800 bar. This procedure gives average values and is more consistent with other treatments.

The smallest value of $\kappa' = 0.7$ Mbar^{-1} in table 3 applies to PnBMA. Such a small value implies that the first Ehrenfest equation is a good approximation for this polymer. [See eqs (5c) and (6b)].

TABLE 3. *Densification rate calculations at atmospheric pressure from PVT data*

Polymer	Ref.	$\Delta\alpha \times 10^4$ K^{-1}	dT_g/dP K/kbar	$dT_g\dagger/dP$ K/kbar	κ'_1 Mbar^{-1}	κ'_2 Mbar^{-1}
PnBMA	43	1.69	20.4	24.3	–	0.7
PVAc	1	4.32	21.2	42.4	8.8	9.2
i-PMMA	44	3.49	21.1	35.2	–	4.9
PVC	47	2.93	13.5	35.5[a]	–	6.4
PVC	48	3.71	14	46	–	12
PVC	2	–	–	–	4.4	–
P4POS	5	–	–	–	7.2	–
P3CS	5	–	–	–	5.8	–
PS	15	2.84	31	71	–	11
PS	47	3.05	30.0	56.4[a]	–	8.1
PS	49	3.15	25.0	49.8	–	7.8
PS	50	2.97	31.6	74.2	–	13
PS	2	–	–	–	5.5	–
PS	4	–	–	–	10	–
PS	5	–	–	–	7.2	–
PS	6	–	–	–	4.3	–
PS	8	–	–	–	5.6	–
PS	9	–	–	–	9.5	–
PS	54	–	–	–	4.5	–
PS	55	3.12	32	73	–	13.8
a-PMMA	48	3.1	18	71	–	15
a-PMMA	47	2.95	23	35.9[a]	–	3.8
a-PMMA	43	2.35	23.6	54.5	–	7.3
a-PMMA	2	–	–	–	5.9	–
a-PMMA	54	–	–	–	4.9	–
PCHMA	43	3.38	22.4	59.8	–	13
P4MOS	5	–	–	–	7.1	–
P4CS	5	–	–	–	9.5	–
PoMS	50	2.71	34.2	73.0	–	11
Pcarb	2	–	–	–	5.1	–
PαMS[b]	56	3.98	39	52	4.9	5.2

[a] The values of $\Delta\kappa$ here are not consistent with those given in Ref. [47]. For distinction, see text and/or Ref. [57].

[b] Tacticity not known to correspond to listings in table 1.

4.4. Theoretical Estimation of the Transition Rate $dT_g^\dagger/dP$

As stated in section 3 the transition rate $dT_g^\dagger/dP = \Delta\kappa/\Delta\alpha$ applicable to the constant formation history, may be estimated from the value of $(\partial T/\partial P)_h$ at T_g. Table 4 summarizes the results of these calculations. In all cases except for PDMSi and PIB the data encompass T_g. With these two polymers the first reference for each applies to the source of data at atmospheric pressure, and the second, at elevated pressures.

Equation (14) and the scaling temperatures and pressures as applied to eq (15) provide the requisite information. The distinction between the values of $(\partial T/\partial P)_h$ in columns A and B is that they correspond to P^* and P^*_{calc}, respectively, in table 2. Values of $dT_g^\dagger/dP$ are included for comparison with those of $(\partial T/\partial P)_h$ in cases where there is sufficient experimental information.

With natural rubber (NR) $\Delta\kappa$ is determined from dynamic compressibility data [60]. This involves the measurement of the adiabatic compressibility in a hydrostatic stress field alternating at low audio frequencies. The low- and high frequency limiting compressibilities are converted from adiabatic to isothermal conditions, providing the difference $\Delta\kappa$. The fact that $\Delta\kappa$ is determined at about 20 K above normal T_g is expected to have no appreciable effect.

Except for PDMSi, the corresponding values of $(\partial T/\partial P)_h$ are nearly the same in columns A and B. The discrepancy for PDMSi is explained by the factors mentioned earlier. (See sec. 4.2.). Excluding this polymer, the relative standard deviation of the differences between corresponding values in these columns is 6 percent, which is considered to be good agreement. For comparison with experiment, the residual standard deviation between corresponding values of $(\partial T/\partial P)_h$ (column A) and $dT_g^\dagger/dP$ is 18 percent. Poor agreement is noted for PnMBa, and two samples of *a*-PMMA.

Over a single substance, for example polystyrene where we have four sets of values, the relative standard deviations with respect to the averages for $(\partial T/\partial P)_h$ (column A) and $dT_g^\dagger/dP$ are 6 and 15 percent, respectively. That for the differences between corresponding values of these quantities is 11 percent. Thus, based on these simple statistics, the most serious limitation is not the inadequacy of the theory, but the uncertainty in the experimental determination of $dT_g^\dagger/dP$. The agreement between values of $dT_g^\dagger/dP$ from different investigators is even worse for *a*-PMMA.

4.5. Application of Hole Theory

After determining the values of $(\partial T/\partial P)_h$ for each substance, κ' may be estimated by eq (16), where dT_g/dP may be determined by means of *PVT* data, dynamic measurements at elevated pressures, or heat capacity and thermal expansion data, both at atmospheric pressure.

PVT Data

Since *PVT* measurements are often made by the variable formation history only (for example, polypropylene, ref. [40]), there is insufficient information to determine $\Delta\kappa$, and hence $dT_g^\dagger/dP$, to be applied to eq (5b). Accordingly, this quantity is replaced by $T^*(\partial\tilde{T}/\partial\tilde{P})_{\tilde{h}}/P^*$ leading to eq (16). The results of these estimates are given in table 5, where κ' corresponds

to κ'_2 in table 3. In all cases $(\partial T/\partial P)_h$ is taken from column A of table 4. Since the expression for κ' involves the difference between two transition rates, its value is very sensitive to $(\partial T/\partial P)_h$. This effect is reflected in the large standard deviation, 2.5 $Mbar^{-1}$, with a relative value of 28 percent, for the differences over 14 pairs of corresponding values of κ'_2 and κ' in tables 3 and 5. The values of PαMS are not included in this calculation because there are insufficient data in ref. [56] to determine the scaling factors applicable to this particular sample. Based on the fact that the standard deviation of κ'_2 for polystyrene (table 3) over five values is 2.8 $Mbar^{-1}$ corresponding to 26 percent, the overall 28 percent value above appears to be dominated by experimental uncertainty.

TABLE 4. *Transition rates calculated from hole theory*

Polymer	Ref.	T_g K	$\bar{T}_g \times 10^5$	$(\partial\bar{T}/\partial\bar{P})_h \times 10^5$	A $(\partial T/\partial P)_h$ K/kbar	B $(\partial T/\partial P)_h$ K/kbar	dT_g/dP K/kbar
PDMSi	36, 37	150[a]	1900	2014	31.4	16.8	–
PIB	37, 38	202[b]	1800	1878	28.8	29.2	–
NR	39	204	2445	2868	–	27.6	24[c]
PP	40	244	2721	3371	35.8	38.6	–
SBR	41	256	2622	3185	–	36.4	–
PMA	42	281	3054	4042	–	33.8	–
PnBMA	43	293	2934	3792	44.8	40.3	24.3
PVAc	1	304	3226	4416	44.3	39.2	42.4
i-PMMA	44	320	2865	3653	40.4	42.2	35.2
PEMA	45	338	2928	3780	–	50.2	–
PET	46	340	3128	4201	–	42.2	–
PVC	47	349	3083	4104	44.9	42.3	41
PVC	48	349	3071	4079	47.4	42.1	46
PS	15	362	2811	3546	68.9	62.3	71.0
PS	47	362	2850	3623	60.2	62.1	56
PS	49	365	3138	4223	62.3	60.8	55.5
PS	50	365	2879	3681	62.6	62.7	74.2
a-PMMA	48	376	3272	4520	57.8	55.2	71
a-PMMA	47	378	3179	4312	55.1	56.8	35.9
a-PMMA	43	378	3171	4295	56.0	57.0	54.5
PCHMA	43	380	3366	4735	63.8	60.8	59.8
PoMS	50	404	3171	4295	73.4	75.1	73.0
Pcarb	51	423	3487	5020	–	66.5	–
PαMS[d]	56	440	3465	4967	–	81.0	52
PαMS (1)	52	448	3528	5118	–	83.4	–
PαMS (2)	52	455	3557	5189	–	86.5	–

[a] T_g taken from ref. [58].
[b] T_g taken from ref. [59].
[c] $\Delta\kappa$ determined from dynamic compressibility data [60] on vulcanized natural rubber with 12 percent combined sulfur. See text.
[d] Scaling factors taken the same as for PαMS (1).

Dynamic Data

From the assumption that the value of dT_g/dP, approximates that of $(\partial T/\partial P)_\omega$, where ω is the angular frequency, frequency-temperature-pressure superposition of dynamic data, including dielectric and ultrasonic, may be used to determine dT_g/dP appearing in eq (16). The validity of this assumption is, of course, subject to the condition that $(\partial T/\partial P)_\omega$ for the T_g -process is essentially independent of frequency. (Numerical comparisons between different experimental transition rates are made below.)

The results of these calculations are given in table 6. Since values of $(\partial T/\partial P)_h$ in column A of table 4 involve fewer assumptions than those in column B, the former are used where there is a choice. The standard deviation of the differences of κ' over eight pairs, where there are values on the same substances in table 3 including κ'_1 for Pcarb, is 2.2 $Mbar^{-1}$ or 30 percent, which is about the same as the experimental uncertainty given above (2.8 $Mbar^{-1}$ or 26 percent) for polystyrene. This value is also about the same as the 28 percent value given for the *PVT* data even though data on different substances are involved. It is possible, however, that dT_g/dP values determined from dynamic data, in particular dielectric, where high resolution is obtained, are more reliable than *PVT* values. T_g determinations from *PVT* data usually involve extrapolations which are not used in the superposition of dynamic data.

TABLE 5. *Densification rate calculations using PVT data and hole theory*

Polymer	Ref.	$\Delta\alpha \times 10^4$ K^{-1}	dT_g/dP K/kbar	$(\partial T/\partial P)_h$ K/kbar	κ' $Mbar^{-1}$
PP	40	4.41	20	35.8	7.0
PnBMA	43	1.69	20.4	44.8	4.1
PVAc	1	4.32	21.2	44.3	10
i-PMMA	44	3.49	21.1	40.4	6.7
PVC	47	2.93	13.5	44.9	9.2
PVC	48	3.71	14	47.4	12
PS	15	2.84	31	68.9	11
PS	47	3.05	30.0	60.2	9.2
PS	49	3.15	25.0	62.3	12
PS	50	2.97	31.6	62.6	12
a-PMMA	48	3.1	18	57.8	12
a-PMMA	47	2.95	23	55.1	9.5
a-PMMA	43	2.35	23.6	56	7.6
PCHMA	43	3.38	22.4	63.8	14
PoMS	50	2.71	34.2	73.4	11
PαMS[a]	56	3.98	39	81	17

[a] Scaling factors taken for PαMS (1), Ref. [52].

Heat Capacity and Thermal Expansion

The estimation of κ' from heat capacity and thermal expansion data is based on the apparent validity of the second Ehrenfest equation [eq (7)]. (This relation is tested in the next section.) The results of the calculations based on eq (17) are summarized in table 7. In this case the statistics may not be meaningful because there are only five values of κ' which correspond to those in table 3 including κ_1 for Pcarb. PαMS is excluded for the reason given above. The standard deviation of the differences is 1.4 $Mbar^{-1}$ or 17 percent, which is somewhat less than the experimental uncertainty (26 percent) based on polysytrene data (table 3). In view of the high experimental uncertainty for all methods, this method of estimating κ' appears to be reliable, except for PDMSi and PαMS.

In ref. [12] a negative value of κ' for PDMSi [based on eq (17)] is reported. This is a surprising, but not necessarily an incorrect result. The analysis of this polymer is hindered by the lack of good thermal expansion data through T_g, largely a consequence of the low temperatures required, and the strong tendency for this polymer to crystallize. The negative value of κ' is obtained by using the value of $\Delta\alpha = 10.28\ K^{-1}$ from table I of ref. [26]. This value is based on the linear thermal expansion data of Weir, Leser, and Wood [58]. After a thorough examination of their results and consultation with Dr. Wood, it was decided that the temperature range for which $V\alpha_l$ was evaluated is too small and too remote from T_g to evaluate $\Delta\alpha$ at T_g. In order to obtain what we consider to be the best available estimate of $\Delta\alpha$, we used the value of $V\alpha_g = 2.7 \times 10^{-4}$ cm³/(g-K) from ref. [58], and $\alpha_l = 8.7 \times 10^{-4}\ K^{-1}$ and $V_g = 0.904$ cm³/g from the density-temperature

TABLE 6. *Densification rate calculations from dynamic data at elevated pressures and hole theory*

Polymer	Ref.	$\Delta\alpha \times 10^4$ K^{-1}	$(\partial T/\partial P)_h$ K/kbar	Ref.	Method	$(\partial T/\partial P)_\omega$ K/kbar	κ' Mbar^{-1}
PIB	37, 38, 59	4.2	28.8	61	U	25	1.6
NR	39	5.40	27.6	60	C	24	1.9
PMA	42	3.7	33.8	62	D	18	5.8
PnBMA	43	1.69	40.3	63	D	16.7	4.0
PVAc	1	4.32	39.2	13	D	22	7.4
PVAc[a]	1	4.32	39.2	64	C	20	8.3
PEMA	45	2.95	50.2	65	D	20	8.9
PVC	47	2.93	44.9	66	D	18	7.9
PVC	47	2.93	44.9	67	S	16.5	8.3
PS	50	2.97	62.6	68	D	32	9.1
a-PMMA	43	2.35	56.0	67	S	24.5	7.4
Pcarb	51	2.81	66.5	13	D	44	6.3

[a] All quantities derived for same sample.
U Ultrasonic
D Dielectric
C Dynamic Compressibility
S Dynamic Shear

TABLE 7. *Densification rate calculations from thermal expansion and heat capacity data and hole theory*

Polymer	Ref.	T_g K	V_g cm^3/g	$\Delta\alpha \times 10^4$ K^{-1}	$(\partial T/\partial P)_h$ K/kbar	Ref.	ΔC_p J/(g-K)	dT_g/dP[a] K/kbar	κ' Mbar^{-1}
PDMSi[b]	58, 30	150	0.904	6.0	31.4	27	0.30	27.0	2.6
PIB	59	202	1.072	4.2	28.8	69	.377	24.1	2.0
NR	39	204	1.023	5.40	27.6	70	.455	24.8	1.5
PP[c]	40	244	1.127	4.41	35.8	71	.51	23.8	5.3
SBR[d]	41	256	0.987	3.92	36.4	72	.456	21.7	5.8
PVAc[e]	1	304	.843	4.32	44.3	16[e]	.50	22.1	9.6
PVC	47	349	.729	2.93	44.9	29[f]	.34	21.9	6.7
PS	50	365	.976	2.97	62.6	29[f]	.368	28.8	10
a-PMMA	43	378	.864	2.35	56.0	29[f]	.33	23.3	7.7
Pcarb	51	423	.854	2.81	66.5	73	.22	46.1	5.7
PαMS[c]	56	440	.958	3.98	81.0	56	.32	52.4	11

[a] $dT_g/dP = T_g V\ \Delta\alpha/\Delta C_P$.
[b] Partially crystalline sample.
[c] All quantities derived from the same sample.
[d] 55 percent Styrene for T_g, V_g and $\Delta\alpha$, 43 percent ΔC_P.
[e] Measurements by J. J. Weeks reported in Ref. 16.
[f] Average over different sources.

equation of Shih and Flory [36]. Although this equation is derived from data at temperatures well above T_g, its nearly linear response apparently allows valid extrapolation to much lower temperatures. The value $V_g\alpha_l = 7.9 \times 10^{-4}$ cm^3/(g-K) is slightly less than the average, 8.7×10^{-4}, of the others for this polymer in table I of ref. [26] which are obtained from different sources of data at higher temperatures not encompassing T_g. Also the extrapolated value of $V_g = 0.904$ cm^3/g above essentially coincides with 0.905 in ref. [26]. The revised thermal expansion values give the positive value of κ' shown in table 7.

4.6. Comparison of Experimental Transition Rates

In tables 6 and 7 the assumptions that dT_g/dP could be replaced by $(\partial T/\partial P)_\omega$ or $TV\Delta\alpha/\Delta C_P$, respectively, are employed. In table 8 values of these quantities are compared for each polymer. A similar table was prepared by O'Reilly [13] in 1962 for glass-forming liquids not restricted to polymers. Values of $\Delta\kappa/\Delta\alpha$ are also included here for comparison; however, agreement with dT_g/dP is not expected since the validity of the inequality

$$dT_g/dP < \Delta\kappa/\Delta\alpha$$

appears to be quite strong and general. In most instances, agreement between dT_g/dP, $(\partial T/\partial P)_\omega$, and $TV\alpha/\Delta C_P$ seems to be within experimental error. Small differences may be anticipated because the conditions under which these quantities are evaluated may be vastly different.

TABLE 8. *Comparison of experimental transition rates*[a]

Polymer	PVT			Dynamic		Thermal	
	Ref.	dT_g/dP	$\Delta\kappa/\Delta\alpha$	Ref.	$(\partial T/\partial P)_\omega$	Ref.	$TV\Delta\alpha/\Delta C_P$
PIB				61	25	59, 69	24.1
NR	39, 60		26[b]	60	24	39, 70	24.8
PP	40	20				40, 71	23.8
PVAc[c]	1	21.2	48.2	64	22	1, 16[d]	22.1
PVC	47	13.5	33.5	66	18	47, 29	21.9
PVC	48	14	46	67	16.5	48, 29	28.6
PS	50	31.6	74.2	68	32	50, 29	28.8
PS[c]	9	31				9	30.5
PS	55	32	73			55	34
a-PMMA	43	23.6	54.5	67	24.5	43, 29	23.3
a-PMMA[c]	9	22				9	32
Pcarb				13	44	51, 73	46.1
PαMS	56	39	52			56	52

[a] All units in K/kbar.
[b] $\Delta\kappa = 1.2 \times 10^{-5}$ bar^{-1} determined from dynamic compressibility.
[c] All given determinations on same sample.
[d] Measurements by J. J. Weeks reported in Ref. [16].

According to these results the Prigogine-Defay ratio

$$r = \Delta\kappa\ \Delta C_P/[TV(\Delta\alpha)^2]$$

is essentially unity for natural rubber and PαMS. Unfortunately, we do not have a PVT value of dT_g/dP for the former to test the validity of the Ehrenfest equations [eqs (6) and (7)]. With PαMS it would appear that although neither of the Ehrenfest equations is obeyed, the Prigogine-Defay ratio is still unity, which is an atypical result. This implies that dT_g^+/dP for volume and entropy are equal, but dT_g/dP is distinct. However, since data in tabular, or even graphical form, are not included in ref. [56], evaluation of these numbers cannot be scrutinized. Poor agreement for PVC in all cases is apparent; however, this may be a result of sample differences including the degree of crystallinity which is difficult to control in this polymer. Also poor agreement is noted for a-PMMA of ref. [9], where both quantities are obtained from the same sample. On the other hand, the data in the row above on the same polymer reveal good agreement including that with dT_g/dP (PVT) of ref. [9]. In all cases agreement is very good for polystyrene.

These results indicate that $dT_g/dP = (\partial T/\partial P)_\omega$ is a valid relation and $dT_g/dP = TV\Delta\alpha/\Delta C_P$ seems to hold most of the time. The validity of the first may be argued on a qualitative phenomenological basis (see sec. 2.) The second relation is evaluated at atmospheric pressure only. There is no apparent reason to assume that the approximation will be as good at elevated pressures.

In section 4.3 we mentioned that PVT data on PnBMA suggest that the first Ehrenfest equation [eq (6b)] is a good approximation for this polymer. This result is tantamount to essentially no densification. (See table 3.) Unfortunately, we have no heat capacity values for this polymer, which are needed to check the second Ehrenfest equation [eq (7)]. In section 3 we noted the possibility of using the "rule of constant ΔC_P" [20] to estimate the heat capacity difference at T_g. (For a comparison of experimental and "bead" values of ΔC_P on polymers, see ref. [28].) For PnBMA the molecular weight of the polymeric repeat unit is 142.2 g/mol. Assigning one bead to each of the two carbon backbones, and one to the oxygen atom, we obtain a total of three beads, which for 11.3 J/(mol-K-bead) gives $\Delta C_P = 0.24$ J/(g-K). Taking this value along with those for $\Delta\alpha$ and T_g from tables 3 and 4, respectively, and $V_g = 0.946$ cm^3/g from ref. [43], we obtain $TV\Delta\alpha/\Delta C_P = 20$ K/kbar, which is in good agreement with 20.4 in table 3. Thus both of the Ehrenfest equations appear to be fairly good approximations for this polymer, along with a corresponding Prigogine-Defay ratio of nearly unity. (The value 1.2 is obtained for PnMBA. The average value obtained from table 8, exclusive of NR and PαMS, which were treated separately, is 2.1.) These results imply that both the density and entropy of PnBMA are essentially independent of formation pressure, at least at low pressures.

4.7. Pressure Dependence of κ' and Limitations Imposed by Chemical Instability

The previous discussions in this paper pertain to the initial values of κ' or at least at very low formation pressures. Most of these are either tangent values at $P' = 0$ (atmospheric pressure) or secant values obtained from $P' = 1$ kbar or less. There are data in the literature, however, which include densifications obtained at different formation pressures.

There are two important physical considerations in optimizing the procedure to obtain "permanent," densified glasses. The first and more obvious, is to select and maintain the temperature of depressurization at temperatures sufficiently below T_g. It is clear that the ambient conditions must be such as to maintain structural relaxation times which are large in comparison to the desired "lifetime" of the glass. Accordingly, high T_g substances are preferable for room temperature stability. The second is to choose T_0, the temperature of isothermal pressurization, large enough that the equilibrium melt is always maintained during pressurization. Stated alternatively, the inequality

$$T_0 > T_g(P') \tag{19}$$

must be approximately satisfied, as illustrated in figure 1. This condition implies that the effective time of the pressurization process must be large in comparison to the structural relaxation time at the final pressure P'. In cases where $T_0 < T_g(P')$ there will be a much smaller contribution to the densification process when the condition $T_0 = T_g(P)$ is approximated and exceeded during pressurization. This situation is revealed by a leveling off in the volume as illustrated schematically in figure 4, where volume changes are plotted with respect to formation pressure at different pressurization temperatures. The densification is expected to be independent of T_0 at low pressures, when ineq (19) is satisfied, as is revealed by the coalescence of these curves with decreasing P'. Such a coalescence is not expected, however, when $T_0 < T_g$ as is illustrated by the data of Shishkin [54] on polystyrene. In figure 4 the dashed line represents the extension of the envelope established from arbitrarily large values of T_0.

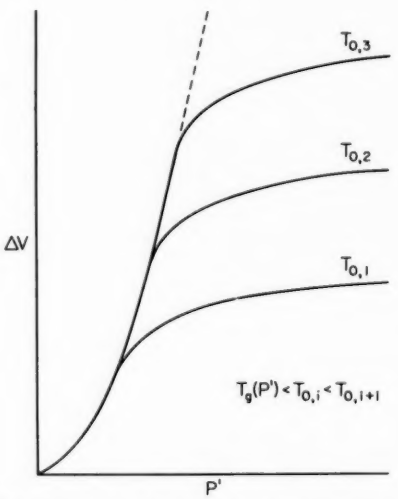

FIGURE 4. Illustration of the influence of the pressurization temperature T_0 on the densification process.
The dashed line is the envelope approached at large temperatures.

One of the better experimental examples which illustrates the behavior shown in figure 4 is provided by the data of Shishkin on PMMA and PS. Formation pressures up to four kbar are applied; but not all of the pressurization temperatures are above $T_g(P')$. At the lower pressures, κ' increases with P' as is indicated by the increasing slopes of Shishkin's volume-formation pressure curves, and as is shown in figure

4. This is the opposite of the trend for the isothermal compressibility κ, which decreases with increasing pressure (see for example refs. [12] and [74]). The data of Shishkin, as well as those of Kimmel and Uhlmann [75] on PMMA, show that some densification is possible with pressurization temperatures below T_g, but the effect is diminished as the difference between these two temperatures is increased. Other examples illustrating the dependence of densification on formation pressure are refs. [6], [9] and [55] on polystyrene, and [56] on PαMS. Yourtee and Cooper [6] observe a very slight decrease in the densification rate with formation pressure for polystyrene over a 6 kbar range. For the same polymer, Weitz and Wunderlich [9] find a much larger dependence with the same trend, where the density gradually becomes nearly constant at 4 kbar. These trends are contrary to the marked increase in the densification rate with formation pressure observed by Shishkin on PS and PMMA and Ichihara et al. [56] on PαMS. κ' does not necessarily have to tend to zero for the volume to be non-negative at large formation pressures. Using our definition of κ', the densified volume tends to zero at arbitrarily large formation pressures when κ' is a positive constant.

According to the experiments of Weitz and Wunderlich on polystyrene, there is a monotonic increase in density at a decreasing rate which the density seems to level off at 4 kbar. Thus, beyond this point the formation pressure would have no effect on the densification process. On the other hand, with most of the other investigations mentioned above, including those on polystyrene, it would appear that chemical stability is the limiting factor. Whether the reaction rate constant of a given rate process increases or decreases with pressure depends upon the sign of its corresponding activation volume [76]. In most cases it is expected that the total activation volume will be positive with a corresponding increase in the effective decomposition temperature with increasing pressure. This behavior may be complicated, however, by the different temperature and pressure dependencies of the various decomposition modes, and, possibly by the initiation of new ones at elevated pressures.

The important consideration here is whether, or not, the decomposition temperature and T_g -pressure curves come sufficiently close at any point to limit the densification process. For example, with polytetrafluoroethylene the increase of decomposition temperature with pressure is only about 3.5 K/kbar [77]. Although this rate is small, the decomposition temperature is sufficiently remote from the observed phase transitions, since its initial (atmospheric pressure) value is about 700°C. In addition, the melting and decomposition curves diverge with increasing pressure over the experimental range of 28 kbar, investigated so far.

In cases where the decomposition temperature T_d increases with pressure, T_0 should also be allowed to increase with pressure to optimize the densification. With polytetrafluoroethylene this process would appear to continue without bound because of the observed divergence mentioned above. In instances where T_d and T_g converge or intersect at a finite pressure, the densification would be essentially limited by the effective intersection temperature as illustrated in figure 5. Except for the polymer mentioned above, pressure dependent pyrolysis data are apparently non-existent in the literature[4].

The results in table 9 summarize an attempt to estimate the optimum densification on a few polymers beyond which thermal decomposition would occur. In the absence of reliable pyrolysis data at elevated pressures, we will estimate optimum densification by commencing isothermal pressurization at $T_0 = T_d$. Since in most cases T_d is expected to increase with pressure, this procedure should underestimate the maximum densification as illustrated by the lower value of P'_{max} obtained by the dashed line path in figure 5.

[4] Preliminary work of this kind on 18 polymers, including PMMA, PS, Pcarb, and PVC, has been reported by H. Eyring and coworkers in Ref. [78]. In all of these the decomposition temperature increases monotonically with pressure. We have been unable to obtain a final report on this activity.

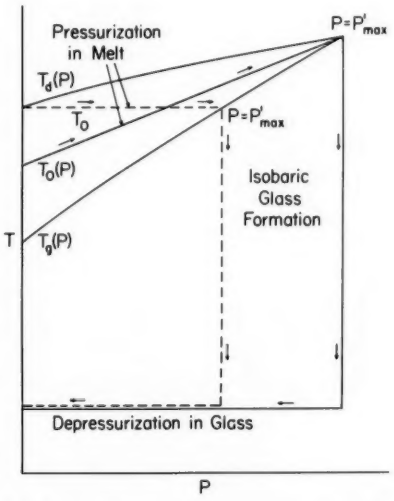

FIGURE 5. *Schematic illustration of temperature-pressure history used to optimize the densification process before the onset of pyrolysis.*

TABLE 9. *Estimation of maximum densification from pyrolysis data*

Polymer	Ref.	ΔH kJ/mol	T K	$k(T)$ %/min	T_d K	T_g K	dT_g/dP K/kbar	P'_{max} kbar	κ' Mbar^{-1}	$-\left(\frac{\Delta V}{V}\right)_{max}$ %
PIB	79	218	593	0.268	558	202	25	14	1.6	2
PP	79	255	623	.069	606	244	20	18	7.0	13
PMA	80	155	558	.270	515	282	18	13	5.8	8
PVAc	81, 82	112	497	5.58	409[a]	304	21.2	5	9.3	5
PVC	83	126	508	0.43	458	349	13.5	8	6.4	5
PS	80	218	608	.163	577	363	30.0	7	8.1	6
a-PMMA	80	230	583	.250	552	378	23.6	7	7.3	5
PαMS	80	243	546	.276	519	448	39	2	4.9	1

[a] Stated to be unstable at temperatures above 463K in Ref. [81]. During sample preparation [1] slight discoloration was observed after heating overnight in a vacuum at 403 K.

In table 9 T_d is taken arbitrarily at the value for which the initial reaction rate constant k = 1%/hr, applicable to the total degredation process. Assuming Arrhenius behavior T_d may be calculated from the relation

$$1/T_d = 1/T - (R/\Delta H)\ell n[(1/60)/k(T)]$$

where $R = 8.314$ J/(mol-K) and ΔH is the activation energy. T is arbitrarly chosen from the closest data point to T_d, which in all cases, but one (PVAc), involves extrapolation. These decomposition temperatures correspond to those given in table 7 of ref. [34], except the latter apparently apply to $k = 1$ percent/min and, accordingly, are larger. The ceiling temperatures in the same table, which apply to the propagation mode at equilibrium, are apparently not relevant to the densification process. T_g, dT_g/dP, and κ' are selected from previous tables in this paper. P'_{max}, the pressure corresponding to the onset of pyrolysis at $T_0 = T_d$ and $-(\Delta V/V)_{max}$, the corresponding maximum densification, are obtained from the simple relations

$$P'_{max} = [T_d - T_g(0)]/(dT_g/dP)$$
$$-(\Delta V/V)_{max} = \kappa' \times P'_{max}.$$

From these results it appears that P'_{max} varies inversely with T_g; however, no trend is apparent for $(\Delta V/V)_{max}$.

4.8. Dependence of Refractive Index on Densification

A reliable estimate of the change of refractive index on densification should be obtained by means of the Lorentz-Lorenz equation,

$$(n^2 - 1)/(n^2 + 2) = K\rho, \qquad (20)$$

where n is the index of refraction and ρ the density. K depends upon the polarizability, which is expected to be essentially independent of formation pressure, or alternatively, the density at constant temperature and pressure. The relative change of index of refraction with formation pressure,

$$\delta' = (1/n)\,(\partial n/\partial P)_{T,P},$$

is obtained explicitly by differentiation of eq (20), viz,

$$\delta' = (1/6n^2)(n^2 - 1)(n^2 + 2)\kappa'. \qquad (21)$$

Table 10 presents the results for polymers for which values for n_D (sodium D line) are available from ref. [35] with κ' selected from our tables. The n_D values are converted to those at T_g by means of the temperature coefficients given in ref. [84]. As seen from the table, these corrections are insignificant. Since all of these values range between 1.48 and 1.58, a very slight (10 percent) error will be incorporated in δ' by taking the function $f(n) = (1/6n^2)(n^2 - 1)(n^2 + 2)$ as a constant, as revealed by the table. Accordingly, in view of the large experimental uncertainties in κ' (35 percent for polystyrene), the additional uncertainties obtained on replacing eq (21) by the approximation

$$\delta' = 0.4\kappa'$$

are slight. The values of δ' in the table however, are calculated from eq (21). We do not have any direct experimental data giving the dependence of the index of refraction on formation pressure.

TABLE 10. *Estimation of change in refractive index from densification rate*

Polymer	T_g °C	$n_D(T)$[a] (°C)	dn_D/dT[b] °C^{-1}	$n_D(T_g)$	$f(n_D)$	κ' Mbar^{-1}	δ' Mbar^{-1}
PIB	−71	1.51[c]	−0.0003	1.54	0.421	1.6	0.7
NR	−69	1.52(25)	−0.00037	1.55	.428	1.9	.8
PP	−29	1.49[c]	([d])	1.51	.400	4.1	1.6
SBR	−16	1.53[c]	([d])	1.54	.421	5.8	2.4
PMA	9	1.47(20)	([d])	1.47	.373	5.8	2.2
PnBMA	20	1.48(25)	([d])	1.48	.380	0.7	0.3
PVAc	31	1.48(20)	−0.0001	1.48	.380	9.1	3.5
PEMA	64	1.48(25)	([e])	1.48	.380	8.9	3.5
PVC	76	1.55[c]	([e])	1.54	.421	7.6	3.2
PS	90	1.59[c]	−0.00013	1.58	.449	8.2	3.7
α-PMMA	105	1.49(20)	−0.00012	1.48	.380	7.4	2.8
PCHMA	107	1.51(20)	−0.00013	1.50	.394	12.6	5.0
Pcarb	143	1.58[c]	([e])	1.57	.442	5.1	2.3

[a] Taken from Ref. [35].
[b] Taken from Ref. [84].
[c] Temperature taken as 25°C.
[d] dn_D/dT taken as −0.0003.
[e] dn_D/dT taken as −0.0001.

These evaluations have potential application in optimization or adjustment of the refractive indices of plastic lenses by appropriately setting the molding pressure. The values in the last column in table 10 give the relative percent changes $(\Delta n/n)$ resulting from a moding pressure of 10 kbar. For PS and PMMA, which are common constituents for plastic lenses, n would change by 4 and 3 percent, respectively. However, it was estimated in the last section that thermal decomposition of these polymers would limit the pressurization to 7 and 8 kbar, respectively. In these analyses isothermal pressurization is considered at the decomposition temperature. If this temperature increases with pressure as indicated by ref. [78] for PS and PMMA, an additional increase in their refractive indices could be obtained by appropriately increasing the temperature during pressurization.

5. Conclusion

Several methods have been evaluated to estimate the densification rate, κ', applicable to glass formation by isobaric cooling at constant rate. Other than the direct measurement of the volume difference in the glass, κ' is always computed from an expression involving the difference between two transition rates, dT_g/dP and $dT_g^{\dagger}/dP$. The hole theory is shown to be sufficiently accurate in estimating $dT_g^{\dagger}/dP$ for the 23 polymers evaluated except for possibly those of dimethyl siloxane and α-methyl styrene. With these it is not clear whether the discrepancies result from experimental error or lack of generality in the application of the theory. Although dT_g/dP is only evaluated experimentally, there are independent alternatives. The simplest of these involves the differences between thermal expansions and heat capacities at T_g for liquid and glass at atmospheric pressure only.

The principal problem in the estimation of densification using these procedures appears to be the large amount of experimental uncertainty in all of the relevant quantities, in particular, the compressibility. Since the expression for κ' involves the difference between two quantities of similar

magnitude, even small experimental errors may have a pronounced effect. Accordingly, it is difficult to assess the relative merits of the different methods employed here, including the application of the hole theory.

The results of these analyses appear to have practical applications. Densifying glasses produces a hardening effect as revealed by an increase in moduli. However, these effects do not appear to be as pronounced, in particular viscosity or relaxation time, as those obtained at the same volume, temperature, and pressure in the glass by commensurately decreasing the cooling rate at atmospheric pressure. This procedure however is usually not practical because of the large times required for glass formation. According to one investigation it is possible to optimize the ultimate properties through the appropriate adjustment of the formation or molding pressure. More work is necessary to establish the generality of this result and to determine the formation pressures for maximum yield stress. Moreover, the relation between the refractive index and densification quantity presented could be used to quantitatively regulate the refractive index of lenses through appropriate adjustment of the molding pressure. The maximum value would appear to be limited by chemical instability at the high temperatures necessary to exceed $T_g(P)$, which increases with pressure. The simple relation given does not include the influence of densification on optical dispersion. Again, experimental work is required to assess the validity of our estimates and the possible influence of densification on dispersion.

This work was supported in part by the National Science Foundation under Grant DMR 75-15401.

6. Appendix

As indicated earlier, eqs (5) in the text involve a linearization of pertinent quantities and proximity to the transition line $T_g(P)$ in figure 3. The experimental data found in the literature often do not satisfy these conditions. Hence we reconsider here the processes depicted in figure 3, by replacing the simplifications adopted earlier by the more general form. This will not only permit the prediction of densification effects under more extreme conditions, but also allow us to gage the quantitative validity of the linearization. Clearly, a knowledge of the equations of state is required for an explicit evaluation, but is certainly not available for the wide range of systems discussed here. However we shall be able to present typical numerical illustrations using PVAc where appropriate data exist [1, 14].

From the definitions of the coefficients α and κ it follows that:

$$V/V_0 = \exp\left[\int_{T_0}^{T} \alpha dT\right];\ V/V_0 = \exp\left[-\int_{P_0}^{P} \kappa dP\right]$$

where the subscript indicates an initial value. However, it will be accurate enough to omit second and higher powers in the expansions of the exponentials. Considering an average, temperature independent value for the liquid, $\langle\alpha\rangle = 8 \times 10^{-4}\ \mathrm{K}^{-1}$, and a temperature interval of 100 degrees, we obtain for the integral a value of 8×10^{-2}. Thus the quadratic term changes the total result by 0.34 percent. The values were chosen so as to magnify the effect. For the glass, the approximation will be even more adequate. With a pressure difference of 2 kbar and $\langle\kappa\rangle = 4 \times 10^{-5}\ \mathrm{bar}^{-1}$, the magnitude of the relative volume change is the same and identical conclusions are obtained as for the α-term.

Denoting the initial temperature in the melt as T_0 and the final temperature in the glass as T_f, with the initial pressure taken as zero, we obtain instead of eq (3), when the pressure dependence of the α's and the temperature dependence of the κ's are taken into account, the following expression:

$$(V_A - V_B)/V_0 = \int_0^{P'}[\kappa_l(T_0, P) - \kappa_{g,c}(T_f, P)]\,dP - \int_{T_g(0)}^{T_g(P')}[\alpha_l(T, 0) - \alpha_{g,c}(T, P')]\,dT + \int_{T_g(P')}^{T_0}[\alpha_l(T, P') - \alpha_l(T, 0)]\,dT - \int_{T_f}^{T_g(0)}[\alpha_{g,b}(T, 0) - \alpha_{g,c}(T, P')]\,dT \tag{A-1}$$

where the subscripts b and c pertain to the low and high pressure glasses respectively. This choice conforms with the nomenclature used in refs. [1] and [14]. In the linearized derivation, α and κ for both liquid and glass are taken to be constants. Accordingly, there is no distinction between the values of $\alpha_{g,b}$ and $\alpha_{g,c}$, and, similarly, $\kappa_{g,b}$ and $\kappa_{g,c}$.

To proceed further, we make use of an explicit equation of state. It is most convenient to employ the extensively tested Tait relations for both melt and glass. To recapitulate the pertinent equation (14), [50]:

$$\kappa(P, T) = C\{[P + B] \times [1 - C\,\ell n(1 + P/B]\}^{-1}$$

where

$$B(T) = a\exp(-bT)$$

and

$$\alpha(T, P) - \alpha(T, 0) = P\kappa(T, P)\,d\ell nB/dT = -bP\kappa. \tag{A-2}$$

The last transforms eq (A-1) into

$$(V_A - V_B)/V_0 = \int_0^{P'}[\kappa_l(T_0, P) - \kappa_{g,c}(T_f, P)]\,dP - \int_{T_g(0)}^{T_g(P')}[\alpha_l(T, 0) - \alpha_{g,c}(T, 0)]\,dT - \int_{T_f}^{T_g(0)}[\alpha_{g,b}(T, 0) - \alpha_{g,c}(T, 0)]\,dT - b_l P' \int_{T_{g(P')}}^{T_0} \kappa_l(T, P')\,dT - b_{g,c}P' \int_{T_f}^{T_{g(P')}} \kappa_{g,c}(T, P')\,dT, \tag{A-3}$$

where the first two terms will predominate.

We now proceed to evaluate the integrals in eq (A-3) which are identified as follows:

$$I_1 = \int_0^{P'} [\kappa_l(T_0, P) - \kappa_{g,c}(T_f, P)]dP \rightarrow \Delta\kappa P'$$

$$I_2 = -\int_{T_g^{(0)}}^{T_{g(P')}} [\alpha_l(T, 0) - \alpha_{g,c}(T, 0)]dT \rightarrow -\Delta\alpha(dT_g/dP)P'$$

$$I_3 = -\int_{T_f}^{T_g^{(0)}} [\alpha_{g,b}(T, 0) - \alpha_{g,c}(T, 0)]dT \rightarrow 0$$

$$I_4 = -b_l P' \int_{T_g}^{T_{0(P')}} \kappa_l(T, P')dT \rightarrow 0$$

$$I_5 = -b_{g,c} P' \int_{T_f}^{T_{g(P')}} \kappa_{g,c}(T, P')dT \rightarrow 0 \qquad \text{(A-4)}$$

where the terms to the right of the arrows are the corresponding linear approximations used in eqs (5) in the text.

Since $C = 0.0894$, the compressibility may be written in good approximation, and consistent with the expansion of the exponentials above, as $C/(B + P)$. Thus we find for I_1,

$$I_1 = C\ell n \left(\frac{1 + P'/B_l(T_0)}{1 + P'/B_{g,c}(T_f)} \right).$$

I_2 and I_3 are evaluated by expressing the atmospheric pressure volume as $V_0 = A_0 + B_0 T + C_0 T^2$ for which $\alpha = (B_0 + 2C_0 T)/V_{av}$ is a good approximation. V_{av} is taken as the average of the two bounds. Finally the general integral corresponding to I_4 and I_5 is

$$\int \kappa(T, P)\, dT = (C/P)\{T + (1/b)\, \ell n\, [P + a \exp(-bT)]\} + f(P).$$

Using the parameters for PVAc given in tables 1 and 2 of ref. [14], the values of the integrals and their linearized counterparts are summarized in table A-1. From ref. [1] $T_g(0) = 30.7$ °C and $T_g(P') = 48.0$ °C. T_0 and T_f are taken to be 90 and 0 °C. These two temperatures are considered to be sufficiently remote from $T_g(P)$, to be characteristic of the equilibrium and glassy states, respectively. The total relative volume differences are given at the bottom of the table followed by the corresponding densification rates. The difference between the two values of κ' amounts to about 4 percent, which is quite satisfactory, since the experimental error on this quantity appears to be considerably larger. This good agreement seen in table A-1 arises however from a cancellation of approximation errors. Moreover, it is gratifying, that the value $\kappa' = 8.8$ Mbar^{-1}, based on the Tait equation is essentially identical to that obtained by directly measuring the volume difference. (See sec. 4.3.) This illustrates the satisfactory performance of the analytical expressions in representing the experimental data.

TABLE A-1. *Values of integrals in eqs (A-4)*

i	Integral Value, I_i	Linear Counterpart
1	2.042×10^{-2}	1.465×10^{-2}
2	-0.649×10^{-2}	-0.733×10^{-2}
3	0.106×10^{-2}	0
4	-0.552×10^{-2}	0
5	-0.242×10^{-2}	0
$(V_A - V_B)/V_0$	0.705×10^{-2}	0.732×10^{-2}
κ' (Mbar^{-1})	8.8	9.2

7. References

[1] McKinney, J. E., and Goldstein, M., J. Res. Nat. Bur. Stand. (U.S.), **78A** (Phys. and Chem.), No. 3, 331–353 (May–June 1974).
[2] Bree, H. W., Heijboer, J., Struik, L. C. E., and Tak, A. G. M., J. Polym. Sci. Polym. Phys. Ed., **12,** 1857 (1974).
[3] Kovacs, A. J., Stratton, R. A., and Ferry, J. D., J. Phys. Chem. **67,** 152 (1963).
[4] Dale, W. C., and Rogers, C. E., J. Appl. Polym. Sci. **16,** 21 (1972).
[5] Wetton, R. E., and Moneypenny, H. G., Br. Polym. J. **7,** 51 (1972).
[6] Yourtee, J. B., and Cooper, S. L., J. Appl. Polym. Sci. **18,** 897 (1974).
[7] Price, C., Polymer **16,** 585 (1975).
[8] Price, C., Williams, R. C., and Ayerst, R. C., in Amorphous Materials, Eds., Douglas, R. W., and Ellis, B., (Wiley-Interscience, 1972), p. 117.
[9] Weitz, A., and Wunderlich, B., J. Polym. Sci., Polym. Phys. Ed. **12,** 2473 (1974).
[10] Simha, R., and Somcynsky, T., Macromolecules **2,** 342 (1969).
[11] Goldstein, M., J. Phys. Chem. **77,** 667 (1973).
[12] McKinney, J. E., Ann. N. Y. Acad. Sci., **279,** 88 (1976).
[13] O'Reilly, J. M., J. Polym. Sci. **57,** 429 (1962).
[14] McKinney, J. E., and Simha, R., Macromolecules **7,** 894 (1974).
[15] Gee, G., Polymer **7,** 177 (1966).
[16] McKinney, J. E., and Simha, R., Macromolecules, **9,** 430 (1976).
[17] Olabisi, O., and Simha, R., Macromolecules **8,** 211 (1975).
[18] Quach, A., and Simha, R., J. Phys. Chem. **76,** 416 (1972).
[19] Berg, J. I., and Simha, R., J. Non-Crystalline Solids, **22,** 1 (1976).
[20] Wunderlich, B., J. Phys. Chem. **64,** 1052 (1960).
[21] Nielsen, L. E., Mechanical Properties of Polymers and Composites. Vol. 2, (Marcel Dekker, New York, 1974) p. 515.
[22] Lee, W. A., and Rutherford, R. A., *in* Polymer Handbook, Ed. Brandrup, J., and Immergut, E. H., (Interscience, New York, 1975) Section III, p. 139.
[23] Brown, D. W., and Wall, L. A., J. Polym. Sci. A-2, **7,** 601 (1969).
[24] Simha, R., and Boyer, R. F., J. Chem. Phys. **37,** 1003 (1962).
[25] Boyer, R. F., and Simha, R., J. Polym. Sci., Polym. Letters Ed., **11,** 33 (1973).
[26] Sharma, S. C., Mandelkern, L., and Stehling, F. C., ibid, **10,** 345 (1972).
[27] Boyer, R. F., J. Macromol. Sci.-Phys. **B7,** 487 (1973).
[28] Wunderlich, B., and Jones, L. D., ibid **B3,** 67 (1969).
[29] Wunderlich, B., and Baur, H., Adv. Polym. Sci. **7,** 151 (1970).
[30] Simha, R., and Wilson, P. S., Macromolecules **6,** 908 (1973).
[31] Madorsky, S. L., Thermal Degradation of Organic Polymers (Interscience, New York, 1964).
[32] Reich, L., and Stivala, S., Elements of Polymer Degradation (McGraw-Hill, New York, 1971).
[33] Wall, L. A., *in* Analytical Chemistry of Polymers, Part II, Ed. Kline, G. M., (Interscience, 1962), p. 181.
[34] Wall, L. A., *in* The mechanisms of pyrolysis, oxidation, and burning of organic materials, Nat. Bur. Stand. (U.S.), Spec. Publ. 357, 199 pages, (June 1972)., Ed. Wall, L. A. p. 47.
[35] Brauer, G. M., and Horowitz, E., in Analytical Chemistry of Polymers, Part III, Ed., Kline, G. M. (Interscience, 1962), p. 46.
[36] Shih, H., and Flory, P. J., Macromolecules **5,** 758 (1972).
[37] Beret, S., and Prausnitz, J. M., ibid **8,** 536 (1975).
[38] Eichinger, B. E., and Flory, P. J., ibid **1,** 285 (1968).
[39] Martin, G. M., and Mandelkern, L., J. Res. Nat. Bur. Stand. (U.S.), **62,** No. 4, 141–146 (Apr. 1959), RP2944.
[40] Passaglia, E., and Martin, G., J. Res. Nat. Bur. Stand. (U.S.), **68A,** (Phys. and Chem.), No. 3, 273–276 (May–June 1964).
[41] Kraus, G., and Gruver, J. T., J. Polym. Sci., Part **A-2,** 571 (1970).
[42] Takahishi, M., Shen, M. C., Taylor, R. B., and Tobolsky, A. V., J. Appl. Polym. Sci. **8,** 1549 (1964).
[43] Olabisi, O., and Simha, R., Macromolecules **8,** 206 (1975).
[44] Quach, A., Wilson, P. S., and Simha, R., J. Macromol. Sci.-Phys. **B9,** 533 (1974).
[45] Rogers, S. S., and Mandelkern, L., J. Phys. Chem. **61,** 985 (1957).
[46] Hellwege, K. H., Hennig, J., and Knappe, W., Kolloid Z.; Z. Polym. **186,** 29 (1962).
[47] Hellwege, K. H., Knappe, W., and Lehmann, P., ibid **183,** 110 (1962).
[48] Heydemann, P., and Guicking, H. D., ibid. **193,** 16 (1963).
[49] Breuer, H., and Rehage, G., ibid. **216–217,** 159 (1967).
[50] Quach, A., and Simha, R., J. Appl. Phys. **42,** 4596 (1971).
[51] Mercier, J. P., Aklonis, J. J., Litt, M., and Tobolsky, A. V., J. Appl. Polym. Sci. **9,** 447 (1965).

[52] Cowie, J. M. G., and Toporowski, P. M., J. Macromol. Sci.-Phys., **1,** 81 (1969).
[53] Simha, R., Wilson, P. S., and Olabisi, O., Kolloid Z.; Z. Polym. **251,** 402 (1973).
[54] Shishkin, N. I., Sov. Phys., Solid State Phys. **2,** 322 (1960).
[55] Ichihara, S., Komatsu, A., Tsujita, Y., Nose, T., and Hata, T., Polym. J. **2,** 530 (1971).
[56] Ichihara, S., Komatsu, A., and Hata, T., Polym. J. **2,** 650 (1971).
[57] Boyer, R. F., Styrene Polymers (Physical Properties-Thermal Characteristics), *in* Encyclopedia on Polymer Science and Technology, Boyer, R. F., Ed., (Wiley and Sons, New York, 1970), p. 297.
[58] Weir, C. F., Leser, W. H., and Wood, L. A., J. Res. Nat. Bur. Stand. (U.S.), **44,** 367–372 (Apr. 1950), RP2084.
[59] Ferry, J. D., and Parks, G. S., J. Chem. Phys. **4,** 70 (1936).
[60] McKinney, J. E., Belcher, H. V., and Marvin, R. S., Trans. Soc. Rheology **4,** 347 (1960).
[61] Singh, H., and Nolle, A. W., J. Appl. Phys. **30,** 337 (1959).
[62] Williams, G., Trans, Faraday Soc. **60,** 1556 (1964).
[63] Williams, G., and Edwards, D. A., ibid **62,** 1329 (1966).
[64] McKinney, J. E., and Belcher, V., J. Res. Nat. Bur. Stand. (U.S.), **67A** (Phys. and Chem.), No. 1, 43–53 (Jan.–Feb. 1963).
[65] Williams, G., Trans. Faraday Soc. **62,** 2091 (1966).
[66] Koppelman, J., and Gielessen, J., Z. für Electrochemie **65,** 689 (1961).
[67] Zosel, A., Kolloid Z.; Z. Polym. **199,** 113 (1964).
[68] Sasabe, H., and Saito, S., Polym. J. **3,** 749 (1972).
[69] Furukawa, G. T., and Reilly, M. L., J. Res. Nat. Bur. Stand. (U.S.), **56,** No. 5, 285–288 (May 1956), RP2676.
[70] Bekkedahl, N., and Matheson, H., J. Res. Nat. Bur. Stand. (U.S.), **15,** 503–515 (Nov. 1935), RP844.
[71] Passaglia, E., and Kevorkian, H. K., J. Appl. Phys. **34,** 90 (1963).
[72] Furukawa, G. T., McCoskey, R. E., and Reilly, M. L., J. Res. Nat. Bur. Stand. (U.S.), 55, No. 3, 127–132 (Sept. 1955), RP2610.
[73] O'Reilly, J. M., Karasz, F. E., and Bair, H. E., J. Polym. Sci., Part C, **6,** 109 (1964).
[74] McKinney, J. E., and Lindsay, R., Density and Compressibility of Liquids, *in* American Institute of Physics Handbook, Gray, D. W., Ed. (McGraw-Hill, New York, 1972). Section 2, p. 167.
[75] Kimmel, R. M., and Uhlman, D. R., J. Appl. Phys. **41,** 2917 (1970).
[76] Lin, S. H., Li, K. P., and Eyring, H., *in* Physical Chemistry, An Advanced Treatise, Vol VII (Academic Press, New York, N.Y., 1975), p. 38.
[77] Tamayama, M., Andersen, T. N., and Eyring, H., Proc. Nat. Acad. Sci. **57,** 554 (1967).
[78] Eyring, H., *in* Proceedings, New Materials from High-Pressure High-Temperature Processes, U.S. Army Research Office-Durham 27–28 Sept. 1967 at Watervliet Arsenal, Watervliet, N.Y.
[79] Madorsky, S. L., and Straus, S., J. Res. Nat. Bur. Stand. (U.S.), **53A** No. 6, 361–370 (Dec. 1954), RP2553.
[80] Wall, L. A., and Madorsky, S. L., J. Polym. Sci. **11,** 491 (1953).
[81] Grassie, N., Trans. Faraday Soc. **48,** 379 (1952).
[82] ibid. **49,** 835 (1953).
[83] Stromberg, R. R., Straus, S., and Achhammer, B. G., J. Polym. Sci. **35,** 355 (1959).
[84] Newman, S. B., ref. [35], p. 284.

(Paper 81A2&3-931)

Publications of the National Bureau of Standards*

On the atomic weight of gallium, G. Marinenko, *J. Res. Nat. Bur. Stand.* (*U.S.*), **81A** (Phys. and Chem.), No. 1, 1–4 (Jan.-Feb. 1977).

Key words: atomic weight; coulometry; electrochemical equivalent; gallium arsenide; gallium atomic weight; stoichiometry.

Accurate measurement of stoichiometry of GaAs provides new data which are used for calculation of the atomic weight of Ga. Using the IUPAC accepted value for the atomic weight of As (74.9216), the atomic weight of Ga based on this work is 69.737 ± 0.006. The mean of two independent chemical values for the atomic weight of Ga, one obtained by Lundell and Hoffman and the other in this work, is 69.735.

Vapor pressure formulation for ice, A. Wexler, *J. Res. Nat. Bur. Stand.* (*U.S.*), **81A** (Phys. and Chem.), No. 1, 5–20 (Jan.-Feb. 1977).

Key words: Clausius-Clapeyron equation; saturation vapor pressure over ice; thermal properties of ice; vapor pressure; vapor pressure at the triple point; vapor pressure of ice; water vapor.

A new formulation is presented for the vapor pressure of ice from the triple point to −100 °C based on thermodynamic calculations. Use is made of the definitive experimental value of the vapor pressure of water at its triple point recently obtained by Guildner, Johnson, and Jones. A table is given of the vapor pressure as a function of temperature at 0.1-degree intervals over the range 0 to −100 °C, together with the values of the temperature derivative at 1-degree intervals. The formulation is compared with published experimental measurements and vapor pressure equations. It is estimated that this formulation predicts the vapor pressure of ice with an overall uncertainty that varies from 0.016 percent at the triple point to 0.50 percent at −100 °C.

Standard pH values for the potassium hydrogen phthalate reference buffer solution from 0 to 60 °C, H. B. Hetzer, R. A. Durst, R. A. Robinson, and R. G. Bates, *J. Res. Nat. Bur. Stand.* (*U.S.*), **81A** Phys. and Chem.), No. 1, 21–24 (Jan.-Feb. 1977).

Key words: acidity; emf; pH; phthalate buffer; potassium hydrogen phthalate; standard for pH.

The standard pH values of the solution of potassium hydrogen phthalate (molality 0.05 mol kg^{-1}) have been redetermined over the temperature range 0 to 60 °C, using SRM 185d. Extensive measurements were made of the emf of cells of the type

$$Pd;H_2(g, 1\ atm)|KH\ phthalate\ (m\ (0.05), KCl\ (m)|AgCl;Ag$$

where m_{KCl} was 0.015, 0.01, or 0.005 mol kg^{-1}, from which values of the acidity function $p(a_H\gamma_{Cl})$ were derived. The pH convention defines γ_{Cl} in the range of ionic strengths 0 to 0.1 mol kg^{-1} and permits conventional values of pa_H to be obtained. According to NBS procedures, pa_H for selected reference solutions is identified with the standard pH(S) in the operational definition of pH. The new values, given in terms of the thermodynamic temperature (T) by

$$pH(S) = (2073.44/T - 13.3270 + 0.045199T - 3.4846 \times 10^{-5}T^2$$

differ, on the average, by 0.003 unit from the results based on the 1944 data of Hamer and Acree.

Atlas of the I_2 spectrum from 19 000 to 18 000 cm^{-1}, J. D. Simmons and J. T. Hougen, *J. Res. Nat. Bur. Stand.* (*U.S.*), **81A** (Phys. and Chem.), No. 1, 25–80 (Jan.-Feb. 1977).

Key words: high-resolution spectrum; iodine spectrum; line identification atlas; rovibronic assignments; spectral analysis; visible absorption spectroscopy.

A line identification band atlas is presented for a 1000 cm^{-1} segment, from 19 000 to 18 000 cm^{-1}, of the molecular iodine absorption spectrum. Each page of the atlas covers a 20 cm^{-1} region of the spectrum and contains a CALCOMP produced photodensitometer trace of the spectrum together with accompanying tabular identification data. The tabular data includes: line identification numbers, observed wavenumbers, calculated wavenumbers, and rotational and vibrational assignments.

The NBS two-pressure humidity generator, Mark 2, S. Hasegawa and J. W. Little, *J. Res. Nat. Bur. Stand.* (*U.S.*), **81A** (Phys. and Chem.), No. 1, 81–88 (Jan.-Feb. 1977).

Key words: calibration; dew point; humidity; hygrometer; mixing ratio; relative humidity; two-pressure generator; volume ratio; water vapor.

A new humidity calibration facility which uses the two-pressure principle for generating gas of known humidity has been developed at NBS for calibrating and testing hygrometers. The relative humidity range of the two-pressure humidity generator is 3 to 98 percent for ambient temperatures −60 to 80 °C and test chamber pressures 5 to 200 kPa (absolute). This is equivalent to a nominal dew/frost point range of −80 to 80 °C. Intercomparison tests were made with the NBS standard gravimetric hygrometer over a portion of the generator's operating range. The estimated maximum uncertainty (three standard deviations) is 0.2 percent *RH* for temperatures 0 to 80 °C which in units of dew point corresponds to an estimated maximum uncertainty of 0.04 °C for dew points −35 to 80 °C.

Humidity fixed points of binary saturated aqueous solutions, L. Greenspan, *J. Res. Nat. Bur. Stand.* (*U.S.*), **81A** (Phys. and Chem.), No. 1, 89–96 (Jan.-Feb. 1977).

Key words: aqueous solution; equilibrium; humidity; relative humidity; salt; saturated salt solution; vapor pressure; water vapor.

An evaluated compilation of equilibrium relative humidities in air versus temperature from pure phase to approximately 10^5 pascal (1 atm) in pressure is presented for 28 binary saturated aqueous solutions. The relative humidities of the solutions range from about 3 to 98 percent. Using a data base from 21 separate investigations comprising 1106 individual measurements, fits were made by the method of least squares to regular polynomial equations with two through four coefficients. Equations and tables are presented along with the estimated uncertainties in the correlated results.

**This listing includes recent NBS papers in the various NBS publication series—defined at end of the listing—as well as NBS-authored papers in non-NBS media—identified by 5-digit numbers. Publications with prices and SD stock numbers may be purchased directly from the Superintendent of Documents, U.S. Government Printing Office, Washington, D.C. 20402 (foreign: one-fourth additional). Microfiche copies of these GPO-published documents, as well as paper copy and microfiche versions of NBS Interagency Reports (NBSIR), may be purchased from the National Technical Information Service (NTIS), Springfield, Va. 22161. Reprints of papers in the NBS Journal of Research and non-NBS media, may often be obtained directly from the authors.*

Frequency dependence of intrinsic stress and birefringence tensor of bead/spring model of polymer solutions, A. Peterlin and J. T. Fong, *J. Res. Nat. Bur. Stand. (U.S.)*, **81A** (Phys. and Chem.), No. 1, 97–107 (Jan.-Feb. 1977).

Key words: bead-spring model; eigenvalues; frequency response; intrinsic optical tensor; intrinsic stress tensor; polymer solution.

The recently obtained complete solution of the simultaneous diagonalization of matrices $\underline{\underline{A}}$ and $\underline{\underline{H}}$ in the hydrodynamic diffusion equation has basically changed the diagonal values ν_p of the symmetric matrix $\underline{\underline{H}}$ of hydrodynamic interaction between all the beads of the elastic random coil model of the isolated macromolecule in solution. Since these values enter explicitly the expression for the intrinsic stress and refractive index tensor in an alternating flow field if based on the concept of internal viscosity of the model one had to recalculate all values obtained formerly by using the then generally accepted erroneous set of ν_p data. The new ν_p equal unity independent of p while the old values were larger than 1 for small p and smaller for large p. Hence their too large contributions in the former range are partially compensated by their too small contributions in the latter region. As a consequence in the whole range investigated, between 3 and 300 chain links, the differences in rheological and rheooptical effects are relatively small, up to a factor of 2, although at higher link number the differences tend to grow with the logarithm of this number.

Diffusion in copper and copper alloys. Part V. Diffusion in systems involving elements of group VA, D. B. Butrymowicz, J. R. Manning, and M. E. Read, *J. Phys. Chem. Ref. Data* **6**, No. 1, 1-50 (1977).

Key words: alloys; antimony; arsenic; bismuth; copper; diffusion; electromigration; liquid metals; nitrogen; phosphorus; ternary diffusion; thermomigration.

A survey, comparison, and critical analysis is presented of data compiled from the scientific literature concerning diffusion in copper alloy systems involving elements in Group VA (As, Bi, N, P, Sb). Here the term "copper alloy system" is interpreted in the broadest sense. For example, the review of diffusion in the Cu-M system reports all diffusion situations which involve both copper and element M, including diffusion of Cu in M or in any binary, ternary, or multicomponent alloy containing M; diffusion of M in Cu or in any alloy containing Cu; and diffusion of any element in any alloy containing both Cu and M. Topics include volume diffusion, grain boundary diffusion, tracer diffusion, alloy interdiffusion, electromigration, thermomigration, strain-enhanced diffusion and diffusion in molten metals. An extensive bibliography is presented along with figures, tabular presentation of data, and discussion of results.

The calculated thermodynamic properties of superfluid helium-4, J. S. Brooks and R. J. Donnelly, *J. Phys. Chem. Ref. Data* **6**, No. 1, 51-104 (1977).

Key words: computed thermodynamic properties; entropy; equation of state; excitation spectrum; helium-4; normal fluid helium-4; phonons; protons; specific heat; superfluid helium-4.

Comprehensive tables of the primary thermodynamic properties of superfluid helium-4, such as the specific heat and entropy, are presented as computed from the Landau quasiparticle model, with the aid of inelastic neutron scattering data. The neutron data are represented by continuous functions of temperature, pressure, and wave number and certain excitation properties such as number density, normal and superfluid densities are calculated directly from it. A discussion of the methods used in our computations is included, and comparisons of computed and experimental results are made where applicable. Certain inadequacies of present theoretical methods to describe the thermodynamic properties are reported, and the use of an effective spectrum is introduced to offset some of the difficulties. Considerable experimental effort is also needed to improve the present situation.

Thermodynamic properties of normal and deuterated methanols, S. S. Chen, R. C. Wilhoit, and B. J. Zwolinski, *J. Phys. Chem. Ref. Data* **6**, No. 1, 105-112 (1977).

Key words: enthalpy of formation; Gibbs energy of formation; ideal gas thermodynamic properties; intermolecular association; normal and deuterated methanols; potential barrier to internal rotation; principal and reduced moments of inertia; structural parameters; vibrational fundamentals; virial coefficients of the equation of state.

Structural and spectroscopic data on CH_3OH, CH_3OD, CD_3OH, and CD_3OD were reviewed. The selected values were utilized to calculate the ideal gas thermodynamic properties in the temperature range of 0 to 1500 K, using the rigid-rotor and harmonic-oscillator model. Experimental data for the standard enthalpy of formation at 298.15 K, the heat capacities, and the third-law entropies at elevated temperatures are available only for CH_3OH in the vapor phase where intermolecular association occurs. The agreement between the observed thermal data and our calculated values is satisfactory within the experimental uncertainties. Finally, the standard chemical thermodynamic values for $\Delta Hf°$, $\Delta Gf°$, and log Kf were generated in the temperature range of 0 to 1500 K.

The spectrum of molecular nitrogen, A. Lofthus and P. H. Krupenie, *J. Phys. Chem. Ref. Data* **6**, No. 1, 113-307 (1977).

Key words: critical review; Franck-Condon integrals; molecular constants; molecular nitrogen; potential energy curves; radiative lifetimes.

This is a critical review and compilation of the observed and predicted spectroscopic data on the molecule N_2 and its ions N_2^-, N_2^+, N_2^{2+}, and the molecule N_3. Each electronic band system is discussed in detail, and tables of band origins and heads are given. In addition to the gas phase electronic, electron and Raman spectra, there are also examined the spectra of condensed molecular nitrogen as well as the pressure- and field-induced infrared and microwave absorption. Dissociation energy of N_2, predissociations, and perturbations are discussed. Potential energy curves are given, as well as radiative lifetimes, f-values, and Franck-Condon integrals. Molecular constants are listed for the known electronic states. Electronic structure and theoretical calculations are reviewed.

Monogr. 147, Suppl. 1. **Relativistic many-body bound systems: Electromagnetic properties,** M. Danos and V. Gillet, *Nat. Bur. Stand. (U.S.), Monogr. 147, Suppl. 1*, 52 pages (Apr. 1977) SN003-003-01754-0.

Key words: electromagnetic properties; form factors; magnetic moments; quadrupole moments; quantum field theory; relativistic many body systems; vector dominance.

The formulae for the calculation of the electron scattering form factors, and of the static magnetic dipole and electric quadrupole moments, of relativistic many-body systems are derived. The framework, given in NBS Monograph 147, is relativistic quantum field theory in the Schrödinger picture; the physical particles, i.e., the solutions of the interacting fields, are given as linear combinations of the solutions of the free fields, called the parton fields. The parton-photon interaction is taken

as given by minimal coupling, $\vec{p} \rightarrow \vec{p} - e\vec{A}$; in addition the contribution of the photon-vector meson vertex of the vector dominance model is derived.

H121. **Waste heat management guidebook,** K. G. Kreider and M. B. McNeil, Eds., *Nat. Bur. Stand. (U.S.), Handb. 121*, 150 pages (Feb. 1977) SN003-003-01669-1.

Key words: boilers; economics; energy conservation; instrumentation; recuperators; waste.

Sources of waste (i.e., discarded) heat in industrial processes are reviewed, and an overview of off-the-shelf technology available for its use is given. Discussions of waste heat measurement technology and economics are included, as are fourteen case studies of successful industrial waste-heat recovery installations.

H122. **Noise emission measurements for regulatory purposes,** D. R. Flynn, W. A. Leasure, Jr., A. I. Rubin, and M. A. Cadoff, *Nat. Bur. Stand. (U.S.), Handb. 122*, 193 pages (Mar. 1977) SN003-003-01750-7.

Key words: acoustics; environmental pollution; machinery and equipment; noise; noise abatement and control; noise emission; regulation; sound.

A review is given of the measurement needs attendant to regulation of the noise generated and emitted by commercial products. The emphasis is primarily on measurement procedures for use in conjunction with point-of-sale regulations as opposed to regulations on the noise which a source actually emits when in operation. The report is divided into three major parts. Part I is a discussion of overall measurement requirements and the type of data and information which are needed in order to promulgate regulations based on appropriate measurement techniques. Part II is designed as a checklist for the evaluation of the suitability of a noise measurement standard for a particular class of products or, in the absence of a suitable standard, as a framework for development of one. The intent is to identify and discuss in some detail those factors which can impact on the accuracy, precision, and applicability of a noise measurement process. Part III consists of a series of flow charts depicting the development of appropriate procedures for the measurement of product noise emission.

SP363. Supplement 1. **Bibliography on atomic energy levels and spectra (July 1971 through June 1975),** L. Hagan, *Nat. Bur. Stand. (U.S.), Spec. Publ. 363 Suppl. 1*, 186 pages (Jan. 1977) SN003-003-01673-0.

Key words: atomic energy levels; atomic spectra; bibliography; energy levels, atomic; spectra, atomic; wavelengths, atoms and ions.

This is the first supplement to the NBS Special Publication 363, "Bibliography on Atomic Energy Levels and Spectra, July 1968 through June 1971," and it covers the most recent literature from July 1971 through June 1975. It contains approximately 2150 references classified by subject for individual atoms and atomic ions. A number index identifies the references. An author index is included. References included contain data on energy levels, classified lines, wavelengths, Zeeman effect, Stark effect, hyperfine structure, isotope shift, ionization potentials, or theory which gives results for specific atoms or atomic ions.

SP400-24. **Semiconductor measurement technology: A laser scanner for semiconductor devices,** D. E. Sawyer and D. W. Berning, *Nat. Bur. Stand. (U.S.), Spec. Publ. 400-24*, 72 pages (Feb. 1977) SN003-003-01739-6.

Key words: electronic reliability; electronics; laser scanner; measurement method; mixer; optics; pre-amplifier; radio receiver; semiconductor device studies.

This is a construction guide and operators manual for a laser scanner built for semiconductor device studies. A very brief discussion of the theory of operation of the scanner is given. The scanner's operation from a systems point of view is described in detail with emphasis on block diagrams. The scanner is described from a hardware point of view with a detailed description of the function of the various controls on the electronic equipment that was built for the laser scanner. A quick guide for the use of the scanner is given so that a person unfamiliar with the instrument can use it effectively. Specifications relating to the scanner's data gathering ability are also given. Mechanical drawings and circuit schematics are given to enable others to build a similar scanner. The optics and their alignment are discussed. Various display modes including color are discussed to enhance operator viewing.

SP400-29. **Semiconductor measurement technology. Progress report, January 1 to June 30, 1976,** W. M. Bullis, Ed., *Nat. Bur. Stand. (U.S.), Spec. Publ. 400-29*, 119 pages (Apr. 1977) SN003-003-01759-1.

Key words: acoustic emission; Auger electron spectroscopy; beam-lead bonds; capacitance-voltage methods; carrier mobility; C-MOS circuits; dopant profiles; electrical properties; electronics; four-probe method; hermeticity; ion implantation; Irvin's curves; leak tests; line-width measurement; measurement methods; microelectronics; optical flying-spot scanner; oxidation particle impact noise detection test; passivation overcoats; photovoltaic method; power-device grade silicon; radioisotope method; resistivity; resistivity variations; safe operating area, transistor; scanning acoustic microscope; scanning electron microscope; scanning low energy electron probe; semiconductor devices; semiconductor materials; semiconductor process control; silicon; silicon dioxide; silicon on sapphire; sodium contamination; spreading resistance; surface roughness; test patterns; thermally stimulated current; transistors, power; TTL circuits; ultrasonic wire bonding; ultraviolet reflectance; x-ray damage.

This progress report describes NBS activities directed toward the development of methods of measurement for semiconductor materials, process control, and devices. Both in-house and contract efforts are included. The emphasis is on silicon device technologies. Principal accomplishments during this reporting period included (1) development of theoretical expressions for electron mobility in silicon based on combinations of scattering mechanisms; (2) successful low-temperature processing of MOS capacitors to permit measurement of thermally stimulated current and capacitance without subjecting the specimens to potentially degrading heat treatments; (3) completion of a study of the thermodynamics of reactions in an oxidation furnace tube which provides a basis for models of the effect of water vapor, chlorine, and tube wall conditions on sodium contamination levels; (4) development of a rapid, nondestructive method for reverse decoration of defects in passivation overcoats; (5) development of the theoretical basis for accurate measurement of small line widths by analysis of a spatially filtered image of the line; (6) extension of the acoustic emission technique to the nondestructive testing of tape-bonded chips and hybrid components; and (7) analysis of the results of a first exploratory interlaboratory evaluation of the radioisotope method for testing hermeticity of semiconductor devices. New tasks were undertaken to develop techniques for measuring resistivity uniformity of and nondopant impurities and defects in power-device grade silicon and to investigate the particle impact noise detection method for screening devices for the

presence of loose particles in the package; initial results were obtained in the study of scanning acoustic microscopy which was begun during the previous reporting period. Because of technical limitations in the methods, efforts to develop both the automated scanning low energy electron probe and in-process ultrasonic bond monitor were terminated. Also reported is other on-going work on materials characterization by electrical and physical analysis methods, materials and procedures for wafer processing, photolithography, test patterns, and device inspection and test procedures. Supplementary data concerning staff, publications, workshops and symposia, standards committee activities, and technical services are also included as appendices.

SP400-31. **Semiconductor measurement technology: Techniques for measuring the integrity of passivation overcoats on integrated circuits,** W. Kern and R. B. Comizzoli, *Nat. Bur. Stand.* (*U.S.*), *Spec. Publ. 400-31*, 120 pages (Mar. 1977) SN003-003-01753-1.

Key words: corona charging decoration; dielectric defect detection; electrophoretic decoration; integrated circuit quality control; selective chemical etching; semiconductor device reliability.

Conventional test methods to evaluate the quality of glass passivation overcoats on semiconductor devices are generally inadequate and/or destructive. Three new methods have been devised that overcome these problems: (1) Sequential selective chemical etching of metal/dielectric structures to detect buried, latent, or partial defects as a function of dielectric layer depth. (2) Electrophoretic cell decoration with uv phosphor particles suspended in an insulating liquid, the sample forming one electrode of the cell. (3) Electrostatic corona charging to selectively deposit surface ions from a high voltage dc discharge on the insulating surfaces of the sample, followed by placing of the charged sample in a suspension of charged carbon black particles in an insulating liquid; depending on the polarity of the ions the particles can be deposited on the insulator surface or at the defect sites. The etching method is most suitable in process research studies, and the electrophoretic technique for demarcating relatively large defects. The corona decoration method, coupled with automated instrumental read-out based on measuring the reflected light intensity, is ideal for routine testing of devices because it is fast, simple sensitive, and nondestructive to devices such as glass passivated bipolar and MOS ICs. The practical benefits of the new test methods can be considerable in production and product control, with cost savings through early detection of production line defects and rapid corrective action.

SP400-33. **Semiconductor measurement technology: The dopant density and temperature dependence of electron mobility and resistivity in *n*-type silicon,** S. S. Li, *Nat. Bur. Stand.* (*U.S.*), *Spec. Publ. 400-33*, 36 pages (Mar. 1977) SN003-003-01742-6.

Key words: dopant density; electron mobility; ionized impurity scattering mobility; lattice mobility; neutral impurity scattering mobility; *n*-type silicon; resistivity; scattering mechanisms; temperature.

Traditional analysis of electron mobility in *n*-type silicon neglects the effects of electron-electron scattering and scattering anisotropy in the mobility calculations. As a result, theory fails to conform with experiment when dopant density exceeds 2×10^{16} cm^{-3}.

In this work, an improved theoretical model for computing mobility and resistivity as functions of dopant density and temperature has been formulated for *n*-type silicon. The model has been applied to phosphorus-doped silicon for dopant densities from 10^{13} to 10^{19} cm^{-3}, temperatures between 100 and 500 K.

The electron mobility was calculated analytically by appropriately combining lattice, ionized impurity, and neutral impurity scattering contributions. The effect of electron-electron scattering on both lattice and ionized impurity scattering mobilities was incorporated empirically for dopant densities greater than 2×10^{16} cm^{-3}. Additionally, the anisotropic scattering effect was also considered in the mobility calculations.

Theoretical calculations of resistivity and ionized donor density were made for phosphorus-doped silicon for temperatures between 100 and 500 K.

Resistivity measurements on seven phosphorus-doped silicon slices with dopant densities from 1.2×10^{14} to 2.5×10^{18} cm^{-3} were carried out for temperatures between 100 and 500 K. Electron mobility at 300 K was deduced from resistivity and junction C-V measurements for dopant densities from 10^{14} to 10^{18} cm^{-3}.

Agreement between theory and experiment for both electron mobility and resistivity of phosphorus-doped silicon was within ± 7 percent in the range of dopant densities and temperatures studied.

SP400-35. **Semiconductor measurement technology: Notes on SEM examination of microelectronic devices,** J. R. Devaney, K. O. Leedy, and W. J. Keery, *Nat. Bur. Stand.* (*U.S.*), *Spec. Publ. 400-35*, 54 pages (Apr. 1977) SN003-003-01755-8.

Key words: backscattered emission; EBIC; microelectronic devices; scanning electron microscope; secondary emission; voltage contrast.

This report reviews selected scanning electron microscope (SEM) techniques which are appropriate for the examination of microelectronic devices. Illustrated are the results of individual variations in SEM operating parameters such as accelerating voltage, specimen tilt, scan line time, and frame time. Techniques which utilize secondary and backscattered electron emissions are compared and electron-beam-induced current and voltage contrast modes are discussed. Specimen preparation and beam-induced charging artifacts are also discussed. This report demonstrates the need for flexibility in selecting and using SEM parameters and analytic procedures to obtain the maximum information when examining semiconductor devices.

SP440. **COLOR—Universal language and dictionary of names,** K. L. Kelly and D. B. Judd, *Nat. Bur. Stand.* (*U.S.*), *Spec. Publ. 440*, 184 pages (Dec. 1976) SN003-003-01705-1.

Key words: centroid colors; color; color designations; calorimetry; color names; color-order systems; Munsell Color System; Universal Color Language; variable accuracy of color designations.

The Universal Color Language (UCL) has been revised and will be published together with the 7th printing of the Color Names Dictionary. It serves as the means of updating the Dictionary. The UCL brings together all the well-known color-order systems and methods of designating color. It interrelates them in six correlated levels of fineness of color designation, each higher level indicating a finer division of the color solid. It follows closely the original requirements for the ISCC-NBS Method of Designating Colors stated in the Color Names Dictionary. They were: a) accurate enough to satisfy a scientist, b) usable enough to satisfy a manufacturer and c) simple enough to be understood by the average person on the street. The first requirement is satisfied by levels 6 and 5, the second by levels 5, 4 and 3, and the third by levels 3, 2 and 1. The UCL is being increasingly used by science, art and industry. Instructions are included for the application of the UCL at each level.

SP461. **Radiation physics.** Proceedings of the International Symposium on Radiation Physics, held at Bose Institute, Cal-

cutta, India, Nov. 30-Dec. 4, 1974, A. M. Ghose, D. V. Gopinath, J. H. Hubbell, and S. C. Roy, Eds., *Nat. Bur. Stand. (U.S.), Spec. Publ. 461*, 268 pages (Jan. 1977) SN003-003-01733-7.

Key words: cross sections; dosimetry; electrons; neutrons; photons, radiation physics; symposium.

These proceedings contain invited and contributed papers presented at the International Symposium on Radiation Physics organized by and held at the Bose Institute, Calcutta, India, Nov. 30-Dec. 4, 1974. The purpose of this symposium, recognizing radiation physics as the thread held in common by a variety of medical, engineering and scientific disciplines, was to bring together specialists from these disciplines to report on, exchange, and make available through these proceedings, information and experiences of common interest to workers in these diverse disciplines. Topics thus brought together in this symposium include new measurements, theoretical developments, compilations and applications of basic cross section and transport data for photon, electron, neutron and heavy ion beams interacting with matter.

SP463. **Materials Information Programs—An interagency review of Federal agency activities on technical information about materials.** Proceedings of a Conference held at the National Bureau of Standards, Gaithersburg, MD, Apr. 16 and 17, 1974, S. A. Rossmassler, Ed., *Nat. Bur. Stand. (U.S.), Spec. Publ. 463*, 271 pages (Jan. 1977) SN003-003-01701-9.

Key words: Commerce; Defense; E.R.D.A.; Federal agencies; interagency review; Interior; Library of Congress; materials; materials data; materials information; N.A.S.A.; U.S.D.A.

The Conference on Materials Information Programs was held on April 16 and 17, 1974, at the National Bureau of Standards, Gaithersburg, Maryland. It was planned, with sponsorship by the Interagency Council for Materials (ICM), as an interagency review of Federal agency activities on technical information about materials. The program was organized by the ICM Working Group on Materials Information and Data. The intent of the review was to develop a common awareness, among operators and sponsors of information activities, of opportunities to help each other solve problems and to improve their services to users. Federal agencies which took part in the Conference, and whose materials information programs are covered in this report, include U.S. Department of Agriculture, Energy Research and Development Administration (formerly A.E.C.), Department of Defense, Department of Interior, National Aeronautics and Space Administration, Department of Commerce, and Library of Congress. Dr. Franklin P. Huddle, of the Congressional Research Service, was the Keynote Speaker; Dr. Emanuel Horowitz, of the National Bureau of Standards, gave the Summary address.

SP467. **Activities of the National Bureau of Standards,** M. Jacobs and S. A. Washburn, Eds., *Nat. Bur. Stand. (U.S.), Spec. Publ. 467*, 40 pages (Mar. 1977) SN003-003-01716-7.

Key words: annual report; computer; energy; environmental; measurement; product safety; research; science; standards; technology.

This publication highlights the major achievements of the National Bureau of Standards and shows how this work contributes to the solution of many problems of national concern. In addition, the report contains sections featuring the Bureau's interaction with the public and private sectors and emphasizes the historical perspective in relation to the Bureau's 75th anniversary and the Nation's bicentennial.

Sections of the report feature: A Word to Our Readers; Introduction; Increasing Measurement Capabilities; Transferring Research and Technology; Promoting Better Materials Use; Aiding Environmental Protection; Conserving Energy Resources; Advancing Building Technology; Protecting Public Safety; Improving Product Performance; Expanding Computer Applications; Providing Information Resources; People; Funds and Facilities; Selected Publications; Directory.

SP468. **MFPG—Prevention of failures in coal conversion systems.** Proceedings of the 24th Meeting of the Mechanical Failures Prevention Group, held at Battelle, Columbus Laboratories, Columbus, OH, Apr. 21-23, 1976, T. R. Shives and W. A. Willard, Eds., *Nat. Bur. Stand. (U.S.), Spec. Publ. 468*, 233 pages (Apr. 1977) SN003-003-01760-4.

Key words: coal conversion; coal gasification; coal liquefaction; corrosion; failure analysis; failure prevention; quality assurance; reliability.

These Proceedings consist of a group of twenty submitted papers and discussions from the 24th meeting of the Mechanical Failures Prevention Group which was held at Battelle, Columbus Laboratories in Columbus, Ohio, on April 21-23, 1976. Prevention of failures in coal conversion systems is the central theme of the Proceedings. A series of overview lectures dealing with reliability problems in coal conversion systems, economics of failures in energy generating systems, corrosion, and gaps in engineering data are presented. In addition, failure analysis, materials problems, and related materials research are discussed.

SP469. **A policy analysis of citizen rights issues in health data systems,** A. F. Westin and F. Isbell, Ed., *Nat. Bur. Stand. (U.S.), Spec. Publ. 469*, 48 pages (Jan. 1977) SN003-003-01730-2.

Key words: citizen rights; computers, confidentiality; data systems; health records; information policy, management principles; medical records; privacy; recordkeeping practices; security.

This is a condensation of the report "Computers, Health Records, and Citizen Rights," by Alan F. Westin, NBS Monograph 157, which investigates the impact of computers on citizen rights in the health recordkeeping area. Under Dr. Alan F. Westin's direction, from July of 1974 to April of 1976, a small interdisciplinary team did the following: (1) examined published literature from medicine and health, law, computing, and social science; (2) conducted interviews with major computer manufacturers, systems developers, health professionals and civil liberties, public interest, consumer, and minority-rights groups; (3) made on-site visits to six representative health-care organizations using computers to handle personal records; (4) corresponded with 70 organizations in the health field; and (5) subjected an initial draft report to review by a conference of experts in September 1975 and subsequently by about 50 outside reviewers. The findings of this investigation were then combined into this four-part report. Part One describes the world of medical data and citizen rights within the framework of three zones—primary health care (by health professionals), service payers and health care reviewers and social uses of health data (such as in employment, life insurance, and welfare); Part Two treats patterns of computerization in health care in each of the above zones; Part Three contains the profiles of the six health-care organizations that were studied in depth; and Part Four analyzes the impact of computerization on personal health records, presents comparisons with six other democratic nations, and states 12 recommended management principles for health care data systems. The full report also contains a 28 page bibliography and 12 appendices with support documents and information.

SP472. **Retrieval and analysis of orthopaedic implants.** Proceedings of a Symposium held at the National Bureau of Standards, Gaithersburg, MD, Mar. 5, 1976, A. Weinstein, E. Horowitz, and A. W. Ruff, Eds., *Nat. Bur. Stand. (U.S.), Spec. Publ. 472*, 130 pages (Apr. 1977) SN003-003-01767-1.

Key words: analysis; implants; metallic; orthopaedic; retrieval.

This book is the formal report of a symposium on Retrieval and Analysis of Orthopaedic Implants. This volume contains the invited lectures that provide a state-of-the-art information base about implant characteristics related to performance; the discussions of a panel addressed to the problems associated with, and the information generated from, implant retrieval analysis; and the reports resulting from a workshop on "What Is the National Need?"

SP475. **The electron factor in catalysis on metals.** Proceedings of a workshop held at the National Bureau of Standards, Gaithersburg, MD, Dec. 8-9, 1975, L. H. Bennett, Ed., *Nat. Bur. Stand. (U.S.), Spec. Publ. 475*, 217 pages (Apr. 1977) SN003-003-01764-7.

Key words: catalysis; characterization; chemisorption; electronic factor; geometric factor; metals; surfaces.

This book presents the proceedings of a Workshop on the Electron Factor in Catalysis on Metals held at the National Bureau of Standards, Gaithersburg, Maryland, on December 8-9, 1975. The Workshop was sponsored by the Institute for Materials Research, NBS, the Devision of Materials Research of the National Science Foundation, and the Division of Conservation Research and Technology of the Energy Research and Development Administration. The purpose of the Workshop was to review the most recent experimental and theoretical investigations on catalysis on metals and related topics, and to bring together chemists, chemical engineers, surface scientists, and solid state physicists and chemists involved in research related to this topic. These proceedings summarize the four panel sessions into which the Workshop was organized: Experimental Techniques, Effect of Alloying, Geometrical Effects, and Electronic Structure.

SP480-8. **A guide to voice scramblers for law enforcement agencies,** R. E. Nelson, *Nat. Bur. Stand. (U.S.), Spec. Publ. 480-8*, 44 pages (Dec. 1976) SN003-003-01735-3.

Key words: LESL; NILECJ; privacy; scramblers; speech scramblers; voice privacy; voice scramblers.

This guideline presents information and suggestions which will assist law enforcement agencies in the selection, procurement, and implementation of voice scramblers in their communications systems. Important points are discussed that need to be considered in choosing the proper scrambler, negotiating the procurement contract, installing the scramblers, and evaluating their performance.

SP500-1. **Computer science and technology: Foreign and domestic accomplishments in magnetic bubble device technology,** R. B. J. Warnar and P. J. Calomeris, *Nat. Bur. Stand. (U.S.), Spec. Publ. 500-1*, 50 pages (Jan. 1977) SN003-003-01724-8.

Key words: amorphous materials; bubble; field-access; garnet; guide-pattern; magnetoresistance; nonvolatility; orthoferrite; photolithography; uniaxial structures.

This document assesses the status of magnetic bubble technology as displayed by non-U.S. research and manufacturing facilities. Non-U.S. research and U.S. accomplishments are described while both technical and economic factors are addressed. Magnetic bubble devices are discussed whenever their application could impact future computer system design. Generally the magnetic bubble device can be applied to a computer system as a peripheral mass memory. Magnetic bubble devices are produced from either synthetic garnet or amorphous materials rather than from familiar silicon material. The document contains a significant bibliography to support certain main points which are supplemented by information supplied by the library of the Information Technology Division (ICST-NBS) and from private interviews with various U.S. technical experts.

SP500-2. **Computer science and technology: Accessing individual records from personal data files using non-unique identifiers,** G. B. Moore, J. L. Kuhns, J. L. Trefftzs, and C. A. Montgomery, *Nat. Bur. Stand. (U.S.), Spec. Publ. 500-2*, 203 pages (Feb. 1977) SN003-003-01726-4.

Key words: data retrieval; file validation; name lookup; nonunique identifiers; personal data files; Privacy Act; probability model; retrieval.

The Privacy Act of 1974 places restrictions on the Federal, state and local agencies' use of the Social Security account number as an identifier. For some agencies, compliance will involve changes in implementation of retrieval algorithms. This report describes methodology applicable to these changes in the more general context of the problem of retrieving individual records from files using nonunique identifiers. State-of-the-art retrieval techniques are discussed, a method for assigning reliability weights to various personal data elements is presented, file validation techniques for the error and omission rates of data items are suggested, and a retrieval probability model—designed to show likelihood of retrieval of a subject's record given a variety of populations, combinations of identifiers, and error/omission rates—is described. A methodology is developed for forming confidence factors from the established error/omission rates for combinations of nonunique identifiers that are candidates for use as retrieval keys. Use of these confidence factors as indices into the precision tables produced by the probability model is described.

SP500-3. **Computer science and technology: Technical profile of seven data element dictionary/directory systems,** B. Leong-Hong and B. Marron, *Nat. Bur. Stand. (U.S.), Spec. Publ. 500-3*, 45 pages (Feb. 1977) SN003-003-01725-6.

Key words: computer software; data base management systems; data element dictionary; data element dictionary/directory; software tool.

A Data Element Dictionary/Directory (DED/D) is a software tool that is used to control and manage data elements in a uniform manner. It can serve data base administrators, systems analysts, software designers, and programmers by providing a central repository for information about data resources across oraganization and application lines. This report describes and classifies DED/D systems and discusses the potential benefits from their use. A technical profile of seven commercially-available DED/D systems is presented with side-by-side exposition of technical features.

SP500-4. **Computer science & technology: Survey of remote terminal emulators,** S. W. Watkins and M. D. Abrams, *Nat. Bur. Stand. (U.S.), Spec. Publ. 500-4*, 80 pages (Apr. 1977) SN003-003-01756-6.

Key words: evaluation; interactive; measurement; performance evaluation; performance measurement; remote terminal emulation; remote terminal emulators; teleprocessing.

This report describes twelve Remote Terminal Emulators (RTE's). The key terminology associated with remote terminal emulation is defined and possible application areas are discussed. Technical implementation details and operational considerations are addressed for each RTE. Summary tables are provided to indicate current RTE capabilities and capacities, as claimed by the RTE developers.

SP500-5. **Computer science & technology: Impact of charge-transfer device technology on computer systems,** R. B. J. Warnar, *Nat. Bur. Stand.* (*U.S.*), *Spec. Publ. 500-5*, 48 pages (Apr. 1977) SN003-003-01758-2.

Key words: bucket-brigade; buried channel; Canada; charge-coupled device; Great Britain; imager CCD's; Japan; peristaltic CCD's; surface channel; The Federal Republic of Germany; The Netherlands; transfer channel.

This document assesses the status of charge-transfer device technology as displayed by foreign research and manufacturing facilities for a period up to September 1975. Capabilities and accomplishments of charge-transfer device research facilities in Japan, Canada, Great Britain, The Netherlands, The Federal Republic of Germany, and the United States are described. Technical and economic factors are addressed and compared. Conclusions are presented which suggest future impacts of charge-transfer devices on current electronic systems, especially computers. Information contained in this report was derived from the open technical literature and from interviews with various U.S. technical experts. The technology assessment resulting in this report was conducted by the Information Technology Division of the Institute for Computer Sciences and Technology, National Bureau of Standards, as part of an "Advanced Computer Technology Survey" project.

SP500-6. **Computer science & technology: Computer network interconnection: Problems and prospects,** I. W. Cotton, *Nat. Bur. Stand.* (*U.S.*), *Spec. Publ. 500-6*, 83 pages (Apr. 1977) SN003-003-01757-4.

Key words: communications networks; computer networks; data communications; interconnection; networks; packet switching; standards.

This report examines the current situation regarding the interconnection of computer networks, especially packet switched networks (PSNs). The emphasis is on identifying the barriers to interconnection and on surveying approaches to a solution, rather than recommending any single course of action.

Sufficient organizational and technical background is presented to permit an understanding and appreciation of the problem. Four major types of interconnections are then surveyed: (1) Circuit Switched Network to PSN, (2) Star Network to PSN, (3) Simple Terminal to PSN, and (4) PSN to PSN. The major barriers to interconnection, both political/legal and technical, are then outlined. The report concludes with some comments on the prospects for overcoming these barriers.

An extensive bibliography, glossary with list of abbreviations, and listing of existing data communications standards relevant to interconnection are also included.

NSRDS-NBS59. **Selected specific rates of reactions of transients from water in aqueous solution. III. Hydroxyl radical and perhydroxyl radical and their radical ions,** N. N. Farhataziz and A. B. Ross, *Nat. Stand. Ref. Data Ser., Nat. Bur. Stand.* (*U.S.*), *59*, 122 pages (Jan. 1977) SN003-003-01731-1.

Key words: aqueous solution; chemical kinetics; data compilation; hydroxyl radical; oxide radical ion; perhydroxyl radical; radiation chemistry; rates; superoxide ion.

Rates of reactions of OH and HO_2 with organic and inorganic molecules, ions, and transients in aqueous solution have been tabulated, as well as the rates for the corresponding radical ions in aqueous solution (O^- and O_2^-). Most of the rates have been obtained by radiation chemistry methods, both pulsed and steady-state; data from photochemistry and thermal methods are also included. Rates for over one thousand reactions are listed.

BSS62. **Evaluation of structural properties of masonry in existing buildings,** S. G. Fattal and L. E. Cattaneo, *Nat. Bur. Stand.* (*U.S.*), *Bldg. Sci. Ser. 62*, 127 pages (Mar. 1977) SN003-003-01738-8.

Key words: analysis; compressive strength; deflection; design; flexural strength; masonry walls; racking strength; seismic loading; shear strength; shear wall; stiffness.

The current state of knowledge on the structural behavior of masonry is synthesized to develop a methodology for the evaluation of the load capacity of masonry walls in existing buildings. A procedure is described for direct sampling and testing of specimens removed from masonry walls of buildings to determine their strength in shear, flexure and compression, and to measure their load-deformation characteristics. A documentation of strength and stiffness properties obtained from available test data is included to provide an alternate source of information on masonry of comparable construction. Sample calculations of masonry building analysis for seismic forces are given in Appendices A and B.

BSS93. **Dynamic performance of a residential air-to-air heat pump,** G. E. Kelly and J. Bean, *Nat. Bur. Stand.* (*U.S.*), *Bldg. Sci. Ser. 93*, 18 pages (Mar. 1977) SN003-003-01691-8.

Key words: cooling and heating coefficients of performance; effective seasonal heating COP; heat pumps; heat pumps and energy conservation; part-load performance; seasonal performance factor.

Information is presented on the dynamic performance of a 5-ton air-to-air heat pump, which was installed in a residence in the Washington, D.C. area. The effect of part-load operation on the heat pump's COOLING and HEATING coefficients of performance (COP) was determined. When the pump operated in the heating mode at outdoor temperatures below 40 °F (4.4 °C), a considerable discrepancy was found to exist between the measured performance and the performance data supplied by the manufacturers. This discrepancy is apparently due to the adverse effects of frost buildup and defrosting of the outdoor coil. The seasonal performance factor (SPF) of the heat pump was estimated and then traced back to the power plant to obtain an "EFFECTIVE SPF" which is then compared with the performance which might be expected from fossil-fuel heating equipment.

BSS94. **Investigation of the Skyline Plaza Collapse in Fairfax County, Virginia,** E. V. Leyendecker and S. G. Fattal, *Nat. Bur. Stand.* (*U.S.*), *Bldg. Sci. Ser. 94*, 91 pages (Feb. 1977) SN003-003-01696-9.

Key words: apartment building; collapse; concrete; concrete strength; construction; flexure; progressive collapse; shear; strength.

The collapse of the Skyline Plaza apartment building A-4 has been studied by using information contained in case records of the Occupational Safety and Health Administration (OSHA), U.S. Department of Labor and obtained from on-site inspections by investigators from the National Bureau of Standards.

Noncompliance with OSHA construction standards has been identified with regard to formwork, field-cured concrete specimens and crane installation. Specifically, the construction procedures did not comply with standards for the removal of supporting forms. It is concluded that premature removal of

forms was a contributing factor to the collapse in building A-4.

An analysis of the 23rd-floor slab indicates that its most likely mode of failure was in shear around one or more columns in section 3 of the floor slab. The strength of the 23rd-floor slab on the day of collapse has been estimated to be at a level that removal of shoring could have produced shear failure in the slab.

BSS96. **Hourly solar radiation data for vertical and horizontal surfaces on average days in the United States and Canada,** T. Kusuda and K. Ishii, *Nat. Bur. Stand. (U.S.), Bldg. Sci. Ser. 96*, 412 pages (Apr. 1977) SN003-003-01698-5.

Key words: computer; energy; radiation; solar.

The majority of the available solar radiation data for the United States and Canada are in the form of either monthly averages of daily total radiation on a horizontal surface or hourly values for cloudless days on horizontal, tilted, and vertical surfaces. Hourly solar radiation data for walls and roofs under "average" solar conditions were computed in order to be able to make estimates of the effect that incident solar radiation has on a building and/or its heating and air conditioning system over a heating and/or cooling season. Calculation procedures developed by Liu and Jordan were modified and hourly solar radiation data were compiled for 80 locations in the United States and Canada. Data were also computed and tabulated for a new parameter called "sol-air temperature for glass."

FIPS PUB 10-2. **Countries, dependencies, and areas of special sovereignty,** H. E. McEwen, Standards Coordinator, *Nat. Bur. Stand. (U.S.), Fed. Info. Process. Stand. Publ. (FIPS PUB) 10-2*, 31 pages (Mar. 1977).

Key words: ADP standards; computers; data elements and codes; data processing; Federal Information Processing Standards; geography; information processing standards; information system; representations and codes; standards; statistical data.

This publication provides a list of geographical-political entities of the world and associated standard codes. These entities include independent states, dependent areas, areas of quasi-independence, noncontiguous territories, possessions without population, areas with special sovereignty associations, areas without sovereignty, political regimes not recognized by the United States, and outlying areas of the United States.

FIPS PUB 46. **Data Encryption Standard,** D. K. Branstad, Ed., *Nat. Bur. Stand. (U.S.), Fed. Info. Process. Stand. Publ. (FIPS PUB) 46*, 17 pages (1977).

Key words: ADP security; computer security; encryption; Federal Information Processing Standard.

The selective application of technological and related procedural safeguards is an important responsibility of every Federal organization in providing adequate security to its ADP systems. This publication provides a standard to be used by Federal organizations when these organizations specify that cryptographic protection is to be used for sensitive or valuable computer data. Protection of computer data during transmission between electronic components or while in storage may by necessary to maintain the confidentiality and integrity of the information represented by that data. The standard specifies an encryption algorithm which is to be implemented in an electronic device for use in Federal ADP systems and networks. The algorithm uniquely defines the mathematical steps required to transform computer data into a cryptographic cipher. It also specifies the steps required to transform the cipher back to its original form. A device performing this algorithm may be used in many applications areas where cryptographic data protection is needed. Within the context of a total security program comprising physical security procedures, good information management practices and computer system/network access controls, the Data Encryption Standard is being made available for use by Federal agencies.

FIPS PUB 47. **Federal Standard COBOL Pocket Guide,** *Nat. Bur. Stand. (U.S.), Fed. Info. Process. Stand. Publ. (FIPS PUB) 47*, 37 pages (1977).

Key words: COBOL; COBOL programming aids; Federal Standard COBOL; programming aids; programming languages.

This document contains a composite language skeleton of Federal Standard COBOL. It is intended to display complete and syntactically correct formats for the High Level of the standard. In addition, the document contains other selected prompts for the COBOL programmer to assist in expediting the programming task.

TN692. **Servo techniques in oscillators and measurement systems,** F. L. Walls and S. R. Stein, *Nat. Bur. Stand. (U.S.), Tech. Note 692*, 23 pages (Dec. 1976) SN003-003-01734-5.

Key words: atomic frequency standard; frequency discrimination; frequency domain stability; frequency-lock loop; phase-lock loop; phase noise; servo techniques; time domain stability.

Nearly every precision oscillator includes a frequency or phase servo system. In the case of cesium standards, a crystal oscillator is frequency locked to a particular resonance line in atomic cesium; in the case of an oscillating hydrogen maser, a crystal oscillator is phase locked to the very weak signal coming from the microwave cavity. The first section of this note treats the errors and offsets of frequency-lock loops which result from background, noise and other effects. Third harmonic lock systems and square wave frequency modulation are analyzed as possible solutions to some of these problems. The second section is a general treatment of servo system response which is applicable to both frequency and phase-lock loops. The effects of noise on such servo systems are discussed in detail, and an example is given of how to obtain optimum performance from a pair of phase-locked oscillators. A simple circuit is suggested for phase-locking high quality oscillators, which has many advantages over previous circuits.

TN933. **An infrared technique for heat-loss measurement,** D. M. Burch, T. Kusuda, and D. G. Blum, *Nat. Bur. Stand. (U.S.), Tech. Note 933*, 52 pages (Apr. 1977) SN003-003-01746-9.

Key words: heat-flow measurements; infrared heat-loss measurement technique; measurement technology; thermography.

This paper describes a newly developed technique for measuring heat-loss rate utilizing an infrared television system. A device called a heat-flow reference pad was developed that makes it possible to measure quantitatively the heat-loss rate through the surface of a building without the need for a conventional heat-flow meter to be mounted on the surface. Technical considerations for the design of a heat-flow reference pad are presented. The infrared measurement technique predicted heat-loss rates in the laboratory and field within approximately 12 percent.

TN934. **Preservation of historic adobe structures—A status report,** J. R. Clifton, *Nat. Bur. Stand. (U.S.), Tech. Note 934*, 35 pages (Feb. 1977) SN003-003-01740-0.

Key words: adobe building materials; adobe soil; mechanical properties; moisture determination; preservation technology.

The physicochemical and mechanical properties of adobe soils and building materials, and the technology of preserving historic adobe structures have been critically reviewed. In most cases, the deterioration of adobe structures can be directly or indirectly correlated with the presence of excess moisture. Therefore, the successful preservation of most historic adobe structures depends largely on effectively protecting these structures from water. This review indicates that the technology of preserving adobe structures needs further development to ensure the longevity of the structures.

Areas in which research is needed have been identified and include: (1) the development of standard methods to characterize the composition and physical properties of adobe soils, and the mechanical properties of adobe brick; (2) nondestructive methods to measure the water contents of and water movement in adobe structures; and (3) the evaluation of the effectiveness of different types of preservation materials and methods.

TN935. **Measurement of energy irradiance from single pulse sources,** A. R. Schaefer and E. F. Zalewski, *Nat. Bur. Stand. (U.S.), Tech. Note 935*, 32 pages (Feb. 1977) SN003-003-01741-8.

Key words: curve fitting; energy irradiance; flashtube; pulsed source; radiometry.

A method of measuring the energy irradiance from a single pulsed source, such as a xenon flashtube, is presented. Details of the approach used in this particular measurement are given, along with a discussion of the data analysis. In particular, we consider some of the inherent problems encountered in curve fitting which are also common to other radiometric and photometric measurements.

TN936. **A FORTRAN program for desmearing small-angle x-ray scattering curves,** J. Mazur, *Nat. Bur. Stand. (U.S.), Tech. Note 936*, 83 pages (Apr. 1977) SN003-003-01752-3.

Key words: FORTRAN program; integral equation; interpolating polynomial; numerical stability; slit correction; small angle scattering; unsmearing.

A FORTRAN program is presented that corrects for collimation effects in small angle x-ray scattering measurements. The method employed in calculations is based on numerical solution of an integral equation, which is written as a Volterrra equation of the first kind. This equation is reduced to a system of simultaneous equations, which are solved by a matrix inversion method. Several different algorithms are tried, based on different interpolating polynomials for I(x), the true scattering intensity which is expressed as a function of the scattering angle x. The problem of numerical stability, which is inherent to the computations algorithms employed in the algebraic solution of integral equation is discussed and exemplified with actual computations.

TN938. **Recommended practice for the use of metric (SI) units in building design and construction,** H. J. Milton, *Nat. Bur. Stand. (U.S.), Tech. Note 938*, 47 pages (Apr. 1977) SN003-003-01761-2.

Key words: International System of Units (SI); metric design and construction; recommended SI practice.

This Technical Note contains a comprehensive set of recommendations for the use of metric (SI) units in building design and construction.

It includes descriptive material dealing with the structure of the International System of Units (SI); rules and recommendations for the presentation of SI units and symbols, and of numerical values associated with SI; a set of tables showing working units and typical applications for SI units in building design and construction; and a section dealing with special considerations in the selection and use of SI units in design and construction. Appendixes show conversion factors for the most common units; superseded metric units not recommended for use with SI; an SI units and relationships chart; and appropriate references.

This document was prepared to provide the technical basis for an ASTM reference standard on recommended practice for the use of metric (SI) units in building design and construction.

NBSIR 75-937. **The national measurement system for medical ultrasonics,** P. A. Hudson, 20 pages (Feb. 1976). Order from NTIS as PB265614.

Key words: electroacoustics; medical diagnostics; radiation safety; radiation therapy (ultrasonic); ultrasonics.

The rapid increase in the use of ultrasonics in medical diagnostics has been brought about by recent advances in imaging techniques employing sophisticated electronic systems. Along with the proliferation of this equipment in the medical community has come concern about possible tissue damage due to this type of radiation. Research on damage thresholds is being carried out in laboratories across this country and overseas. Agreement between various researchers is hampered by lack of accurate standards for measurement of transducer beam power and intensity.

The National Measurement System for medical ultrasonics is, at this time, inadequate, fragmented and largely uncoordinated. The Electromagnetics Division is in process of developing standards for measurement of transducer beam power, intensity, and beam pattern. These standards will be disseminated widely throughout the country to provide the needed accuracy and measurement agreement among biomedical researchers and ultimate users (hospitals, physicians, clinics, etc.). Interim standards for beam power were developed 1 1/2 years ago and are already in use by standards laboratories of manufacturers and universities. It is estimated that another 5 years will be required to bring the measurement system under some form of control.

NBSIR 75-938. **The National Measurement System for Acoustics,** D. S. Pallett and M. A. Cadoff, 95 pages (Mar. 1977). Order from NTIS as PB264290.

Key words: acoustical measurements; acoustics; audiometry; national measurement system; noise; noise control; noise emissions; sound; sound level meters.

This report describes acoustical measurement processes which are motivated by societal concern over noise and which have broad relevance to our contemporary technological society. The emphasis of this study of the National Measurement System for Acoustics has been to review the status of the system in order to determine the adequacy of these important physical measurements and to promote improvements within

the measurement system. The relevant physical quantities are indicated, and the interactions occurring between participants as well as the roles of acoustical standardization institutions are specified. Technological, social and economic impacts are outlined. Finally, the status and trends of the system and the NBS role in adapting to changing technology are discussed.

NBSIR 75-945. **The National Measurement System for Surface Properties,** C. J. Powell, 81 pages (Mar. 1977). Order from NTIS as PB264258.

Key words: National Measurement System for Surface Properties; surface atomic structure; surface characterization; surface composition; surface electronic structure; surface properties.

An analysis is given of the National Measurement System for Surface Properties. Emphasis is placed on the properties needed to characterize a solid surface, particularly surface composition, surface atomic structure and surface electronic structure; these characteristics directly affect many important surface properties or processes that occur on surfaces (e.g., electrical and optical properties, adhesion, bonding, catalytic activity, plating, durability, corrosion, decoration, segregation, lubrication and reactivity). The above three forms of surface characterization are widely utilized in surface-science experiments while measurements of surface composition are routinely made to solve a wide variety of problems in the semiconductor, chemical, petroleum and metallurgical industries for applications ranging from process and device development, process control, process evaluation to failure analysis. Surface-characterization measurements in government laboratories support a variety of agency missions. Surface science and surface technology have both grown rapidly in the past ten years, and further growth is expected. At this time, there is a complete lack of standards, standard procedures, and standard materials to support surface-characterization measurements. In short, there is no established national system for the measurement of surface properties. Recommendations for NBS action are given to improve and extend the measurement services required to promote surface science and surface technology and thereby to establish a satisfactory system for the measurement of surface properties.

NBSIR 76-837. **Characterization of a superconducting coil composite and its components,** A. F. Clark, W. F. Weston, V. D. Arp, J. G. Hust, and R. J. Trapani, 143 pages (July 1976). Order from NTIS as PB261709.

Key words: fiberglass cloth; mechanical properties; stress analysis; superconducting coil composite; superconducting wire; thermal properties.

The physical properties of a superconducting coil composite and its components are studied in order to accurately predict the coil behavior under a variety of operating conditions. This second interim report includes data on the Young's moduli, the Poisson's ratios, the shear moduli, and the thermal conductivity of the coil composite as well as the compressive modulus of the fiberglass cloth and the thermal expansion of the superconducting wire. In addition, the development of an acoustic technique for the determination of the elastic moduli of the coil composite and the stress analysis of transversely isotropic magnet coils are reported.

NBSIR 76-844. **A microwave vector voltmeter system,** K. C. Roe and C. A. Hoer, 70 pages (Aug. 1976). Order from NTIS as PB264300.

Key words: amplitude; computer controlled; diode detectors; microwave measurements; phase angle; self-calibration; seven-port junction; vector voltmeter.

This report presents a system description and operating procedure for a vector voltmeter system which covers the frequency range .5 to 12 GHz. The design is based upon a seven-port junction where phase and amplitude information is obtained using only power detectors. The system is computer controlled and self-calibrating for ratio measurements.

NBSIR 76-848. **Semi-annual report on materials research in support of superconducting machinery,** R. P. Reed, J. G. Hust, M. B. Kasen, H. M. Ledbetter, H. I. McHenry, D. T. Read, R. E. Schramm, L. L. Sparks, and R. L. Tobler, 322 pages (Oct. 1976). Order from NTIS as PB261996.

Key words: aluminum alloys; composites; elastic properties; engineering materials; fatigue; fracture; iron alloys; cryogenic temperatures; maraging steels; mechanical properties; nickel alloys; phenolformaldehyde; stainless steels; superconducting machinery; thermal conductivity; titanium alloys.

Results are reported of a six-month study, ending September 1976, on candidate materials for superconducting-machinery components. The results cover five areas—advanced composites, elastic properties, fatigue resistance and fracture toughness, magnetothermal conductivity, and thermal conductivity. Material properties were studied over the temperature range 4 to 300 K. Materials studied include: aluminum alloy 5083, copper-0.3, cadmium-0.3 tin, copper-28 nickel, iron-48 nickel, 3.5 Ni and 9 Ni steels, titanium-4 aluminum-6 vanadium, titanium-5 aluminum-2.5 tin, stainless steel 21-6-9, several austenitic stainless steels of the 300 series, 300-grade maraging steel, phenolformaldehyde, and the composites boron/aluminum, boron/epoxy, graphite/epoxy, and niobium-titanium/copper. Some notable results of the study are: anomalous elastic properties of stainless steel 21-6-9 due to a Nèel transition; complete sets of elastic constants for two composties, B/Al and NbTi/Cu; thermal conductivities of Ti-6Al-4V and Fe-48Ni are reduced by a magnetic field while those of Cu-0.5 Sn and Cu-28Ni are unaffected; a screening method for composites of possible cryogenic use; general trends regarding temperature effects on the fracture toughness and fatigue-crack-growth resistances of structural alloys are correlated with crystal structure class; and the tensile-yield-strength and fracture-toughness data for fourteen commercial structural alloys at 4 K and 295 K are compared demonstrating an inverse relationship between these properties and indicating the optimum combination of properties that are technologically possible. Also, the materials and properties studied experimentally during the three-year program are summarized. This work was supported by the Advanced Research Projects Agency of the U.S. Department of Defense.

NBSIR 76-994. **A numerical solution of the time dependent partial differential equations which describe a one-dimensional, laminar, premixed flame,** R. L. Brown, 178 pages (Jan. 1976). Order from NTIS as PB263100.

Key words: combustion; differential equations; flame chemistry; flame modeling; laminar flames; numerical solution of flame equations.

The set of time dependent, parabolic differential equations, which describe the physical and chemical processes in a one-dimensional, laminar, premixed flame is solved by adapting a solution procedure originally developed to solve the two-dimensional steady state boundary layer equations. The flame equations are integrated by an implicit method until the steady state is reached. This corresponds to a flame propagating steadily through a mixture of combustible gases. By a suitable choice of boundary conditions, it is also possible to model a flame which is stabilized on a burner. Solution of the flame equations

yields the concentration profiles of the different chemical species as well as the temperature profile. From these one can also calculate the production rates of each species, the rate of each chemical reaction, and the heat release rate at each point in the flame. The velocity of the freely propagating flame can be calculated from the integrals over the whole flame zone of any of the species production rates. The model incorporates realistic thermodynamic data and transport property data that are functions of both temperature and concentration. A complete documentation of the computer program which accomplishes the integration is presented.

NBSIR 76-1030. **The effect of sample orientation in the smoke density chamber,** L. Breden and M. Meisters, 32 pages (May 1976). Order from NTIS as PB263633.

Key words: fire performance; horizontal and vertical smoke measurements; smoke; smoke density chamber; smoke suppressants.

Smoke measurements were compared for various materials in the vertical and horizontal positions. There appeared a significant difference for thermoplastic materials because of the melting away from the incident heat flux in the vertical position. The horizontal mode in addition allows one to relate the chemistry of polymeric materials to the amount of smoke production. Finally, smoke measurements are made of products containing various amounts of smoke suppressants.

NBSIR 76-1078. **Piezoelectric polymer transducers for dynamic pressure measurements,** A. S. DeReggi, S. Edelman, and S. C. Roth, 42 pages (June 1976). Order from NTIS as PB264125.

Key words: piezoelectric; polymer; polyvinylidene fluoride; pressure sensor; pyroelectric; transducer.

This report describes the construction, testing and calibration of piezoelectric polymer sensing transducers of two sizes. The piezoelectric material was obtained by poling 25 μm thick, polyvinylidene fluoride sheet. Sensors with an active area of 1 cm diameter, intended for dynamic interface-pressure measurements, were calibrated in a fixture generating normal pressure transients by means of piston impact. Sensors with an active area of 2 mm diameter, intended for measuring dynamic pressures while implanted in the cranium of rhesus monkeys, were calibrated in an oil cell with a piston-cylinder seal which provided hydraulic pressure transients by means of impact on the piston. The larger sensors had a normal-pressure sensitivity around 3 μV/Pa (20 mV/psi) and the smaller sensors a hydraulic-pressure sensitivity around 0.7 μV/Pa (5 mV/psi).

NBSIR 76-1094. **Standards for computer aided manufacturing,** J. M. Evans, Jr., J. T. O'Neill, J. L. Little, J. S. Albus, A. J. Barbera, D. W. Fife, E. N. Fong, D. E. Gilsinn, F. E. Holberton, B. G. Lucas, G. E. Lyon, B. A. S. Marron, A. J. Neumann, M. V. Vickers, and J. C. Walker, 41 pages (July 1976). Order from NTIS as ADA030098.

Key words: CAM architectures; computer aided manufacturing; computer systems; standards; system integration; voluntary standards.

This report identifies and evaluates those existing and potential standards which will be useful to the Air Force in the development and implementation of integrated computer aided manufacturing (ICAM) systems. Such systems, when implemented by the Air Force and by Air Force contractors, will increase productivity in discrete part batch manufacturing by several thousand percent. The use and importance of standards are considered in the context of CAM systems. Since the Air Force will develop the detailed ICAM architecture after this study is complete, existing system concepts and architectures are examined to identify the common elements to guide the further presentation and discussion of relevant standards.

NBSIR 76-1113. **A ten year history of National Bureau of Standards activities under the Brooks Act (Public Law 89-306),** G. Burns and S. Radack, Eds., 93 pages (Feb. 1977). Order from NTIS as PB263526.

Key words: ADP standards; Brooks Act; computer science research; computers in the Federal Government; scientific and technological advisory services.

This report presents the principal findings of a National Bureau of Standards task force which reviewed the activities and accomplishments of NBS from 1965 to 1975 under Public Law 89-306, the Brooks Act. The Brooks Act is concerned with the effective use of computers by the Federal Government and assigns the National Bureau of Standards responsibility for providing scientific and technological advisory services for automatic data processing, developing uniform Federal ADP standards and undertaking necessary research in computer science and technology. Program activities and a history of funding for each of these three major responsibilities are covered. Also included are case studies of individual program initiatives.

NBSIR 76-1135. **Radiation-hardness testing of electronic devices: A survey of facility dosimetry practices,** J. C. Humphreys and S. E. Chappell, 45 pages (Sept. 1976). Order from NTIS as PB263630.

Key words: dosimeter calibration; electronic devices; ionizing radiation; radiation dosimetry; radiation hardness testing; radiation sources; thermoluminescence dosimeters; total dose.

As part of a program to develop better quality assurance in the measurement of total dose in the field of radiation-hardness testing of electronic devices, a survey was conducted at twelve radiation test facilities. The survey was carried out through personal visits at which time various characteristics of the test facilities and dosimetry procedures were noted. This report summarizes the results of the survey. Particular attention is given to the types of dosimetry problems perceived by the dosimetry personnel at the facilities as well as to general observations by the surveyor.

The observations and information obtained through this survey led to some conclusions on where problems in total-dose measurements may occur. Some specific recommendations result and give direction to the program plan for developing more consistent measurement procedures within the radiation-hardness testing community.

NBSIR 76-1142. **Considerations and standards for visual inspection techniques,** G. T. Yonemura, 17 pages (Oct. 1976). Order from NTIS as PB263099, $3.50.

Key words: nondestructive testing; modulation transfer function; vision; visual acuity; visual capacities.

When we look at the capacity of the human visual system we see that it has many capacities depending on the circumstances under which it is used. The sensory data show that man can adjust to a wide variety of operating conditions. But, unless we have detailed information of the conditions for which these processes are to be optimized and quantitative descriptions of the tasks to be performed, the advantages to be obtained by visual science applications cannot be optimally utilized. Physical correlates of the response should be quantified, followed by a systematic scaling of the physical correlates for application to nondestructive testing. The Modulation Transfer Function widely used in optical imaging assessments would be an evaluation technique applicable to hardware, processing and image description.

NBSIR 76-1145. **Interlaboratory comparison of force calibrations using ASTM method E74-74. Phase I,** R. W. Peterson and R. L. Bloss, 35 pages (Aug. 1976). Order from NTIS as PB265110.

Key words: force; force calibration; interlaboratory comparison; load cell; static force.

This report covers the first phase of an intercomparison of force calibrations coordinated by the National Bureau of Standards in conjunction with Committee E28.01 of the American Society for Testing and Materials. Results obtained show that the provisions of ASTM Method E74-74, "Standard Methods of Calibration of Force-measuring Instruments for Verifying the Load Indication of Testing Machines" can be met by a variety of calibration laboratories. In general, uncertainties computed from the data are of the magnitude expected based upon the NBS results. An important byproduct of the program is the mechanism for self-evaluation by each laboratory of its own force calibration capability.

NBSIR 76-1148. **Characterizing the inter-fiber bond strengths of paper pulps in terms of a breaking energy,** J. C. Smith and E. L. Graminski, 39 pages (Oct. 15, 1976). Order from NTIS as PB264689.

Key words: breaking energy; inter-fiber bond strength; mixed waste paper; paper recycling; pulp characterization; 2.5 g/m² handsheets.

The inter-fiber bond strength of paper is an important but an arduous property to measure. In order to characterize a pulp completely, the quality of bondability must be known especially for pulps produced from a mixture of waste paper. It has been postulated that a measure of bond strength can be obtained by measuring 2.5 g/m² handsheets to tensile failure, recording the number of bonds broken with a sensitive tensile tester and plotting a curve of number of bonds broken as a function of cumulative work done on the system. The value of the minimum slope of this curve is equal to the average energy dissipated per bond break. Results obtained on two different softwood kraft pulps indicate the proposed method may be useful in assessing bond strengths.

NBSIR 76-1174. **Skid resistance measurement test procedures for intercomparing FHWA national and regional reference systems,** R. W. Kearns and J. F. Ward, 35 pages (Dec. 1976). Order from NTIS as PB262366.

Key words: friction, pavement; highway safety; measurement, skid resistance; pavement, skid resistance; test procedures, skid resistance measuring systems; tire-pavement interface forces.

The measurement of the skid resistance of highways, under wet weather conditions, is part of the Federal Highway Administration (FHWA) skid-accident reduction program. A national reference system and regional reference systems are operated to improve the method of measurement, to reduce differences in results between systems and to include measurement assurance in the program. State highway measuring systems are intercompared with reference systems at FHWA regional field test centers. This document describes the objectives, the scope and the general procedures of the tests used to intercompare the regional reference systems with the national reference system operated by the National Bureau of Standards. Listing of the general equipment required are included.

NBSIR 76-1178. **Air leakage and thermal performance of a MARK III relocatable Lewis building,** C. W. Phillips, B. A. Peavy, and M. E. Kuklewicz, 42 pages (Dec. 1976). Order from NTIS as PB264211.

Key words: air leakage of buildings; building heat transfer; honeycomb panel construction; relocatable buildings; wind-load racking.

This report presents the findings of air leakage and heat transfer tests of a Mark III relocatable building at the National Bureau of Standards, Building Environment Division, for the U.S. Department of the Navy. Quantitative and qualitative (smoke trace) air leakage tests with the building pressurized, and the heat transfer test, were performed with the building erected in an environmental laboratory. The quantitative air leakage tests were performed in two phases. One was with the building racked to simulate a wind load and the other was without racking. The building was of prefabricated honeycomb panel construction using aluminum skins. Included are photographs of the building and test equipment and tables and charts showing the magnitude of air leaks at the windows and doors. Racking had negligible effect on the air leakage rate.

NBSIR 76-1180. **Standardization and measurement services in Guyana,** H. S. Peiser, N. C. Beck, and K. S. Stephens, 100 pages (Feb. 1977). Order from NTIS as PB265087.

Key words: cottage industry; developing countries; Guyana; less developed countries; measurement services; standardization; testing facilities.

A survey of standardization and measurement services in Guyana was carried out in July, 1976, as part of a National Bureau of Standards program sponsored by the Office of Science and Technology of the Agency for International Development. The Survey Team included three members, one of whom was an NBS staff member and the other two, U.S. participants. The survey was conducted at the request of Dr. Dennis Irvine, Chairman of the National Science Research Council (NSRC) and Vice Chancellor of the University of Guyana.

The NBS team's specific objectives were: 1) to survey domestic and export oriented industries and related GOG and private sector organizations, and 2) to advise the NSRC on optimum means for establishing a National Bureau of Standards and related activities to assist effectively industrial development in Guyana.

NBSIR 76-1182. **The thermal performance of a two-bedroom mobile home,** G. J. Teitsma and B. A. Peavy, 104 pages (Jan. 1977). Order from NTIS as PB263883.

Key words: air infiltration; energy conservation; mobile home; part-load efficiency; thermography.

Tests were conducted on a mobile home located in an Environmental Climatic Laboratory for the purpose of evaluating its thermal performance. The heating demand greatly affected the part-load efficiency of a gas-fired, forced-air, sealed-combustion furnace system. The practice of installing oversized heating plants was shown to result in low seasonal operating efficiencies. Air leakage measurements were performed using a pressurization technique to quantify the amount of air leakage through the various parts of the mobile home. Separate air infiltration tests using the SF_6 tracer-gas technique that somewhat higher air infiltration rates were induced by operation of the mobile home heating plant. A thermographic survey of interior surfaces showed that the technique used to install the wall insulation may allow wrinkles formed in the surface of the insulation to form air paths running the height of the wall cavity. Convective air flow through these paths may create heat leaks on the building surface which can have an impact on the overall heat-loss rate. Separate tests were also conducted to identify places in the mobile home envelope having high condensation potential.

NBSIR 76-1190. **Report on an NBS/AID survey of standardization and measurement services in Thailand,** H. S. Peiser and R. S. Marvin, Eds., 80 pages (Feb. 1977). Order from NTIS as 264917.

Key words: measurements; quality control; standardization; testing facilities; Thailand.

A survey of standardization and measurement services available in Thailand was carried out in May and June of 1973 as part of a National Bureau of Standards program sponsored by the Office of Science and Technology of the Agency for International Development. The Survey Team included five NBS staff members, three third-country participants, and an approximately equal number of professional Thai participants, headed by the overall Survey Director, Dr. Charoen Vashrangsi of the Department of Science in the Thai Ministry of Industry. A total of universities, government departments and private organizations were visited by some or all of the Team. The schedule of visits was so heavy that no time was available for discussion and formulation of formal recommendations. Thus the report is largely a brief factual account of the various visits, although a few comments and suggestions are included.

NBSIR 76-1191. **A survey of calibration techniques for atmospheric ozone monitors,** J. A. Hodgeson, 30 pages (Dec. 1976). Order from NTIS as PB263534.

Key words: air pollution; calibration; iodometry; monitoring; ozone; ultraviolet photometry.

A survey is presented of recent studies on calibration techniques for atmospheric ozone (O_3) monitors. These calibration techniques are based on iodometry, ultraviolet photometry (UV) and gas phase titration (GPT). The iodometric procedures include the 1 percent neutral buffered potassium iodide (NBKI) technique used by the Environmental Protection Agency (EPA), a 2 percent NBKI method of the California Air Resources Board and a 1 percent unbuffered KI technique previously used by the Los Angeles Air Pollution Control District (LAAPCD). The UV and GPT approaches are of rather recent application and brief descriptions of the calibration procedures are given. In summary the data show excellent agreement between O_3 determinations by UV or GPT and demonstrate that absolute measurements of trace O_3 concentrations can be made by either technique. On the other hand, the NBKI methods yield O_3 measurements 1 to 13 percent higher than absolute values when O_3 in dry air is analyzed. In the presence of humid air the NBKI measurements are high by factors ranging from 15 to 30 percent.

NBSIR 76-1193. **Earthquake related activities of the Center for Building Technology,** C. G. Culver, 24 pages (Mar. 1977). Order from NTIS as PB265103.

Key words: buildings; design; disaster mitigation; earthquakes; engineering.

This report describes activities related to earthquake engineering being carried out by the Center for Building Technology as part of the Center's overall Disaster Mitigation Program. Laboratory and field research, post disaster investigations and efforts to develop comprehensive eartquake resistant design provisions are included. The professional disciplines within the Center and the laboratory facilities are discussed. Recent accomplishments and mechanisms employed for facilitating implementation of the Center's research results are also discussed.

NBSIR 76-1194. **A study of fire spread in multi-family residences: The causes—The remedies,** B. M. Vogel, 22 pages (Feb. 1977). Order from NTIS as PB264368.

Key words: apartments; building codes; fire; fire resistivity; firestopping; fire walls; garden apartments; multi-family residences.

This report identifies the major elements contributing to the spread of fire in multi-family buildings, where the fire is beyond the area of origin. The data has been collected from 84 separate fires involving low-rise (garden apartments) residential buildings in the Washington, D.C. metropolitan area. This report categorizes the contributing factors of the fire spread into construction deficiencies, design deficiencies, and possible code violations; and suggests the need for specific revisions to building codes.

NBSIR 77-1195. **The world of EDP standards,** M. F. Hill and J. L. Walkowicz, 154 pages (Dec. 1976). Order from NTIS as PB263771.

Key words: ADP standards; international standardization; national standardization; national standards bodies; practice; procedures; regional standardization; standardization; standards development.

This publication describes the activities and relationships of the many organizations and individuals involved at the national, regional, and international levels in the development of standards for computers and information processing. A generalized description of the standardization process is presented first and then used as a basis for describing the activities of the principal organizations that comprise *The World of EDP Standards*. This Second Edition of *The World* brings up-to-date the information contained in the First Edition and retains the format used therein. The description of each organization is structured in a uniform manner and includes the history of each organization, its objectives, membership, organization, finance, relationship to other organizations, and its technical work.

NBSIR 77-1207. **Performance of the engine-generators used in the Jersey City total energy plant,** J. B. Coble, M. E. Kuklewicz, and J. H. Hebrank, 22 pages (Mar. 1977). Order from NTIS as PB264427.

Key words: diesel engine performance; engine-generator efficiency; engine-generator performance; heat recovery; total energy systems.

Each of five 600-kilowatt (kW), diesel engine-generators which were to be installed in a total energy plant was performance tested under NBS direction at the engine-generator vendor's plant. These tests provided a basis for acceptance of the engine-generators and for comparison with installed performance.

This testing was performed as a part of a comprehensive study to assess engineering, economic, and environmental aspects of a total energy plant which supplies all electrical power, hot water, and chilled water to an apartment complex in Jersey City, New Jersey. Under sponsorship of the Department of Housing and Urban Development (HUD), the National Bureau of Standards (NBS) has instrumented the total energy site for engineering data and is collecting economic and environmental data.

The engines were tested at seven power levels ranging from 0 to 110 percent rated electrical load. In the tests, fuel consumption, electrical output, and jacket-water heat recovery were measured, as well as many other parameters. Results are reported for fuel consumption, electrical efficiency, and electrical-plus-thermal efficiency, and comparisons are made with measured data from the total energy plant.

NBSIR 77-1208. **NBS space processing research,** E. Passaglia and R. L. Parker, 115 pages (Feb. 1977). Order from NTIS as PB264286.

Key words: convection; crystal growth; crystal perfection; microgravity; purification; space processing.

This report describes NBS work for NASA in support of NASA's Space Processing Program covering the period January 1, 1976-December 31, 1976.

The results obtained for each task are given in detailed summaries in the body of the report. Briefly, in Task 1—Crystal Perfection in Czochralski Growth—large nickel single crystals have been grown having dislocation densities as low as 400 lines/cm² as assessed by x-ray dynamical diffraction techniques. In Task 2—Evaporative Purification of Ultra-High Purity Materials—Part A—it was determined that the use of sessile drops as a means of support for the study of molten alumina places severe restrictions on the type and validity of the data that can be obtained in view of temperature measurement and control problems encountered. In Part B, rates of evaporative purification were determined for Nb-Mo and for Mo-Zr alloys at elevated temperatures using R.F. levitation of molten drops. In Task 3—Vapor Transport Synthesis and Crystal Growth—the growth of 1.5 cm diameter crystals of mercurous chloride crystals by a vapor Bridgman technique is described. In Task 4—Melt Shape in Weightless Crystal Growth, thermocapillary forces on air bubbles in a viscous oil were measured, and the shape of axisymmetric liquid zones and their stability with respect to perturbations has been investigated numerically.

NBSIR 77-1210. **Equipment maintenance for energy conservation,** J. Levy, 56 pages (Feb. 1977). Order from NTIS as PB264297.

Key words: dynamic programming; economic analysis; energy conservation; equipment maintenance; Markow decision process; policy improvement algorithm.

A general model of equipment performance as a function of maintenance is developed that permits quantification of the optimal level of maintenance in terms of performance attainment and relative factor costs. The model formulation is that of a finite state, finite action Markovian decision process. The report supplies a listing for a program in BASIC of the policy improvement algorithm for finding a best policy. The model will help maintenance engineers, building managers and/or others responsible for making decisions concerning maintenance policies in selecting economically efficient levels of maintenance for elements of building service equipment. The report also contains an illustrative example applying the model to the maintenance of an air handling unit.

NBSIR 77-1213. **Skid resistance measurement tests of new FHWA reference systems at the Eastern Field Test Center,** R. W. Kearns and J. F. Ward, 132 pages (Mar. 1977). Order from NTIS as PB265102.

Key words: accident reduction, skidding; correlation, skid resistance; highway safety; measurement, skid resistance; pavement, skid resistance; pavement wetting system; skid resistance, measurement; tire-pavement interface forces; wet pavement skid resistance.

The Federal Highway Administration (FHWA) is developing a program to improve the method of measuring wet weather pavement skid resistance (SN) and to reduce the variation in results. At the national level, an interim reference system (IRS) is maintained and operated by the National Bureau of Standards. At the regional level, an area reference system (ARS) is maintained and operated at each FHWA Field Test Center. Intercomparisons between these reference systems and the highway measuring systems at the state level provide measurement assurance.

In this report, the first correlations between three identical, newly manufactured systems (ARS 1, 2, 3) and the IRS are given. Computed standard deviations of midrange predicted SN values are typically less than 0.1 SN. SN is given as a function of test speed for each system, on two test surfaces. Speed gradients of SN are found to be characteristic of the surface.

The test program is explained, from preparations and calibrations of subsystems through dynamic measurement on the surfaces. Controlled and uncontrolled variables are identified, discussed, and in some cases, investigated experimentally. A ranking of the sources of dispersion is given.

A ground station for improved SN calculation precision and on-site statistical analysis, operated in parallel with traditional SN data acquisition methods, is found to perform reliably.

NBSIR 77-1217. **Safety problems associated with pressure containers,** S. K. Wakamiya and N. J. Calvano, 42 pages (Mar. 1977). Order from NTIS as PB264691.

Key words: container; corrosion; explosion; extinguisher; fire; gas; injury; liquefied; petroleum; standards.

Accident reports from hospital emergency rooms and reports of interviews with accident victims were reviewed to determine the probable causes of accidents involving two types of pressure containers: fire extinguishers and liquefied petroleum (LP) gas tanks. The data collected and reviewed during the study suggests that some of the safety problems associated with fire extinguishers involve: 1) incompatibility of the contents of an extinguisher with its shell; 2) faulty method attachment of plastic pressure gages on some dry chemical extinguishers; and 3) widespread use of obsolete extinguishers.

The primary hazard associated with LP gas containers appears to be leakage from various parts of the LP system. In many instances leaking gas accumulated in a closed area and was accidentally ignited, resulting in an explosion.

Engineering standards relevant to the safety of fire extinguishers and LP gas tanks were reviewed. Although the present standards governing these pressure containers address most safety problems adequately, a few of the requirements in some of these standards appear to be of questionable value in preventing certain types of accidents.

NBSIR 77-1218. **Risks associated with certain sports activities,** W. B. Beine, 106 pages (Jan. 1977). Order from NTIS as PB264666.

Key words: accident; associated factors; injuries; literature; NEISS; recommendations; review; safety; sports.

This study provides the Consumer Product Safety Commission with recommendations for assigning priorities to tasks associated with reducing the incidence and severity of sports related injuries. Recommendations were derived from an analysis of the published literature and the NEISS data. They emphasize the need for collecting additional data, improving surveillance capabilities, stimulating research, and developing and promulgating equipment safety standards.

NBSIR 77-1219. **Optical materials characterization,** A. Feldman, D. Horowitz, and R. M. Waxler, 37 pages (Mar. 1977). Order from NTIS as PB264692.

Key words: BaF_2; CaF_2; KBr; KCl; LiF; NaF; refractive index; SrF_2; thermal coefficient of refractive index; ZnSe.

The refractive indices of three prisms of chemical vapor deposited ZnS were measured at room temperature over the wavelength range 540 nm to 1.083 μm. The refractive indices of eight specimens of CaF_2 doped with Er were measured from 404.7 nm to 1.083 μm. The doping range was 0.001 to 3 percent Er. Interferometric measurements of dn/dT were made over the temperature range −180 to 200 °C at the wavelengths 632.8 nm and 3.39 μm on single crystal specimens of BaF_2, CaF_2, reactive atmosphere processed (RAP) KBr, RAP KCl,

KCl doped with KI, LiF, NaF and SrF_2, and on chemical vapor deposited (CVD) ZnSe and hot forged CaF_2.

NBSIR 77-1221. **Proceedings of a symposium: Communicating for product improvement October 13-14, 1976,** C. Hulick, Ed., 52 pages (Feb. 1977). Order from NTIS as PB264919.

Key words: procurement incentives; product improvement system; product innovation; user need.

The general objective of the conference was to establish a continuing dialogue between private industry and government agencies on the ways and means of product improvement, placing particular emphasis on methods of communicating specific product needs to manufacturers and making purchasing offices more responsive to these needs at the Federal, State and local level. Workshops were organized to consider Product Improvement System, User Need and Industry Response, Procurement Incentives and Techniques, and The Role of Professional Organizations. Reports and recommendations of these Workshops are included.

NBSIR 77-1222. **Reproducibility of the radiant panel test method (ASTM E 162-67) using polyurethane foam, neoprene, and hardboard specimens,** T. G. Lee, 40 pages (Mar. 1977). Order from NTIS as PB265089.

Key words: ASTM E 162; coefficient of variation; flame spread tests; flexible polyurethane; hardboard; interlaboratory evaluation; neoprene; radiant panel test; round robin; test method.

Interlaboratory evaluation of the Radiant Panel Method (ASTM E 162-67) for flame spread testing of two flexible foam and one hardboard specimens was made. Results obtained by 13 laboratories based on 4 replicate tests, showed that the between-lab coefficient of variation on the flame-spread index (I_s) was 21 percent for Hardboard A, 35 percent for Urethane B and 45 percent for Neoprene C. The within-lab coefficient of variation for the Hardboard was 9.9 percent. The higher variability of results for the foam materials was caused by the rapid melting of the Urethane B and unstable flame front of the Neoprene C specimens during the tests. An important source of error for some laboratories was in the determination of β, the calibration constants, and the inappropriate use of base stack temperature correction. Statistics on the reproducibility of the flame-spread factor (F_s), heat evolution (Q) and I_s are also given. A new pilot burner and other modifications of the method were found useful.

NBSIR 77-1229. **Accelerometer calibration—A comparison between CESTA and NBS,** J. D. Pollard, 22 pages (Jan. 1977). Order from NTIS as PB265477.

Key words: accelerometers; calibration; measurements; vibration; vibration exciters; vibration standards.

This report describes a vibration measurement interchange between a French laboratory (CESTA) and the National Bureau of Standards (NBS). Methods of calibration at NBS and results of the calibration of two commercially available double ended or "piggy-back" type accelerometers are discussed. No difficulties were encountered in the calibration of System 1, however, above 4000 Hz difficulties were experienced in the calibration of System 2.

NBS-GCR-ETIP 76-24. **A framework for analyzing commodity supply restrictions,** 242 pages (Sept. 1976). Order from NTIS as PB258093.

Key words: applied microeconomic framework; commodity supply crises; econometric analysis; economic impacts; efficiency impacts; income distribution effects; policy alternatives.

Study addresses commodity supply crises due to producer country export policies, and considers the issue of resource exhaustion only as it relates to this problem. The primary concern is with *economic* impacts and policies. Crises in commodity supplies may well have political impacts, but detailed treatment of such effects is beyond the scope of the study. Possible political and diplomatic constraints on U.S. policies are considered, but the primary concern is with economic impacts.

Policies differ in their effects on the distribution of income between producers and consumers. Such effects are considered, where appropriate. Concentration is on efficiency impacts, however, and there is no attempt to address effects on the size distribution of income.

The basic analytical approach is that of the applied microeconomist working in a supply and demand framework. This framework allows the use of available qualitative economic, econometric and engineering information. There has been no use of mathematical programming or input-output techniques as it is believed that the techniques employed are, for the purposes of this study, more productive within time and budget constraints.

NBS-GCR-ETIP 76-25. **Cartelization in the world cobalt market: Economic analysis and policy implications,** 96 pages (Sept. 1976). Order from NTIS as PB264386.

Key words: cartels; economic policy options; foreign supply disruptions; stockpiling; technology; U.S. demand structure.

This volume applies the analytical framework to study supply, demand, and price formation in the cobalt market as a background for policy formation. It also analyzes the effects and likelihood of a producer country cartel or supply disruption. Finally, it presents policy and technological strategies in response to cartel formations or supply cutoffs.

The major policy implication of this study is that maintenance of a moderate contingency stockpile of between five and ten million pounds provides adequate insurance for possible supply disruptions. This range includes both public and private contingency stocks. Promotion of research and development to find substitutes for cobalt and cobalt alloys might be warranted, but only if the costs to the public sector are very low relative to the potential reduction in consumption. Subsidies to potential domestic producers would be advisable only if a prolonged disruption seemed likely; in such a situation, promoting recovery of cobalt from undersea manganese nodules might be preferable to subsidizing landbased production.

NBS-GCR-ETIP 76-26. **Value incentive program. Energy conservation compressors for computer room air conditioning systems,** 39 pages (Oct. 1976). Order from NTIS as PB259998.

Key words: Experimental Technology Incentives Program (ETIP); Federal Supply Service; life cycle costing; procurement policy; specifications; value incentive.

This case study covers the use of the Value Incentive Clause by a GSA/FSS contractor to make product improvement suggestions on Energy Conservation Compressors for Computer Room Air conditioning Systems. The use of this clause allows for contractors who hold FSS contracts to make suggestions to reduce the overall cost of procurement to the government and to share in the savings resulting from their suggestion. Copies of the GSA order, and the clause itself are included in addition to the specific changes proposed for the energy conservation compressors for computer room air conditioning systems.

NBS-GCR-ETIP 76-27. **Value incentive program. Reduce welding/brazing on wardrobe hinge,** 41 pages (Oct. 1976). Order from NTIS as PB260523.

Key words: Experimental Technology Incentives Program (ETIP); Federal Supply Service; life cycle costing; procurement policy; specifications; value incentive.

This case study covers the use of the Value Incentive Clause by a GSA/FSS contractor to make product improvement suggestions to Reduce Welding/Brazing on Wardrobe Hinge. The use of this clause allows for contractors who hold FSS contracts to make suggestions to reduce the overall cost of procurement to the government and to share in the savings resulting from their suggestion. Copies of the GSA order, and the clause itself are included in addition to the specific changes proposed to reduce welding/brazing on wardrobe hinge.

NBS-GCR-ETIP 76-28. **Policy implications of producer country supply restrictions: The world platinum and palladium markets,** 153 pages (Sept. 1976). Order from NTIS as PB264387.

Key words: cartels; economic policy options; foreign supply disruptions; stockpiling; technology; U.S. demand structure.

Analysis of the supply and demand conditions in the world markets for platinum and palladium and the nature of the U.S. dependence on foreign supplies. Objective is to evaluate the probability and consequences of disruptions in the supply of new platinum metals to the United States or of cartel sponsored increases in the prices of these metals. The analysis of the consequences of supply disruptions and cartelization of the platinum and palladium markets is based on both qualitative assessment of the characteristics of those industries and a theoretical model of firm behavior applied to the industries which use platinum metals as a capital good.

The study is organized into chapters on consumption, supply, market organization and price history (including past crises), qualitative analysis of the impact of supply disruptions, a theoretical analysis of the impact of supply disruptions and an analysis of alternative government policies to protect against disruptions.

NBS-GCR-ETIP 76-29. **Policy implications of producer country supply restrictions: The world manganese market,** 210 pages (Sept. 1976). Order from NTIS as PB264388.

Key words: cartels; economic policy options; foreign supply disruptions; stockpiling; technology options; U.S. demand structure.

This volume analyzes the likelihood and the consequences for the United States of nonmilitary disruptions in foreign supplies of higher grade manganese ores, materials which the U.S. does not mine domestically. Information about foreign producers is studied for indications of the probability and nature of potential nonmilitary supply disruptions which would result either from formal cartels explicitly formed for economic gain, or from more tacit forms of collusion. Considerable attention is given to the demand of U.S. steelmakers for manganese at various prices, from which the economic cost which higher manganese prices would inflict can be inferred. Finally, economic policy options are investigated in terms of minimizing the total expected welfare loss for the economy. Stockpiling policy is investigated in detail both because it is a fundamental policy response, and because the most relevant analysis of other policy options, such as investment in technological projects, generally assumes a coordinated stockpile policy. A coordinated tariff policy is also considered.

NBS-GCR-ETIP 76-30. **Policy implications of producer country supply restrictions: The world copper market,** 121 pages (Aug. 1976). Order from NTIS as PB264389.

Key words: cartels; economic policy options; foreign supply disruptions; stockpiling; technology options; U.S. demand structure.

This volume examines the likelihood of future crises in copper supply and the policy alternatives available to the United States. The major conclusion is that supply crises are fairly unlikely and that the potential damage to the U.S. economy from such crises would be minimal. Even when very pessimistic assumptions are made about the ability of the United States and other countries to adapt to disruptive export policies of CIPEC (the organization of foreign copper producers), it appears that CIPEC does not have enough market power to cause severe economic damage to the principal consuming countries.

The analysis addresses the likelihood of a number of potential supply crises. Each type of supply crisis will lead to a significant welfare loss only if the United States becomes substantially dependent on imports before the interruption occurs. Therefore, an important question for analysis in this report is whether copper imports are likely to play an important role in future U.S. supply patterns, and if so, why.

NBS-GCR-ETIP 76-31. **Policy implications of producer country supply restrictions: The world chromite market,** 247 pages (Oct. 1976). Order from NTIS as PB264390.

Key words: cartels; economic policy options; foreign supply disruptions; stockpiling technology options; U.S. demand structure.

This volume presents an analysis of the likelihood and the consequences for the United States of disruptions in our foreign supplies of chromium, a material which we do not mine domestically. Information about foreign producers is studied for indications of the probability and nature of potential supply disruptions, whether caused by cartels formed for economic gain or by actions of individual supplying countries. Considerable attention is given to assessing the market behavior of U.S. consumers of chromium, from which can be inferred the economic cost which higher chromium prices would inflict. Finally, economic policy options, particularly the standard tools of stockpiles and tariffs, are investigated in terms of minimizing the total expected welfare loss for the economy. Investments in technological projects which would ameliorate U.S. vulnerability to chromium supply disruptions are subject to general analysis, assuming a coordinated stockpile and tariff policy. Finally, in a brief historical review, potential past crises in the chromite market are assessed for lessons relevant to possible future supply disruptions.

NBS-GCR-ETIP 76-32. **Policy implications of producer country supply restrictions: The world aluminum/bauxite market,** 275 pages (Mar. 1977). Order from NTIS as PB264391.

Key words: applied microeconomic framework; commodity supply crises; econometric analysis; economic impacts; efficiency impacts; income distribution effects; policy alternatives.

Analyzes the impact on the world bauxite and aluminum markets of the recently formed International Bauxite Association (IBA), a cartel organized by the bauxite producing and exporting nations. Examines the probable price and output policies of the IBA and the potential effect of these policies on the U.S. economy. The resource loss to the United States resulting from the cartel's actions is estimated, and alternate U.S. government policies for modifying the IBA's behavior and reducing the resource loss resulting from cartel pricing and possible supply cutoffs are analyzed. Particular emphasis is given to the role of innovative technology.

NBS-GCR-ETIP 76-33. **Policy implications of producer country supply restrictions: The world energy market,** 382 pages (Nov. 1976). Order from NTIS as PB264392.

Key words: applied microeconomic framework; commodity supply crises; econometric analysis; economic impacts; efficiency impacts; income distribution effects; policy alternatives.

A number of policies have been proposed to reduce U.S. dependence on imported oil or to reduce U.S. vulnerability in some other way. Among the policies proposed are stockpiling, quotas and tariffs, subsidies to domestic oil producers, accelerated development of nuclear power, and conversion of oil fired generating plants to coal. Of special concern is the proposal that U.S. government subsidize or offer other incentives to the development of synthetic fuels, since these technologies have not yet been significantly developed on a commercial scale in the United States. This study examines these different policies, their benefits and costs, and compares them as instruments to reduce the impact of future supply disruptions.

The policy measures chosen for analysis are representative of types of actions currently under consideration to mitigate the effects of OPEC. The policy analysis treats the price of oil, the strength of OPEC, and the prospect for future embargoes as given, determined effectively by forces other than the policies themselves. Policy measures primarily aimed at weakening OPEC and encouraging its collapse require a different kind of analysis and are not within the scope of this study, though considerations bearing on OPEC's cohesiveness are discussed.

NBS-GCR-ETIP 76-34. **Developing incentives for pest control methods. Proceedings of a conference Oct. 26-27, 1976,** 92 pages (Jan. 1976). Order from NTIS as PB263275.

Key words: impact of government on the economy; pesticides; R&D incentives; regulation; technology.

The conference, which is the subject of these proceedings, represented the culmination of a joint study effort by Experimental Technology Incentives Program/National Bureau of Standards (ETIP/NBS) and Office of Pesticide Programs/U.S. Environmental Protection Agency (OPP/EPA) to develop incentives through which the Federal Government could encourage continued research and development of pest control methods. The project is part of the regulatory programs of ETIP seeking data and policy recommendations on how regulatory process can be improved in a way that will benefit desirable technological growth in the private sector.

The purpose of the conference was to assemble representatives of the parties at interest (government agencies, industry and public interest groups) in order to examine and evaluate the incentives that had been developed by the study contractor, Arthur D. Little, Inc. The two-day meeting was organized into working groups who reported to a plenary session at the close of their discussions. The result is a consensus concerning the incentives and their implementation. The report contains summaries of the workshops, their recommendations for the parties at interest to follow, and the reactions of participants after the conference was held.

NBS-GCR-ETIP 76-35. **Post-marketing surveillance of new drugs: A preliminary review of the current state-of-the-art,** W. M. Wardell, M. C. Tsianco, H. T. Davis, and S. N. Anavekar, 46 pages (Dec. 1976). Order from NTIS as PB263273.

Key words: adverse reaction detection; biostatistics; drug regulation; pharmaceutical regulation; phase IV; post marketing surveillance; regulatory experiments; system design.

The study had the aim of gathering information to (1) identify examples of post-marketing surveillance that have been carried out, (2) review the methodology available for PMS in relation to the aims of studies involved, using the actual examples upon which data could be obtained, (3) analyze the examples in technical terms, particularly experimental design and statistical power, (4) examine their costs and benefits where sufficient data exist. The case examples selected for this study were those upon which the data could be obtained in a limited time period and in some cases published data were used. Examples of controlled experiment studies, controlled cohort surveys, uncontrolled cohort surveys, case-control surveys, and spontaneous voluntary reporting are provided. These examples are not the products of a formal system of PMS but are studies which have been carried out to meet a variety of perceived needs. A main conclusion is that no single design approach for a PMS system will by itself be sufficient to carry out all that is needed from a PMS system. As one moves from descriptive approaches to analytic studies, power, bias, and costs become dominating features.

NBS-GCR-ETIP 77-36. **Policy implications of producer country supply restrictions: Overview and summary,** 264 pages (Feb. 1977). Order from NTIS as PB264393.

Key words: applied microeconomic framework; commodity supply crises; econometric analysis; economic impacts; efficiency impacts; income distribution effects; policy alternatives.

This volume summarizes the other eight volumes of the study which seeks to evaluate alternative federal policies which deal with restrictions initiated by producer countries on supplies of major imported materials. A major premise of CRA's effort was that rational policy analysis must proceed from a realistic and market specific analysis of risks to a similarly concrete evaluation of potential damage, and then to consideration of a range of policy instruments including not only government encouragement of technological change, but also stockpiling, tariffs and quotas, subsidies, and other measures.

The analytical approach combined an assessment of real dangers to the U.S. economy in various materials markets with an analysis of the costs of different policies designed to reduce the impacts of foreign supply restrictions. The assessment of the dangers involved an analysis of both the economic costs of various possible contingencies with an assessment of the probabilities of these contingencies. The analysis of the potential policies also involved the measurement of the transfer payments (income redistributions) and the identification of the noneconomic costs, such as environmental consequences, of each policy.

NBS-GCR-76-77. **A basic investigation of the extinguishability of various fabrics,** L. B. Miles, 95 pages (Sept. 22, 1976). Order from NTIS as PB257767.

Key words: extinguishability; fabric flammability; flammability ranking; heat flux; heat transfer rate; linear burning rate.

In considering extinguishability hazards both the inherent qualities of a fabric as well as human reactions are important. This study concentrates on the former aspect. Linear burning rate and heat flux are measured for twelve fabrics within a TRI Flammability Analyzer cabinet. Initial work deals with ambient oxygen effects on the burning rate and heat flux of each fabric measured at four levels of oxygen. From the resulting data, a series of relationships were studied by regression techniques. The latter work investigates heat sink/intersticial effects on burning rate and heat flux. Two heat sink designs were evaluated using temperature and distance as variables. In studying

cooling effects, each fabric was tested at three heat sink distances. Burning rate and heat flux were plotted as functions of inverse heat sink distance. In the oxygen effects study, analyses showed that linear burning rate was dependent on fiber type and construction, that heat flux was basically fiber dependent, and that mass burning rate was not entirely independent of construction. In the heat sink effects study, burning rate and heat flux were mainly dependent on distance of the heat sink. A comparison of oxygen and heat sink data showed that in both cases oxygen supply was the controlling factor.

NBS-GCR-76-78. **An investigation of certain design parameters of the mushroom apparel flammability tester,** A. K. Stratton, 112 pages (July 1976). Order from NTIS as PB257836.

Key words: apparel; fabrics; flammability testing; heat transfer rates; Mushroom Apparel Flammability Tester; standards; test development; textiles.

This paper describes the effect of variations in design parameters of the apparatus on the heat transfer rates measured by the "Mushroom Apparel Flammability Tester." In this instrument, cylindrical specimens of apparel fabrics are suspended from a circular top plate, and the rate of heat transfer to the top plate and a cylinder inside the specimen are measured. The paper describes the effect of changing the cylinder diameter, and of introducing rods between the specimen and the cylinder to prevent deposition of molten polymer on the cylinder. Heat transfer rates measured on the top plate and on the cylinder are compared. Design parameters for the present version of this instrument and the corresponding test method were chosen on the basis of this investigation. The paper is in the form of a Master of Science thesis; the experimental work was performed at NBS.

NBS-GCR-76-79. **A problem in fire safety: Flame spreading across liquid fuels,** F. L. Dryer, I. Glassman, W. A. Sirignano, 30 pages (Sept. 15, 1976). Order from NTIS as PB259127.

Key words: combustion models; flame spread; fluid flow; laser doppler velocimetry; liquid fuels; solid fuels; surface tension.

This report provides a brief summary of experimental and theoretical work carried out at Princeton University on flame spreading across liquid fuels. The importance of surface tension driven flows ahead of the flame front in controlling flame spread across liquids at temperatures below the flash point was demonstrated experimentally. Buoyancy and radiation effects were also present but were of lesser importance. Variations in the temperature of the liquid surface are attributed to eddies in the gas phase ahead of the flame front. These eddies may also play a role in flame propagation across solid combustibles. It is proposed to investigate these eddies by means of laser doppler velocimetry. A two-dimensional, steady-state computer program is under development for use as a tool in studying flame propagation above liquid and solid fuels.

NBS-GCR-76-80. **Scaling of radiative characteristics of turbulent diffusion flames,** G. H. Markstein, 51 pages (June 1976). Order from NTIS as PB259126.

Key words: flame radiation; radiant flux density; radiation measurement; radiative heat transfer; turbulent flames.

The following measurements were performed on single buoyancy-controlled turbulent propane diffusion flames within the range $44 \leq q \leq 412$ cm^3/s of fuel rate q: 1) total radiative power P, determined with a wide-view-angle radiometer, 2) total radiative power ΔP emitted by a horizontal flame slice of known height Δz, measured with a wide-view-angle radiometer that looks at the flame through a horizontal slit, and 3) radiance emitted along a flame diameter, N_{max}, measured with a collimated beam radiometer. The latter two quantities were measured simultaneously as functions of height z above the burner nozzle over the entire length L of the flame. Total radiative power was found to scale with the first power of flow rate, $P = \chi Q = \chi \Delta h_c q$, where the fraction χ of total rate of release Q emitted as radiation was 0.264 and $\Delta h_c = 86.821$ J/cm^3 is the heat of combustion per unit volume of fuel. From the local radiative properties $S = \Delta P/\Delta z$ and N_{max}, flame diameter $D = \pi^{-2} S/N_{max}$ and volumetric radiant power $p = 4\pi^3 N^2_{max}/S$ were derived. It was found further that the dependence of the data on flow rate q could be scaled by power law relationships, with the dependence on height z expressed by two dimensionless functions $s(\zeta)$, $n(\zeta)$ of the dimensionless height $\zeta = z/L$.

NBS-GCR-77-82. **Detector sensitivity and siting requirements for dwellings—Phase 2,** S. W. Harpe, T. E. Waterman, and W. J. Christian, 379 pages (Feb. 1977). Order from NTIS as PB263882.

Key words: detector sensitivity; detector siting; escape time; fire tests; gas detectors; heat detectors; residential fires; smoke detectors.

The contract for a field investigation of the effectiveness of residential smoke detectors was extended to cover 36 additional tests investigating details not completely covered in the first report. The objective of the second phase of the program was to gather information on fires under summer/fall conditions without air conditioning and to expand available information on high volume, two story structures. The effects of open windows, new technical developments in photoelectric detector design, and the response of semiconductor type residential gas detectors and mechanically powered heat detectors were also included.

The tests reinforced the conclusions of the first phase of testing. They showed that open windows have little appreciable affect of life safety and detection times, and that semiconductor gas sensing fire detectors exhibit fuel specific response characteristics which seriously degraded the effectiveness in certain types of fires.

This column lists all outside publications by the NBS staff, as soon as possible after issuance as practical. For completeness, earlier references not previously reported may be included from time to time.

16659. Mehlman, G., Weiss, A. W., Esteva, J. M., **Revised classification of Mg II levels between 59 and 63 eV,** *Astrophys. J.* **209,** 640-641 (Oct. 15, 1976).

Key words: atomic processes; line identifications.

A total of 68 new resonances in the absorption spectrum of magnesium were previously identified by two of the authors. The tentative classification proposed for 10 of the Mg II levels was erroneous. A revised labeling is proposed in this note for these lines.

16660. Newman, M., **Asymptotic formulas related to free products of cyclic groups,** *Math. Comp.* **30,** No. 136, 838-846 (Oct. 1976).

Key words: asymptotic formulas; classical modular group; cyclic groups; free groups; free products; tables.

Asymptotic formulas for the number of subgroups of a given index of the free product of finitely many cyclic groups are given. The classical modular group Γ is discussed in detail and a table of the number of subgroups of Γ of index n is given for $1 \leq n \leq 100$.

16661. Lawton, R. A., Andrews, J. R., **Electrical strobing of a photoconductor cuts sampling oscilloscope's risetime,** *Laser Focus Mag.*, pp. 62-65 (Nov. 1976).

Key words: optical; oscilloscope; photoconductor; sampling; waveforms.

An oscilloscope capable of directly sampling optical waveforms has been developed at NBS. It uses a GaAs photoconductor strobed by an electrical impulse. The transition time of the oscilloscope is 100 ps.

16662. Dodge, M. J., Malitson, I. H., **Refractive index of high purity KCl and KI doped KCl,** *Proc. 5th Conf. on Infrared Laser Window Materials, Las Vegas, NV, Dec. 1-4, 1975*, pp. 216-223 (Air Force Materials Laboratory, Wright-Patterson Air Force Base, OH, Feb. 1976).

Key words: potassium chloride; refractive index; temperature coefficient of index.

The refractive indexes of a sample of potassium chloride made by reactive atmosphere processing (RAP) and a sample of potassium chloride doped with potassium iodide were determined from 0.25 μm to 15.5 μm. Measurements were made by means of the minimum-deviation method on both samples at a controlled room temperature near 20 °C and on the RAP specimen near 34 °C. Each set of experimental data was fitted to a Sellmeier-type dispersion equation which permits refractive index interpolation within several parts in 10^{-5}. Temperature coefficients of index as a function of wavelength are also given. A comparison of these data with values of commercially grown KCl is presented.

16663. Engen, G. F., **Theorem giving limits for $|S_{22}|$ when $|S_{11}|$ and the two-port efficiency are known,** *IEEE Trans. Instrum. Meas.* **IM-20,** No. 1, 78 (Feb. 1971).

Key words: lossless two-port; scattering parameters.

A well-known condition on the scattering parameters of a lossless two-port may be written $|s_{22}| = |s_{11}|$. For low-loss two-ports it may be expected that this condition is approximately satisfied; this result is of potential value in certain types of system evaluation.

16664. Lovas, F. J., Johnson, D. R., Buhl, D., Snyder, L. E., **Millimeter emission lines in Orion A,** *Astrophys. J.* **209,** No. 3, 770-777 (Nov. 1, 1976).

Key words: interstellar, molecules; line identifications; nebulae, individual; radio sources, lines.

During the course of a search of Orion A for signals from three large, organic molecules, several millimeter wave lines from known interstellar molecules were observed. Results of observations on methanol (CH_3OH), methyl cyanide (CH_3CN), methyl acetylene (CH_3CCH), acetaldehyde (CH_3CHO) and ^{29}SiO are reported here. Emission signals from two hydrogen recombination lines (H41α and H42α) detected from the H II region of Orion A are also reported. Negative results were obtained for several millimeter wave transitions of ethylene oxide (CH_2OCH_2), acetone [$(CH_3)_2CO$], and cyclopropenone (HCCOCH).

16665. Madden, R. P., Hughey, L. R., **Radiometry with synchrotron radiation,** *Proc. Synchrotron Radiation Facilities, Quebec Summer Workshop, Quebec, Canada, June 15-18, 1976*, Chapter 10.4, pp. 10-51—10-77 (1976).

Key words: calibration facilities; photodiodes; radiometry; spectrometer calibration; synchrotron radiation; transfer standard detectors.

Transfer standard detectors are calibrated at NBS by comparing their output with that of a double-ionization chamber. In this instance the synchrotron radiation from the NBS electron storage ring (SURF) is utilized as a convenient source of radiation in the wavelength range of 190 to 600 Å. Synchrotron radiation is also used as an absolute irradiance standard. Numerous experimental checks of Schwinger's theoretical predictions have demonstrated agreement within the limits of accuracy of the measurements. SURF is a well characterized storage ring. The magnetic field and electron radius are known to about .01 percent. The major source of uncertainty is the determination of the number of electrons in orbit (n_e). n_e is measured with a narrow band photodiode calibrated by the NBS Optical Radiation Section. This method provides n_e to about 2.4 percent and an overall uncertainty of less than 5 percent for wavelengths in excess of 40 Å.

16666. Motz, J. W., Danos, M., **The potential for exposure reduction in diagnostic radiology,** *Proc. Digest of the 4th Int. Conf. on Medical Physics, Special Issue of Physics in Canada, Ottawa, Canada, July 25-30, 1976*, **32,** 13.3 (Le Droit-Leclerc, Ottawa, Canada, July 1976).

Key words: diagnostic radiography; exposure reduction; imaging information content; image processing; mammography; x-ray radiography.

Based on considerations of the statistical noise generated by the detection of a given number of particles in a given resolution element, a method is developed for determining the quantitative dependence of the image information content on the patient exposure. Data are given which show: (1) the minimum exposures required for the detection of image signals from six sample structures encountered in diagnostic radiology, as a function of the spatial resolution and x-ray energy, (2) the number of gray levels attainable for a given patient exposure, body thickness, and x-ray energy, and (3) the quantitative effects of x-ray grids in increasing the image contrast and gray level number, and in reducing the exposure required for the detection of a given image signal. The implications of these results for reducing exposures and for detecting low contrast objects below the visibility threshold will be discussed.

16667. Beeghly, H. F., Mears, T. W., Michaelis, R. E., **Standard materials for analysis and testing,** Paper in *Treatise on Analytical Chemistry*, I. M. Kolthoff and P. M. Elving, Eds., **3,** Part III, 1-45 (John Wiley & Sons, 1976).

Key words: chemical analysis; measurement systems; physical measurement units; standard reference materials; physical measurement units.

Emphasis in this chapter is on reference materials, with particular concern for carefully characterized materials, certified by a responsible, impartial agency or organization. Attention is given to materials useful in making meaningful measurements over the span of needs by science, industry, and government for "benchmark" or reference point materials for calibrating and checking measuring instruments and methods.

16668. Crawford, M. L., **Techniques for measurement of electromagnetic radiation and susceptibility of electronic equipment,** *Proc. 1st Symp. and Technical Exhibition on Electromagnetic Compatibility, Montreux, Switzerland, May 20-22, 1975*, pp. 38-44 (Electromagnetic Compatibility, Montreux, Switzerland, 1975).

Key words: electronic equipment; EMC measurements; low-Q enclosures; radiated susceptibility; TEM transmission cell.

This paper describes two alternative approaches to conventional screen room measurements for determining radiation from electronic equipment and the susceptibility of equipment to continuous wave and pulsed electromagnetic fields. Details of EMC measurements performed using the two techniques: (1) use of underground mine tunnels (low-Q enclosure), and (2)

use of TEM transmission cells, are given along with a brief discussion of factors influencing the measurement results.

The TEM cell is particularly high-lighted because of its potential for making accurate ($\leq$ 1-2 dB for radiated susceptibility at levels up to 600 V/m, and 3-5 dB for radiated emission at levels down to 10 μV/m) measurements with a minimum of additional equipment.

16669. Kanda, M., **An improved solid state noise source,** *Proc. Int. IEEE-MTT-S Microwave Symp., Cherry Hill, NJ, June 14-16, 1976*, pp. 224-226 (The Institute of Electrical and Electronics Engineers, Inc., Piscataway, NJ, June 1976).

Key words: argon gas discharge noise source; silicon avalanche diode; solid state noise source; stability.

An improved solid state noise source is discussed. By implementing such modifications as 1) heat sinking of a silicon avalanche noise diode, 2) proper DC RF decoupling, and 3) impedance matching, the stability of the NBS solid state noise source is improved significantly over that of typical commercial solid state noise sources. The paper describes these modifications, how they are implemented, and the resulting improvement in stability.

16670. Ederer, D. L., **Photoabsorption in inner-shells of atoms,** (Proc. 2nd Int. Conf. on Inner Shell Ionization Phenomena, Freiburg, Germany, Mar. 29-Apr. 2, 1976), Paper in *Second International Conference on Inner Shell Ionization Phenomena*, W. Mehlhorn and R. Brenn, Eds., pp. 145-165 (Universität Freiburg, Freiburg, Fed. Rep. Germany, 1976).

Key words: atoms, correlation; configuration interaction; exchange interaction; inner shells; photoabsorption.

Inner-shell optical photon excitations in atomic gases are discussed in this paper. Special emphasis is given to electron correlations arising from configuration interaction and the exchange interaction. Because these interactions are largest at photon energies $\leq$ 200 eV the scope of the paper will be limited to this part of the spectrum. The subject is approached from the point of view of experimental physics emphasizing excitations in noble gases and metal vapors. The first section of the paper deals with excitations to discrete states that decay by an Auger or an autoionization process, and the next section explores the role exchange and correlation plays in the continuum photoionization cross section of gaseous systems. Finally recent measurements will be reviewed that use the technique of photoelectron spectroscopy to measure the partial photoionization cross section of each group of subshell electrons.

16671. Wacker, P. F., **Non-planar near field measurements: Spherical scanning,** *AFAL-TR-75-38*, 55 pages (Air Force Avionics Laboratory, Air Force Systems Command, Wright-Patterson Air Force Base, OH, Apr. 1975).

Key words: antennas; arrays; coordinate transformations; data processing; group representations; measurements; near field; nonplanar; patterns; scanning; spherical; symmetry.

The advantages and limitations of near-field antenna measurements are compared with those of conventional far-field measurements. Further, the advantages and limitations of planar, circular cylindrical, and spherical scanning are compared.

Spherical scanning is advantageous for arrays steered well off-axis and for antennas with wide angle side lobes, but the data processing has been quite impractical except for very simple antennas and probes. A new highly efficient data processing scheme is given for spherical scanning with and without probe pattern correction. The translation-of-centers transformation of the probe pattern coefficients (required only with the probe pattern correction) is carried out once and for all for a given probe, scanning radius, and frequency. The routine computations involve Fast Fourier "Transforms" and multiplication by matrices with constant elements, matrices which are independent of the detailed nature of the probe, the radius of the scanning sphere, the points at which measurements are made, and the nature of the test antenna. The FFT's and matrix multiplications supplant matrix inversion, ordinary solution of simultaneous equations in more than two unknowns, ordinary numerical integration, and (in routine processing) ordinary evaluation of functions, even for computation of the far field. Except for the truncation of the infinite series of spherical modes, no analytical or data processing approximations are made, even in the use of the FFT.

So that readers may draw from their understanding of planar and cylindrical scanning, a unified theory of near-field data processing is given, treating planar, cylindrical, and spherical scanning as mere special cases.

16672. Lawn, B. R., Fuller, E. R., Wiederhorn, S. M., **Strength degradation of brittle surfaces: Sharp indenters,** *Am. Ceram. Soc.* **58,** No. 5-6, 193-197 (May-June 1976).

Key words: brittle solids; ceramic surfaces; degradation; fracture; indentation; strength.

A theory of strength loss for brittle surfaces in contact situations, developed in a previous paper for "blunt" indenters, is extended to the case of "sharp" indenters. A prior fracture mechanics analysis of crack growth beneath ideal cone indenters serves as the basis for predetermining the prospective surface degradation of ceramic components in service. Compared to blunt indenters, sharp indenters can cause severe degradation at lower contact loads. However, at high loads, the extent of degradation becomes remarkably insensitive to details in the indenter geometry. Essential theoretical predictions are verified by bend tests on glass slabs. Effects of indenter "sharpness" and initial specimen surface flaw state are investigated systematically, along with some secondary rate effects in the contact process. The possibility of minimizing degradation via adjustment of material parameters (including hardness) or surface condition (e.g. residual stresses, frictional properties) is briefly discussed.

16673. Wasik, S., Chesler, S., **Use of a nematic liquid crystal for the gas-liquid chromatographic separation of naphthalene homologues,** *J. Chromatogr.* **122,** 451-458 (1976).

Key words: gas-liquid chromatography; liquid crystal; naphthalene homologues; nematic phase; supercooled phase.

The gas-liquid chromatographic separations of methyl-, ethyl-, and dimethyl-naphthalene isomers on the nematic and supercooled regions of N,N'-bis(*p*-methoxybenzylidene)-α,α'-bi-*p*-toluidine are presented and compared with the results obtained on other materials. The unique selectivity of this liquid crystal, based upon differences in the molecular length-to-breadth ratio of the solute positional isomers, has enabled the complete separation of these naphthalene homologues.

16674. Collins, L. A., Lane, N. F., **Quantum-mechanical calculations of rotational-excitation cross sections for HCl, DCl, DF, and HF in slow collisions with He,** *Phys. Rev. A* **14,** No. 4, 1358-1367 (Oct. 1976).

Key words: atom-molecule scattering; collisions of He with diatomic hydrides; heavy particle collisions; rotational excitation in atom-molecule scattering.

Low-energy rotational-excitation cross sections have been calculated for collisions between ground-state helium atoms and the diatomic molecules HCl, DCl, DF, and HF from model-potential surfaces. Solutions of the coupled radial equations are

obtained in the close-coupling coupled-channels (CC) formulation and the j_z-conserving coupled-states (CS) approximation, including as many channels (open and closed) as needed for convergence. Trends in the behavior of the cross sections with respect to variations in the potential surface and the spacing of rotational levels are discussed with particular emphasis on the isotope effects. In addition, cross sections calculated for various CS approximations are compared with CC results and comment is made on the influence of the closed channels.

16675. Clark, F. O., **Asymmetric HCN line profiles from the Orion Nebula,** *Astrophys. J.* **200,** L115-L117 (Sept. 1, 1975).

Key words: molecules, interstellar; Orion Nebula.

The hyperfine components of the HCN $J = 1$-0 transition in Orion are observed to be asymmetric. This asymmetry apparently indicates some inhomogeneity of the molecular cloud and is interpreted as due to radial motions in the source. The magnitude of these implied motions is discussed and the sense examined. Alternate interpretations are also discussed.

16676. Johnson, C. R., **Multiplicativity and compatibility of generalized matrix norms,** *Linear Algebra and Appl.* **16,** 25-37 (1977).

Key words: compatible; generalized matrix norm; Hadamard product; multiplicative; spectral radius; vector norm.

It is well known that if a generalized matrix norm is multiplicative, then it has a compatible vector norm associated with it. The converse, however, is invalid, and the precise relation between multiplicativity and compatibility is here explored for a generalized matrix norm. In the process, certain methods for deriving one norm from another are mentioned.

16677. Costrell, L., **Evolution, definition, and status of IEEE Standard 583: Standard modular instrumentation and digital interface system (CAMAC),** *Proc. Electro 76 Professional Program, Boston, MA, May 11-14, 1976,* No. 29, Paper No. 4, 1-8 (Institute of Electrical and Electronics Engineers, Inc., New York, NY, 1976).

Key words: CAMAC; computer interfacing; instrumentation; interfacing; standards.

Incompatible instruments have long been the rule in laboratories and industrial organizations. The problems they pose are enormous and expensive. The concern is with interfaces, mechanical, electrical, and from a signal standpoint. Besides the inefficiency inherent in a multiplicity of different interfaces, the man hours of design effort is staggering and this effort is needlessly repeated for installation after installation. IEEE Standard 583 defines a standardized instrumentation system designated CAMAC, for Computer Automated Measurement and Control, that has been developed to alleviate this problem and that is gaining wide international acceptance. The system features a fully specified data highway (Dataway) together with modular functional units that are completely compatible with each other and that are available from diverse sources. Additional levels of compatibility are achieved through the use of standardized parallel and serial highways that have been developed for use with the basic CAMAC system.

16678. Costrell, L., **CAMAC instrumentation system—Introduction and general description,** *U.S. NIM Committee on CAMAC Tutorial Articles, (Computer Automated Measurement and Control), ERDA Report No. TID-26618,* 8 pages (Energy Research and Development Administration, Washington, DC, Oct. 1976).

Key words: CAMAC; Dataway; instrumentation; modules; nuclear; standards.

The CAMAC instrumentation system is described in a general way in this introductory paper which is followed by papers that discuss the system in greater detail. This paper is an updated version of the introductory paper that appeared in the April 1973 IEEE Transactions on Nuclear Science.

16679. Costrell, L., **Highways for CAMAC systems—A brief introduction,** *U.S. NIM Committee on CAMAC Tutorial Articles, (Computer Automated Measurement and Control), ERDA Report No. TID-26618,* 7 pages (Energy Research and Development Administration, Washington, DC, Oct. 1976).

Key words: CAMAC; highway; interface; instrumentation; standards.

The interconnection between CAMAC crates and between the crates and a computer is called the CAMAC highway. The purpose of this paper is to present a brief summary of CAMAC highway configurations to put in perspective the highway papers that follow and to serve as a starting point for the panel discussion on CAMAC highways.

16680. Ghigo, F. D., Shelus, P. J., Silverberg, E. C., Faller, J. E., **Laser range measurements using non-Gaussian pulse shapes,** *Appl. Opt.* **15,** No. 11, 2621-2623 (Nov. 1976).

Key words: laser range measurement; pulse shapes; ranging systems.

Many optical ranging systems currently use laser pulses with approximately Gaussian shape of a few nanoseconds or less. In those cases where the number of photoelectrons in the return signal is small, either on a single shot basis or where a number of shots are combined to build up an "equivalent" single shot, the accuracy of the range measurement is proportional to $W/\sqrt{N}$, where W is the width of the laser pulse and N the number of photoelectrons received. We show that a considerable improvement in accuracy can be obtained if the unbounded, Gaussian pulse shape is modified so that it can be considered a bounded distribution of finite duration.

16681. Fong, J. T., Rehm, R. G., Graminski, E. L., **Weibull statistics and a microscopic degradation model of paper,** *Tappi* **60,** No. 1, 156-159 (Jan. 1977).

Key words: durability; fatigue; fiber length; flexing; low cycle fatigue; mechanical properties; microstructure; modelling; paper; pore size; statistical analysis; Weibull distribution.

Motivated by scanning electron micrographs showing microstructural degradation of several grades of paper under repetitive loadings, a crude statistical approach in defining two micro-variables, namely, an "effective" fiber length and an "equivalent" void diameter, is presented. The approach is based on the mathematical properties of a shape-sensitive statistical distribution originally derived by Weibull. Two microstrength parameters, the fiber-breaking load and the fiber-to-fiber bond strength, are also given a Weibull statistical analysis. Two distinct mechanisms for explaining the loss of modulus due to repetitive flexing are presented for constructing a self-consistent microscopic degradation model of paper.

16682. Morrison, M. A., Collins, L. A., Lane, N. F., **Theoretical study of low-energy electron-CO_2 scattering,** *Chem. Phys. Lett.* **42,** No. 2, 356-360 (Sept. 1, 1976).

Key words: theoretical elastic e-CO_2 scattering; theoretical electron-CO_2 scattering; theoretical electron-molecule scattering.

A study of electron collisions with ground-state CO_2 molecules in the energy range 0.07-10.0 eV is reported. An accurate static potential is augmented with a local exchange

potential and induced polarization terms, and coupled radial equations are solved in a spherical coordinate system. Converged total and momentum-transfer cross sections are presented and discussed, and comparison is made with existing experimental measurements.

16683. McCamy, C. S., **Theory of optical wedges as flux modulators,** *J. Opt. Soc. Am.* **66,** No. 12, 1350-1355 (Dec. 1976).

Key words: calibration; density; photography; reflectance; transmittance; wedges.

Many optical experiments and applications require the use of devices called optical wedges which are thin-sheet optical modulators having a continuous, usually linear, change in optical density with either distance or angle. The optical density of a sample area on an optical wedge depends on the size and shape of the aperture and the characteristics of the wedge. The relationship of the effective density of the whole sample to the density at the center of the sample has been derived for wedges of rectilinear and circular form and sampling apertures in the form of rectangles, circles, and circular sectors. The theory has applications in the microdensitometry of photographic edges.

16684. Krauss, M., Liu, B., **The energy curve of XeF, $X^2\Sigma^+$,** *Chem. Phys. Lett.* **44,** No. 2, 257-260 (Dec. 1, 1976).

Key words: charge transfer; dissociation energy; energy curve; overlap; van der Waals; XeF.

The energy curve of the ground state of XeF is obtained theoretically assuming that the energy is represented by the sum of the "first order energy" and the dispersion energy. Since the inverse power expansion of the dispersion energy is not valid when the atoms overlap significantly, the dispersion energy is estimated in the overlap region by noting that the Coulomb integrals now vary exponentially with internuclear distance. The onset of overlap was chosen to occur over a range of distances which then permits a range of well depths to be determined. Comparison with recent experimental results indicates that the σ of the analogous van der Waals well provides agreement with the well depth. The energy curve has an unusual shape which suggests that the region around the minimum is determined by a small mixing of charge transfer into the ground state. Since this study is intended to determine the qualitative electronic basis of the binding in molecules like XeF, no attempt was made to calculate the vibrational spectrum but it is clear from the curve shape that the spectrum could be fit only with a large anharmonicity coefficient.

16685. Halsey, N., Marlowe, D. E., Mitchell, R. A., Mordfin, L., **Non-metallic antenna-support materials pultruded rods for antenna guys, catenaries and communications structures,** *AFML-TR-76-42*, 126 pages (Air Force Materials Laboratory, Wright-Patterson Air Force Base, OH, May 1976).

Key words: aramid; composite materials; end fittings for FRP rod; environmental resistance of FRP rods; fiber-reinforced plastic (FRP); glass; guys, antenna; pultrusion; reinforced plastics; stress rupture of FRP rod; test methods; weatherability of FRP rods.

Both E-glass and Kevlar 49 (aramid) fibers were used to reinforce an isophthalic polyester resin. These materials were used, in turn, to form pultruded antenna rod hardware for structural tests. The aramid material exhibited substantially improved strength-retention properties over the glass-reinforced material under prolonged exposure to heat and humidity. The aramid material offers the promise of superior weatherability in antenna-support applications although further testing is warranted. The stress-rupture properties of pultruded rod, under high humidity, possess unusual temperature and time dependencies. These are explained in terms of the mechanisms whereby moisture is transported from the environment to the fiber/matrix interface. The stress-rupture properties, as well as the tensile properties, may be improved by appropriately modifying the pultrusion process.

Two new end fittings, generally capable of attaining the full tensile strength of glass fiber-reinforced pultruded rod, were developed.

Several new test methods were developed, including an environmental stress-rupture test, two methods for investigating the quality of the fiber/matrix interface, and a method for examining the rate sensitivity of the tensile strength. A significant rate sensitivity was observed for glass fiber-reinforced rod but not for aramid fiber-reinforced rod.

16686. Dikkers, R. D., **Development and implementation of standards for solar heating and cooling applications,** *Proc. Joint Solar Energy Conf. on Sharing the Sun 76 Solar Technology in the Seventies, Winnipeg, Manitoba, Canada, Aug. 15-20, 1976,* **1,** 83-90 (Pergamon Press, Elmsford, NY, 1976).

Key words: buildings; cooling; heating; laboratory accreditation; performance criteria; solar energy; standards.

Solar energy program activities being conducted by the National Bureau of Standards (NBS) are primarily centered around projects related to the development and implementation of standards and performance criteria for solar heating and cooling applications. In support of the Energy Research and Development Administration (ERDA) and the Department of Housing and Urban Development's (HUD) solar energy research and demonstration programs, NBS has prepared interim performance criteria for residential solar energy systems, and test procedures for determining the thermal performance of solar collectors and thermal storage devices. Currently, NBS is developing: (1) interim performance criteria for commercial solar energy systems; (2) intermediate standards for solar heating and domestic hot water systems that can be used in conjunction with HUD's Minimum Property Standards; (3) draft standards for materials (i.e., sealants, cover plates, insulation) to be used in solar systems; (4) plans for establishing a solar collector testing laboratory accreditation program; and (5) plans for identifying and developing other needed standards in cooperation with various standards-writing organizations such as ASTM and ASHRAE.

16687. Lindgren, R. A., Bendel, W. L., Jones, E. C., Jr., Fagg, L. W., Maruyama, X. K., Lightbody, J. W., Jr., Fivozinsky, S. P., **Electroexcitation of the $T_0 + 1$ giant $M1$ resonance in ^{58,60}Ni,** *Phys. Rev. C* **14,** No. 5, 1789-1799 (Nov. 1976).

Key words: electron scattering; inelastic; isospin; magnetic; multipolarity; sum rule.

Using inelastic electron scattering, several isobaric analog 1^+ states between 9 and 13 MeV excitation in ^{58}Ni and ^{60}Ni have been found. They are identified as components of the $T_0 + 1$ giant $M1$ state in ^{58,60}Ni.

16688. Staffa, J. A., Zervos, C., Mighell, A. D., Hubbard, C. R., ***S*-carboxymethyl-L-cysteine sulfoxide (configuration 2*R*:4*R*),** *Acta Cryst.* **B32,** Part 11, 3132-3135 (Nov. 1976).

Key words: absolute configuration; amino acid derivative; crystal structure; *S*-carboxymethyl-L-cysteine sulfoxide; x-ray determination; zwitterion.

$C_5H_9SO_5N$, orthorhombic, $P2_12_12_1$; $a = 4.786$ (2), $b = 8.312$ (1), $c = 18.914$ (5) Å; $Z = 4$, $D_x = 1.723$, $D_m = 1.732$ (5) g cm^{-3} (flotation at 21 °C). The structure has been determined by standard Fourier techniques from x-ray diffractometer data and refined by least-squares methods to $R = 0.035$ for 924 independent reflections. As found by x-ray analysis, the title com-

pound exists as an "apparent" zwitterion. The cysteine carboxyl and the methyl carboxyl groups of adjacent molecules are involved in a very strong hydrogen bond [O...O 2.449 (3) Å].

16689. Lafferty, W. J., Suenram, R. D., Johnson, D. R., **Microwave spectrum of acetylene-d_2,** *J. Mol. Spectrosc.* **64,** 147-156 (1977).

Key words: acetylene-d_2; *l*-type doubling constants; microwave spectrum; rotational constants; Stark effect; vibrational transition moment.

Eight *P*-branch transitions from the ν_5^1-ν_4^1 difference band of C_2D_2 have been observed in the microwave region. Significant improvements in the spectroscopic constants for the two states involved in the difference band have been obtained by combining infrared and microwave data. The Stark shifts for the observed C_2D_2 lines are discussed in some detail. The vibrational transition moment is found to be $\mu_{vib} = 0.0358 \pm 0.0020$ D.

16690. Fraker, A. C., **The microstructural influence of a 2 wt pct Mo addition to a Ti-1.5 wt pct Ni alloy,** *Metall. Trans. A Commun.* **7A,** 1793-1796 (Nov. 1976).

Key words: corrosion resistant alloys; microstructures; molybdenum additions; precipitation; titanium alloys; transmission electron microscopy.

Microstructural changes resulting from adding 2 wt.% Mo to the crevice corrosion resistant Ti-1.5 wt.% Ni alloy have been studied. Light microscopy of bulk specimens and thin foil transmission electron microscopy show that the Mo addition produces a finer and more elongated grained microstructure and increases the martensitic reaction. The Mo addition also delays precipitation and growth of the intermetallic phase, Ti_2Ni, and increases the hardness of the material.

16691. Green, R. B., Keller, R. A., Schenck, P. K., Travis, J. C., Luther, G. G., **Opto-galvanic detection of species in flames,** *J. Am. Chem. Soc.* **98,** No. 26, 8517-8518 (Dec. 22, 1976).

Key words: dye laser; flame analysis; flame fluorescence; laser; opto-galvanic effect; spectroscopy; tunable laser.

A recently reported, opto-galvanic effect (OGE) in electrical discharges has been found to occur in flames. Specifically, if the current from a constant voltage source is passed through the flame, the current is found to change when the flame is irradiated by intense monochromatic radiation (laser) corresponding to an absorption of a species present in the flame. This change in current is easily detected by standard electrical measurement techniques and can be used for spectroscopy, analytical determinations, and flame analysis. As an example of the analytical application of this technique, the quantitative analysis of sodium in a flame is described.

16692. Rossmassler, S. A., **The National Standard Reference Data System,** *Proc. AGARD Conf. on Advancements in Retrieval Technology as Related to Information Systems, Arlington, VA, Oct. 20-21, 1976, AGARD-CP-207,* 10-1—10-4 (Available from National Technical Information Service, Springfield, VA 22161, Dec. 1976).

Key words: data compilation; data evaluation; information retrieval; NSRDS; Omnidata; reference data.

The National Standard Reference Data System is a coordinated, but decentralized, effort to increase the *reliability* and *availability* of numerical data used in and produced by the physical sciences and engineering. Individual data projects on specific technical subjects are established to extract, evaluate, and compile, in a systematic manner, all relevant data from the scientific journal and technical report literature. The evaluation process compresses the original data, and the systematic treatment aids the user in filling his data needs. Sophisticated data-handling capabilities—including on-line information and data retrieval—are developed in individual data centers and also in a central data systems design group.

16693. Hermach, F. L., Flach, D. R., **An investigation of multijunction thermal converters,** *IEEE Trans. Instrum. Meas.* **IM-25,** No. 4, 524-528 (Dec. 1976).

Key words: ac current measurements; ac-dc comparator; ac-dc transfer standard; ac voltage measurement; multijunction converter; thermal converter.

The relative ac-dc differences of a group of multii-junction thermal converters (MJTC's) have been determined over the frequency range 30 Hz-10 kHz. These MJTC's are of different ranges and were obtained from several sources. Differences were observed at low frequencies when converters of various ranges were intercompared. For voltage measurements, the use of matched resistors in series with the MJTC heater resistors greatly reduced these errors and contributed to the reduction of other errors as well. It is believed that the average ac-dc difference of this group is less than 0.3 ppm at 160 Hz and 0.5 ppm up to 10 kHz.

16694. Hermach, F. L., **Ac-dc comparators for audio-frequency current and voltage measurements of high accuracy,** *IEEE Trans. Instrum. Meas.* **IM-25,** No. 4, 489-494 (Dec. 1976).

Key words: ac current measurement; ac-dc comparator; ac-dc transfer standard; ac voltage measurement; thermal converter.

This paper surveys recent developments in high-accuracy ac-dc comparators, the basic standards for ac current and voltage measurements at audio and higher frequencies. These instruments compare the unknown ac quantity with a dc reference. The ac-dc transfer characteristics of thermal converters, the most widely used comparators, can be evaluated to about 10 ppm at audio frequencies in national metrology laboratories. With recent developments even better accuracies, and greater convenience with automatic comparisons, are feasible.

16695. Geltman, S., **Theory of laser-induced inelastic collisions,** *J. Phys. B Letter to Editor* **9,** No. 18, L569-L574 (1976).

Key words: atomic collision; excitation transfer; laser stimulation; orbiting; saturation; selection rules; van der Waals.

A theory of laser-induced inelastic collisions is presented, containing atomic selection rules and specific intensity and velocity dependences. It is applied to the case of the process $Sr(5p\ ^1P^o) + Ca(4s^2\ ^1S) + \hbar\omega\ (6408.6\ Å) \rightarrow Sr(5s^2\ ^1S) + Ca(4d\ ^1D)$, for which the intensity and wavelength dependence of the cross section is evaluated.

16696. Rubin, R. J., Mazur, J., Weiss, G. H., **Spans of polymer chains,** *Pure Appl. Chem.* **46,** 143-148 (1976).

Key words: polymer chain statistics; random walk statistics; spans of polymer chains.

The span of an *N*-segment chain in a given direction, *e*, is defined as the maximum distance between parallel planes normal to *e* which contain segments of the chain. We present a simple derivation of Daniel's result for the span of a random chain. We have generalized this simple derivation and have calculated: (1) $\langle X_{ring} \rangle$, the average span of an *N*-segment random polymer ring; (2) $\langle X_{surf.} \rangle$, the average span in the direction normal to the solution surface of an *N*-segment chain which is attached at one end to the surface; (3) In addition, we have obtained the exact solution of a problem treated by Holling-

sworth, the calculation of $\langle R_{Holl.} \rangle$, the average distance between the first segment and the most distant segment in an N-segment polymer chain. The results are:

$$\langle X_{ring} \rangle = (\pi N/6)^{1/2} \cong 0.724 N^{1/2}$$

$$\langle X_{surf.} \rangle = 2 \ln 2(\pi N/6)^{1/2} \simeq 1.003 N^{1/2}$$

$$\langle R_{Holl.} \rangle = \tfrac{1}{2}\pi(\pi N/6)^{1/2} \cong 1.137 N^{1/2}.$$

For reference purposes we note that the average span calculated by Daniels for an N-segment polymer chain is $\langle X \rangle = 2(2N/3\pi)^{1/2} \cong 0.921 N^{1/2}$ and the root-mean-square end-to-end distance is $\langle r_N^2 \rangle^{1/2} = N^{1/2}$.

The spans of each chain configuration in the directions defined by the principal components of the square radius of gyration of the chain have been determined. The relative values of the average squares of the spans in the directions of the largest, intermediate, and smallest components of the square radius of gyration are found to be 6.7:2.2:1 in the case of the unrestricted polymer chain model. For the same model, Solc and Stockmayer obtained the following set of relative values of the ordered principal components of the square radius of gyration, 11.7:2.7:1. We have determined that the apparent difference between these two sets of relative average dimensions arises from a different segment density distribution in the different principal directions.

16697. Williams, E. S., **Thermal current converters for accurate ac current measurement,** *IEEE Trans. Instrum. Meas.* **IM-25,** No. 4, 519-523 (Dec. 1976).

Key words: ac-dc difference; current comparator; current measurements; thermoelement.

A new 14-range set of thermal current converters consisting of shunted thermoelements has been constructed to measure ac-dc difference and ac current from 10 mA to 20 A at 20 Hz to 50 kHz. The ac-dc difference corrections for all ranges can be determined relative to two ranges by a 7-step intercomparison of certain adjacent ranges.

16698. Field, B. F., Hesterman, V. W., **Laboratory voltage standard based on 2e/h,** *IEEE Trans. Instrum. Meas.* **IM-25,** No. 4, 509-511 (Dec. 1976).

Key words: Josephson junction; standard cell; superconducting; voltage measurement; voltage reference.

The increased dependence of a standards laboratory on a stable voltage reference has made the maintenance of a "volt" by standard cells a costly and time consuming process. This paper describes an instrument designed to calibrate cadmium-sulfate standard cells directly against a time-invariant superconducting Josephson junction voltage reference, thus replacing the large groups of cells typically used as a voltage reference. An induced voltage of 5.2 mV is produced across the Josephson junction by irradiating the junction with microwaves of a known frequency. A specially designed potentiometer is used to scale this voltage up to 1.01 + V where it can be compared to a standard cell. The overall accuracy (2σ) of the system is 0.4 ppm or better.

16699. Tsang, W., Walker, J. A., **Instrument for the generation of reactive gases,** *Anal. Chem.* **49,** No. 1, 13-17 (Jan. 1977).

Key words: acetaldehyde; acrolein; calibration; diffusion cell; formaldehyde; instrumentation; pyrolysis; reactive gases.

An instrument has been constructed which is capable of generating reactive gases over wide concentration ranges [from ppm on up]. Its operational characteristics and performance have been evaluated with specific application to the generation of formaldehyde, acetaldehyde, and acrolein vapors of micrograms/minute rates.

16700. Interrante, C. G., Hicho, G. E., **Removal of iron-sulfide deposits from fracture surfaces,** *Am. Soc. Test. Mater. Spec. Tech. Publ.* **610,** pp. 349-365 (1976).

Key words: crack propagation; ductility; failure; fractography; fracture tests; hydrogen; steels; stress corrosion.

Steels are most commonly used at moderate strength levels at which they have high ductility and resistance to subcritical crack growth due to hydrogen. Thus, in testing the susceptibility to hydrogen damage of these steels, severe charging conditions are commonly used, and hydrogen sulfide is often used in low-pH solutions to obtain the desired high fugacity for the test. The fracture faces of specimens tested in this type of solution become covered with iron and other sulfides that are difficult to remove without affecting the underlying metal as well. The removal of these sulfide deposits from the fracture surfaces is a prerequisite to fractographic analysis of the failure mode, and it was attempted by various methods. Hydrogen reduction of the sulfides at elevated temperatures followed by ultrasonic cleaning in alcohol was found to be much more successful than the other methods studied. This is true principally because the hydrogen-reduction treatment did not attack the fracture surface. Procedures for four different cleaning treatments are described, and they are rated in terms of their relative capability for cleaning sulfide-contaminated fracture surfaces without affecting the underlying metal. Evaluations of these methods for double-cantilever-beam and Charpy V-notch specimens of a 2¼Cr-1Mo steel with fracture surfaces that were created at various stress-intensity levels provides information needed for studying the cracking mechanism under severe sulfide exposure conditions.

16701. Hruska, G. R., Magrab, E. B., Penzes, W. B., **Environmental effects on microphones of various constructions,** *J. Acoust. Soc. Am.* **61,** No. 1, 206-210 (Jan. 1977).

Key words: calibration; ceramic; condenser; electret; humidity; microphones; reciprocity; sensitivity; temperature.

The pressure sensitivities of two ½-in electret, two 1-in ceramic, and two back-vented 1-in condenser microphones were measured for numerous combinations of temperature, percentage relative humidity, and frequency. The two condenser microphones were calibrated by the reciprocity technique at each combination of temperature, relative humidity, and frequency. The condenser microphones were then used as calibrated sources to determine the pressure sensitivities of the other microphones. Insert voltage techniques were used to eliminate the environmental effects on the electronics. It was found that the backvented condenser microphones are insensitive to changes in relative humidity. At frequencies considerably below their resonance frequencies they exhibited only a very small change in sensitivity with temperature. At frequencies closer to the resonance frequency the temperature coefficient increases approximately fourfold. The temperature and humidity coefficient for the electret and ceramic microphones could not be determined due to the instability in their sensitivities which produced changes that were larger than those induced by the temperature and humidities.

16702. Magrab, E. B., **Natural frequencies of elastically supported orthotropic rectangular plates,** *J. Acoust. Soc. Am.* **61,** No. 1, 79-83 (Jan. 1977).

Key words: Galerkin; natural frequencies; orthotropic; plates; rotary inertia; transverse shear; vibration.

An expression is derived from which the natural frequencies of a rectangular orthotropic plate, under any combination of

simply supported, elastically supported, or clamped boundary conditions, can be obtained. The Mindlin-Timoshenko theory, which includes the effects of transverse shear and rotary inertia, is used to describe the plate motion. The solution is obtained with a previously developed extension of the Galerkin technique. Comparison of results with the limited results of previous investigations is very good. New results are presented for the fundamental frequencies of rectangular and square plates for boundary conditions on all four edges that vary continuously from simply supported to clamped, and for various combinations of length-to-thickness ratios and material constants. Additional results are presented for orthotropic plates simply supported and clamped on all four edges.

16703. Rebbert, R. E., Ausloos, P. J., **Gas-phase photodecomposition of carbon tetrachloride,** *J. Photochem.* **6,** 265-276 (1976/77).

Key words: absorption cross section; carbon tetrachloride; chlorine atom; photochemistry; primary processes; quantum yields; troposphere; ultraviolet.

The gas-phase photolysis of CCl_4 was investigated at 213.9, 163.3 and 147.0 nm in the presence of HCl, HBr, and C_2H_6. Quantum yields of the products measured in these mixtures at a temperature of 300 K led to the conclusion that at 213.9 nm over 90 percent of the photodecomposition can be attributed to the photodissociative process:

$$CCl_4 + h\nu \rightarrow CCl_3 + Cl \text{ (quantum yield } \geq 0.9)$$

independent of pressure (5-60 torr). At 163.3 nm, CCl_2 is formed via the photodecomposition process:

$$CCl_4 + h\nu \rightarrow CCl_2 + 2Cl \text{ (quantum yield } \sim 0.75)$$

Contrary to earlier suggestions, CCl_2 is unreactive toward CCl_4. Combination with other radicals and insertion into HCl are the major modes of reaction of CCl_2.

Experiments carried out at 313.0 nm show evidence for the occurrence of photodissociation of CCl_4. On the assumption that absorption of a photon by CCl_4 invariably leads to the detachment of a chlorine atom, the absorption cross-section at 313.0 nm is $\leq 3.7 \pm 0.4 \times 10^{-26}$ cm^2 molecule^{-1} (300 K). This result indicates that photodecomposition of CCl_4 in the troposphere is of minor importance as compared to other processes including diffusion up to the earth's stratosphere.

16704. Bright, D. S., **Miniature helical stirrer,** *Anal. Chem.* **49,** No. 1, 191 (Jan. 1977).

Key words: cuvette; helix; mixer; spectrophotometry; stirrer; vortex.

A novel and easily made helical stirring device is described that rapidly stirs small samples in long thin volumes, e.g., 1 cm spectrophotometric cuvettes. This stirring device overcomes some difficulties encountered with the conventional magnetic stirring device. Also described is a modified cuvette designed to enhance total mixing.

16705. Fenves, S. J., Wright, R. N., **The representation and use of design specifications,** (Proc. Symp. on Structural and Geotechnical Mechanics, Urbana, IL, Oct. 2-3, 1975), Paper in *Structural and Geotechnical Mechanics*, W. J. Hall, Ed., pp. 278-304 (Prentice-Hall, Inc., Englewood Cliffs, NJ, 1977).

Key words: building codes; computer programming; decision tables; graph theory; performance specifications; standards.

Design specifications are presented as the primary communication and control tool for the design and construction industry. Requisite properties of completeness, uniqueness, and correctness are identified, and the role of performance and limit state concepts in specifying intent of the specifications are emphasized. Formal representational methods are presented at three levels: decision tables for specification provisions, an information network for related provisions, and argument trees for organizing and outlining. An idealized process for specification development is presented, and the use of the representation tools for checking specifications and providing strategies for textual expression is described and illustrated. Development of computer aids for specification processing in design and conformance checking is described.

16706. Steinberg, H. L., **Standard Reference Collections of forensic science materials: Status and needs,** *LESP-RPT-0601.00*, 90 pages (U.S. Department of Justice, Law Enforcement Assistance Administration, National Institute of Law Enforcement and Criminal Justice, Washington, DC, Feb. 1977).

Key words: criminalistics; evidential materials; forensic reference collections; forensic science; reference materials; standard reference collections.

An overview of criminalistics is given, stressing the potential forms and uses of Standard Reference Collections (SRCs).

A set of 34 classes of materials of Forensic Science import (FSM classes) is presented. A brief introduction to each FSM class is then given, along with a recommended action. Where a recommendation for SRC development or for further consideration is made, some elaboration of relevant factors is given. Fourteen FSM classes are so recommended. Fifteen classes were not recommended for further SRC consideration at this time. Five FSM classes were classified as "indeterminate," due to an insufficient data base.

An extensive bibliography is included.

16707. Morrow, J. J., **NBS automated one-ohm resistance measurements,** *Quality Progress* **IX,** No. 11, 22-25 (Nov. 1976).

Key words: automated resistance measurement; automation; dc current comparator; digital nanovoltmeter; resistance; resistance measurements.

A one-ohm resistance measurement system at NBS utilizes a dc current comparator potentiometer and a digital nanovoltmeter (DNM) with a sensitivity of one nanovolt. The circuit configuration for automated measurements is the same as that for manually balanced measurements except that the DNM replaces the galvanometer and the circuit is not balanced. Accuracies of 1 part in 10^7 are easily achieved with the system.

16708. Culver, C. G., **Live-load survey results for office buildings,** *J. Struct. Div. Proc. Am. Soc. Civil Eng.* **102,** No. ST12, 2269-2284 (Dec. 1976).

Key words: buildings; live loads; load surveys; structural engineering.

Live load data obtained from a survey of twenty-three office buildings located in various regions throughout the United States are presented. The buildings ranged in height from two stories to forty-nine stories. Data for government and private office buildings are included. Statistical summaries of the data are presented and the effects of various factors such as building height, building age, geographic location, room use and room size are discussed. A mathematical model expressing the relationship between the live load in offices and the significant factors affecting the load magnitude is also presented. The data presented may be used to evaluate current requirements for design loads for buildings and also for research studies of load effects in buildings.

16709. Truhlar, D. G., Van-Catledge, F. A., **Tests of INDO/1*s* and INDOXI/1*s* methods for the calculation of the static potential for electron scattering by CO,** *J. Chem. Phys.* **65,** No. 12, 5536-5538 (Dec. 15, 1976).

Key words: carbon monoxide molecules; dipole moment; electron scattering; electrostatic potential; intermediate neglect of differential overlap (INDO); molecular orbital theory; quantum chemistry; static potential.

We have previously used semiempirical molecular orbital theory (INDO, INDO/1*s* and INDOXI methods) to calculate the equilibrium-geometry ground state static potential $V_s(r,\theta;R_e)$ for N_2 and CO as functions of r and θ; where $V_s(r,\theta;R_e)$ is the interaction energy of a fixed electron with the unperturbed ground-state charge distribution of a molecule fixed at its equilibrium internuclear distance, r is the magnitude of the vector $r[\equiv(r,\theta,\phi)]$ from the center-of-mass of the molecule to the electron, and θ is measured with respect to the internuclear axis. The static potential is useful for electron scattering calculations and for estimating the reactivity of molecules with electrophilic reagents.

16710. Wagner, H. L., Hoeve, C. A. J., **The Mark-Houwink equation and chain dimensions of linear polyethylene in theta solvents,** *J. Polym. Sci. Polym. Symp. No. 54,* 327-339 (1976).

Key words: biphenyl; chain dimensions; dodecanol; linear polyethylene; Mark-Houwink equation; NBS Standard Reference Material 1475; theta solvents; 3,3,5-trimethylhexyl acetate.

In order to ascertain whether the fractions used to determine the molecular weight distribution of the NBS standard polyethylene sample SRM 1475 by gel-permeation chromatography are linear, the exponent a in the Mark-Houwink equation was determined in three theta solvents: biphenyl, dodecanol, and 3,3,5-trimethylhexyl acetate. Our data indicate that a might exceed the theoretical value of 0.5. This is attributed to the fractions below molecular weight 20,000, which approach free-draining coils in their behavior. When an exponent of 0.5 is assumed and fractions below 20,000 are omitted, the characteristic size ratio $\langle r_0^2\rangle/nl^2$ is found to be 7.21 at 140 °C. The average value at 140 °C derived from available data, including ours, is 6.79, in excellent agreement with the theoretical value of 6.89. We conclude that standard sample SRM 1475 is linear polyethylene.

16711. Mountain, R. D., **Generalized hydrodynamics,** *Adv. Mol. Relaxation Processes* **9,** 225-291 (1976).

Key words: correlation function; density fluctuations; fluctuations; hydrodynamics; light scattering; liquid state; molecular dynamics; neutron scattering; shear wave; statistical mechanics; time correlation function; transverse current; ultrasonics.

Equations of motion for time correlation functions of molecular quantities, such as the density-density correlation function, can be obtained in the form of generalized hydrodynamic equations. The generalization considered here leads to wave vector dependent generalizations of thermodynamic coefficients and to wave vector and frequency dependent generalizations of transport coefficients in linear equations of motion for the correlation functions. The motivation for describing collective effects in fluids at the molecular level from this viewpoint is discussed in this review and several ways of deriving such equations of motion are compared. An explicit derivation is carried out for the density-density correlation function, the quantity studied by neutron and light scattering studies. The intent of this discussion is to provide a perspective view of the subject. Several applications of the theory are described. These include molecular dynamics, neutron scattering and light scattering studies of density-density correlations, molecular dynamics and light scattering studies of transverse current correlations, hydrodynamic studies of long time tails in molecular correlation functions of the currents of the hydrodynamic variables and ultrasonic studies of fluids in the critical region and in the rarified gas region. Some unresolved aspects of the theory are considered in the last section.

16712. Brown, P. W., Clifton, J. R., **Nondestructive techniques for evaluating metallic artifacts of historical interest,** *Bull. Assoc. Preserv. Technol.* **VIII,** No. 4, 2-21 (1976).

Key words: compositional analysis; instrumental methods; metallic artifacts; microstructural analysis; nondestructive evaluation techniques.

This paper describes a variety of nondestructive evaluation (NDE) techniques which can be used to characterize the compositions and methods of fabrication of metallic artifacts, to form a basis for approximating their ages and determining their sources. This paper was prepared with the objective of showing preservation technologists how NDE methods can be used in the course of their work. This paper was written in response to a request by Mr. L. H. Nelson, editor of the Bulletin of the Association for Preservation Technology. Because the paper is addressed to an audience not versed in this area, it has been reviewed by Mr. Nelson who approves of the format and the level of technical content.

16713. Childers, C. B., Dziuba, R. F., Lee, L. H., **A resistive ratio standard for measuring direct voltages to 10 kV,** *IEEE Trans. Instrum. Meas.* **IM-25,** No. 4, 505-508 (Dec. 1976).

Key words: direct voltage measurements; high voltage measurements; Kelvin-Varley divider; ratio standard; voltage dividers; volt boxes.

A highly accurate guarded voltage-ratio standard has been developed for measuring direct voltages from the range of a standard cell to 10 kV. The ratio standard has a resolution capability of 0.1 ppm for ratios of 1:1 to 10 000:1 with an estimated uncertainty of 0.2 ppm. It is designed for operation at a rating of 2 kΩ/V and consists of an adjustable reference section in series with three resistance groups each containing nine nominally equal sections. The resistance ratios are determined by a self-calibration technique using a 1:1 bridge. A series-parallel mode of calibration provides an additional check on the accuracies of the ratios. The standard is housed in a temperature-controlled oil bath whose oil is filtered to remove moisture and contaminants.

16714. Stroik, J. S., **Physical security of door assemblies and components,** *NILECJ-STD-0306.00,* 33 pages (U.S. Department of Justice, Law Enforcement Assistance Administration, National Institute of Law Enforcement and Criminal Justice, Washington, DC, May 1976).

Key words: burglary resistance; door assemblies; door components; doors; frames; hardware; hinges; locks; security standards.

Security standards for doors have been developed at the National Bureau of Standards to evaluate burglar-resistance of door assemblies and components. Criteria were established by analysis of available data on burglary methods, by duplication of the attacks, and finally by measurement of the duplicated attacks applicable to the standards' scope. The scope includes development of standards designed to resist only burglary attacks defined as "common" or "opportunity" attacks on residences and small businesses. Four classes were established, from class I which includes attributes for the lowest level of re-

sistance, up to class IV with attributes for the highest level of resistance. Requirements are specified as performance criteria with test methods described in detail. Two classification methods were established, one for door assemblies, the other for door assembly components. Included in an appendix is a description of the test equipment used at the National Bureau of Standards.

16715. Interrante, C. G., Early, J. G., Hicho, G. E., **Analysis of findings of four tank-car accident reports,** *DOT Report No. FRA-OR&D 75-50*, 70 pages (Available as PB251097 from the National Technical Information Service, Springfield, VA 22161, Jan. 1975).

Key words: metallurgy; tank cars.

A comprehensive overview of the findings and metallurgical analyses of tests conducted at the National Bureau of Standards on samples of tank-car materials submitted by the Federal Railroad Administration is presented. The submitted samples were taken from tank cars which had been involved in accidents during the period January 1970 to January 1971. The testing conducted during the metallurgical analyses included full chemical analyses, ambient temperature tensile tests on longitudinal and transverse specimens, quantitative metallography to determine ferrite grain size, peralite colony size, and inclusion content, size, and shape, hardness tests, bend tests on longitudinal and transverse specimens, and a very comprehensive program of impact testing, which is covered in a separate report on Impact Properties.

16716. Interrante, C. G., **Impact properties of steels taken from four failed tank cars,** *DOT Report No. FRA-OR&D 75-51*, 157 pages (Available as PB255854 from the National Technical Information Service, Springfield, VA 22161, June 1976).

Key words: metallurgical; tank cars.

An overview of the results and metallurgical analyses of the findings of impact tests conducted at the National Bureau of Standards on samples of tank-car materials submitted by the Federal Railroad Administration is presented. The submitted samples were taken from tank cars which had been involved in service accidents during the period January 1970 to January 1971. One of these tank cars had been fabricated from ASTM A212 steel and the remaining four tank cars from AAR TC128 steels. The impact test data were reported earlier in four tank-car accident reports.

16717. Early, J. G., Interrante, C. G., **A metallurgical investigation of a full-scale insulated rail tank car filled with LPG subjected to a fire environment,** *DOT Report No. FRA-OR&D 75-52*, 67 pages (Available as PB250587 from the National Technical Information Service, Springfield, VA 22161, Jan. 1975).

Key words: metallurgical; tank cars.

An analysis of the failure of an insulated rail tank car, RAX 202, which had been tested to failure in a fire environment at White Sands Missile Range, New Mexico, was requested by the Federal Railroad Administration, Department of Transportation.

The tank car, filled with approximately 33,000 gallons of liquified petroleum gas (LPG), failed after approximately 94 minutes of exposure to a JP-4 jet fuel fire. The car fractured into four fragments which were examined in the field. Five plate samples from the four fragments were selected for laboratory study at the National Bureau of Standards.

16718. Early, J. G., **Mechanical properties of AAR M128-69-B steel plate samples taken from insulated fire tested tank car RAX 202,** *DOT Report No. FRA-OR&D 76-74*, 57 pages (Available as PB255907 from the National Technical Information Service, Springfield, VA 22161, June 1976).

Key words: metallurgical; tank cars.

Studies were undertaken to measure the elevated-temperature mechanical properties and to determine the elevated-temperature fracture behavior of selected AAR M128-B steel plates. In addition, the ambient-temperature mechanical properties were measured to determine if the requirements of specification AAR M128-69-B were satisfied. The NBS results of check chemical analyses, hardness surveys, thickness measurements, macroscopic observations, and metallographic analyses of the plate samples had been reported previously. The results of ambient-temperature tensile tests showed that all plate samples met the strength and tensile ductility requirements of specification AAR M128-69-B. The results of hot-tensile tests showed a continuous decrease in strength properties and an increase in tensile ductility as the test temperature was increased from 1100 F to 1250 F. An analysis of stress-rupture data for specimens from all plate samples in the same temperature range indicated that a straight line in a log-log plot of initial stress versus rupture life reasonably represented the data at each test temperature. In the temperature and stress range studied, a decrease in the initial stress of about 20 to 30 percent resulted in a twelvefold increase in rupture life from 15 minutes to three hours. A comparison of the results of the metallographic analysis of hot-tensile and representative stress-rupture specimens with the previously reported metallographic results on the initial rupture site in the failed shell course indicate the presence of the identical fracture mode. This mode is characterized by many intergranular voids which originate primarily at the proeutectoid ferrite-pearlite boundaries. These results confirm the previously reported finding that the initial rupture of the tank car was a stress-rupture crack.

16719. Interrante, C. G., Hicho, G. E., Harne, D. E., **A metallurgical analysis of five steel plates taken from a tank car accident near Crescent City, Illinois,** *DOT Report No. FRA-OR&D 75-48*, 87 pages (Available as PB250530 from the National Technical Information Service, Springfield, VA 22161, Mar. 1972).

Key words: metallurgy; tank cars.

A metallurgical analysis of five steel samples (numbered FRA-1 through FRA-5) was requested by the Bureau of Railroad Safety, Federal Railroad Administration, Department of Transportation. These steel samples were taken from two tank cars (numbered SOEX 3037 and SOEX 3219) which had been involved in an accident near Crescent City, Illinois. Samples FRA-1, FRA-4, and FRA-5 were reported to be shell plates and sample FRA-3, a head plate. Sample FRA-2 was a welded sample of head plate and shell plate and it was used for most of the mechanical properties determinations in this report.

An investigation was conducted at the National Bureau of Standards to determine if the samples conformed with the appropriate specifications for tank car materials and to gather information pertinent to the question of the suitability of these steels for use as plate materials of tank cars. Samples FRA-1, -2, and -5 were reportedly produced to the specification for ASTM A 212-65 Grade B, flange quality steel (A 212-B); and FRA-3 and -4 were reportedly produced to specification AAR M128 Grade B, flange quality steel (M128-B).

16720. Interrante, C. G., Hicho, G. E., **Metallurgical analysis of a steel shell plate taken from a tank car accident near South Byron, N.Y.,** *DOT Report No. FRA-OR&D 75-47*, 56 pages (Available as PB250063 from the National Technical Information Service, Springfield, VA 22161, Oct. 1971).

Key words: metallurgy; tank cars.

A metallurgical analysis of a steel plate sample (the South Byron sample) was requested by the Federal Railroad Administration. The steel sample was taken from a tank car (number PPGX9990) which had been involved in an accident near South Byron, New York. This sample was reported to have been produced to specification AAR-M-128-65-DTD-1966-Flange Quality-Grade B, and it was reportedly taken from the second course of shell plate of car number PPGX9990. The fracture in this course circumscribed the tank car and resulted in the division of the car into two sections.

An investigation was conducted at the National Bureau of Standards to determine if the plate sample conformed with the above Association of American Railroads (AAR) Specifications for Tank Cars and to gather information pertinent to the question of the suitability of this type of steel for use as the shell plate of tank cars.

16721. Gans, W. L., **Present capabilities of the NBS Automatic Pulse Measurement System,** *IEEE Trans. Instrum. Meas.* **IM-25,** No. 4, 384-388 (Dec. 1976).

Key words: automated measurement; pulse; rise time; sampling oscilloscope; spectrum amplitude; time domain; transient.

In 1972, NBS began development of an Automatic Pulse Measurement System (APMS) consisting essentially of a minicomputer-controlled wide-band sampling oscilloscope. The objective of the work was to produce a fast general purpose pulse waveform acquisition and processing instrument with spectral capability in the frequency range dc-18 GHz. The purpose of this paper is to report the highlights of work done on the APMS from early 1975 to present.

The measurement applications of the APMS now consist of both publicly offered calibration services and in-house experimental measurements. In the first category, calibration services are available for the following physical parameters: a) Impulse generator spectrum amplitude; b) Wide-band coaxial attenuation/gain; c) Pulse generator transition time.

Still in the experimental stage are measurements involving reflection coefficient and impedance, group delay, pulse distortion, and wide-band antenna characteristics.

16722. Jesch, R. L., **Repeatability of SMA coaxial connectors,** *IEEE Trans. Instrum. Meas.* **IM-25,** No. 4, 314-320 (Dec. 1976).

Key words: insertion loss; reflection coefficient; repeatability; SMA connectors.

SMA connectors in three different configurations were investigated for variation of reflection coefficient magnitude and insertion loss for a given SMA connector connect-disconnect sequence. Repeatability measurements were taken over the frequency range of 2 to 18 GHz on the NBS Automatic Network Analyzer. Plots are given that show the SMA connector repeatability for both reflection coefficient magnitude and insertion loss as a function of frequency.

16723. Larsen, N. T., **A new self-balancing dc-substitution RF power meter,** *IEEE Trans. Instrum. Meas.* **IM-25,** No. 4, 343-347 (Dec. 1976).

Key words: bolometer; microwave; power measurement.

Problems intrinsic in self-balancing Wheatstone bridges have led to the development of a new dc substitution microwave power meter. The new instrument allows four-terminal measurement of bolometer resistance and affords improved accuracy and lower noise at a lower cost than earlier instruments. Measurement errors due to imperfect behavior of the servo system are typically less than 0.01 percent.

16724. Hoer, C. A., Roe, K. C., Allred, C. M., **Measuring and minimizing diode detector nonlinearity,** *IEEE Trans. Instrum. Meas.* **IM-25,** No. 4, 324-329 (Dec. 1976).

Key words: diode detector; diode model; temperature compensation.

This paper describes two techniques for measuring the linearity of amplitude detectors in general, and for measuring the deviation from square-law E of point-contact diode detectors in particular. A general mathematical model is given for determining the RF input power as a function of the detector output voltage. It is shown how to choose the value and the temperature coefficient of the video load resistance to minimize E and make E independent of temperature.

16725. Andrews, J. R., **Impulse generator spectrum amplitude measurement techniques,** *IEEE Trans. Instrum. Meas.* **IM-25,** No. 4, 380-384 (Dec. 1976).

Key words: calibration; electromagnetic interference; fast Fourier transform; impulse generator; radiometer; sampling oscilloscope; spectrum amplitude; spectrum analyzer; spectrum intensity.

Various techniques that have been used to calibrate impulse generators and to measure spectrum amplitude are surveyed. A summary of experiments comparing the various techniques is included. The NBS measurement service for calibrating impulse generators is described.

16726. Engen, G. F., **Determination of microwave phase and amplitude from power measurements,** *IEEE Trans. Instrum. Meas.* **IM-25,** No. 4, 414-418 (Dec. 1976).

Key words: automatic network analyzer; automation; microwave; microwave measurement; six-port.

Although straightforward in principle, the extension of existing designs for automatic network analyzers (ANA's) to the higher microwave frequencies is difficult in the current state of the art. What appears to be needed is a basically different approach to the microwave detection problem. One promising alternative is provided by the so-called "six-port" techniques, which eliminate the need for modulation or for frequency conversion, local oscillators, phase detectors, etc. Recent theoretical studies have provided new insights into the basic concept and lead to "five-port" configurations which require three instead of four amplitude detectors. Of particular interest is the projected measurement dynamic range of 50-60 dB corresponding to a dynamic range requirement in the amplitude detectors of a nominal 20 dB or less.

16727. Estin, A. J., **Scattering parameters of SMA coaxial connector pairs,** *IEEE Trans. Instrum. Meas.* **IM-25,** No. 4, 329-334 (Dec. 1976).

Key words: coaxial connectors; microwave connectors; RF connectors; scattering parameters.

A technique is described for making reflection and insertion loss measurements on microwave connectors, without the need for reference to calibrated or precision standards. The effects of connectors used in the measuring system are removed from the results, thus providing a means for testing and selecting cables from a group for specific critical applications. Results are given for a group of eight sections of Type 141 solid dielectric line having SMA connectors, and generic behavior is predicted for the SMA connector.

16728. Wells, J. S., Streit, G. E., Petersen, F. R., **Absolute spin-flip Raman laser frequency measurements with metal-insulator-metal diodes,** *Opt. Commun.* **19,** No. 2, 248-252 (Nov. 1976).

Key words: frequency measurements on tunable lasers; IFS with a tunable laser; infrared frequency synthesis; SFRL frequency measurement; spin flip Raman laser.

Infrared frequency synthesis techniques with metal-insulator-metal (MIM) diodes have been extended to include absolute frequency measurement of a spin-flip Raman laser (SFRL). As a result of this extension, spectroscopy in the 5.3 μm region more readily can be put on a frequency rather than a wavelength metrology basis. Additional observations with the diode are in qualitative agreement with recent work relating to nonlinear tuning over axial SFRL modes.

16729. Maienthal, E. J., Becker, D. A., **A survey on current literature on sampling, sample handling, for environmental materials and long term storage,** *Interface* **5,** No. 4, 49-62 (1976).

Key words: chemical analysis; environmental samples; long-term storage; microbiologicals; organics; pesticides; radionuclides; sample handling; sampling; trace elements.

In order to aid in the development of criteria for the possible establishment of a National Environmental Specimen Bank for the Environmental Protection Agency, a large portion of the recent literature concerning sampling and storage of environmental specimens has been examined. This has been done both manually and by use of bibliographical retrieval services such as Medline, Chemcon, Biosis, Cain, Defense Documentation Center and others. Also, the advice and opinion of workers in various aspects of the field has been obtained. A summary of the results of this survey is found below, separated into the various areas of concern.

16730. Waxler, R. M., Horowitz, D., Feldman, A., **Precision interferometer for measuring photoelastic constants,** *Appl. Opt.* **16,** No. 1, 20-22 (Jan. 1977).

Key words: crystals; fused silica; interferometers; optics; photoelasticity.

A stable polarizing interferometer has been adapted for measuring small changes in optic path induced by small stresses in optical materials. With this instrument we measured the piezo-optic constants of fused silica at 0.6328 μm by applying stresses up to 1.34×10^7 N/m^2 and found good agreement with previous workers who employed much higher stresses. The standard deviation of the fringe shift from a linear fit of optical path change as a function of stress was less then $\lambda/500$. This technique is valuable for measuring the piezo-optic constants of materials that cannot withstand large stresses.

16731. Riad, S. M., Nahman, N. S., **Application of the homomorphic deconvolution for the separation of TDR signals occurring in overlapping time windows,** *IEEE Trans. Instrum. Meas.* **IM-25,** No. 4, 388-391 (Dec. 1976).

Key words: homomorphic deconvolution; time domain reflectometry.

The homomorphic transformation is used to separate a time domain reflectometry (TDR) signal into its rapidly and slowly varying components, respectively. The separation (deconvolution) technique is successful in the case where the multiple reflections cannot be viewed in nonoverlapping time windows as is required by the conventional TDR method.

16732. Chiu, H. Y., Adams, P. J., Linsky, J. L., Basri, G. S., Maran, S. P., Hobbs, R. W., **High-resolution stellar vidicon spectrophotometry. I. Variable mass loss from arcturus and the hypothesis of giant convective elements,** *Astrophys. J.* **211,** No. 2, 453-462 (Jan. 15, 1977).

Key words: Ca II emission; stars, chromospheres; stars, individual; stars, late type; stars, mass loss.

High-resolution spectrophotometry of the variable Ca II K-line in the K2 IIIp star α Boo was performed on five occasions over the period 1974 April-1976 February with the McMath Solar Telescope at Kitt Peak National Observatory and an experimental SEC vidicon camera. The results are compared with *Copernicus* observations of the Mg II *h* and *k* lines (1973 May 19; 1974 May 20) and with earlier Ca II data of Griffin, and it is found that either of two states may typically occur in the Arcturus chromosphere. From comparison with the results of model calculations for expanding chromospheres, it is concluded that these correspond respectively to a "normal" state in which the mass loss $dM/dt < 10^{-9} M_\odot$ yr^{-1} and an "abnormal" state in which $dM/dt \approx 8 \times 10^{-9} M_\odot$ yr^{-1}. In the latter case, the expansion velocity is ~ 13 km s^{-1} at optical depth unity in the K-line, which exceeds the local sound speed. It is suggested that the abnormal state represents the rise to the photosphere of a very large convective element ($d \approx r^*$) as hypothesized for red giants by Schwarzschild.

16733. Holton, J. K., **Interfacing building design and solar energy research and standards,** *Proc. 1976 Joint Solar Energy Conf., on Sharing the Sun: Solar Technology in the Seventies, Winnipeg, Manitoba, Canada, Aug. 15-20, 1976,* **9,** 74-82 (Pergamon Press, Elmsford, NY, 1976).

Key words: communication of research and standards; National Bureau of Standards; solar energy standards; standards users.

An extensive program of solar energy research and standards development has been undertaken by the National Bureau of Standards in support of the national effort to expedite the introduction of solar usage. The communication between researchers and the building community, who will utilize the products of this research, is of critical importance for effective conduct of this program. This paper examines a number of the programs being conducted at NBS, identifies the intended user groups, and describes some of the paths of communication that are being used. It is hoped that a clearer understanding of the research/user linkage will lead to more effective communication between those working in the field.

16734. Tucker, J. C., **Alternative models of the decision-making process and their implications for information packaging,** *Proc. 39th Annual Meeting of the American Society for Information Science on Information-Politics, San Francisco, CA, Oct. 4-9, 1976,* **13,** 10 pages (American Society for Information Science, Washington, DC, 1976).

Key words: decision maker; decision model; information packaging; information processing; managment information.

The organization of data into information for decision-making depends not only on the problem addressed, but also on the decision maker's thought processes. Three types of decision makers are described: the satisficer or cybernetic decision maker, the rational decision maker, and the adaptivizer. The rational decision maker is the classic type, described in economic and management literature. The cybernetic model of the decision maker is based on studies in cognitive psychology, which attempt to model the processes of the mind. The concept of the adaptive decision maker is relatively new, growing out of the present environment of uncertainty, rapid change, and interdependence, which requires flexibility.

After examining the information processing characteristics of each of these types, the paper suggests some ways in which the information specialist might organize information to be presented to each type of decision maker to have maximum effect on the decision process. Care must be taken, however, not to cross the line between effective presentation and manipulation of the decision maker.

16735. Parks, S. I., Linzer, M., **Application of pulse compression techniques to medical ultrasound,** (Proc. of the Society of Photo-Optical Instrumentation Engineers, Conf., Washington, DC, Sept. 16-19, 1976), Paper in *Application of Optical Instrumentation in Medicine V*, R. K. Cacak, et al., Eds., **96,** 349-353 (Society of Photo-Optical Instrumentation Engineers, Palos Verdes Estates, CA, 1976).

Key words: chirp radar; medical diagnosis; pulse compression; signal processing; ultrasound.

The application of pulse compression to medical ultrasound is discussed. This approach can decrease peak power and increase sensitivity in ultrasonic diagnosis. A prototype system with 8:1 compression ratio and 0.6 μs resolution is described. Compressed echo waveforms were obtained from an aluminum bar and from a human heart *in vivo*.

16736. Morton, M., Fetters, L. J., **Homogeneous anionic polymerization of unsaturated monomers,** Paper in *Macromolecular Reviews*, A. Peterlin, M. Goodman, S. Okamura, B. H. Zimm, and H. F. Mark, Eds., **2,** 71-113 (Interscience Publishers, John Wiley & Sons, New York, NY, 1967).

Key words: block copolymers; homogeneous anionic polymerization; monodisperse polymers; unsaturated monomers.

This review discusses the polymerization of unsaturated monomers by carbanionic mechanisms. Particular emphasis is placed on the synthetic possibilities of these systems, i.e., monodisperse polymers, block copolymers, and polymers having reactive end-groups.

16737. Bright, R. G., **Status and problems of fire detection for life safety in the United States,** (Proc. Symp. National Academy of Sciences-National Research Council on Fire Detection for Life Safety, Washington, DC, Mar. 31-Apr. 1, 1975), Paper in *Fire Detection and Life Safety*, pp. 3-14 (1977).

Key words: building fires; fire detection devices; heat detectors; ionization chamber detectors; photoelectric detectors; smoke detectors.

About 12,000 persons lose their lives in fires each year in the U.S. Two-thirds of these persons die in home fires. If fire detectors for life safety are to be effective, their use in dwellings is indicated.

Any of the three conventional fire detector types, flame, heat, or smoke, can serve for life safety. Comparing advantages and disadvantages of each type of detector indicates smoke detectors should be the most effective of the three. There are, however, some technical and design deficiencies with smoke detectors which must be overcome if these devices are to realize their maximum potential as life saving devices.

16738. Waterstrat, R. M., Manuszewski, R. C., **The niobium-osmium constitution diagram,** *J. Less-Common Met.* **51,** 55-67 (1977).

Key words: atomic ordering; constitution diagram; niobium alloys; osmium alloys; phase diagram.

The Nb-Os alloy system has been investigated over the entire composition range using metallographic, x-ray diffraction and electron microprobe techniques. The ϵ-Os solid solution extends to about 27 at.% Nb at high temperatures but this is reduced to about 20 at.% Nb at lower temperatures. Three intermediate phases occur in this system and all of them possess topologically close-packed structures of the Frank-Kasper type. These phases are χ (α-Mn type), σ(σ-phase type) and β(A15 or βW-type). The α-Nb solid solution extends to about 19 at.% Os at high temperatures but only to about 13 at.% Os at lower temperatures. Two eutectic reactions occur at about 2120 °C and 2175 °C. The χ-phase is formed by a peritectic reaction at about 2270 °C, the σ-phase melts congruently at about 2200 °C and the β-phase forms by a peritectoid reaction at about 1975 °C. All the intermediate phases possess highly ordered structures with the larger (Nb) atoms preferring the sites having high coordination while the smaller (Os) atoms prefer the sites of lowest coordination.

16739. Brown, W. E., Gregory, T. M., Chow, L. C., **Effects of fluoride on enamel solubility and cariostasis,** *Caries Res.* **11,** (Suppl. 1), 118-141 (1977).

Key words: chemical potential; dental caries; enamel; fluorapatite; fluoride; hydroxyapatite; solubility.

The known caries-reducing effect of fluoride is frequently attributed to its ability to reduce the solubility of enamel. Solubility data are presented which show that under a caries-like condition, the difference in the amounts of enamel that would dissolve in the absence and in the presence of fluoride ions is not significant. A new theory for the physicochemical action of fluoride is proposed which is based on the view that fluoride increases the chemical potential of the component H_3PO_4 and decreases the chemical potential of the component $Ca(OH)_2$ of the solution within the lesion, thereby lowering diffusion out of the enamel or hastening remineralization. Solid solutions between hydroxyapatite and fluorapatite are an important means of incorporation of fluoride into enamel crystals, but the thermodynamic properties exhibited by such solid solutions in the presence of F^- ions and under cariogenic conditions are likely to mimic those of the end member, fluorapatite because of the formation of surface coatings. A distinction is made between "lattice" and "interfacial" fluorides; addition of acid to an equilibrated mixture would cause release of "lattice" fluoride to the solution and, at the same time, an uptake of fluoride by the "interface."

16740. Truhlar, D. G., Brandt, M. A., Srivastava, S. K., Trajmar, S., Chutjian, A., **Quantum mechanical and crossed beam study of vibrational excitation of N_2 by electron impact at 30-75 eV,** *J. Chem. Phys.* **66,** No. 2, 655-663 (Jan. 15, 1977).

Key words: close-coupling calculations; crossed beams; cross sections; differential cross sections; electron scattering; inelastic scattering; nitrogen molecules; resonances; scattering; vibrational excitation.

The ratios of differential cross sections for excitation of the first excited vibrational state and for elastic scattering for electron impact on N_2 have been measured at scattering angles ranging from 20° to 135° at 30, 35, 40, 45, and 75 eV impact energies and from 25° to 90° scattering angle at 20 eV impact energy. The results at 20 eV are in good agreement with two previous sets of measurements. Using previously measured and normalized elastic differential cross sections for N_2, the ratios have been converted to inelastic cross sections. Calculations using a four-state vibrational-rotational basis set and an effective interaction potential developed previously are reported at the five energies in the 30-75 eV region. It is shown that the potential scattering model can account for the magnitude and the qualitative behavior of the cross sections at 35-75 eV but there are some significant quantitative differences between theory and experiment. The most striking of these is the way the theoretical model overestimates the scattering at scattering angles less than about 50°. Core-excited resonances apparently make an appreciable contribution to the vibrationally inelastic scattering at 30 eV.

16741. Jordan, T. H., Schroeder, L. W., Dickens, B., Brown, W. E., **Crystal structure of stannous hydroxide phosphate, a**

reaction product of stannous fluoride and apatite, *Inorg. Chem.* **15,** No. 8, 1810-1814 (1976).

Key words: asymmetric coordination; crystal structure; Sn bonding; tin hydroxy phosphate; tin phosphate.

Stannous hydroxide phosphate, $Sn_5(OH)PO_4$, crystallizes in the monoclinic unit cell, $a = 7.176$ (4) Å, $b = 7.051$ (1) Å, $c = 10.453$ (4) Å, and $\beta = 103.96$ (3)°, with space group $P2_1/n$ and $Z = 4$. Refinement of the structure concluded with $R_w = 0.035$ and $R = 0.053$. A total of 1332 x-ray data of measurable intensity were collected from a single crystal using Mo radiation and θ-2θ scans. The data were not corrected for absorption, and the refinements allowed for anomalous dispersion but not for secondary extinction. Each of the Sn atoms is coordinated by three oxygen atoms; with Sn...O distances of ~ 2.1 Å. All three coordinated oxygens are within the same hemisphere about Sn, presumably because of repulsion by a lone pair of electrons in the other hemisphere about Sn. The hydroxyl hydrogen atom has been located approximately, and forms a hydrogen bond with an oxygen of the PO_4. The O-P-O angles in the PO_4 group show little deviation from tetrahedral because there is no Sn coordination to PO_4 edges. Each oxygen atom of the PO_4 group forms one strong bond to Sn. Three of these oxygen atoms also form weaker bonds to Sn and the fourth forms a hydrogen bond with the hydroxyl group. The average P-O distance is 1.539 Å. Structural consideration of the Sn-PO_4 coordinations and the PO_4 geometry imply that Sn...O bonds are predominantly ionic in tin phosphates.

16742. Schroeder, L. W., Prince, E., **Hydrogen-bonded dimers in Tin(II) hydrogen phosphate,** *Acta Cryst.* **B32,** Part 12, 3309-3311 (Dec. 1976).

Key words: hydrogen-bonded dimers; neutron diffraction; stannous hydrogen phosphate.

$SnHPO_4$, monoclinic, $P2_1/c$, $a = 4.608$ (2), $b = 13.603$ (4), $c = 5.823$ (2) Å, $\beta = 98.76$ (1)°, $Z = 4$. This neutron diffraction study has shown that the HPO_4^{2-} ions are linked together by two asymmetric hydrogen bonds [d(O...O) = 2.560, d(O-H) = 1.017 Å ∠O-H...O = 178.1 °] to form dimers. Tin-phosphate-oxygen coordination takes place primarily in layers with the hydrogen bonds occurring between these layers.

16743. Henderson, M. M., **The Federal sector,** Chapter in *The Information Age: Its Development, Its Impact*, D. P. Hammer, Ed., pp. 91-121 (The Scarecrow Press, Inc., Metuchen, NJ, 1976).

Key words: Federal library and information activities; library and information sciences; review.

This chapter reviews the significant accomplishments in library and information sciences in the Federal Government over a ten year period (1965-1975). Federal librarians and information scientists were faced with a number of problems but also offered some special promises: major support for innovative developments came from Federal sources, for example, and cooperative programs have resulted in resource sharing on a number of fronts. The chapter follows a chronological path to trace developments and activities; those discussed in different context in other chapters are not covered in detail in this one. A list of sources and recommended reading is included for the reader's reference.

16744. Stein, R. J., **Electron transmission measurements of electron mean free path in supported thin films from 1-5 keV,** *Surf. Sci.* **60,** 436-444 (1976).

Key words: Auger-electron spectroscopy (AES); electron attenuation lengths; electron spectroscopy for chemical analysis (ESCA); electron transmission through thin films; inelastic electron mean free path; supported thin films.

Measurements are made of the transmission of medium energy electrons through in vacuo deposited films in order to determine the inelastic electron mean free path as a function of energy. Films of Al, Ge and Au are deposited in small increments on 20-30 Å carbon substrates supported by "holey" carbon films. The no-loss electron current is measured for each thickness as a continuous function of incident energy in the range of 1-5 keV. Although this preliminary experiment does not result in a precise separation of elastic and inelastic scattering effects, the attenuation lengths estimated are in reasonable agreement with measured and calculated inelastic mean free paths. Elastic scattering cross sections appear to be smaller than estimated by simple theory.

16745. Gerhold, W. F., **Corrosion behavior of ductile cast-iron pipe in soil environments,** *J. Am. Water Works Assoc.* **68,** No. 12, 5506-5510 (Dec. 1976).

Key words: carbon steel; corrosion; ductile cast-iron; soils; statistical analysis; underground.

Ductile cast-iron pipe was buried for up to fourteen years in a variety of soil environments. This final report, comparing its performance to that of carbon steel buried in the same soils, suggests the two substances corrode at nearly the same rates when encased in some soils. Different soils, however, alter the corrosion rates considerably for both materials.

16746. Bennett, H. S., Cantrell, C. D., **Inclusions in cadmium telluride: Estimates for damage thresholds,** *J. Appl. Phys.* **48,** No. 2, 522-529 (Feb. 1977).

Key words: cadmium telluride; elastic compliance tensor; elastic moduli; extrinsic damage thresholds; high-power lasers; infrared materials; tensile stress.

One problem frequently encountered in high-power laser systems is the thermal extrinsic damage to the laser materials, which arises from absorbing inclusions. Absorbing inclusions are impurities with physical and optical properties which differ substantially from those of the host material. Such inclusions may absorb sufficient radiation from the incident laser beam to produce major stresses within the host. In this paper, estimates of the maximum tensile stress as a function of inclusion size, laser pulse width, and laser power are computed for the common precipitates in CdTe. Our computations suggest that the heating of such precipitates when subjected to power densities of about 100 MW/cm² may produce stresses comparable to or greater than the breaking strength of the CdTe host.

16747. Gadzuk, J. W., **Angle resolved Auger surface spectroscopy,** *Surf. Sci.* **60,** 76-84 (1976).

Key words: adsorption; angle resolved; Auger; chemisorption; electron spectroscopy; surfaces.

The angular distribution of electrons ejected in core-valence-valence Auger transitions of atoms chemisorbed on metal surfaces is considered theoretically. Since the valence electrons participating in the Auger transition are also involved in chemical bonding to the surface, these initial states contain information pertaining to the chemisorption bonding geometry. The role of the initial state symmetry in determining the angle resolved Auger surface spectrum (ARASS) is investigated through model calculations and is found to be small. Thus the ARASS is expected to be a smoothly varying function of angle with $\lesssim \pm 15$ percent modulations due to diffraction effects, in agreement with recent experimental results for S adsorbed on Ni(100).

16748. Penn, D. R., **Electron mean free paths for free-electron-like materials,** *Phys. Rev. B* **13,** No. 12, 5248-5254 (June 15, 1976).

Key words: electron mean free path; free-electron-like metal; 100 to several 1000 eV.

Mean free paths for electrons in bulk jellium are calculated for electrons with energies from a few hundred to a few thousand eV and for values of r_s for 1.5 to 5 where r_s is the average distance between valence electrons measured in units of the Bohr radius. Account is taken of exchange and correlation effects in an approximate way. The present theory is compared to previous theories and to experiments on Al, Be, Si, SiO_2, and Al_2O_3, and in most cases the agreement between theory and experiment is quite good.

16749. Gadzuk, J. W., **Vibrational excitation in photoemission spectroscopy of condensed molecules,** *Phys. Rev. B* **14,** No. 12, 5458-5465 (Dec. 15, 1976).

Key words: adsorption; molecules; photoelectron spectroscopy; surfaces; vibrational excitation.

Photoelectron spectra of gas-phase molecules display sharp vibrational structure. The envelope of the spectrum is determined by the Franck-Condon factor. On the other hand, photoelectron spectra of the same molecules, adsorbed or condensed onto metal surfaces show a broad band whose shape resembles the gas-phase Franck-Condon envelope but with no sharp structure. The smearing out of the vibrational structure is usually attributed to lifetime effects or site inhomogeneities. A new mechanism involving intrinsic phonon sidebands in photoemission from condensed molecules is suggested and the details of the theory are worked out. Experimental ultraviolet photoelectron spectra from condensed CO are considered in the light of this theory.

16750. Houck, J. C., **Mercury-melting-line determination by latent heat method,** *J. Appl. Phys.* **48,** No. 2, 605-609 (Feb. 1977).

Key words: high pressure; latent heat detection; melting and freezing equilibrium; mercury.

The equilibrium pressure for the melting and freezing of mercury was observed for the temperature range $-38.834-0.023$ °C by latent heat detection. The corresponding pressure range was $0.14-757.32$ MPa (MPa = 10^6 N/m^2). The least-squares fit was obtained for this range of pressure with a standard deviation of the residuals of 0.055 MPa for pressure expressed as a third-order polynomial in temperature.

16751. Tsai, D. H., MacDonald, R. A., **An atomistic view of shock wave propagation in a solid,** (Proc. 5th European Conf. on Thermophysical Properties of Solids at High Temperatures, Moscow, USSR, May 18-21, 1976), *High Temp. High Pressures* **8,** 403-418 (1976).

Key words: anharmonic crystal; computer simulation; energy transport; equation of state; interatomic potential; molecular dynamics; second sound; shock wave; stress relaxation; structural relaxation; thermal relaxation.

Molecular dynamical studies of the propagation of strong one-dimensional shock wave in a perfect fcc or bcc monatomic lattice in one, two, and three dimensions are reported. Various two-body interatomic potentials ranging from a harmonic potential to one which simulates that in α-iron are used. The classical equations of motion for the atoms are solved numerically under appropriate initial and boundary conditions, and the properties of the lattice are obtained from averages of the atomic motion. With a realistic potential the shock wave velocity u_s increases approximately linearly with increasing particle velocity u_p, in agreement with experiment. The results show the structure of the shock wave on an atomic scale, and give such details as the thickness of the shock front and the equilibration of stresses and energies in the compressed region. Under certain conditions structural relaxation accompanied by stress relaxation is also observed. The implications of some of these details on the determination of equation of state data from shock wave experiments are examined.

16752. Cheron, B., Scheps, R., Gallagher, A., **Noble-gas broadening of the 6 $^2P_{1/2}$-7 $^2S_{1/2}$ (377.6 nm) 6 $^2P_{3/2}$-7 $^2S_{1/2}$ (535 nm) thallium lines,** *Phys. Rev. A* **15,** No. 2, 651-660 (Feb. 1977).

Key words: line broadening; satellites; thallium.

The shapes of the thallium (Tl) 535- and 377.6-nm resonance lines broadened by 500-1500 torr of noble gases have been measured at 743 K. The reported normalized emission intensities yield absorption coefficients in absolute units for all portions of the line. The shift and broadening of the Lorentzian-shaped line cores, the wavelengths of the transition to non-Lorentzian wings, wing shapes, and satellite positions, shapes, and intensities are reported. As an example, a pair of excited and ground-state interaction potentials are given for the Xe case to explain the shift, width, and intensities in all portions of the line wings.

16753. Wiederhorn, S. M., Tighe, N. J., Evans, A. G., **New design techniques for brittle materials,** *Proc. 43rd AGARD Meeting Structures Panel, London, England, Sept. 27-30, 1976,* pp. 41-55 (Technical Editing and Reproduction, Ltd., Harford House, London, England, Dec. 1976).

Key words: brittle materials; ceramics; delayed failures; design techniques; flaw detection techniques.

Methods of design for improving the reliability of ceramics in structural applications are described. Based on the science of fracture mechanics, these methods provide a rational basis for estimating the lifetime of structural components that are subjected to applied loads. Data obtained by standard strength or fracture mechanics techniques are used to develop design diagrams from which component performance is evaluated. Three types of diagrams are described, depending on whether the critical flaw size in a component is estimated by nondestructive evaluation, proof testing, or statistical evaluation. The validity of the theory has been tested experimentally, and, on the whole, agreement between theory and experiment is satisfactory. However, additional experimentation is suggested to fully evaluate the limits of the theory.

16754. Lind, M. A., **Measurement of the absolute spectral response of detectors,** *Proc. of the Technical Program—Electro-Optical Systems Design Conf. 1976—International Laser Exposition, New York, NY, Sept. 14-16, 1976,* pp. 55-58 (1976).

Key words: absolute spectral response; detector uniformity; linearity; photodetectors; silicon detectors.

There are many parameters that affect the absolute spectral response of any photodetector. The question of how to measure these parameters and thereby characterize a detector is the subject of this paper. For brevity, this paper will confine itself to the discussion of the techniques used to measure those parameters which have the greatest potential effect on silicon photodiodes operated in the short circuit or current mode. In general, these same parameters also affect all other photodetectors to some extent.

16755. Johnson, C. R., **The inertia of a product of two hermitian matrices,** *J. Math. Anal. Appl.* **57,** No. 1, 85-90 (Jan. 1977).

Key words: eigenvalue; hermitian matrix; inertia; stability.

Given the inertias of H and K, hermitian and nonsingular, the precise set of possible inertias of HK is determined. Several consequences are given.

16756. Hodgeson, J. A., Hughes, E. E., Schmidt, W. P., Bass, A. M., **Methodology for standardization of atmospheric ozone measurements,** *Proc. Int. Conf. on Photochemical Oxidant Pollution and Its Control, Research Triangle Park, NC, Sept. 12-17, 1976, EPA-600/3-77-001a, Ecological Research Series*, **1,** 3-12 (Environmental Sciences Research Laboratory, Research Triangle Park, NC, Jan. 1977).

Key words: ozone; potassium iodide; techniques; ultraviolet photometer.

Preliminary intercomparisons have been made among several techniques for the calibration of atmospheric ozone monitors. These procedures include the 1 percent neutral buffered potassium iodide method; a modification of this method employing 0.1 molar boric acid rather than the phosphate buffer; a 3-meter double-beam ultraviolet photometer; and gas phase titration. The potassium iodide reagent with boric acid gave a more stable color development and much closer agreement with the ultraviolet measurements than that obtained with the neutral buffered reagent. Ozone calibration data with the 3-meter photometer agreed within 1 and 2 percent with gas phase titration and ultraviolet photometric ozone measurements respectively made at the Environmental Protection Agency facility in Research Triangle Park, North Carolina.

16757. Shiloh, M., Gayer, B., Brinckman, F. E., **Preparation of nitrides by active nitrogen. II. Si_3N_4,** *J. Electrochem. Soc.* **124,** No. 2, 295-300 (Feb. 1977).

Key words: activation parameters; active nitrogen; iodine; kinetics; microwave discharge; nitride; plasma; reaction mechanism; silicon; synthesis; thin film; vapor transport.

A general method for the preparation of nitrides is described by which active nitrogen, excited in a microwave cavity, is subsequently reacted with SiI_4 vapors formed *in situ* by passing iodine vapors over heated silicon powder. The temperature dependence of the deposition of Si_3N_4 on polished Si wafers was measured and compared with calculated thermodynamic data of similar reactions with nonactive nitrogen. The kinetic measurements were related to the special flow characteristics of the system. The over-all reaction

$$4(N)_g + 3(SiI_4)_g \rightarrow (SiN_4)_s + 6(I_2)_g$$

was found to be exothermic. Two regions of different slopes were obtained from the Arrhenius plot

$$\Delta E_{(280\ -450\,^\circ C)} = -3070 \text{ cal/mole}$$

$$\Delta E_{(450\ -500\,^\circ C)} = -8600 \text{ cal/mole}$$

The calculated temperature dependence of the enthalpy change of the corresponding reaction with nonactive nitrogen was shown to be almost constant in the range studied. Similar values of negative activation energy were obtained for the assumed second-order rate-determining reaction: $N + SiI_4 \rightarrow SiN + 2I_2$.

16758. Hummer, D. G., **Line formation in expanding atmospheres,** (Proc. IAU Symp. No. 70, on Be and Shell Stars, Bass River, MA, Sept. 1975), Paper in *Be and Shell Stars*, A. Slettebak, Ed., pp. 281-312 (Reidel, Dordrecht-Holland, 1976).

Key words: high speed aerodynamics; radiative transfer; spectral line formation; stellar atmospheres.

The current state of understanding of line formation processes in expanding atmospheres is reviewed, and the successes and limitations of current computational techniques are summarized. Some results for differential rotation are also given, although very little work has been done in this area. Special attention is given to the severe difficulties that are encountered in inferring the structure of rapidly expanding or rotating atmospheres from observed line profiles because of the failure under these conditions of the Eddington-Barbier relation in integrated light; the value in this respect of continuum and interferometric observations is emphasized.

16759. Wineland, D. J., Allan, D. W., Glaze, D. J., Hellwig, H. W., Jarvis, S., Jr., **Results on limitations in primary cesium standard operation,** *IEEE Trans. Instrum. Meas.* **IM-25,** No. 4, 453-458 (Dec. 1976).

Key words: cesium standard; clock, operating; magnetic shielding; microwave feed; primary cesium standard.

We report on the most recent design changes in our two primary cesium standards, their current operational use, results obtained, and limitations. NBS-4, the shorter device with an interaction length of $L = 0.52$ m, has been extensively used for many months as a clock. After improvements in the magnetic shielding and microwave feed, we have obtained σ_y (1 week $< \tau <$ 2 weeks) $= 7 \times 10^{-15}$ in a 10-Hz bandwidth for its frequency stability. NBS-6, the longer, more accurate device ($L = 3.75$ m), features a linewidth (< 30 Hz), which is believed to be the narrowest linewidth ever reported for a cesium device. NBS-6 has been operated to give a short-term stability σ_y (1 s) $= 7 \times 10^{-13}$ in a 10-Hz bandwidth and has capability of easy beam reversal. The current and past rates of the International Atomic Time (TAI) in terms of our primary cesium standards are reported and compared with the results of other laboratories. With NBS-6 we have calibrated the rate of the NBS time scale of an uncertainty of 0.9×10^{-13}.

16760. Lutz, G. J., **Activation analysis with a californium-252 source,** (Proc. Educational Seminar on Use of Californium-252 in Teaching and Research, Karlsruhe, Germany, Apr. 14-18, 1975), *IAEA-SR-3/3*, Chapter in *Some Physical, Dosimetry and Biomedical Aspects of Californium-252*, pp. 73-87 (International Atomic Energy Agency, Vienna, Austria, 1976).

Key words: activation analysis; californium-252; inland waters and sediments; in vivo analysis; mineral exploration; nuclear safeguards; oceanography; on-stream analysis; well logging.

Aside from the great disparity in fluxes, neutron activation analysis with a ^{252}Cf source differs in two ways from the more traditional methods with a reactor. Firstly, in situ analyses require that the bombarding source and detector conform to the requirements of the sample, e.g. material on a conveyor belt or minerals in a bore hole, and hence frequently use ^{252}Cf sources; secondly, prompt capture gamma rays, the photons produced virtually simultaneously with the capture of a neutron by the nucleus, are frequently used for detection in californium activation analysis. They are rarely used in activation analysis with a reactor. This review discusses the major "field" applications of ^{252}Cf activation analysis—on-stream analysis, well logging, terrestrial mineral exploration, in vivo analysis, oceanography, studies of inland waters and sediments, and for nuclear safeguards. This is followed by a discussion of more conventional laboratory activation analysis with the isotope source.

16761. Richmond, J. C., **A simple test for evaluating the spectral responsivity of monochrome television cameras,** *LESP-RPT-0310.00*, 24 pages (U.S. Department of Justice, Law Enforcement Assistance Administration, National Institute of Law Enforcement and Criminal Justice, Washington, DC, Feb. 1977).

Key words: diffuser; interference filters; spectral responsivity; spectral transmittance; television camera tubes; television cameras; test methods.

This report describes a light source designed for measuring the spectral responsivity of monochrome television cameras, and a simple procedure for making such measurements. The light from a quartz-halogen lamp is diffused and passes through an array of twelve interference filters, of 50 nm bandpass each, with peak wavelengths at about 50 nm intervals from 400 to 950 nm. The spectral transmittance of the diffuser, and of each interference filter-diffuser combination was measured, and factors are supplied to compute the radiance of the light transmitted by each filter from the measured luminance of the diffuser.

A step wedge, with 21 steps, in which the ratio of the transmittance of adjacent steps is about $\sqrt{2}$, is located below the array of interference filters. The gamma of the television camera is evaluated by use of the step wedge. The voltage of the video signal produced when the image of each filter impinges on the face of the camera tube is measured, and divided by the radiance of the filter raised to the gamma power, to obtain the relative spectral responsivity of the camera at the peak wavelength of the filter. The results are normalized by dividing each value by the maximum value obtained, and the quotients plotted as a function of wavelength to produce the spectral responsivity curve of the camera.

16762. Jenkins, E. B., Snow, T. P., Upson, W. L., Starrfield, S. G., Gallagher, J. S., Friedjung, M., Linsky, J. L., Anderson, R., Henry, R. C., Moos, H. W., *Copernicus* **observations of Nova Cygni 1975,** *Astrophys. J.* **212,** No. 1, 198-202 (Feb. 15, 1977).

Key words: Novae; OAO-3; spectra-ultraviolet.

Near-ultraviolet radiation from Nova Cygni 1975 was detected by the *Copernicus* satellite on five occasions from 1975 September 1 to 1975 September 9. The nova was not seen in the UV after this date. The principal result was the observation of a broad emission feature from the Mg II doublet at 2800 Å. The absence of strong UV radiation at shorter wavelengths suggests that these lines are produced by collisional excitation in the outer layers of an expanding shell with $T_e \sim 4000$ K. The absence of observed emission lines from highly ionized species indicates that the amount of material with $4.4 < \log T < 5.7$ is less than 10^{-3} times that which produces the Mg II emission. The continuum flux in the near-UV decreased as the nova evolved, showing that the total luminosity decreased as the nova faded in the visible.

16763. Pallett, D. S., Bartel, T. W., Voorhees, C. R., **Recent reverberation room qualification studies at the National Bureau of Standards,** *Noise Control Eng.* **7,** No. 2, 71-80 (Sept.-Oct. 1976).

Key words: acoustical measurements; acoustics; acoustics facility; automated sound measurement; computer-controlled instrumentation; reverberation room; reverberation room qualification; sound power.

A computer-controlled instrumentation system has been implemented to ascertain room "qualification" (per ANS S1.21-1972) for sound power measurements, to measure radiated sound power, and to measure acoustic absorption in the NBS reverberation room. Preliminary studies performed with this system indicate the effectiveness of rotating diffuser elements and the use of a 12-microphone array in achieving a qualified condition. Initial sound power measurements made under qualified conditions appear to show a measurement repeatability that is generally consistent with and within the bounds of the uncertainties indicated in Table 1 of S1.21.

16764. Voorhees, C. R., Pallett, D. S., **Laboratory measurements in acoustics,** *Noise Control Eng.* **7,** No. 2, 52-56 (Sept.-Oct. 1976).

Key words: acoustical measurements; acoustics; acoustics facilities; laboratory facilities; noise measurement; sound measurement.

A detailed questionnaire on the topic of "Laboratory Measurements of Noise Emission and of Acoustical Properties of Building Elements and Materials" was initiated by the Board of Directors of the Institute of Noise Control Engineering in September 1974. Topics dealt with cover the use of facilities for sound power, acoustical absorption, transmission loss, and impact noise measurements, and the use of reference sound sources and anechoic chambers. Results of the survey, which are presented and briefly discussed, indicate the extent and type of activity in these areas. They also reveal a general feeling among respondents that acoustic measurements could be made more accurate with the implementation or improvement of existing facility qualification (performance) criteria, calibration data, measurement standards, and measurement methodology.

16765. Lawton, S. A., Novick, S. E., Broida, H. P., Phelps, A. V., **Quenching of optically pumped $O_2(b^1\Sigma_g^+)$ by ground state O_2 molecules,** *J. Chem. Phys. Letters to the Editor* **66,** No. 3, 1381-1382 (Feb. 1, 1977).

Key words: laser; metastable; oxygen molecules; photoluminescence; quenching.

A flashlamp-pumped tunable pulsed dye laser operating near the head of the O_2 atmospheric B band at 688 nm was used to excite the first vibrational level of the $b^1\Sigma$ state. The quenching rate constant was determined from the dependence of the $b^1\Sigma$ decay constant on O_2 density. The rate for quenching of the $b^1\Sigma$ state by O_2 was found to be $(3.8 \pm 0.3) \times 10^{-17}$ cm^3 molecule^{-1} sec^{-1}.

16766. Holmer, C. I., **Qualification of an acoustic research facility for sound power determination,** *Noise Control Eng.* **7,** No. 2, 87-92 (Sept.-Oct. 1976).

Key words: acoustic test facility; noise; noise measurement; reverberation room; sound power measurement; standard test procedures for sound power measurement.

Modifications to a test facility that were required in order to bring the facility to within the qualification requirements of American National Standard S1.21 for sound power measurement of sources emitting pure tones are described. The facility is unique in that two nearly identical rooms, of substantially smaller volume than recommended (i.e. 90 m^3), were found to be "qualifiable" with suitable modifications. The modifications included the use of an eight microphone array, fixed and rotating diffusers, low frequency absorption and multiple source locations. The modifications, and some of their objective effects on the qualification measurements, are discussed.

16767. Cezairliyan, A., McClure, J. L., **Temperature and energy of $\alpha \rightarrow \beta$ transformation in hafnium-3%$_0$ zirconium,** *High Temp. High Pressures* **8,** 461-467 (1976).

Key words: hafnium; high-speed measurements; high temperature; solid-solid phase transformation; thermodynamics.

Measurements of the temperature and energy of the $\alpha \rightarrow \beta$ transformation of hafnium containing $3 \cdot 12$%$_0$ zirconium using a millisecond-resolution pulse-heating technique are described. The results yield 2012 K for the transformation temperature and $33 \cdot 1$ J g^{-1} for the transformation energy. The normal spec-

tral emittance (at 0·65 μm) at the transformation point is determined to be 0·42. Estimated maximum inaccuracies of the measured properties are: 10 K for the transformation temperature, 10 percent for the transformation enery, and 5 percent for the normal spectral emmittance.

16768. Brown, P. W., Berger, R. L., Clifton, J. R., Frohnsdorff, G., **Limitations to fly ash use in blended cements,** *Proc. 4th Int. Ash Utilization Symp., St. Louis, MO, Mar. 24-25, 1976,* pp. 518-529 (Energy Research & Development Administration, Morgantown, WV, 1976).

Key words: blended cements; fly ash; specifications.

The production and utilization of blended cements containing fly ash is less than one million tons a year in the U.S. This accounts for only about one percent of the cement produced. It has been demonstrated that utilization of fly ash with portland cement to make blended cement results in energy and raw materials savings almost directly proportional to the amount of ash used. In view of the benefits derived from ash utilization in this way the level of production of blended cement may be expected to increase. However, additional property data need to be developed to address uncertainties and misconceptions regarding the performance of blended cements. Facilitation of blended cement use requires the development of data to be used by voluntary consensus standards organizations as a basis for standard test procedures and specifications.

16769. Chang, S. S., **Stored energy in poly(vinyl chloride) from pelletizing process,** *J. Chem. Thermodyn.* **9,** 189-197 (1977).

Key words: adiabatic temperature drift; enthalpy; glass transition; heat capacity; pelletization; poly(vinyl chloride), pressure densification; relaxation; stored energy; strain energy.

From the heat capacities measured from 5 to 375 K on three poly(vinyl chloride) samples, evidence of residual strain energies stored in the sample appeared near the glass-transition temperature in the pelletized materials. The three samples were derived from suspension- and bulk-polymerized powder stocks and were measured either pelletized or as received. The stored energies began to be released at temperatures about 30 to 40 K below the glass-transition temperature of about 355 K. The stored energies were estimated to be (2.7 ± 0.1) and (3.5 ± 0.1) J g^{-1} for samples pelletized under 140 and 500 MPa of pressure, respectively.

16770. Kusuda, T., **Energy calculations for energy conservation design of buildings,** *APEC J.*, pp. 18-22 (Automated Procedures for Engineering Consultants, Dayton, OH, Winter 1976-1977).

Key words: computerized energy analysis; energy conservation standards; new building design; retrofit design.

Since energy calculation is an essential element of energy conservation standards, an accurate and comprehensive yet "easy-to-use" computer program for such calculation is most desirable. This paper reviews the existing state of energy-analysis procedures and identifies the areas for needed improvement. The paper also points out that the computational procedures suitable for new building design could be simpler than those required to simulate the energy consumption performance of existing buildings.

Standardization of input and output is also considered a key factor for the "easy-to-use" issue for the implementation of computerized energy calculation for building energy conservation standards.

16771. Scheide, E. P., Durst, R. A., **Indirect determination of sulfate in natural waters by ion-selective electrode,** *Anal. Lett.* **10,** No. 1, 55-65 (1977).

Key words: environmental analysis; ion-selective electrode; lead electrode; natural waters; rainwater; seawater; sulfate.

The indirect determination of sulfate in natural waters (seawater and simulated rainwater) was accomplished by titration with lead nitrate solution using the lead ion-selective electrode as the titration sensor. The indirect determination of sulfate is based on the formation of $PbSO_4$ which is quantified by measurements with a lead electrode. The measurements were carried out in 80 percent isopropanol using a double-junction reference electrode. The data evaluation was performed by a Gran plot of the titration of sulfate samples with standard lead nitrate. Samples containing between 2 and 100 ppm sulfate concentration were analyzed directly, while samples of higher sulfate concentration were diluted prior to analysis. The seawater samples were diluted 100-fold prior to analysis.

16772. Durst, R. A., **Tris(hydroxymethyl)aminomethane physiologic-pH buffer—Liquid-junction error,** *Clin. Chem.* **23,** No. 2, 298 (1977).

Key words: clinical pH; liquid junction; pH analyzers; pH error; pH; physiologic pH; tris pH buffer.

Studies using clinical blood-pH instrumentation confirm the reported existence of a residual liquid junction potential which produces an error in the observed pH value. The magnitude of the effect depends on the type of liquid junction and may include contributions from errors in instrument temperature control. The buffer is useful as a secondary standard of pH for the detection of instrumental malfunctions in pH analyzers.

16773. Scheide, E. P., **The piezoelectric-crystal mercury dosimeter,** *Phys. Teach.* **15,** No. 1, 47-51 (Jan. 1977).

Key words: environmental analysis; industrial hygiene; mercury vapor; personal dosimeter; piezoelectric sensors; quartz crystal microbalance.

A personal dosimeter for mercury vapor in air based on the use of a piezoelectric sensor with a selective coating has been developed and evaluated. The philosophy behind the use of such devices is explained along with the basic physics concerning this scientific principle. The sensor is a gravimetric device which indicates an integrated total exposure to mercury vapor. Calibration curves are given in the industrial hygiene range of interest and the device was evaluated from an industrial hygiene point of view. Short summaries are given describing current research and new directions in this field.

16774. McKinney, J. E., **Application of hole theory to estimate the pressure-induced densification of polymers,** *Ann. N.Y. Acad. Sci.* **279,** 88-93 (Oct. 15, 1976).

Key words: compressibility; densification; glass; glass transition; hole theory; liquid; polymer; pressure; thermodynamic.

Forming a glass by isobaric cooling at an elevated pressure produces a larger density than that obtained by cooling at the same rate at atmospheric pressure. Simple phenomenological theory is used to obtain a relation to estimate the densification from glass transition properties obtained by experiment. It is shown how the hole theory of Simha and Somcynsky may be used to facilitate the estimation of densification through the application of a universal reduced function that replaces the quantity most difficult to obtain experimentally in this relation.

16775. Glaze, D. J., Hellwig, H., Allan, D. W., Jarvis, S., Jr., **NBS-4 and NBS-6: The NBS primary frequency standards,** *Metrologia* **13,** 17-28 (Feb. 1977).

Key words: bias uncertainty; frequency accuracy; frequency bias; frequency stability; primary frequency standard; time dispersion.

The NBS primary frequency standard NBS-4 has been operating since January 1973. NBS-5 operated from January 1973 until March 1974. At this time NBS-5 was modified significantly and redesignated NBS-6. The extent and character of these design changes are discussed. NBS-6 operation and evaluation began in March 1975. Results obtained from NBS-4, NBS-5 and NBS-6 are given, along with intercomparisons of some significant parameters.

During 1975, NBS-4 was operated as a clock and a time dispersion of 2.5 ns was obtained for one day. The NBS approach to long term clock operation of the primary standards is discussed. These techniques will probably involve "accuracy servo" methods, and may lead to very accurate clocks with time dispersion less than 1 ns per day.

16776. Bergquist, J. C., Lee, S. A., Hall, J. L., **Saturated absorption with spatially separated laser fields: Observation of optical "Ramsey" fringes,** *Phys. Rev. Lett.* **38,** No. 4, 159-162 (Jan. 24, 1977).

Key words: nonlinear spectroscopy; Ramsey fringes; saturated absorption.

We have observed Ramsey's interference fringes in the optical region using saturated-absorption techniques in a fast atomic beam. We discuss their physical origin and describe an optical configuration that guarantees fringes of high symmetry. This technique, with its high-resolution potential, should lead to dramatic improvements in spectral measurements.

16777. Grant, W. H., Smith, L. E., Stromberg, R. R., **Radiotracer techniques for protein adsorption measurements,** *J. Biomed. Mater. Res. Symp.* **8,** 33-38 (1977).

Key words: adsorption; proteins; radiotracer; techniques.

Factors which contribute to measurement errors associated with the use of radiotracers to measure protein adsorption are considered. Techniques for removal of excess adsorbent solution and for estimation of surface area are described. Artifacts induced by the incorporation of a radio-label both by specific adsorption of the labeling atom and by changes in the protein are discussed.

16778. Bridges, J. M., Ott, W. R., **Vacuum ultraviolet radiometry. 3: The argon mini-arc as a new secondary standard of spectral radiance,** *Appl. Opt.* **16,** No. 2, 367-376 (Feb. 1977).

Key words: argon; light source; mini-arc; radiometry; spectral radiance; standard; ultraviolet.

A miniature argon arc has been designed and tested as a new transfer standard of spectral radiance for the wavelength range from 114 nm to 330 nm. Calibration has been performed using two primary standard sources: the hydrogen arc from 130 nm to 330 nm and the blackbody line radiator from 114 nm to 130 nm. The mini-arc provides an intense, stable, and reproducible uv continuum with dc power requirements of less than 1.5 kW. The arc characteristics have been investigated, and the sensitivity of the radiant power output to various operating parameters has been measured. The rms uncertainty in the spectral radiance is estimated to be 5.3 percent above 140 nm and 10.1 percent between 114 nm and 140 nm, due primarily to uncertainties in the primary standard sources.

16779. Lin, S. L., Bardsley, J. N., **Monte Carlo simulation of ion motion in drift tubes,** *J. Chem. Phys.* **66,** No. 2, 435-445 (Jan. 15, 1977).

Key words: drift tube; ion; Monte-Carlo; swarm; theory; velocity distribution.

The motion of a swarm of ions in a uniform electric field is studied by simulating the motion of a single ion through many collisions with neutral atoms in order to obtain the drift velocity, average energy, and velocity distribution for the ions. For K^+ ions in He at low field strengths, the results agree well with the solutions of the Boltzmann equation by Kumar and Robson; and for K^+ in Ar at all field strengths, the computed mobilities demonstrate that the Viehland-Mason moment method can give useful results, especially if carried through to third order. The velocity distributions computed for O^+ ions in He and Ar are used in the accompanying paper by Albritton *et al.*, to analyze drift tube measurements of O^+ reaction rates. Significant deviations from the Maxwell-Boltzmann form have been found and are seen to have important effects in that application. Velocity distributions have also been obtained for Li^+ in He. The sensitivity of ionic mobilities to changes in the ion-atom interaction potential is examined with particular reference to K^+ ions in Ar.

16780. Hardy, S. C., **A grain boundary groove measurement of the surface tension between ice and water,** *Philos. Mag.* **35,** No. 2, 471-484 (Feb. 1977).

Key words: grain boundary groove; ice-water interface; ice-water surface tension; Nash-Glicksman theory; surface energy.

The surface tension between ice and water has been measured by observations of the equilibrium shape of grain boundary grooves at an interface stabilized by an imposed temperature gradient. The experiments have been designed to minimize the perturbing effects of heat flow in the cell walls which contain the samples. The observed grooves are in agreement with the theory of Nash and Glicksman (1971) which predicts groove shapes for the case of unequal thermal conductivities in the two phases. The measurements give a value of 29.1 ± 0.8 mJ m^{-2} for the ice-water surface tension.

16781. Okabe, H., **Photodissociation of thiophosgene,** *J. Chem. Phys.* **66,** No. 5, 2058-2062 (Mar. 1, 1977).

Key words: $CS(A^1\pi)$; photodissociation; thiophosgene; ΔHf° (SCCl); ΔHf° ($SCCl_2$).

The photolysis of thiophosgene produces $CS(A^1\pi)$ below the incident wavelength (1270 Å) from which $\Delta Hf^\circ_0(SCCl_2) \leq 7.92 \pm 1$ kcal mol^{-1} (33.1 ± 4 kJ mol^{-1}) is derived. The quantum yield for the production of Cl atoms has been determined from the amounts of HCl produced from the photolysis of thiophosgene-heptane mixtures. At 2537 Å the yield is unity over the pressure region 0.4-80 torr (0.05-10 kPa) of thiophosgene, indicating that the primary photochemical process is almost entirely SCCl + Cl. Both at 3660 and 4358 Å the quantum yield of Cl production increases with a decrease in thiophosgene pressure and is 0.90 ± 0.17 and 0.38 ± 0.19, respectively, as the pressure approaches zero. From the pressure dependence of the quantum yield the lifetime of the excited state $^1A_2$ is estimated to be about 55 nsec at 4358 Å and about 6 nsec at 3660 Å. The photolysis data of the $^1A_2$ state of thiophosgene are correlated with the fluorescence lifetime measured previously. $D^\circ_0(SCCl{-}Cl) = 63.4 \pm 0.5$ kcal mol^{-1} (265.3 ± 2 kJ mol^{-1}) and $\Delta Hf^\circ_0(SCCl) = 43 \pm 1$ kcal mol^{-1} (180 ± 4 kJ mol^{-1}) ar- derived. The photochemistry of thiophosgene is compared with that of phosgene and formaldehyde. A new method of Cl isotopic enrichment is suggested.

16782. Anderson, W. E., Davis, R. S., **Measurement of ac insulation losses at cryogenic temperatures,** *IEEE Trans. Elec. Insulation* **EI-12,** No. 1, 51-54 (Feb. 1977).

Key words: cryogenic; dielectric loss; dissipation factor; high voltage; low temperature polymer.

The design of superconducting high voltage transmission lines requires engineering data which, until recently, have been largely unavailable. The selection of a suitable dielectric for a tape-insulated ac cryogenic cable, for example, requires the knowledge of insulation dissipation factors at high voltage, which are typically 20×10^{-6} or smaller. We present here dissipation factor measurements made on several dielectric tapes under consideration by a superconducting power transmission line project as well as on epoxies which appear mechanically suitable as low-temperature bushing material. The measurement technique and instrumentation are described.

16783. Braun, W., Tsang, W., **Mechanism of alkyl halide photolysis by a pulsed CO_2 TEA laser,** *Chem. Phys. Lett.* **44,** No. 2, 354-359 (Dec. 1, 1976).

Key words: alkyl halides; CO_2 laser; infrared; kinetics; mechanisms; photochemistry; pyrolysis.

A CO_2 TEA laser has been used to photolyze dilute samples of various alkyl halides in helium. The mechanism of the high intensity infrared photolysis of these molecules involves the decomposition of molecules into molecular or radical fragments. The reaction pathway is always dissociation into the lowest thermal dissociation channel(s) of the molecule photolyzed. Products from the initial process are also photo-dissociated by the laser pulse and their decomposition pathways are similarly governed. The molecules being photolyzed are not thermally equilibrated with the bath or with each other and the molecular-specific nature of the laser excitation is demonstrated.

16784. Goodman, S., Shier, D., **On designing a reliable hierarchical structure,** *SIAM J. Appl. Math.* **32,** No. 2, 418-430 (Mar. 1977).

Key words: dynamic programming; graph; network; organization; probability; reliability; trees.

This paper considers the design and analysis of a class of managerial structures which are perhaps best illustrated by a spy network. The problem is formulated as a reliability problem on organizational trees, and two probabilistic performance measures are studied. With respect to either measure, it is possible to analyze the value of any given hierarchical structure. In addition, optimal organizational designs can be synthesized with respect to either criterion using for the one a dynamic programming approach and for the other a graph-theoretic solution method.

16785. Manning, R. G., Kurylo, M. J., **Flash photolysis resonance fluorescence investigation of the temperature dependencies of the reactions of $Cl(^2P)$ atoms with CH_4, CH_3Cl, CH_3F, CH_2F_2, and C_2H_6,** *J. Phys. Chem.* **81,** No. 4, 291-296 (1977).

Key words: chemical kinetics; chlorine atoms; flash photolysis; hydrogen metathesis methanes; resonance fluorescence; vibrational excitation.

The flash photolysis resonance fluorescence technique was employed to investigate the temperature dependencies of the reactions $Cl + CH_4 \rightarrow HCl + CH_3$ (k_1); $Cl + CH_3Cl \rightarrow HCl + CH_2Cl$ (k_2); $Cl + CH_3F \rightarrow HCl + CH_2F$ (k_3); $Cl + CH_3F \rightarrow HCl + CH_3F$ (k_3); $Cl + C_2H_6 \rightarrow HCl + C_2H_5$ (k_4). The following rate expressions were obtained in units of cm^3 $molecule^{-1}$ s^{-1}: $k_1(218-322\ K) = (7.93 \pm 1.53) \times 10^{-12} \exp[-(2529 \pm 101)/RT]$; $k_2(233-322\ K) = (3.36 \pm 0.71) \times 10^{-11} \exp[-(2484 \pm 113)/RT]$; $k_3(216-296\ K) = (4.79 \pm 1.05) \times 10^{-12} \exp[-(1535 \pm 107)/RT]$; $k_4(222-322\ K) = (7.29 \pm 1.23) \times 10^{-11} \exp[-(121 \pm 87)/RT]$ where $R = 1.987$ cal deg^{-1} mol^{-1}. At 227 and 296 K k_3/k_3 was observed to be ≤ 1.3.

16786. Ravechè, H. J., **Metastable states in the Lennard-Jones fluid,** *Ann. N.Y. Acad. Sci.* **279,** 36-42 (Oct. 15, 1976).

Key words: algorithm; Lennard-Jones; metastable states; Monte Carlo.

Metastable states associated with the fluid-solid transition in the classical Lennard-Jones system are simulated by means of the Monte Carlo algorithm in statistical mechanics. The simulations are concerned with both the thermal and structural properties of undercooled or overcompressed monatomic fluids.

16787. Tung, M. S., **Characterization and modification of permselective properties of apatite membranes,** *J. Dental Res.* **55,** Spec. Issue D, D77-D85 (1976).

Key words: apatites; caries mechanism; caries prevention; membrane potentials; permselective properties; surface properties.

Compressed apatite disks were used as models for tooth enamel. Their permselective properties were studied as functions of the pH of the gradient solutions, the composition of the apatites, and the pretreatments with anionic phosphate compounds and cationic proteins. The results are discussed in relation to the caries mechanisms.

16788. Finnegan, T. F., Holdeman, L. B., Wahlsten, S., **Microwave phenomena in thin-film Josephson junctions coupled to a contiguous microstrip resonator,** *IEEE Trans. Magn.* **MAG-13,** No. 1, 392-395 (Jan. 1977).

Key words: coherent microwave emission; e/h voltage standard; Josephson junction; microstrip resonator; microwave coupling; parametric plasma oscillation; thin-film device.

A half-wavelength microstrip resonator has been used to couple microwave radiation between Josephson junctions and an external 50 Ω transmission line, and various microwave properties of these resonator-coupled junction devices have been studied. The advantages of these devices in applications including coherent radiation emission, 2e/h precision voltage sources, and parametric plasma-related effects are described.

16789. Lambropoulos, M., Moody, S. E., **Design of a three-stage alkali beam source,** *Rev. Sci. Instrum.* **48,** No. 2, 131-134 (Feb. 1977).

Key words: atomic beam; effusive oven; sodium beam.

A three-stage effusive alkali beam source is described in detail. Among the advantages of this device over ordinary effusive ovens are greatly increased intervals between refillings, and the production of beams with significantly reduced alkali dimer densities.

16790. Grundl, J. A., Spiegel, V., Eisenhauer, C. M., Heaton, H. T. II, Gilliam, D. M., Bigelow, J., **A californium-252 fission spectrum irradiation facility for neutron reaction rate measurements,** *Nucl. Technol.* **32,** 315-319 (Mar. 1977).

Key words: calibration; californium-252; cross sections; design; errors; fission neutrons; irradiation devices; measuring methods; neutron reactions; neutron sources.

Spontaneous fission sources of ^{252}Cf, lightly encapsulated and with neutron source strengths approaching 10^{10} n/s, have been developed especially for integral cross-section measurements and neutron reaction rate calibrations. An irradiation facility at the National Bureau of Standards makes use of these sources in two well-investigated geometries. A free-field neutron flux in the range of 10^7 n/(cm² s) (10^5 n/mm²·s) and fluences of up to 10^{13} n/cm² (10^{11} n/mm²) are established at the facility based only on a distance measurement and the absolute source strength of the national standard Ra-Be photoneutron source.

The error in the ^{252}Cf source strength ($\pm$ 1.1%) dominates the total free-field flux uncertainty of $\pm$ 1.4 percent (1 σ). Neutron scattering effects in the source capsule and support structures and neutron return from concrete and earth boundaries have been calculated and investigated experimentally. In the worst case, they contribute $\pm$ 0.7 percent to the total flux response uncertainty for all observed neutron reaction rates, including those with sensitivity to low-energy neutrons.

16791. Hanley, H. J. M., **Prediction of the viscosity and thermal conductivity coefficients of mixtures,** *Cryogenics* **16,** No. 11, 643-651 (Nov. 1976).

Key words: corresponding states; dense liquid; mixture; modified Enskog theory; prediction; thermal conductivity coefficient; viscosity coefficient.

A corresponding states procedure to predict the viscosity and thermal conductivity coefficients of a pure fluid or mixture is discussed. We show the transport properties of a fluid or mixture can be calculated to within experimental error given only corresponding values for a reference fluid and equation of state data. With methane, as the reference fluid, we consider nitrogen, ethane, propane, butane, carbon dioxide, and mixtures of these fluids. LNG is also included. It is shown that the conventional corresponding states approach is not sufficient to predict correctly the transport properties. The effect of internal degrees of freedom on the thermal conductivity coefficient and the enhancement in the critical region for this coefficient is discussed briefly.

16792. Haynes, W. M., **Simplified magnetic suspension densimeter for absolute density measurements,** *Rev. Sci. Instrum.* **48,** No. 1, 39-41 (Jan. 1977).

Key words: absolute measurements; barium ferrite buoy; densimeter; experimental; liquid, magnetic; modification; suspension.

A magnetic suspension densimeter, incorporating three support coils, has been reduced to a system using only one coil. This simplifies considerably the design of the apparatus and the procedures involved in the measurements. This instrument can be used for absolute density measurements; i.e., it does not have to be calibrated with reference fluids of known density.

16793. Heimbach, C. R., Lehman, D. R., O'Connell, J. S., **Two-body electrodisintegration of ^3He: Faddeev calculation,** *Physics Lett.* **66B,** No. 1, 1-4 (Jan. 1977).

Key words: Coulomb excitation; electron scattering; Faddeev equations; helium-three; monopole transition; separable potential.

$^3He(e,e')pd$ and $^3He(e,e'p)d$ cross sections are calculated with Faddeev formalism. At low excitation energies, forward electron scattering cross sections are dominated by the Coulomb monopole transition. Backward electron scattering is dominated by the magnetic quadrupole transition.

16794. Hellwig, H., **Design principles and characteristics of frequency and time standards,** *IEEE Trans. Nucl. Sci.* **NS-23,** No. 6, 1629-1635 (Dec. 1976).

Key words: frequency; standards, time; time standards.

Today's precision oscillators and clocks are discussed. They include cesium standards, rubidium standards, hydrogen masers, and quartz crystal oscillators. A brief review of their basic design philosophy and performance characteristics is given. Block diagrams of schematics of the physics packages as well as of the electronic systems are given, and it is pointed out quantitatively (where possible) which parameter changes cause frequency shifts and/or performance deterioration. Particular attention is focused on those parameters which are likely to change under nuclear radiation.

16795. Holdeman, L. B., Holdeman, J. T., Jr., **Magnetic torque on a shielded superconducting gyroscope,** *J. Appl. Phys.* **47,** No. 11, 4936-4943 (Nov. 1976).

Key words: electrodynamics; gyroscope; London moment; magnetic torque; relativity; satellite experiment; superconducting.

The torque on a superconducting sphere rotating in an arbitrary magnetic field is calculated. The result is expressed in terms of the coefficients of the expansion of the magnetic field in spherical harmonic functions, but in general a boundary-value problem must be solved to obtain these coefficients. The boundary-value problem is solved and the torque calculated for configurations pertinent to the gyroscope relativity experiment, a proposed satellite experiment which is to test various theories of gravitation. Typical numerical results for these torques are given and compared with the predicted relativistic effects.

16796. Moulder, J. C., Clark, A. F., **Time-resolved spectroscopy of laser-initiated metal combustion,** (Proc. Unconventional Spectroscopy, San Diego, CA, Aug. 24-25, 1976), *SPIE* **82,** 66-74 (Society of Photo-Optical Instrumentation Engineers, Palos Verdes Estates, CA, 1976).

Key words: laser effects; luminescence; metal combustion; spectroscopy; titanium alloys.

A rapid-scan spectrometer employing a silicon-target vidicon detector was used to study the time-resolved emission spectra of laser-ignited metals. Bulk specimens of Ca, Mg, Zr, Ti and several Ti alloys were ignited with a 90 W cw CO_2 laser in air or under a gentle flow of oxygen. Line and band emissions observed between 300 and 1100 nm during combustion help to identify vapor phase reactants and products and their locations in the flame. Disappearance of discrete spectra during the transient combustion of Ti and Zr gives information on the accumulation of molten oxide products. Observations of the continuum radiation emitted by laser-irradiated flames indicate a laser-stimulated luminescence from condensed metal oxide particles.

16797. Radebaugh, R., **Thermal conductance of indium solder joints at low temperatures,** *Rev. Sci. Instrum.* **48,** No. 1, 93-94 (Jan. 1977).

Key words: beryllium; copper; cryogenics; indium; joints; solder; thermal conductance.

The thermal conductances of two indium solder joints were measured between 2 and 130 K. One joint was between two copper pieces and the other joint between beryllium and copper. Both joints gave nearly the same results even though beryllium is much more difficult to wet with indium. The thermal conductances of the joints at 4 K were considerably higher than those of joints using alloy solders such as lead-tin. The maximum conductance per unit area was about 100 W/cm^2 K, which occurred at about 20 K.

16798. Siegwarth, J. D., **Polarization and dielectric constant of $SrTiO_3$ glass ceramics at low temperatures,** *J. Appl. Phys.* **48,** No. 1, 1-4 (Jan. 1977).

Key words: dielectric constant; dielectric relaxation; electret; glass ceramic; polarization; strontium titanate.

Peaks observed in the temperature dependence of the dielectric constant of $SrTiO_3$ glass ceramics do not appear in the dc polarization. A remanent polarization is observed between 4 and 77 K. The dielectric properties at low temperature are attributed to the relaxation of permanent dipoles to an electret state rather than to antiferroelectric ordering.

16799. Smith, E. W., Giraud, M., **Calculations of rotational linewidths in HCl perturbed by argon,** *J. Chem. Phys.* **66,** No. 4, 1762-1764 (Feb. 15, 1977).

Key words: anisotropic interactions; HCl-Ar; linear molecules; rotational line widths; semiempirical potential; theoretical potential.

Calculations of rotational line widths in HCl perturbed by Argon are calculated using a recently developed theory for the broadening of linear molecules by atoms. Calculations are made with a semiempirical potential and with a recent purely theoretical potential and comparisons are made with experimental data measured for the 0-0 and 0-1 vibrational bands. The inaccuracy of potentials extracted solely from line profile data is discussed and the importance of high order anisotropic contributions to the interaction is stressed.

16800. Stock, M., Drullinger, R. E., Hessel, M. M., **Comparison between electron beam and optically produced mercury excimer fluorescence,** *Chem. Phys. Lett.* **45,** No. 3, 592-594 (Feb. 1, 1977).

Key words: kinetics; Mercury excimers; time resolved spectroscopy.

Significant differences have been observed between the mercury excimer fluorescence produced by electron beam and optical excitation. We have used time resolved fluorescent spectroscopy to study the evolution of the excimer system following a 4 ns optical excitation pulse.

16801. Tobler, R. L., **Low temperature effects on the fracture behaviour of a nickel base superalloy,** *Cryogenics* **16,** No. 11, 669-674 (Nov. 1976).

Key words: fatigue; fracture; low temperature tests; mechanical properties; nickel alloys; superalloys.

The mechanical properties of a solution treated and double aged nickel—18 percent iron—18 percent chromium alloy (Inconel 718) were studied to assess its utility at temperatures in the ambient-to-cryogenic range. Uniaxial tensile property measurements using unnotched specimens at decreasing temperatures between 295 and 4 K show that yield and ultimate strengths increase by 20 and 29 percent, respectively, while ductility remains virtually constant. Fracture mechanics tests using 2.54 cm thick compact specimens revealed that the fatigue crack growth resistance of this alloy improves slightly at extreme cryogenic temperatures, and its plane strain fracture toughness, K_{Ic}, increases from 96.3 MPa $m^{1/2}$ at 295 K to 112.3 MPa $m^{1/2}$ at 4 K. These results are compared with similar data for Inconel 750 alloys.

16802. Blais, N. C., Truhlar, D. G., **Monte Carlo trajectory study of Ar + H_2 collisions. I. Potential energy surface and cross sections for dissociation, recombination, and inelastic scattering,** *J. Chem. Phys.* **65,** No. 12, 5335-5356 (Dec. 15, 1976).

Key words: argon; collisions; dissociation; hydrogen; inelastic; molecular potential; recombination; scattering; theoretical; theory.

Modified statistical electron-gas calculations using the methods of Gordon, Kim, Rae, Cohen, and Pack are carried out to obtain the interaction energy of Ar with H_2 as a function of geometry. The results are combined with the accurate pairwise interactions, the long-range nonpairwise interaction, and the potential LeRoy and van Kranendonk fit to spectral data on the van der Waals' complex to obtain a potential energy surface which is as accurate as possible at all geometries. This surface and the pairwise additive surface are then used in a Monte Carlo quasiclassical trajectory study of the cross sections (under shock-tube high-energy collision conditions) for complete dissociation, for production of quasibound states of H_2, and for *V-T*, *R-T*, and *V-R-T* energy transfer. Except for *R-T* energy transfer, the accurate surface yields smaller cross sections than the pairwise additive surface does. The cross sections for dissociation are much smaller than predicted by the available-energy hard-sphere model but are larger than the inelastic cross sections for excitation to the highest bound vibrational energy levels. Initial vibrational excitation energy is more effective than rotational energy or relative translational energy in causing dissociation. Using the full potential surface the recombination cross section of the $v = 13$, $j = 8$ quasibound state of H_2 is calculated at $E_{rel} = 0.026$ eV and is in good agreement with the result previously calculated by Whitlock, Muckerman, and Roberts using a less accurate, pairwise additive potential surface.

16803. Blais, N. C., Truhlar, D. G., **Monte Carlo trajectory study of Ar + H_2 collisions. II. Vibrational and rotational enhancement of cross sections for dissociation,** *J. Chem. Phys.* **66,** No. 2, 772-778 (Jan. 15, 1977).

Key words: argon; cross section; dissociation collisions; hydrogen; theory; vibrational and rotational enhancement.

Integral cross sections and properties of the dissociated trajectories were calculated for the reactions Ar + H_2 → Ar + H + H and Ar + H_2(qb) → Ar + H + H, where H_2(qb) is a quasibound H_2. Integral cross sections were also calculated for Ar + H_2 → Ar + H_2(qb). Twenty-four different (21 bound, 3 quasibound initial vibrational-rotational states of H_2 are considered. The potential surface (which we presented previously) is based on modified statistical calculations at small distances and dissociates to an accurate potential in the van der Waals region and to accurate diatomic curves. At a total energy 1 eV above the energetic threshold for dissociation, we find reagent vibrational energy is very effective in promoting dissociation (the vibrational bias parameter of Kiefer, Joosten, and Breshears is about 11 to 13), rotational energy is second most effective, and relative translational energy is least effective. Except for the topmost vibrational level we find dissociation cross sections are much smaller than predicted by the hard-sphere available-energy theory.

16804. Smeyers, P., **Influence of magnetic fields on nonradial stellar oscillations,** *Proc. Solar and Stellar Pulsation Conf., Los Alamos, NM, Aug. 3-5, 1976,* pp. 140-149 (Los Alamos Scientific Laboratory, University of California, Los Alamos, NM, Oct. 1976).

Key words: nonradial; perturbation theory; stellar oscillations; weak magnetic fields.

A perturbation method is presented which allows us to determine the effect of a weak magnetic field on the linear and adiabatic nonradial oscillations of a star. The method has been applied to a model with uniform density pervaded by a magnetic field with both a poloidal and a toroidal component, and to a polytropic model with a magnetic field which is purely toroidal and has only a ϕ-component.

16805. Olver, F. W. J., **Connection formulas for second-order differential equations with multiple turning points,** *SIAM J. Math. Anal.* **8,** No. 1, 127-154 (Feb. 1977).

Key words: asymptotic analysis; Bessel functions; boundary-value problem; connection formula; diffraction theory; error analysis; Liouville-Green approximation; ordinary differential equation; turning point.

A study is made of the differential equation

$$d^2w/dx^2 = [u^2f(u, x) + g(u, x)]w, a_1 < x < a_2,$$

in which u is a positive parameter. For each value of u, $\partial^2 f(u, x)/\partial x^2$ and $g(u, x)$ are assumed to be continuous in the finite or infinite open interval (a_1, a_2). The function $f(u, x)$ is real and its only zero within (a_1, a_2) is a single zero of multiplicity $m-2$, where m (≥ 2) is an arbitrary integer. For large values of u, asymptotic approximations for the solutions are constructed in terms of Bessel functions of order $1/m$, subject to certain restrictions on the behavior of $f(u, x)$ and $g(u, x)$ as $u \to \infty$. These restrictions are satisfied, for example, if $f(u, x)$ is independent of u and $g(u, x) = O(u^\omega)$, where $\omega < \min(4/m, 1)$. Each approximation is uniformly valid throughout (a_1, a_2) and is accompanied by a strict and realistic bound for the error term.

In the case in which a_1 and a_2 are singularities of the differential equation, the uniform approximations are applied to solve the problem of connecting the known asymptotic solutions in terms of elementary functions (the Liouville-Green approximations) valid in a neighborhood of a_2, with the corresponding asymptotic solutions valid in a neighborhood of a_1.

16806. Green, D. C., **A CAMAC parallel branch driver for the Harris 6024/5 computer,** *IEEE Trans. Nucl. Sci.* **NS-24,** No. 2, 931-932 (Apr. 1977).

Key words: branch driver; CAMAC; CAMAC standards; computer interfaces; digital interfaces; Harris computer.

A CAMAC parallel Branch Driver has been developed for the Harris 6024/5 series computers used in neutron physics research at the National Bureau of Standards. The Branch Driver allows either programmed transfers or programmed interrupt transfers of data between the computer and a CAMAC Branch Highway.

16807. Faulkner, D. J., **Mode interaction in U TrA,** *Proc. Solar and Stellar Pulsation Conf., Los Alamos, NM, Aug. 3-5, 1976,* pp. 66-75 (Los Alamos Scientific Laboratory, University of California, Los Alamos, NM, Oct. 1976).

Key words: beat Cepheids; double-mode Cepheids; Fourier analysis of stellar variations; mode interaction; stellar instabilities; U Trianguli Australis.

Photoelectric observations of the double-mode Cepheid U TrA previously reported by Oosterhoff (1957a) and Jansen (1962) have been reanalyzed using Fourier techniques. The two reported periods have been confirmed and it has been shown that no further statistically significant periodicity is present. The two observed modes are subject to a strong mode interaction, but it is not yet clear whether this will have any implications for the pulsational masses derived for double-mode Cepheids.

16808. Vorburger, T. V., Sandstrom, D. R., Waclawski, B. J., **The displacement of hydrogen by carbon monoxide on the (100) face of tungsten: A photoemission and thermal desorption study,** *Surface Sci.* **60,** 211-230 (1976).

Key words: carbon monoxide; chemisorption; coadsorption; desorption; displacement; hydrogen; photoemission; thermal desorption; tungsten; ultraviolet photoelectron spectroscopy.

Photoelectron spectra ($h\nu = 21.22$ eV) and thermal desorption data were obtained for CO and H coadsorbed on W(100) at 80 K. When the clean surface is exposed to a saturation dose of H_2, subsequent exposure to CO results in the formation of a state whose emission spectrum is similar to that of molecular α-CO. Upon heating to ~280 K, a structural rearrangement occurs in which most of the adsorbed CO is converted to the strongly bound β form as the hydrogen is simultaneously desorbed. These data plus the observation that H_2 cannot be adsorbed to any significant degree on a saturated layer of β-CO suggest that adsorbed β-CO and H occupy the same atomic sites on the W(100) surface. The distinction between long and short range repulsive CO-H interactions is discussed. For CO adsorbed on clean W(100), the range of activation energies for virgin to β conversion is calculated from the UPS data to be 45-62 kJ/mol.

16809. Ayres, T. R., Linsky, J. L., Rodgers, A. W., Kurucz, R. L., **Stellar model chromospheres. V. Alpha centauri A (G2 V) and alpha centauri B (Kl V),** *Astrophys. J.* **210,** No. 1, Pt. 1, 199-210 (Nov. 15, 1976).

Key words: flare stars; stellar chromospheres; stellar evolution; stellar photospheres; stellar spectra; stellar transition regions.

We propose models for the upper photospheres and lower chromospheres of α Cen A and B based on a partial redistribution (PRD) analysis of the Ca II K line cores and damping wings. Coudè spectrograms of the Ca II regions in these stars obtained with the Mount Stromlo 74 inch (1.9 m) telescope are calibrated by fitting the far wing profiles of K with synthetic fluxes based on radiative equilibrium (RE) models. The RE calibrations are verified by comparison with independent calibrations using Willstrop's absolute photometry and narrow band fluxes obtained at Mount Stromlo. Deviations of the empirical profiles from the RE fluxes in the inner wings of K suggest departures from radiative equilibrium in the upper photosphere of α Cen A comparable to those found previously for the Sun and Procyon. Alpha Cen B shows similar departures from RE when the effects of CO cooling near the temperature minimum are taken into account. We find similar ratios of T_{min}/T_{eff} for both stars, which are within the range of T_{min}/T_{eff} ratios determined previously for the Sun, Procyon, and Arcturus. In addition, we find similar mass column densities at the 8000 K levels of the α Cen A and B chromospheres comparable to those determined for the Sun and Procyon. Finally, α Cen A appears to be more evolved and possibly much older than the Sun, despite its similar chromosphere structure.

16810. Beaty, E. C., Hesselbacher, K. H., Hong, S. P., Moore, J. H., **Triple-differential three-dimensional cross sections for low-energy electron impact ionization of helium,** *J. Phys. B: Atom. Molec. Phys.* **10,** No. 4, 611-620 (1977).

Key words: cross section; differential; electron; helium; ionization; measurements.

Measurements are reported of the triple-differential cross section for ionization of helium by electron impact. Experimental conditions were chosen to help clarify the situation in the theory of ionization. Data are presented for primary energies of 100, 105, 125 and 165 eV. Unlike previous measurements in this energy regime, data are included for the circumstance where the three electron trajectories are not in a plane.

16811. Parris, G. E., Blair, W. R., Brinckman, F. E., **Chemical and physical considerations in the use of atomic absorption detectors coupled with a gas chromatograph for determination of trace organometallic gases,** *Anal. Chem.* **49,** No. 3, 378-386 (Mar. 1977).

Key words: arsenic; atomic absorption; gas chromatography; organometal; selenium; tin.

A commercial atomic absorption spectrophotometer with a heated graphite-tube furnace atomizer (HGA) was adapted as a detector for a gas-liquid chromatograph. The combined system was applied to the determination of elements (i.e., As, Se, Sn) known to be methylated by microorganisms. The system was optimized by assessing the effects of varying the

atomization temperature, the inner surface of the furnace (i.e., fused silica, alumina, bare graphite and pyrolytic carbon surfaces) and the carrier gas (i.e., pure argon and argon with hydrogen). Using conservative, statistically-based numerical techniques, the system detection limits for arsenic, selenium, and tin (introduced as trimethylarsine, dimethylselenium and tetramethyltin gas solutions with nitrogen diluent) were found to be 5 ng As, 7 ng Se, and 12 ng Sn. To obtain these limits, the bare graphite furnace was run continuously at about 1800 °C while the compounds were eluted from the chromatograph with argon to which 10 percent hydrogen was added. Optimization of the furnace conditions requires an understanding of the thermodynamics and kinetics associated with thermal and chemical decomposition of the analyte compounds.

16812. Stone, E. J., Lawrence, G. M., Fairchild, C. E., **Kinetic energies and angular distributions of oxygen atom photofragments produced by photodissociation of O_2 and N_2O in the vacuum ultraviolet,** *J. Chem. Phys.* **65,** No. 12, 5083-5092 (Dec. 15, 1976).

Key words: atomic; experimental; lifetimes; N_2O; oxygen; radiation; time-of-flight.

A gas phase chemi-ionization process is used to detect O atoms produced by photodissociation of O_2 and N_2O. For the photon energies used here the accessible O atom states are within the ground ^3P levels and the metastable ^1D and ^1S levels. Kinetic energies of the O atom photofragments are determined using an atomic beam time-of-flight technique, and the O atom angular distributions are determined by varying the angle between the direction of the photon beam and the atomic beam flight path. Dissociative transitions within the Schumman-Runge continuum of O_2 and the principal vacuum ultraviolet absorption continuum of N_2O yield results in agreement with previous predictions. For the dissociation of O_2 at wavelengths of 120 and 124 nm, the principal dissociation products are $O(^3P) + O(^1D)$; and, at these wavelengths, the O atom angular distribution is consistent with previous conclusions that predissociation is important. Using existing theories of photofragment angular distributions, an asymmetry parameter having a value of (-0.61 ± 0.05) is obtained for predissociation in O_2 at the 10.0 and 10.3 eV absorption features.

16813. Krasny, J. F., Peacock, R. D., **Comments on "Flammability assessment of apparel fabrics",** *Textile Chem. Colorists* **9,** No. 4, 32-33 (Apr. 1977).

Key words: burn injury; flammability; Mushroom Flammability Tester; test methods.

The heat transfer rate from burning fabrics, measured on the Mushroom Apparel Flammability Tester, is compared with flammability assessments reported in a paper by Galil and Lomartire. Agreement between the two methods was found for only a few fabrics.

16814. Sparrow, J. H., Dick, C. E., **Pulsed high intensity monoenergetic low energy x-ray source and absolute x-ray monitor,** *Nucl. Instrum. Methods* **141,** 283-292 (1977).

Key words: absolute x-ray detectors; electron excitations; monoenergetic x rays; pulsed x-ray source; x-ray detector calibration; 1.5-8 keV x rays.

An x-ray source of 1.5, 4.5, or 8.0 keV with 10 ns durations has been produced utilizing a pulsed electron source to excite the characteristic K-line radiation of elemental targets. A parallel plate ionization chamber was calibrated in the NBS standard monoenergetic K x-ray beams and used with Ross filters to measure the pulsed source K x-ray fluence. Typical measured peak x-ray flux intensities are 10^{18}-10^{19} K x-rays per sr per s. The pulsed source contains four identical ports for simultaneous measurement of the K x-ray intensity by the ionization chamber and detectors being calibrated. The pulsed K x-ray source and the NBS standard steady state K x-ray source, which differ in intensity by 10 orders of magnitude, have been utilized to determine the responses of a photoelectric diode, a scintillator-vacuum photodiode combination, and a silicon PIN diode.

16815. Bennett, H. S., Forman, R. A., **Relative dominance of bulk or surface absorption in highly transparent materials by transient methods,** *J. Appl. Phys.* **48,** No. 3, 1217-1222 (Mar. 1977).

Key words: absorption; barothermal gas cell; bulk absorption; highly transparent; infrared materials; optical materials; surface absorption.

For the case in which a pulsed laser beam passes through the weakly absorbing windows of a gas cell containing a nonabsorbing gas, the time rate of change of the relative pressure rise immediately after the cessation of the laser beam correlates directly with the relative dominance of bulk and surface absorption in highly transparent materials. Whenever bulk absorption dominates, the time derivative of the pressure rise in the gas for times shortly after cessation of the pulse is positive; when surface absorption dominates, it is negative; and when bulk and surface absorption are comparable, it is very close to zero. This, suggests then, a relatively simple experimental procedure by which one may determine nondestructively the relative dominance of bulk or surface absorption in highly transparent materials.

16816. Ekin, J. W., Clark, A. F., **Effect of strain on the critical current of Nb_3Sn and NbTi multifilamentary composite wires,** (Proc. Joint MMM-Intermag Conf., Pittsburgh, PA, June 15-18, 1976), *AIP Conf. Proc. No. 34, Magnetism and Magnetic Materials—1976,* J. J. Becker and G. H. Lander, Eds., pp. 81-83 (American Institute of Physics, New York, NY, 1976).

Key words: aluminum stabilization; copper stabilization; critical current; critical-current degradation; multifilamentary wires; Nb_3Sn; NbTi; strain; stress.

The critical currents of flexible Nb_3Sn and NbTi composite wires have been observed to decrease as a function of strain. Characteristic samples of the data are presented along with a brief summary and intercomparison of the results for each wire type. In the NbTi wires the decrease commenced at strains of about 0.5 percent, but did not become appreciable (i.e., greater than ~ 5%) until strains exceeded about 1.5 percent. The effect is almost totally reversible and the magnitude of the decrease is not strongly dependent on sample configuration or stabilization material. In the Nb_3Sn composites the degradation in critical current is relatively much larger, becoming significant at strains ranging from 0.1 to 0.3 percent depending on the reinforcement technique used in the wires' construction. At high strains, the effect in Nb_3Sn is only partially reversible. Also in the Nb_3Sn composites, stress-induced resistivities as high as 10^{-10} Ωcm were observed at currents well below I_c. This leads to significant Joule heating of the superconducting wire and ambiguities in the operational definition of "critical current."

16817. Han, C. C., Mozer, B., **Conformation of PS-PMMA diblock copolymer in toluene by small angle neutron scattering,** *Macromolecules* **10,** No. 1, 44-51 (Jan./Feb. 1977).

Key words: conformation; deuterated polystyrene-poly(methylmethacrylate); diblock copolymer; radius of gyration; small angle neutron scattering.

A deuterated polystyrene-poly(methyl methacrylate) (dPS-PMMA) diblock copolymer and its deuterated polystyrene homopolymer precursor were studied by small angle neutron

scattering and light scattering experiments using toluene as the solvent. The radii of gyration of the deuterated PS homopolymer ($M = 88\,000$) measured by both methods and that of the PMMA block ($M = 203\,000$) in the diblock copolymer measured only by neutron scattering were determined as 210 and 85 Å, respectively. In addition, the second virial coefficients and the chain excluded volume exponents were also obtained. The copolymer chain conformation in toluene at 23 °C is inferred from these measurements. It is suggested that the PMMA block forms the interior core from which the PS block exudes out as an expanded chain.

16818. Wisdom, J., Hartquist, T. W., Lane, N. F., **He(2^3S) bubble in liquid helium,** *Phys. Rev. B, Comments and Addenda* **14,** No. 9, 4205-4208 (Nov. 1, 1976).

Key words: helium absorption; liquid helium bubble; metastable helium atoms.

Using the phenomenological model of Padmore and Cole, we have reinvestigated the nature of the "bubble" surrounding a 2^3S metastable helium atom in liquid helium. The principal result of this work is that a reasonable $2^3S \rightarrow 2^3P$ absorption line shift is obtained in good agreement with the model of Hickman, Steets, and Lane, and with experiment, and that a local liquid-helium density function is obtained in good agreement with that determined in a very different manner by Hansen and Pollock.

16819. Johnson, C. R., **Functional characterizations of the field of values and the convex hull of the spectrum,** *Proc. Am. Math. Soc.* **61,** No. 2, 201-204 (Dec. 1976).

Key words: convex hull; eigenvalue; field of values; positive semidefinite; semistable.

The only compact, convex set-valued homogeneous and translatable function of square complex matrices which is an indicator function for the matrices with positive semidefinite real part is the classical field of values. An analogous characterization of the convex hull of the spectrum is given.

16820. Klebanoff, P. S., Frenkiel, F. N., **On the small-scale turbulence structure,** (Proc. Bat-Sheva Int. Seminar, Ben-Gurion Univ. of Negev, Beersheva, Israel, Mar. 17-20, 1975), Paper in *MHD-Flows and Turbulence*, H. Branover, Ed., pp. 147-151 (Halsted Press, Div. John Wiley & Sons, Inc., New York, NY, 1976).

Key words: boundary-layer; higher-order moments; hot-wire anemometry; log-normal distribution; small-scale turbulence.

The results of an experimental investigation into the nature of the small-scale turbulence structure involving the measurement of higher-order moments of turbulent velocity gradients are described. Comparisons with atmospheric investigations and theory are given.

16821. Klebanoff, P. S., McMichael, J. M., **On MHD pipe flow,** (Proc. Bat-Sheva Int. Seminar, Ben-Gurion Univ. of Negev, Beersheva, Israel, Mar. 17-20, 1975), Paper in *MHD-Flows and Turbulence*, H. Branover, Ed., pp. 73-80 (Halsted Press, Div. John Wiley & Sons, Inc., New York, NY, 1976).

Key words: liquid metals; magnetohydrodynamics; pipe flow; resistance coefficients; turbulence.

A description of the liquid metal flow facility at NBS is presented. Data demonstrating the operation of the facility, including wall pressure measurements over a range of Hartmann numbers and Reynolds numbers extending up to 1350 and 340,000, respectively, are discussed.

16822. McCrackin, F. L., **Calibration of gel permeation chromatography columns using polydisperse polymer standards,** *J. Appl. Polymer Sci.* **21,** 191-198 (1977).

Key words: calibration; column broadening, GPC; gel permeation chromatography; nonlinear regression.

Two methods of calibrating gel permeation chromatography columns are given. The first method uses polymer standards that may have broad molecular weight distributions. Either the weight-, number-, or viscosity-average molecular weight of each standard must be known. This method neglects column peak spreading. The second method requires polymer standards of moderately narrow molecular weight distributions for which both the weight- and number-average molecular weights are known. However, the second method determines both the column peak spreading and calibration of the column. The second method is applied to calibration of a column using polystyrene standards. The column peak spreading is found to be small and independent of molecular weight for this column.

16823. Maki, A. G., Sams, R. L., Pearson, R., Jr., **Microwave and infrared spectra of isotopically substituted carbonyl selenide (OCSe),** *J. Mol. Spectrosc.* **64,** 452-459 (1977).

Key words: bond distances; carbonyl selenide; energy levels; force field; infrared; microwave; molecular structure; spectra; spectroscopy.

Infrared and microwave spectral measurements are given for three isotopically enriched species of carbonyl selenide. The high-resolution infrared measurements (made near 2000 and 2600 cm^{-1}) provide constants for the following transitions: $10^00\text{-}00^00$ for $^{16}O^{12}C^{80}Se$; $10^00\text{-}00^00$ and $11^10\text{-}01^10$ for $^{18}O^{12}C^{80}Se$; and $10^00\text{-}00^00$, $11^10\text{-}01^10$, $10^01\text{-}00^01$, and $10^01\text{-}00^00$ for $^{16}O^{13}C^{80}Se$. Microwave measurements are given for the $J = 4 \leftarrow 3$, and $3 \leftarrow 2$ transitions of $^{18}O^{12}C^{80}Se$ and $^{16}O^{13}C^{80}Se$ in the 00^00, 01^10, 02^00, 02^20, and 00^01 states. Equilibrium rotational constants are given for all three isotopic species and the equilibrium bond distances are determined to be r_e(C-O) = 1.1535 ± 0.0001 Å and r_e(C-Se) = 1.7098 ± 0.0001 Å.

16824. Needham, P. B., Jr., Driscoll, T. J., Powell, C. J., Stein, R. J., **Determination of the Be-Auger-electron attenuation length in Be using 160-keV protons,** *Appl. Phys. Lett.* **30,** No. 7, 357-359 (Apr. 1, 1977).

Key words: attenuation length; Auger-electron yield; beryllium; electron scattering; proton bombardment.

We report the first results of a method for determining the inelastic attenuation length of low-energy electrons in the surface region of a solid from a yield of characteristic Auger electrons excited by proton bombardment. Samples of evaporated beryllium were bombarded by 160-keV protons, and the attenuation length of 100-eV electrons in Be was determined to be 6.1 Å.

16825. Pella, P. A., **Measurement of the vapor pressures of** TNT, **2,4-**DNT, **and** EGDN, *J. Chem. Thermodyn.* **9,** 301-305 (1977).

Key words: DNT; EGDN; electron-capture gas chromatography; measurements; TNT; vapor pressures.

The vapor pressures of 2,4,6-trinitrotoluene (TNT), 2,4-dinitrotoluene (2,4-DNT), 2,6-dinitrotoluene (2,6-DNT), and ethylene glycol dinitrate (EGDN) have been measured by an electron-capture gas-chromatographic method in the temperature range from 287.15 to 329.65 K for TNT, 277.15 to 344.15 K for 2,4-DNT, 277.15 to 323.15 K for 2,6-DNT, and 240.15 to 298.15 K for EGDN. The temperature dependence of the vapor pressure is given by the equations: TNT: $\log_{10}(p/\text{torr}) = (12.31 \pm 0.34) - (5175 \pm 105)\text{K}/T$; 2,4-DNT: $\log_{10}(p/\text{torr}) = (13.08 \pm$

0.19)−(4992 ± 59)K/T; 2,6-DNT: $\log_{10}(p/\text{torr}) = (13.99 \pm 0.18)-(5139 \pm 52)\text{K}/T$; EGDN: $\log_{10}(p/\text{torr}) = (10.55 \pm 0.08)-(3476 \pm 22)\text{K}/T$.

The values for the enthalpy of sublimation are ΔH_{sub}(TNT) = (23.7 ± 0.5) kcal_{th} mol^{-1}, ΔH_{sub}(2,4-DNT) = (22.9 ± 0.3) kcal_{th} mol^{-1}, and ΔH_{sub}(2,6-DNT) = (23.5 ± 0.2) kcal_{th} mol^{-1}. The enthalpy of vaporization for EGDN is (15.9 ± 0.09) kcal_{th} mol^{-1}. The indicated uncertainties are standard errors.

16826. Penn, D. R., **Secondary-electron energy distribution in high-energy photoemission,** *J. Vac. Sci. Technol.* **14,** No. 1, 300-302 (Jan./Feb. 1977).

Key words: energy distribution; photoemission; secondary electron.

We have calculated the energy distribution of secondary electrons observed in core-level XPS or core-level synchroton photoemission experiments on Al. The secondary electrons are produced when the photoexcited primary electrons scatter inelastically from the valence electrons via the mechanisms of bulk and surface plasmon production and electron-hole production. The scattering cross sections for these events are determined from the Lindhard dielectric function, although the plasmon dispersion and broadening are taken from experimental measurements. Multiple scattering is taken into account by means of the Wolff-Spencer-Fano integral equation for the electron-energy distribution. The calculated results are compared to experiment.

16827. Ruff, A. W., **Characterization of debris particles recovered from wearing systems,** *WEAR* **42,** 49-62 (1977).

Key words: debris; electron microscopy; particles; wear; x-ray emission.

Studies have been conducted on wear debris collected from various systems involving both sliding and rolling contacts. Results of size, shape and chemical composition analyses of typical debris particles are presented. Different techniques for debris recovery and analysis are discussed. Some results are presented on electron transmission studies of individual debris particles. The effect of small particle size on x-ray emission microanalysis is also described.

16828. Spal, R. D., **Production of uniform field gradients for magnetometers by means of current-carrying strips,** *J. Appl. Phys.* **48,** No. 3, 1338-1341 (Mar. 1977).

Key words: Faraday magnetometer design; homogeneity; magnet design; magnetic field gradients; magnetometer design.

Current-carrying strips are a convenient means to produce a uniform field gradient for use in a Faraday magnetometer. An expression is derived for the magnetic field gradient, taking into account the images of the strips in the pole pieces. Tables are presented giving the magnitude and homogeneity of the gradient for various strip widths and locations. The performance in the laboratory of a set of strips is reported.

16829. Vorburger, T. V., Waclawski, B. J., Plummer, E. W., **Evidence for the distortion of C_2H_4 and C_2H_2 chemisorbed on W(100),** *Chem. Phys. Lett.* **46,** No. 1, 42-47 (Feb. 15, 1977).

Key words: acetylene; adsorption; chemisorption; dehydrogenation; ethylene; photoemission; tungsten; ultraviolet photoelectron spectroscopy.

The adsorption of C_2H_4 on W(100) has been studied by ultraviolet photoelectron spectroscopy with $h\nu = 21.22$ eV. The spectrum measured after an initial saturation exposure at 80 K exhibits structure which correlates well with energy levels recently calculated by Demuth and Eastman (DE) for sp^3 rehybridized C_2H_4. Dehydrogenation of the adsorbate, either by subsequent heating to 295 K or direct adsorption at 295 K, yields a spectrum which correlates with DE's calculation for sp^2 rehybridized C_2H_2. These results suggest that C_2H_4 and C_2H_2 may be distorted from their planar and linear structures respectively and that the C-C bonds on these molecules are stretched by adsorption on W(100). Qualitative arguments suggest that the bonding site for both molecules is directly over a W atom and that the Dewar-Chatt model for π-d bonding in organometallic compounds is applicable.

16830. Pella, P. A., Mills, R. M., **A trace vapor generator for testing explosives vapor detectors,** *LESP-RPT-0604.00,* 24 pages (U.S. Department of Justice, Law Enforcement Assistance Administration, National Institute of Law Enforcement and Criminal Justice, Washington, DC, Mar. 1977).

Key words: DNT; EGDN; explosive detection; limits of detection; sensitivity test; TNT; vapor generator; vapor pressure.

A vapor generator for law enforcement applications was developed to produce known trace concentrations of vapors of 2,4,6 trinitrotoluene (TNT), 2,4-dinitrotoluene (2,4 DNT), 2,6-dinitrotoluene (2,6 DNT), and ethylene glycol dinitrate (EGDN). Known equilibrium vapor concentrations of these explosives are generated at several temperatures by passing dry nitrogen through a temperature-controlled column packed with the explosive dispersed on an inert support. The equilibrium vapor enters a dynamic gas-blending system in which the vapor is precisely diluted with air to provide output explosives vapor concentrations below 1 ppb. The system was evaluated by measuring output vapor concentrations of TNT, 2,4 DNT, 2,6 DNT, and EGDN using gas-chromatographic analysis. The applicability of the generator for testing sensitivities and limits of detection of commercial explosives vapor detectors is demonstrated.

16831. Quindry, T. L., Stenbakken, G. N., **Sound sensing units for intrusion alarm systems,** *NILECJ-STD-0308.00,* 18 pages (U.S. Department of Justice, Law Enforcement Assistance Administration, National Institute of Law Enforcement and Criminal Justice, Washington, DC, Mar. 1977).

Key words: alarm; audio alarm; burglar alarm; intrusion alarm; intrusion detector; sound sensing; standard.

This standard establishes performance criteria for sound sensing alarms intended for use in protective intrusion systems to monitor for attempts to enter a room or building. These devices cause the initiation of an alarm signal to a police panel, central station, or local audible alarm device. Included are requirements and test methods for performance, electrical properties and materials. The characteristics addressed are those which affect the reliability of the devices with emphasis on those performance characteristics which affect their false alarm susceptibility and its tamper resistance.

JOURNAL OF RESEARCH of the National Bureau of Standards—A. Physics and Chemistry
Vol. 81A, Nos. 2 and 3, March–June 1977

INDEX TO VOLUME 81A

January–June 1977

A

Acidity 21
Alkyl iodides 267
Aqueous solution 89
Atlas of the I_2 spectrum from 19 000 to 18 000 cm^{-1} 25
Atomic weight 1

B

Bates, R. G., Hetzer, H. B., Durst, R. A., Robinson, R. A., Standard pH values for the potassium hydrogen phthalate reference buffer solution from 0 to 60 °C 21
Bead/spring model 97
Bennett, H. S., Kayser, R., Jr., Evaporation of liquid droplets in hot gases 257
Brown, W. E., McDowell, H., Gregory, T. M., Solubility of $Ca_5(PO_4)_3OH$ in the system $Ca(OH)_2$-H_3PO_4-H_2) at 5, 15, 25, and 37 °C 273

C

Calibration 81
Cezairliyan, A., McClure, J. L., Taylor, R. Thermophysical measurements on 90Ti-6Al-4V alloy above 1450 K using a transient (subsecond) technique 251
Clapeyron equation 5
Compressibility 283
Concentration dependent diffusion coefficient 243
Concentration front 243
Confluent hypergeometric functions 257
Coulometry 1

D

Densification 283
Dew point 81
Diffusion with discontinuous swelling. III. Type II diffusion as a particular solution of the conventional diffusion equation 243
Discontinuous swelling 243
Dissolution 273
Droplet 257
Durst, R. A., Hetzer, H. B., Robinson, R. A., Bates, R. G., Standard pH values for the potassium hydrogen phthalate reference buffer solution from 0 to 60 °C 21

E

Eigenvalues 97
Electrical resistivity 251
Emf 21
Equilibrium 89
Evaporation of liquid droplets in hot gases 257

F

Fong, J. T., Peterlin A., Frequently dependence of intrinsic shear and birefringence tensor of bead/spring model of polymer solutions 97
Frequency dependence of intrinsic shear and birefringence tensor of bead/ spring model of polymer solutions 97
Frequency response 97

G

Gallium arsenide 1
Gallium atomic weight 1
Glass 283
Glass transition 283
Greenspan, L., Humidity fixed points of binary saturated aqueous solutions 89
Gregory, T. M., McDowell, H., Brown, W. E., Solubility of $Ca_5(PO_4)_3OH$ in the system $Ca(OH)_2$-H_3PO_4-H_2O at 5, 15, 25, and 37 °C 273

H

Hasegawa, S., Little, J. W., The NBS two-pressure humidity generator, Mark 2 81
Heat capacity 251
Hetzer, H. B., Durst, R. A., Robinson, R. A., Bates, R. G., Standard pH values for the potassium hydrogen phthalate reference buffer solution from 0 to 60 °C 21
High-resolution spectrum 25
High-speed measurements 251
High temperatures 251
Hougen, J. T., Simmons, J. D., Atlas of the I_2 spectrum from 19 000 to 18 000 cm^{-1} 25
Humidity 81, 89
Humidity fixed points of binary saturated aqueous solutions 89
Hydroxyapatite 273
Hygrometer 81

I

Intrinsic optical tensor 97
Intrinsic stress tensor 97
Iodine spectrum 25
Ion-molecule reactions 267
Ion pairs 273
Isotope effects 267
Isotope effects in the association reactions of methyl and ethyl iodide cations 267

K

Kayser, R., Jr., Bennett, H. S., Evaporation of liquid droplets in hot gases 257

L

Line identification atlas 25
Liquid 283
Little, J. W., Hasegawa, S., The NBS two-pressure humidity generatire, Mark 2 81

M

Marinenko, G., On the atomic weight of gallium 1
Mass spectrometry 267
McClure, J. L., Cezairliyan, A., Taylor, R., Thermophysical measurements on 90Ti-6Al-4V alloy above 1450 K using a transient (subsecond) technique 251
McDowell, H., Gregory, T. M., Brown, W. E., Solubility of $Ca_5(PO_4)_3OH$ in the system $Ca(OH)_2$-H_3PO_4-H_2O at 5, 15, 25, and 37 °C 273
McKinney, J. E., Simha, R., Thermodynamics of the densification process for polymer glasses 283

Page

Melting 251
Mixing ratio 81
Moving boundary problem 257

N

Normal spectral emittance 251

O

On the atomic weight of gallium 1

P

Peterlin, A., Diffusion with discontinuous swelling. III. Type II diffusion as a particular solution on the conventional diffusion equation 243
—, *Fong, J. T.*, Frequency dependence of intrinsic shear and birefringence tensor of bead/spring model of polymer solutions 97
pH 21
Photo-ionization 267
Phthalate buffer 21
Polymer 283
Polymer solution 97
Potassium hydrogen phthalate 21
Preheat 257
Pressure 283
PVT 283
Pyrolysis 283

R

Radiance temperature 251
Rate constants 267
Refractive index 283
Relative humidity 81, 89
Robinson, R. A., Hetzer, H. B., Durst, R. A., Bates, R. G., Standard pH values for the potassium hydrogen phthalate reference buffer solution from 0 to 60 °C 21
Rovibronic assignments 25

S

Salt 89
Saturated salt solution 89
Saturation vapor pressure over ice 5
Sieck, L. W., Isotope effects in the association reactions of methyl and ethyl iodide cations 267
Simha, R., McKinney, J. E., Thermodynamics of the densification process for polymer glasses 283

Page

Simmons, J. D., Hougen, J. T., Atlas of the I_2 spectrum from 19 000 to 18 000 cm^{-1} 25
Solubility 273
Solubility isotherms 273
Solubility of $Ca_5(PO_4)_3OH$ in the system $Ca(OH)_2$-H_3PO_4-H_2O at 5, 15, 25, and 37 °C 273
Solubility product 273
Specific heat capacity 251
Spectral analysis 25
Standard for pH 21
Stoichiometry 1

T

Taylor, R., Cezairliyan, A., McClure, J. L., Thermophysical measurements on 90Ti-6Al-4V alloy above 1450 K using a transient (subsecond) technique 251
The NBS two-pressure humidity generator, Mark 2 81
Thermal coefficient at solubility 273
Thermal expansion 273
Thermal properties of ice 5
Thermal radiation properties 251
Thermodynamic 283
Thermodynamics 251
Thermodynamics of the densification process for polymer glasses 283
Thermophysical measurements on 90Ti-6Al-4V alloy above 1450 K using a transient (subsecond) technique 251
Titanium alloy 251
Tooth mineral 273
Transient heat conduction 257
Two-pressure generator 81

U

Unconventional diffusion 273

V

Vapor pressure 5,89
Vapor pressure at the triple point 5
Vapor pressure formulation for ice 5
Vapor pressure of ice 5
Velocity of concentration front propagation 243
Visible absorption spectroscopy 25
Volume ratio 81

W

Water vapor 5, 81, 89
Wexler, A., Vapor pressure formulation for ice 5

NBS TECHNICAL PUBLICATIONS

PERIODICALS

JOURNAL OF RESEARCH—The Journal of Research of the National Bureau of Standards reports NBS research and development in those disciplines of the physical and engineering sciences in which the Bureau is active. These include physics, chemistry, engineering, mathematics, and computer sciences. Papers cover a broad range of subjects, with major emphasis on measurement methodology, and the basic technology underlying standardization. Also included from time to time are survey articles on topics closely related to the Bureau's technical and scientific programs. As a special service to subscribers each issue contains complete citations to all recent NBS publications in NBS and non-NBS media. Issued six times a year. Annual subscription: domestic $17.00; foreign $21.25. Single copy, $3.00 domestic; $3.75 foreign.

Note: The Journal was formerly published in two sections: Section A "Physics and Chemistry" and Section B "Mathematical Sciences."

DIMENSIONS/NBS (formerly Technical News Bulletin)—This monthly magazine is published to inform scientists, engineers, businessmen, industry, teachers, students, and consumers of the latest advances in science and technology, with primary emphasis on the work at NBS. The magazine highlights and reviews such issues as energy research, fire protection, building technology, metric conversion, pollution abatement, health and safety, and consumer product performance. In addition, it reports the results of Bureau programs in measurement standards and techniques, properties of matter and materials, engineering standards and services, instrumentation, and automatic data processing.

Annual subscription: Domestic, $12.50; Foreign $15.65.

NONPERIODICALS

Monographs—Major contributions to the technical literature on various subjects related to the Bureau's scientific and technical activities.

Handbooks—Recommended codes of engineering and industrial practice (including safety codes) developed in cooperation with interested industries, professional organizations, and regulatory bodies.

Special Publications—Include proceedings of conferences sponsored by NBS, NBS annual reports, and other special publications appropriate to this grouping such as wall charts, pocket cards, and bibliographies.

Applied Mathematics Series—Mathematical tables, manuals, and studies of special interest to physicists, engineers, chemists, biologists, mathematicians, computer programmers, and others engaged in scientific and technical work.

National Standard Reference Data Series—Provides quantitative data on the physical and chemical properties of materials, compiled from the world's literature and critically evaluated. Developed under a world-wide program coordinated by NBS. Program under authority of National Standard Data Act (Public Law 90-396).

NOTE: At present the principal publication outlet for these data is the Journal of Physical and Chemical Reference Data (JPCRD) published quarterly for NBS by the American Chemical Society (ACS) and the American Institute of Physics (AIP). Subscriptions, reprints, and supplements available from ACS, 1155 Sixteenth St. N.W., Wash., D.C. 20056.

Building Science Series—Disseminates technical information developed at the Bureau on building materials, components, systems, and whole structures. The series presents research results, test methods, and performance criteria related to the structural and environmental functions and the durability and safety characteristics of building elements and systems.

Technical Notes—Studies or reports which are complete in themselves but restrictive in their treatment of a subject. Analogous to monographs but not so comprehensive in scope or definitive in treatment of the subject area. Often serve as a vehicle for final reports of work performed at NBS under the sponsorship of other government agencies.

Voluntary Product Standards—Developed under procedures published by the Department of Commerce in Part 10, Title 15, of the Code of Federal Regulations. The purpose of the standards is to establish nationally recognized requirements for products, and to provide all concerned interests with a basis for common understanding of the characteristics of the products. NBS administers this program as a supplement to the activities of the private sector standardizing organizations.

Consumer Information Series—Practical information, based on NBS research and experience, covering areas of interest to the consumer. Easily understandable language and illustrations provide useful background knowledge for shopping in today's technological marketplace.

Order above NBS publications from: Superintendent of Documents, Government Printing Office, Washington, D.C. 20402.

Order following NBS publications—NBSIR's and FIPS from the National Technical Information Services, Springfield, Va. 22161.

Federal Information Processing Standards Publications (FIPS PUB)—Publications in this series collectively constitute the Federal Information Processing Standards Register. Register serves as the official source of information in the Federal Government regarding standards issued by NBS pursuant to the Federal Property and Administrative Services Act of 1949 as amended, Public Law 89-306 (79 Stat. 1127), and as implemented by Executive Order 11717 (38 FR 12315, dated May 11, 1973) and Part 6 of Title 15 CFR (Code of Federal Regulations).

NBS Interagency Reports (NBSIR)—A special series of interim or final reports on work performed by NBS for outside sponsors (both government and non-government). In general, initial distribution is handled by the sponsor; public distribution is by the National Technical Information Services (Springfield, Va. 22161) in paper copy or microfiche form.

BIBLIOGRAPHIC SUBSCRIPTION SERVICES

The following current-awareness and literature-survey bibliographies are issued periodically by the Bureau:

Cryogenic Data Center Current Awareness Service. A literature survey issued biweekly. Annual subscription: Domestic, $25.00; Foreign, $30.00.

Liquified Natural Gas. A literature survey issued quarterly. Annual subscription: $20.00.

Superconducting Devices and Materials. A literature survey issued quarterly. Annual subscription: $30.00. Send subscription orders and remittances for the preceding bibliographic services to National Bureau of Standards, Cryogenic Data Center (275.02) Boulder, Colorado 80302.

U.S. DEPARTMENT OF COMMERCE
National Bureau of Standards
Washington, D.C. 20234

OFFICIAL BUSINESS
Penalty for Private Use $300

POSTAGE AND FEES PAID
U.S. DEPARTMENT OF COMMERCE
COM-215
SPECIAL FOURTH-CLASS RATE
BOOK

JOURNAL OF RESEARCH of the National Bureau of Standards — Vol. 81A, Nos. 2&3 Mar.–June 1977
A. Physics and Chemistry

Contents

	Page
Diffusion with discontinuous swelling. III. Type II diffusion as a particular solution of the conventional diffusion equation. Anton Peterlin.	243
Thermophysical measurements on 90Ti-6Al-4V alloy above 1450 K using a transient (subsecond) technique. A. Cezairliyan, J. L. McClure, and R. Taylor.	251
Evaporation of liquid droplet. Richard Kayser, Jr., and Hebert S. Bennett.	257
Isotope effects in the association reactions of methyl and ethyl iodide cations. L. Wayne Sieck.	267
Solubility of $Ca_5(PO_4)_3OH$ in the system $Ca(OH_2$-H_3PO_4-H_2O at 5, 15, 25, and 37°C. H. McDowell, T. M. Gregory, and W. E. Brown.	273
Thermodynamics of the densification process for polymer glasses. John E. McKinney and Robert Simha.	283
Publications of the National Bureau of Standards.	299
Index to volume 81A, January to June 1977.	343

SJRA UNIVE300UAISSDUE003R 1
UNIVERSITY MICROFILMS INC
ATTN SERIALS SECTION
300 NORTH ZEEB RD
ANN ARBOR MI 48106

Library of Congress Catalog Card Number: 62-37059

For sale by the Superintendent of Documents, U.S. Government Printing Office,
Washington, D.C. 20402. Order by SD Catalog
No. C 13.22/sec. A:81(1&2). Single copy price varies. Subscription price: $17.00 a year; $4.25 additional for foreign mailing.

UNITED STATES GOVERNMENT PRINTING OFFICE, WASHINGTON: 1977